

**Stratigraphy and Facies of the Pliocene Mayrán  
Lacustrine Basin System, Northeast México**

A thesis submitted to The University of Manchester for the degree of  
Doctor of Philosophy in the Faculty of Engineering and Physical Sciences

**2012**

**Natalia Amezcua Torres**

School of Earth, Atmospheric and Environmental Sciences

## CONTENTS

<i>Contents</i>	2
<i>List of figures</i>	5
<i>List of tables</i>	7
<i>List of appendices</i>	7
<i>Abstract</i>	8
<i>Declaration</i>	9
<i>Copyright statement</i>	10
<i>Acknowledgments</i>	11
<b>SECTION ONE: INTRODUCTION AND BACKGROUND</b>	12
<b>Chapter 1. Introduction</b>	13
1.1 Rationale	13
1.2 Aim and objectives	14
1.3 Study area	15
1.4 Research Methods	17
1.4.1 Field methods	17
1.4.2 Laboratory	18
1.4.2.1 Petrographic techniques	18
1.4.2.2 Geochemical Techniques	19
1.5 Thesis structure	22
1.6 Publication status and notes	24
<b>Chapter 2 Background literature</b>	26
2.1 Introduction	26
2.2 General aspects on lakes	26
2.3 Lake Basins controls on sediment fill	28
2.3.1 Sequence stratigraphy applied to lacustrine deposits	28
2.3.2 Sequence expression in lake basin types	30
2.4 Carbonate lake facies models	32
2.5 Carbonate sedimentology some considerations	36
2.6 Geology of the Mayrán Formation	38

<b>Chapter 3</b>	<b>Cascading carbonate lakes of the Mayrán Basin System, Northeast México: The interplay of inherited structural geometry, bedrock lithology and climate</b>	42
3.1	Abstract	42
3.2	Introduction	43
3.3	Geologic Setting	44
3.4	The Mayrán Basin system	47
3.4.1	Geomorphology	47
3.4.2	Facies associations	48
3.4.2.1	Non-channelized conglomerates	48
3.4.2.2	Channelized conglomerates and pebbly sandstones	49
3.4.2.3	Calcareous sandy mudstones and siliciclastic mudstones	50
3.4.2.4	Horizontally bedded limestones	51
3.4.2.5	Tufa clinofolds	53
3.4.2.6	Evaporites	55
3.4.3	Spatial distribution of facies	55
3.4.4	Facies interpretation and paleogeography	59
3.5	Discussion	62
3.5.1	Basin geomorphology	63
3.5.2	Sediment sources and partitioning	64
3.5.3	Allogenic vs. autogenic controls on sediment stacking patterns	65
3.6	Conclusion	67
3.7	Acknowledgements	68
<b>Chapter 4</b>	<b>Prograding tufa clinofolds in cascading lake basins</b>	70
4.1	Abstract	70
4.2	Introduction	71
4.3	Geologic setting	72
4.4	The Mayrán Basin system Prograding Tufa Lobes	74
4.4.1	Spatial distribution and external form	74
4.4.2	Stratigraphy and Sedimentology	77
4.5	Discussion	81
4.6	Conclusions	85

<b>Chapter 5</b>	<b>Lacustrine carbonate lithofacies in the Late Neogene Mayrán Formation, Northeast Mexico</b>	<b>87</b>
5.1	Abstract	87
5.2	Introduction	88
5.3	Geologic setting	90
5.4	Methods	92
5.4.1	Nomenclature of Mayrán carbonates	94
5.5	Lithofacies analyses	95
5.5.1	Ostracode mudstone	98
5.5.2	Clotted boundstone	103
5.5.3	Gastropod Wackestone-Packstone	106
5.5.4	Oncoid Wackestone-Packstone	109
5.5.5	Stromatolites	111
5.5.6	Charophyte Wackestone -Packstone	114
5.5.7	Macrophyte Boundstone	116
5.5.8	Marlstone	118
5.5.9	Crystalline carbonate	119
5.5.10	Evaporites	121
5.6	Discussion and interpretation	125
5.6.1	Detritus derived components	125
5.6.2	Locally produced components	126
5.6.3	Early diagenetic components	128
5.6.4	Spatiotemporal facies variation	131
5.7	Concluding comments	132
5.8	Acknowledgements	133
<b>Chapter 6</b>	<b>U-Pb Dating of carbonates in the Mayrán Formation, Northeast México</b>	<b>135</b>
6.1	Abstract	135
6.2	Introduction	136
6.3	Geologic Setting	138
6.3.1	Stromatolites, oncoids and botryoidal cements	140
6.4	Analytical Techniques	142
6.5	Results	143

6.6	Discussion	147
6.7	Conclusion	152
6.8	Acknowledgements	153
<b>SECTION THREE</b>		154
<b>Chapter 7: Synthesis, Discussion, Conclusions and Further work</b>		155
7.1	Introduction	155
7.2	Synthesis and Discussion	155
7.2.1	Cascading carbonate lakes of the Mayrán Basin system	155
7.2.2	Prograding tufa clinofolds in cascading lake basins	158
7.2.3	Lacustrine carbonate lithofacies in the Late Neogene Mayrán Formation	160
7.2.4	U-Pb dating of carbonates in the Mayrán Formation	164
7.3	Overall conclusions	165
7.4	Future work	168
<b>REFERENCES</b>		170
<i>List of figures</i>		5
Figure 1.1	The Mayrán Basin System northeast Mexico.	16
Figure 2.1	Schematic lake-basin type model as a function of both sediment + water supply, and potential accommodation	31
Figure 2.2	Representative attributes of the three major lacustrine facies associations.	32
Figure 2.3	Low energy bench type lake margin	34
Figure 2.4	Low energy ramp type lake margin	35
Figure 2.5	Locations of geological and geographical context of northeast México	38
Figure 2.6	Several depositional events in the study area	40
Figure 3.1	Geologic map of study area	45
Figure 3.2	Simplified structure and N-S cross section across the study area	46
Figure 3.3	The Mayrán Basin system	47
Figure 3.4	Panorama view to the Mayrán Formation overlying onto the angular unconformity	49
Figure 3.5	Paleocurrent measurements of channelized and nonchannelized	50

	conglomerates	
Figure 3.6	Simplified N-S cross section across the Mayrán Basin system and representative logs of subbasins	52
Figure 3.7	Examples of clastic and carbonate facies in the Mayrán Formation	54
Figure 3.8	Laterally continuous horizontally bedded limestones	56
Figure 3.9	Digital elevation model draped with aerial photographs	58
Figure 3.10	Photopanorama and (B) interpretation of the subbasins II, III, and IV	61
Figure 3.11	N-S transect across the boundary between subbasins II and III	62
Figure 3.12	Model of the Mayrán Basin system	63
Figure 4.1	The Mayrán Basin system indicating locations of prograding tufa lobes.	73
Figure 4.2	Large scale prograding tufa clinoform lobes in the Mayrán Basin system.	75
Figure 4.3	Field exposure of the large scale prograding tufa clinoform lobes	78
Figure 4.4	Detail of prograding tufa clinoforms in tufa lobe IIA	79
Figure 4.5	Idealized stratigraphic log of prograding tufa lobe	80
Figure 4.6	Stalbe isotope plot of calcite cements in tufa lobes	80
Figure 4.7	Idealized model for large scale prograding tufa clinoforms formation	83
Figure 5.1	Simplified map with location and distribution of the Mayrán Formation	91
Figure 5.2	Stratigraphic logs of the Mayrán Formation	97
Figure 5.3	Ostracod mudstone-wackestone	99
Figure 5.4	Isotope plot of micrite and calcite spar of the lacustrine carbonates in the sub-basins	102
Figure 5.5	Plot of Total organic carbon (TOC) and organic carbon stable isotopes values of the lacustrine carbonates	102
Figure 5.6	Clotted boundstone	105
Figure 5.7	Gastropod mudstone-packstone	107
Figure 5.8	Oncoid wackestone-packstone	110
Figure 5.9	Stromatolites	113
Figure 5.10	Charophyte wackestone-pakestone	115
Figure 5.11	Macrophyte Boundstone	117
Figure 5.12	Marlstone and Crystalline carbonate	120

Figure 5.13	Sulphates and Halite	123
Figure 5.14	Schematic lateral distribution of microfacies types	124
Figure 5.15	Idealized paleoenvironmental reconstruction of Mayrán lakes	130
Figure 6.1	Map of the Mayrán Basin system, and U-Pb samples location	137
Figure 6.2	Generalized stratigraphic section of the study area	139
Figure 6.3	Stromatolite and calcite botryoids from the Mayrán Formation	141
Figure 6.4	Laser ablation on samples N18B-3 and N26-1	144
Figure 6.5	Terra-Wasserburg Concordia plots showing results of LA-ICP-MS screening analyses	149
Figure 6.6	Composite Terra-Wasserburg Concordia diagram for sample N18B-3	150
Figure 6.7	Pliocene Mayrán Formation overlying on angular unconformity onto Cretaceous bedrock and recent deposits	151
Figure 6.8	Present day model of the Mayrán Basin system	152
Figure 7.1	Model of the Mayrán Basin system	158
Figure 7.2	Idealized model for large scale prograding tufa clinofolds formation	160
Figure 7.3	Idealized paleoenvironmental reconstruction of the carbonate lakes	163
Figure 7.4	Present day model of the Mayrán Basin system	165

### ***List of tables***

Table 4.1	Dimensions of major prograding tufa clinofold bodies	76
Table 5.1	Summary of lithofacies types in the Mayrán Formation	96
Table 5.2	Stable oxygen and carbon isotopes from lacustrine limestones	100
Table 5.3	Total organic carbon and organic carbon isotopes from lacustrine limestones	101
Table 6.1	Summary of LA-ICP-MS U-Pb results screening of Mayrán carbonate	146
Table 6.2	U-Th-Pb isotopic data for sample N18B-3	148

### ***List of appendices***

Appendix 1	Total Organic Carbon laboratory results chart	188
Appendix 2	Paragenetic sequence inferred for the Mayrán carbonate	190
Appendix 3	Basin scale log location map	191
Appendix 4	Figure key and abbreviations	192
Appendix 5-17	Additional stratigraphic logs from the Mayrán Formation	193

Total Number of Words: 48,006

## Abstract

Lake basins contain depositional systems whose stratigraphy and sedimentology are highly influenced by allogenic and authigenic processes. Identifying the relative roles of these controls is complicated in settings where both tectonic and climate influences control sediment inputs and accommodation availability. In order to identify how these controls may interact in carbonate lake basins the lacustrine Mayrán Formation, northeast México was investigated. The Mayrán Formation is well exposed and the strata geometries are well preserved. The necessary data needed to unravel these complexities was obtained using field based techniques (geological and structural mapping, sedimentary logging and sampling), combined with optical and electron optical microscopy, mineralogical (XRD), and geochemical (oxygen and carbon stable isotopes, total organic carbon [TOC], organic carbon isotopes, and U-Pb carbonate dating) techniques, to characterise the lake basins.

These data reveal that the Mayrán Formation was deposited in four, northerly, down-stepping, broadly coeval, hydrologically linked, carbonate-dominated lake subbasins (the Mayrán Basin system), that formed at different elevations spanning ~500 m. Subbasin geomorphology was controlled by the inherited topography of the exhumed and eroded Parras foreland fold-and-thrust belt, as a result, the subbasins are compartmentalized by prominent sandstone ridges that form sills between subbasins. Sedimentary infill of the subbasins consists of a fluvio-lacustrine succession (carbonate and clastic) that overly an angular unconformity truncating the folded and faulted Cretaceous bedrock. Clastic sediments were preferentially trapped in the most proximal subbasin in the south, adjacent to the mountain front. In more distal settings to the north, carbonate production resulted in deposition of horizontally bedded lacustrine limestones with subordinated siliciclastics and evaporite minerals.

Carbonate deposition occurred during overfilled to balance filled conditions. Prominent aggradational to progradational tufa clinoforms form at the spillover points between the subbasins, and interfinger up- and down-dip with the horizontally bedded lacustrine limestones. The tufas consist of steeply dipping clinoforms that prograde northwards. They formed by inorganic and biogenically mediated calcite precipitation as waters from the topographically upper lake overflowed the sill. U-Pb dating of speleothem cements formed in the tufas yield a Pliocene age ( $3.06 \pm 0.2$  Ma). The horizontally bedded limestones that predominantly fill the subbasins are composed of nine lithofacies. These are: ostracode mudstone-wackestone, clotted boundstone, gastropod wackestone-packstone, oncoid wackestone-packstone, stromatolite, charophyte wackestone-packstone, marlstones, crystalline carbonate and evaporite minerals. These lithofacies contain variable proportions of production-derived components, with subordinated detrital and diagenetic components. They overall contain inorganic and organic calcite (average 91%), organic matter (average 12.6 % TOC) and subordinated detrital quartz, feldspar and clay. Stable isotope conditions from stromatolite laminations ( $\delta^{13}\text{C}$  -6.3‰ and  $\delta^{18}\text{O}$  -8.0‰), and micritic matrix from samples in all the subbasins ( $\delta^{13}\text{C}$  -5.7‰ and  $\delta^{18}\text{O}$  -8.4 ‰), indicate that overall calcite deposition occurred in freshwater lakes, under predominantly oxic conditions. Carbonate particles deposited mainly by *in situ* disaggregation and by settling. Significant preservation of the organic matter likely occurred because of the fine grained carbonate matrix, and because of moderate rates of both carbonate sediment and organic matter production. Stacking patterns in the lake successions show an overall shallowing upward cyclicality. It is considered, that the effects of inherited basin geomorphology and climate, ultimately controlled facies variability and strata geometries in these subbasins.



## **Declaration**

The author declares that no portion of the work referred to in the thesis has been submitted in support of an application for another degree or qualification of this or any other university or other institute of learning.

Natalia Amezcua Torres

## **Copyright statement**

- i. The author of this thesis (including any appendices and/or schedules to this thesis) owns any copyright in it (the “Copyright”) and he has given The University of Manchester the right to use such Copyright for any administrative, promotional, educational and/or teaching purposes.
- ii. Copies of this thesis, either in full or in extracts, may be made only in accordance with the regulations of the John Rylands University Library of Manchester. Details of these regulations may be obtained from the Librarian. This page must form part of any such copies made.
- iii. The ownership of any patents, designs, trade marks and any and all other intellectual property rights except for the Copyright (the “Intellectual Property Rights”) and any reproductions of copyright works, for example graphs and tables (“Reproductions”), which may be described in this thesis, may not be owned by the author and may be owned by third parties. Such Intellectual Property Rights and Reproductions cannot and must not be made available for use without the prior written permission of the owner(s) of the relevant Intellectual Property Rights and/or Reproductions.
- iv. Further information on the conditions under which disclosure, publication and exploitation of this thesis, the Copyright and any Intellectual Property Rights and/or Reproductions described in it may take place is in the University IP Policy (see <http://documents.manchester.ac.uk/DocuInfo.aspx?DocID=487>), in any relevant Thesis restriction declarations deposited in the University Library, The University Library’s regulations(see <http://www.manchester.ac.uk/library/aboutus/regulations>) and in The University’s policy on Presentation of Theses.

## **Acknowledgments**

I would like to take this opportunity to thank all the people who helped, encourage and support me through the completion of this Ph.D. Project.

Special thanks to my supervisors Rob Gawthorpe, Joe MacQuaker and Simon Brocklehurst, for their support, guidance and encouragement over the course of this project.

I would like to acknowledge the financial support of the National Council of Science and Technology (CONACYT), and the Mexican Geological Survey (SGM).

I am very grateful to Roxana, Graham, Ingrid, Leonardo, Ana and Cath for their support, and to Cathy Hollis and Martin Pedley for they constructive feedback.

Finally, without the unconditional support of my husband, Samuel and our son Edgar, I would never have been able to complete this thesis.

**SECTION ONE:**  
**INTRODUCTION AND BACKGROUND**

## Chapter 1. Introduction

### 1.1. Rationale

Lake deposits can provide high resolution paleoclimate records and may also contain resources of economic interest. In order to exploit the information preserved within the lacustrine record and the resources they host, it is necessary to understand the key controls on their facies variability and architecture. The fill of lake basins is controlled by a complex interaction of forcing mechanisms including, regional climate, basin hydrology, basin geology, geomorphology and tectonics (Glen and Kelts, 1991; Sarg, 2001; Bohacs et al., 2003). These forcing mechanisms ultimately control: i) accommodation, ii) lake level variations, iii) type of sediment yield iv) water chemical composition; v) and lithofacies variability (Eugster and Hardie, 1975; Talbot and Livingstone, 1989; Smoot and Lowenstein, 1991, Bohacs et al., 2000a, Carroll and Bohacs, 1999 and 2001, Gierlowski-Kordesch 2010).

Understanding the responses of lakes to the variable controlling factors is complex, and generally difficult to interpret (Bohacs, et al., 2003). However, carbonate lakes are particularly suitable for study of the relative controls on basin fill because: i) they are susceptible to the volume and type of sediment yield into the lake, ii) they develop where the inputs of siliciclastic detritus are either episodic or restricted, iii), and because carbonate precipitation in these settings is largely dependent upon how much detrital carbonate enters the lake, and how much dissolved carbonate is present in the inflow waters (Cohen, 2003; Gierlowski-Kordesch et al., 1988, Gierlowski-Kordesch, 2010). The Mayrán Basin system is a natural laboratory for the study of lacustrine carbonate basins. This is because it comprises four individual, coeval, hydrologically linked, carbonate-dominated lake basins; each containing varying proportions of clastic sediment. Moreover the succession is well preserved in excellent exposures, where lateral and vertical facies variability and strata geometries can be recognized.

Questions arising from this carbonate dominated system are:

- Why are carbonate-dominated successions deposited in a series of individual lake basins with siliclastic bedrock?
- What is the origin of the large volumes of carbonate sediments that infill the basins?

- What type of facies occur in such a sedimentary system?
- What are their spatio-temporal variations, and what controls them?
- When did the fill occur?

## 1.2. Aim and objectives

The principal aim of this thesis is to investigate the controls on the stratigraphy and sedimentology in carbonate lake basins.

In order to achieve this aim the following research objectives have been identified. Objectives 1 and 2 form the basis of a paper (Chapter 3) that investigates the basin scale controls on carbonate lake basin formation and basin scale facies variability. Objective 3 forms the basis of a paper (Chapter 4) that analyses the development of prominent tufas that are key features in interpreting basin hydrology, and creates a link that relates to the rest of the aims. Objectives 4 to 7 form the basis for a paper (Chapter 5), that investigates the complex processes that control lithofacies variability in carbonate-dominated lake basins, it considers information described in previous chapters. Objective 8 forms the basis of a paper (Chapter 6) that explores the application of U-Pb dating a novel technique in continental carbonates.

These objectives effectively form the theme of Chapters Three to Six and are each the basis of a paper:

1. To investigate the relative roles of inherited structural geometry, bedrock lithology, sediment production, and basin hydrology as key controls on fluvio-lacustrine facies in the Mayrán Formation, in the Mayrán Basin system.
2. To identify how basin scale inputs of clastic detritus are partitioned in adjoining sedimentary basins with a localized clastic sediment source.
3. To document and determine the origin of a series of large scale prograding tufa clinofolds that occur exposed in the Mayrán Basin system, analysing their location, geometry, stratigraphy, and sedimentology.

4. To analyse the rocks in the field and laboratory and integrate these observations to determine the main facies, the various components within the facies and the location and interrelationships between facies.
5. To analyse the roles of detrital input, autochthonous sediment production, organic matter production and early diagenetic processes operating during the fill of the Mayrán lake subbasins.
6. To document and determine the origin of a series of large scale prograding tufa clinoforms that are exposed in the Mayrán Basin system, analyzing their location, geometry, stratigraphy, and sedimentology.
7. To investigate how primary production, variable inputs of clastic detritus and diagenesis (linked to basin hydrology, and geomorphology, and climate) overall controlled basin scale carbonate lithofacies variability in a series of linked lacustrine subbasins.
8. To assess the suitability of Mayrán carbonates for isotope dilution analyses, and provide accurate U-Pb data to constrained an age for the Mayrán Formation.

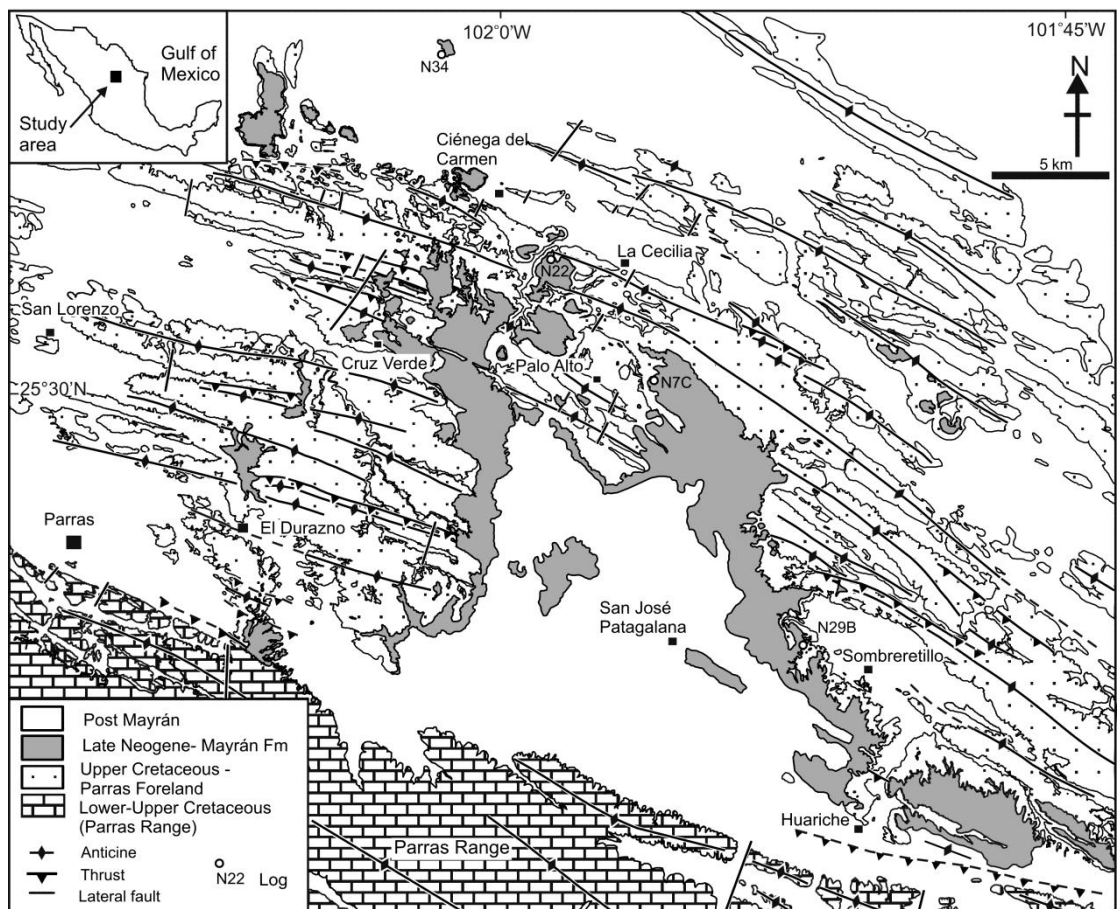
### 1.3. Study area

Controls on lacustrine basin fill are highly variable and are reflected in the complex sedimentology and stratigraphy of their sedimentary successions. This complexity arises because lacustrine lithofacies are controlled by the interplay of authigenic, or intrabasinal processes such as hydrologic balance, biodiversity, pre-existing topography and basin morphology; and by allogenic processes such as tectonics and climate (Glenn and Kelts, 1991).

Identifying ancient basins where these parameters can be separated from one another is commonly difficult, as the rocks are not always well-exposed and the products of these processes are typically intimately mixed. Well-exposed lake basins composed of linked sub-basins, in which different sediment supply processes dominated, offer unique

opportunities to study the relative influence of allogenic and authigenic processes responsible for the fill.

This study focused on the Mayrán Formation, deposited in a series of adjoining subbasins here named the Mayrán Basin system in northeast México (Fig. 1.1). The study area offers an excellent opportunity to study the sedimentological processes responsible for lacustrine basin fill because exceptional exposures exist in the area, due to the semi-arid climate and lack of vegetation, in addition the Mayrán Formation carbonates have been quarried, and are accessible by roads. Crucially in this lake system, the clastic sediment being supplied to the basin was mainly restricted to one geographic source and its dispersal was limited by the presence of physical barriers between the basins, yet the hydrology of all the basins was closely linked. In this setting detailed facies analyses, in the context of basin scale sedimentological variability; means that the controls on basin-scale variability can be identified and distinguished.



**Figure 1.1** The Mayrán Basin System northeast México.



## 1.4. Research Methods

In order to meet the aims and objectives of this study and specifically meet the requirement for integrating multi-scale observations to the varying methods where adopted.

### 1.4.1 Field methods

Three field work seasons of one month (2007), two months (2008), and two weeks (2009), were carried out in Parras de la Fuente, Northeast Mexico. Five structural sections, south to north documented, were measured from south to north in the Basin System, in order to constraint the structure of the basin, geometry, and the controls on the distribution of the Mayrán subbasins. Detailed outcrop descriptions included: photophanoramic images taken, drawing of outcrop sketches describing outcrop-scale strata geometries descriptions, stratigraphic logs measurements (at the scale of 1:10), clastic imbrication measurements, and collection of suitable rock samples, , were performed in carefully selected sites, after basin wide recognisance, in order to constraint basin scale lateral and vertical facies variability, stratal geometry and overall large scale stratigraphic relations. Geological field data and satellite imagery (Spot, Aster, QuickBird), were processed with the Geographic Information System ArcMap 9.3<sup>®</sup>. Construction of a digital elevation model of the basin was also performed using this software. Only one structural section is presented in the thesis (Chapter 1), and it was constructed based on the *Kink method*. The geological cross-section was constructed using the Kink Method (see Suppe, 1983, 1985, for further detail). This method assumes that: 1) folds are parallel, have straight limbs and may have angular hinges, and 2) any given stratum measured perpendicular to bedding is locally uniform (Suppe, 1985).

The cross-section shows the deformation oriented perpendicular to trend of the structures (South to North), and composes of 4 discontinuous but parallel segments, due to accessibility in the field area. The geologic contacts (rock types), bedding dips, major fold limbs, and fault locations that were observed in the field were measured and added to the topographic profile. Axial surfaces that bisect fold limbs were positioned, and axial surfaces projected to depth were merged to form new axial surfaces that also bisect fold limbs. Intersection of two axial surfaces will form a new axial surface. Folds were interpreted where changes in dip and stratigraphy occurred, and thrust faults where either abrupt changes in the stratigraphic succession were identified. Once constructed, the cross section was digitized using CorelDraw4<sup>®</sup>, where the fold inflection points were smoothed.

The clast imbrication data were plotted using the StereoNett software and subsequently exported to Corel Draw 4<sup>©</sup> software for final edition of plots in figures

## 1.4.2 Laboratory

### 1.4.2.1 Petrographic techniques

Petrographical techniques were used to characterize the rock textures, the biological production, clastic and detrital derived components in thin-sections from the Mayrán Formation. Thin section preparation and petrographical analyses were performed at the Williamson Research Centre for Molecular Environmental Science, at Manchester University. The individual petrographic techniques and operating conditions of the equipment are outlined in the following sections.

#### *Thin section preparation and scanning*

Polished thin sections typically 20-30  $\mu\text{m}$  thick were made from each sample in either large (50mm by 70 mm) or small (26 mm by 48 mm), format glass slide. To minimize sample damage during preparation, an oil (Castrol Ilocut 430) media was used (Adams et al., 2006). Thin sections were scanned at medium resolution in an Epson Perfection 1250 Photo Flatbed scanner to obtained larger field view of the textures in the thin section.

#### *Optical Microscope*

Textural and mineralogical information in thin sections was analysed under both plane-polarized light (PPL), and cross-polarised light (XPL) on 195 thin-sections. This was achieved using a Nikon Optiphot 2.0-POL microscope, equipped with a Progress C10 Plus Digital Camera. Photomicrographs duplicates in XPL and PPL, were taken at different magnifications (X2, X4, X10 and X20), using the software Progress Capture Pro. 2.

#### *Scanning Electron Microscope*

Prior to SEM examination, thin sections were carbon coated to increase their electronic conductivity, and to prevent charging. The SEM examination was carried out on a JEOL 6400 scanning electron microscope equipped with a Link four-quadrant backscattered electron detector, and Princeton Gamma-Tech, energy- dispersive spectrometer. The SEM was operated at a working distance of 15 mm, at 20kV and 1.5 nA. SEM and Backscattered electron images (X20 to X2500 magnifications) were recorded digitally using the Semafore software. Mineralogical composition was determined based on their

backscattered coefficients ( $\eta$ ), and by elemental results yield by the dispersive spectrometer. The backscattered coefficient ( $\eta$ ) is in function of the electron density and is a value that describes the efficiency of a solid to a backscattered beam of incident electrons (Lewis and McConchie 1994).

#### *Cold Cathodoluminescence Microscopy*

Cathodoluminescence (CL) of 24 samples was achieved using a CITL, (model CCL8200 MkIII) cold cathode luminoscope, with operating conditions of 10-120 kV accelerating voltage, gun current of 250-300  $\mu$ A and 0.2 Torr vacuum, in order To assess the characterization of carbonate types (e.g. Dickson, 1966).

The photographs obtained from the different petrographic techniques were annotated and scaled using Corel Draw 4 and 5 and Adobe Photoshop CS2.

### **1.4.2.2 Geochemical Techniques**

#### *XRD Analyses*

Whole-rock mineralogy (of 122 samples) was carried out (to identify and confirm initial petrographic characterization) in the X-Ray Laboratory at the University of Manchester. A total of 22 samples were analysed using a Philips PW1730 X-ray diffractometer at 20 mA, utilising a copper K( $\alpha$ ) radiation with a step size and time constant of 0.01° and 2.00 s. Additionally, 100 samples were analyzed using a Bruker D8 Advance diffractometer set at 40 KV and 40mA. Sample was prepared by mixing approximately 0.2 g of the powdered sample with a few drops of amyl acetate, smeared and then left to air dry on a small glass slide. Analysis was performed using Eva 14 to match the data to standards from the ICDD (International Centre for Diffraction Data) database. The data output is .raw/.eva files, for the raw data/processed data on the Bruker and .rd files from the Philips. A custom written (by Brian Smith) DOS program to convert the .rds to .raw files for analysis on the Bruker was used, and a File Exchange program to change the .raw files to .uxd, in order to be read by excel. The alignment of the Bruker diffractometer was checked regularly using a quartz standard and the data is repeatable to 0.004 degrees accuracy. For the Philips, Si was regularly used as an internal standard, or sometimes Si was run alone to check alignment.

### *Total Organic Carbon*

Thirty samples from three stratigraphic sections in subbasin II were also selected to perform TOC and  $\delta^{13}\text{C}_{\text{organic}}$  analyses to know the proportions of organic matter and potential producers. The samples were prepared by decarbonating whole rock powder with 1N HCl, rinsed in distilled water and dried for 24 hours at 50°C, and analyzed with a Carlo Erba NA1500 Series II Elemental Analyzer, coupled to a ThermoElectronDeltaVPlus Mass Spectrometer, at the Stable Isotope Laboratory of Memorial University of Newfoundland, Canada.

### *Stable isotopes*

Fifty three  $\delta^{18}\text{O}$  and  $\delta^{13}\text{C}$  stable isotope analyses were performed on two specific carbonate components present in samples from subbasin I to IV to constrain the origins of these components. The two components were: i) micrite present in matrix, coated grains, and other microbial laminations, and ii) calcite spar cement occluding pore space in both matrix and allochems. About 2 to 5 mg of these components were obtained by microdrilling selected areas of polished slabs, under petrographic microscope observation. The measurement of carbon and oxygen isotope ratios was analyzed on an automated VG SIRA 12 mass spectrometer at the University of Liverpool. Carbon and oxygen isotope data are reported in conventional delta ( $\delta$ ) notation in “parts per mil” (‰) relative to V-PDB (Pee Dee Belemnite Standard). Accuracy and reproducibility of the isotopic analyses was assessed by replicate analysis of BCS2 (internal calcite standard) against NBS-19 and two internal calcite standards.

### *U-Pb Dating*

U-Pb dating applied to carbonates require a combination of petrographic screening and micro-sampling for isotopic analyses. In order to effectively tackle this suite of samples we employed a two-stage U-Pb analytical program: (1) in-situ analyses using laser ablation inductively coupled plasma multiple collector mass spectrometer (LA-ICP-MC-MS) to rapidly assess U and Pb concentrations, U/Pb ratios and their variation related to the petrography, followed by (2) isotope dilution (ID) isotope ratio mass spectrometry on select samples for which the LA-ICP-MS results indicated potential for geochronologically useful data.

For the in-situ screening stage, samples were analysed by LA-ICP-MC-MS at National Environmental Research Council (NERC) Isotope Geoscience Laboratory

(NIGL), British Geological Survey in Keyworth, UK. Samples were ablated using a New Wave Research UP193FX (193 nm) excimer laser ablation system coupled to a Nu HR MC-ICP-MS. The laser sampling protocol employed ablation with a spot size of 100 $\mu$ m, a dwell time of 15 seconds, and a fluence at 10Hz at  $\sim$ 6.7J/cm<sup>2</sup>. NIST 614 glass was used as an ablation standard monitor for approximate quantification, with the Mayran Formation carbonate samples normalized to NIST 614 according to the deviation of the measured average session values using the concentrations and isotopic composition measured for NIST 614 relative to the expected ratios for NIST 614 (Woodhead et al., 2008).

For isotope dilution analyses, U was measured by MC-ICP-MS in wet plasma mode with static detection using a multiple collector Faraday cup array whereas Pb was measured using a Thermo Triton TIMS instrument fitted with an axial secondary electron multiplier (SEM) allowing the small Pb signal to be detected in dynamic single-collector mode on the SEM. Pb and U standards SRM 981 (TIMS) and U500 (MC-ICP-MS) were analysed to monitor mass spectrometer performance. For details of mass spectrometry and column chemistry see Slama et al (2008). Moles of Pb and U, and the U/Pb ratio were determined using a mixed <sup>205</sup>Pb-(<sup>230</sup>Th)-<sup>233</sup>U-<sup>235</sup>U double spike with a U/Pb ratio of  $\sim$ 110 which was calibrated against a metals derived (NBS 982 Pb and CRM 112a natural U) gravimetric shelf solution with the error in the U/Pb ratio estimated to be  $\sim$ 0.1%. Data reduction, error propagation and plotting were carried out using customized data reduction spreadsheets based on Schmitz and Schoene U-Pb ID-TIMS data reduction Excel workbook and Isoplot version 3.00. The decay constants used were those proposed by Jaffey et al. (1971).

#### *Nomenclature of Mayran Carbonates*

In carbonate depositional environments, hydrodynamic, biogenic and diagenetic processes determine rock fabric and texture (Dunham, 1962; Tucker and Wright, 1990). Continental carbonates are characterized by containing particles derived from a wide variety of origins (both from within the basin and derived from inputs to the basin) and exhibit a wide range of microfabrics. For practical purposes, the classification scheme of Dunham (1962) is used here to describe the carbonate lithofacies texture, whereas the terminology for crystal textures and fabrics is based on the classification scheme defined by Friedman (1965).

## 1.5 Thesis structure

The structure of this PhD Thesis follows the alternative format style where Chapters 3 to 6, are in a format suitable for submission to further publication in peer-reviews journals. Additional chapters are written in standard format thesis. In order to achieve the research objectives set out in Section 1.2, the thesis is organized into seven chapters. The first two chapters provide an overall introduction to the study and provide geological context to the study. Chapters three to specifically address each of the objectives mentioned above and chapter 7 summarises the conclusions overall. Since each publication style chapter forms a self-contained contribution, some overlap and repetition of the background information, methodologies, and references is inevitable.

Chapter 3. *Cascading carbonate lakes of the Mayrán Basin System, Northeast México: The interplay of inherited structural geometry, bedrock lithology and climate.* This chapter provides the first description of the Mayrán Basin system. In it, the geologic and structural framework of the basin are summarized and the data are used to address the geomorphological and sedimentological controls on the fill of each of the lacustrine sub-basins. This study includes geological-structural mapping of the Mayrán Basin system, stratigraphic sections, lithologic descriptions of the sedimentary facies that filled the subbasins, and interpretation of the spillover points linking the sub-basins. It includes a basin model to illustrate the interrelationships between sedimentary sub-environments within the basin system. The compartmentalization of a lake basin into a series of sub-basins with different elevation linked by spillover points is relatively rare in post-tectonic (or pre-tectonic) phases of basin evolution. The observations made here on the cascading lakes of the Mayrán Basin System may therefore be applicable to syn-tectonic lake basins where compartmentalization by active structures can readily lead to sub-basin formation, each with its own base level.

Chapter 4. *Prograding tufa clinof orm bodies in cascading lake basins.* Prograding tufa clinof orms commonly have low preservation potential in the rock record, and ancient large-scale features like those encountered here are therefore rare. In this chapter where, why and how these particularly tufa clinof orms formed is documented. This study includes detailed sedimentological and stratigraphical

analyses of the tufa deposits forming the tufa “deltas”, and utilizes satellite imagery (Landsat and Quick Bird) integrated to a Digital Elevation Model (DEM) to illustrate their role in the evolution of the Mayrán Basin system.

Chapter 5. *Lacustrine carbonate lithofacies in the Late Neogene Mayrán Formation, Northeast Mexico.* This chapter focuses on the detailed sedimentological and stratigraphic analysis of the carbonate lithofacies that comprise the lacustrine deposits of the Mayrán Formation. It explains the main mechanisms involved in sediment production, supply and diagenesis that overprint each lithofacies present. Using these data, the spatio-temporal facies variability of the lacustrine deposits are described, and a depositional model is proposed. The new data provided here illustrate the complexity and variability of facies deposited in carbonate-dominated lacustrine subbasins with a common hydrology yet very different inputs.

Chapter 6. *U-Pb dating of carbonates in the Mayrán Formation, Northeast México.* This chapter focuses on the age determination of the carbonates that comprise the Mayrán Basin system lakes. This chapter applies a novel U-Pb isotopic technique to date these relatively young carbonate deposits. The new data provided by the U-Pb dating of Mayrán carbonates are used to constrain: i) the age, with implications to the Neogene geological evolution of Northeast México, and ii) provide insight into the climatic controls on large lacustrine and fluvial systems formed in northeast México and southeast USA during the Neogene.

Chapter 7. *Synthesis ad future research directions* provide a synthesis and discussion of the study where the research major findings are summarized. This chapter reviews how each of the aims of this thesis have been fulfilled and discusses uses and limitations of the research. The chapter then discuss of several ideas for further research.

**1.6 Publication Status and Notes**

Chapter 3. Published in: The Geological Society of America Bulletin. Its topics cover the entire range of the earth sciences, and it is #10 ranked "geosciences, multidisciplinary" peer-reviewed journal. As lead author I was responsible for the fieldwork, and both data collection and integration. Co-authors MacQuaker and Gawthorpe provided supervision throughout the course of the work and manuscript revision.

Chapter 4. Is being prepared for submission to: *Geology* (Geological Society of America). As a lead author I was responsible for the fieldwork, data collection, and integration of data. Co-authors MacQuaker and Gawthorpe provided supervision throughout the course of the work and manuscript revision.

Chapter 5. Is being prepared for submission to either the: *Journal of Sedimentary Research* or *Sedimentology*. The complete manuscript is in revision by co-authors, and will be submitted to any of the mentioned international peer review journals. As a lead author I was responsible for the fieldwork, samples collection, analytical work (petrographic and geochemical methods), and interpretation of the results. Co-authors MacQuaker, Gawthorpe and Marshall provided supervision throughout the course of the work and manuscript revision.

Chapter 6. Is being prepared for submission to: *Palaeogeography, Palaeoclimatology, Paleoecology*. As a lead author I was responsible for the fieldwork, samples collection, detailed petrographic analysis focused on sample selection, sample preparation, dating analysis, and interpretation of the results. Co-author Condon supervised the dating analytical work and did data processing and revision of manuscript. Gawthorpe and MacQuaker provided supervision throughout the course of the work and manuscript revision.



## **Chapter 2**

## Chapter 2. Background literature

### 2.1 Introduction

In order to understand the Mayrán Basin system development and the lateral and vertical facies variability present in lacustrine carbonate successions, an overview of lakes, lacustrine basins and controls on sedimentary fill are introduced, together with a summary of the general depositional environments in carbonate lakes. Some chemical considerations are also introduced. An overview of some chemical considerations on carbonate precipitation, are illustrated and the geology of the Mayrán Formation is reviewed.

### 2.2 General aspects on lakes

Lakes are inland bodies of standing water that occupy depressions on the earth crust. As such, lakes exhibit a wide range of possible settings, sizes, chemistries, and morphologies (Gierlowski-Kordesch and Kelts, 1994). This variability is expressed in their complex sedimentology and stratigraphy (Bohacs et al., 2003). Lake classification varies depending on whether geological, chemical, hydrological (Glenn and Kelts, 1991) considerations are taken into account. Considering the balance of water input versus evaporation, lakes may be hydrologically open or closed. Open lake systems with permanent outlets tend to have relatively stable shorelines, and a limited residence time for solutes (Bohacs et al., 2003). These lakes may also be linked to cascading chains. Closed lake systems, with no surficial outlet, have unstable shorelines and complex deposits in littoral zones, controlled by annual flooding, microbial mats, and receding waters with rapid salinity changes (Glenn and Kelts, 1991).

As inland water bodies, lakes may develop a density stratification which influences the deposition of fine-grained sediment (Cohen, 2003; Nichols, 2004). Lakes may be well mixed (poly- or oligo-mictic) to permanently stratified (meromictic); with low nutrient and productivity levels (oligotrophic) to high productivity and nutrient levels (eutrophic) (Cohen, 2003, Gierloski-Kordesch, 2010). Anoxic bottom waters may result from thermal or chemical stratification or from high rate of organic matter input. Seasonal variations affect water conditions such as temperature, pH, oxygen availability, water density, viscosity and visibility, and consequently the primary production (Cohen, 2003). The

wind-mixed surface water layer, the epilimnion, is separated from the deeper water mass, the hypolimnion, by the thermocline; the zone with highest thermal gradient in the metalimnion (Glenn and Kelts, 1991). Depending on ion concentrations, lakes can be fresh water or saline lakes. Fresh water lakes have low concentrations of salts and occur in areas of moderate to high water input, exceeding evaporation rates. Saline lakes have high concentration of dissolved ions (greater than 5gr1 of solutes; Eugster and Hardie, 1978). These lakes develop in arid or semiarid regions where evaporation equals or exceeds water input, concentrating the salts with time (Eugster and Hardie, 1978, Nichols, 2004). The bedrock geology of underlying and catchment areas influences lake sedimentology and chemistry (Dean et al.1983; Platt and Wright, 1991).

Biological diversity in lakes is strongly correlated with habitat area (Cohen, 2003), and its influence on lake sedimentation is even more important than it is in marine carbonate environments (Tucker and Wright, 1990). Some small aquatic algae such as Charophytes (e.g. *Nitella* and *Chara*) are important contributors of calcareous sediment as they have calcify reproductive structures (gyrogonites) or develop stem encrustations (Dean, 1981, Burne et al., 1980). Microbial communities such as cyanobacterial mats, biofilms, some forming mounds are common in littoral and sublittoral areas in lakes (Cohen, 2003). In hardwater to moderate alkaline lakes these microbial communities may precipitate calcite forming microbialites (stromatolites), which are common features in lake fossil record (Arp et al., 1999; Golubic et al., 2000, Gierlowski-Kordesch, 2010). Macrophytes (vascular plants) inhabit the littoral zone of lakes, and based in their attachment to the substrate can be submerged, emerged, rooted-floating species and unattached or free floating (Wetzel, 2000). Ostracodes are one of the most important organisms in lakes, and provide a mainly benthonic microfossil that archives precise palaeoenvironmental information through their taxonomy, shell structure, trace element geochemistry and stable isotopes of carbon and oxygen (Delrome, 1989; Palacios-Fest et al., 1994). Lacustrine molluscs (gastropods and bivalves) are the most ubiquitous organisms in lake deposits (Cohen, 2003; Gierlowski-Kordesch, 2010). Gastropods include both aquatic forms (Basomatophora and Prosobranchia) and not specifically aquatic forms (Styolomatophora) adapted to subaereal conditions in the lake marginal areas (Ložek, 1986). Studies on fossils of paleolake deposits are important paleoenvironmental proxies because of the sensitivity of organisms to lake conditions.

### 2.3 Lake basins types and controls on sedimentary fill

Lake basins occur in many continental settings and lake basin forming processes can be classified according to different criteria. The initial classification of Davies (1882) included three main classes of lake basins: construction or orographic basins, destruction or erosion basins, and obstruction basins. Following Davis' criteria, Hutchinson (1957) recognized 76 types of lake basins within 11 major categories: glacial and periglacial, tectonic, fluvial, coastal, volcanic, eolic, solution, landslide damming, and artificial reservoirs. Overall, lake basins and lake basin sedimentary fill is largely controlled by tectonics, climate and inherited topography (Bohacs et al., 2003).

#### 2.3.1 *Sequence Stratigraphy applied to lacustrine deposits*

Sequence Stratigraphy is an evolving field of research now applied in the study of non-marine environments. Lacustrine basins provide an ideal setting for the application of sequence stratigraphic concepts (Talbot, 1994). However, due to the differences in their stratigraphic forcing mechanism it would be inappropriate to apply an unmodified marine sequence-stratigraphic model to lacustrine deposits (Bohacs et al 2000b). A sequence stratigraphic approach, looking at a hierarchical arrangement of rock packages bounded by various types of surfaces, can be used having in mind that the expression of the depositional sequences varies in function of each lake depositional system (Bohacs et al., 2000b). As a result, lacustrine sequence stratigraphic concepts and models are still developing (Keighley et al., 2003).

Lacustrine basins are subject to a variety of tectonic and climatic controls together with the influences of sediment supply and thus exhibit a diverse lithofacies both in vertical and lateral successions (Keighley et al., 2003). The understanding of sedimentological controls upon sequence development is very important for the application of sequence stratigraphic concepts in lake basins (Talbot, 1994).

As depositional systems, lakes present distinctive characteristics such as: high sensitivity to changes in accommodation space and climate; high variation in water chemistry and lake ecology over short stratigraphic intervals; direct relations between lake level and sediment supply; lake shorelines moves basinward either by progradation or withdrawal of water; and the lake system is directly controlled by relative rates of potential accommodation (tectonics / inherited topography) and supply of sediment + water (climate

and hydrology), within a time span (Bohacs et al., 2000a; Carroll and Bohacs, 1999; Carroll et al., 2006; Gierlowski-Kordesch and Kelts, 1994).

Changes in lake levels exert a fundamental control on lacustrine and fluvial systems that drain into the lake, affecting the stratigraphy (Shanley and McCabe, 1994). Lake levels also have an effect on the area of water exposed to the wind-generated waves, which controls the degree to which density stratification and/or mixing occur within the water column. Periods of fluvial incision or lacustrine aggradation near the lake shore may correspond with lake levels, decreasing their correlation basinwards (Shanley and McCabe, 1994). Regional climate and hydrology exert important effects on lake levels and sediment influx. Indicators of past lake levels include erosional truncation surfaces, bench berms, and lowstand progradational deltaic deposits. Unconformities in the form of erosional truncation surfaces may be indicators of areas and episodes of subaerial exposure within a sedimentary section (Scholz, 2001). Rising in relative lake level is often seen as onlap in all directions as the lake expands (Sladen, 1994).

In lacustrine sequence stratigraphy the sequence boundary concept has been applied under two different criteria. Milligan and Chan (1988) suggested that it should be either based on the established lake-level hydrograph rather than physical stratal surfaces. Alternatively, using the physical definition of sequence boundaries and strata surfaces (cf. Van Wagoner et al., 1990 in Keighley et al., 2003) when these surfaces fulfil the physical criteria (Milligan and Chan, 1998; Van Wagoner et al., 1990)

Based on sequence stratigraphic analysis in part of the Green River Formation, Keighley et al. (2003) made these interpretations: Sequence boundaries are marked by the base of the first channelized fluvial deposits or the top of the first well developed paleosol above lacustrine-dominated strata. Major flooding surfaces can be identified most clearly at the base of lacustrine dominated intervals where carbonate overlies fluvial sandstone or paleosol. Maximum flooding surfaces are identified where profundal oil shales cap some of the clastic parasequences. Flooding surfaces by definition (Van Wagoner et al. 1988) bound parasequences. The parasequences may display a coarsening upwards trends defined by the abundance of oncoids, ooids, or other fossil material toward the top. These carbonate parasequences are <2m thick. Successions assigned to the Lowstand System Tracts are capped by the first significant transgressive surface, and are characterized by amalgamated fluvial channels that finie upwards, with a shift to lenticular

sand bodies of higher sinuosity, maybe in response to a reduced fluvial gradient and early base-level rise. Transgressive Systems Tracts are bounded by the initial transgressive surface below and the maximum flooding surface above. Beneath the maximum flooding surface, the succession typically comprises a lacustrine dominated interval consisting of carbonate parasequences. The Highstand System Tract is bounded by the maximum flooding surface and the succeeding sequence boundaries. According to Fisher et al. (2007) during periods of lake highstand, channels of the fluvial systems may flow into the body of water forming a series of deltaic lobes (Fisher et al., 2007)

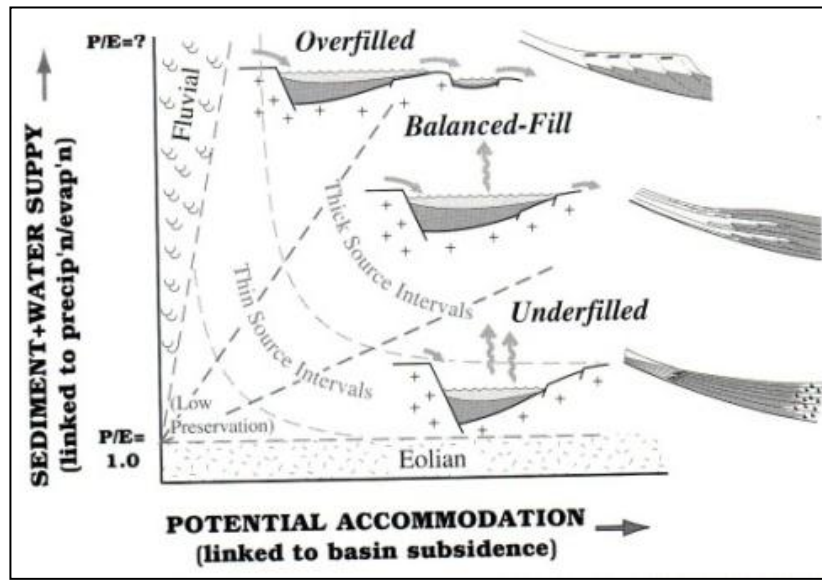
### 2.3.2 Sequence expression in lake basin types

According to Bohacs et al. (2000a) the relative balance of rates of potential accommodation change (mostly tectonically controlled) with the sediment + water supply (mostly climate) controls the occurrence, distribution, and character of lake strata at meso- and macro scales (one to tens of meters and hundreds of meters scale). Within a sequence stratigraphic framework and based on observations of lithofacies association, and fundamental controls on stacking patterns of lake strata of ancient and modern lacustrine systems, Bohacs et al. (2000a) recognized three types of lake basins: Overfilled, Balancefilled and Underfilled (Fig. 2.1 and 2.2)

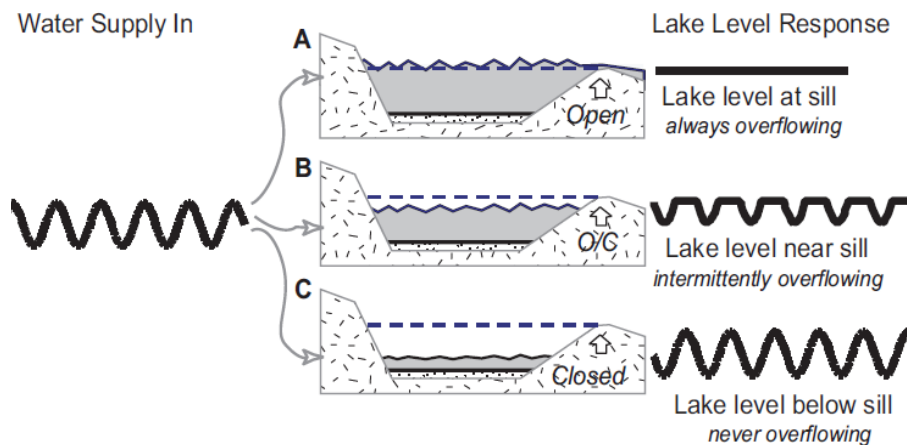
**Overfilled basins** are characterized by the rate of sediment / water supply exceeding potential accommodation (generally when precipitation/evaporation is relatively high or rate of tectonic subsidence is low). Fluvio-Lacustrine siliciclastic deposits that accumulate in hydrologically open lakes are the most common facies association, and parasequence development is driven mainly by shoreline progradation and delta channel avulsion.

**Balance filled lake** basins occur when the rates of sediment/water supply are in balance with potential accommodation. Carbonate and siliciclastic facies can accumulate in lakes that are alternatively hydrologically open or closed. Carbonates are generally abundant in these lakes. Successions record not only progradational parasequences but also aggradation of chemical sediments due to desiccation. Generally this type of lake basin accumulates a fluctuating profundal facies association.

**Underfilled lake basins** are characterized by rates of accommodation that exceed the rate of supply of sediment and water. In hydrologically closed lakes, deposition of evaporites dominates, and parasequences record vertical aggradation due to desiccation, which is the evaporative facies association. Changes in climate or tectonic subsidence influence the lacustrine system evolution and may change from one stage (type) to another (Bohacs et al., 2000a).


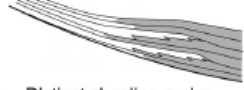
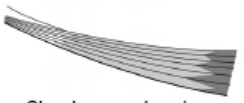


A



B

**Figure 2.1.-** (A) Schematic lake-basin type model as a function of both sediment + water supply, and potential accommodation (from Bohacs et al., 2000a after Carroll and Bohacs, 1999). (B) High of the sill relative to lake level changes (Bohacs et al., 2003).

Lacustrine facies association; lake basin type	Stratigraphy	Stratal stacking patterns	Sedimentary structures	Lithologies	Organic matter
Fluvial-lacustrine; overfilled lake basin	Maximum progradation:  <ul style="list-style-type: none"> <li>Parasequences related to lateral progradation</li> <li>Maximum fluvial input</li> </ul>	Dominantly progradation Indistinctly expressed parasequences	Physical transport: ripples, dunes, flat bed Root casts Burrows (in- and epifaunal)	Mudstone, marl Sandstone Coquina Coal, coaly shale	Freshwater biota Land-plant, charophytic and aquatic algal OM Low to moderate TOC Terrigenous and algal biomarkers
Fluctuating profundal; balanced-fill lake basin	Mixed progradation and desiccation:  <ul style="list-style-type: none"> <li>Distinct shoaling cycles common</li> <li>Fluvial input variable</li> </ul>	Mixed progradation and aggradation Distinctly expressed parasequences	Physical and biogenic: flat bed, current, wave, and wind ripples; stromatolites, pisolites, oncolites Mudcracks Burrows (epifaunal)	Marl, mudstone Siltstone, sandstone Carbonate grainstone, wackestone, micrite Kerogenite	Salinity tolerant biota Aquatic algal OM Minimal land plant Moderate to high TOC Algal biomarkers
Evaporative; underfilled lake basin	Maximum desiccation:  <ul style="list-style-type: none"> <li>Closely spaced packages of wet-dry lithologies</li> <li>Minimum fluvial input</li> </ul>	Dominantly aggradation Distinctly to indistinctly expressed parasequences	Physical, biogenic, and chemical: climbing current ripples, flat bed, stromatolites, displacive fabrics, cumulate textures	Mudstone, kerogenite Evaporite Siltstone, sandstone Grainstone, boundstone, flat-pebble conglomerate	Low-diversity, halophytic biota Algal-bacterial OM Low to high TOC Hypersaline biomarkers

*Note:* OM—organic matter; TOC—total organic carbon. Table adapted from Bohacs et al., 2000b.

**Figure 2.2** Representative attributes of the three major lacustrine facies associations. Taken from Bohacs et al., 2003.

## 2.4 Carbonate lake facies models

Carbonate accumulation in lakes is strongly dependent on the proportions of carbonates or calcium rich rocks exposed at the surface or subsurface (Gierlowski-Kordesch, 2010). Carbonate minerals are important components in lake deposits, in addition to clastic detritus, biogenic silica, sulphates, and organic matter; the relative proportions of these components can be an indicator of lake evolution, and basin geological characteristics (Dean and Fouch, 1983). The gradient of a lake influences sedimentation patterns (Gierlowski-Kordesch, 2010). Platt and Wright (1991) proposed a facies model for carbonate lakes, describing the type of basin margins and slope gradient based on the littoral, sublittoral, pelagial (profundal) settings:

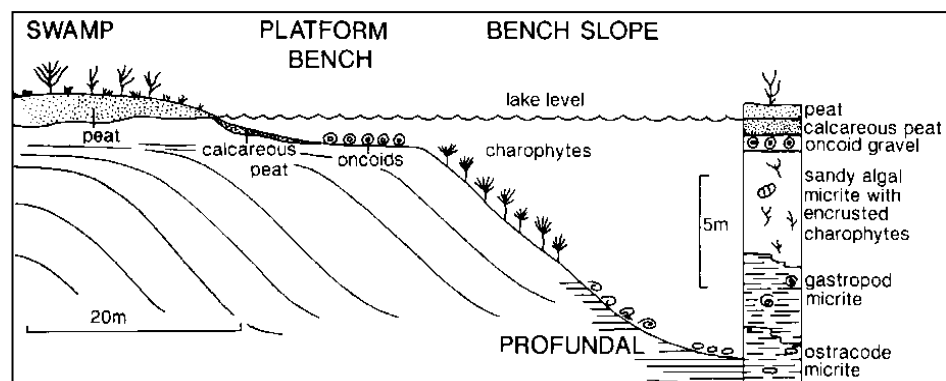


**Lake Margins** are areas of carbonate production which are controlled by photosynthesis mediated by biogenic or bioinduced processes in shallow waters (<10m) (Dean and Fouch, 1983). Shoreline areas are dominated by bioclasts, and microbial carbonate production in the form of cyanobacterial stromatolites and oncoids (Platt and Wright, 1991; Cohen and Thouin, 1987). In these shallow water areas, lime mud is also produced by disaggregation of carbonate encrustations on aquatic or submerged plants, and algae (Pedley, 1990; Platt and Wright, 1991). Charophyte algae may grow on low to moderate high energy substrates down to 15 to depth (Leithch, 1991). Stromatolite/tuffa bioherms commonly occur adjacent to slope breaks on prograding margins (Dean and Fouch, 1983). Littoral carbonates may change laterally into floodplain or fluvial clastic deposits, but also some evaporites or peat horizons can be deposited during low lake stands, although peat if present is rarely preserved due to oxidation. Subaerial exposure of lake marginal areas may induce pedogenetic processes (Platt, 1989).

**In pelagic lake** areas, carbonate sediment is mainly supplied from either bioclasts or by bio-induced processes. The input of organic matter, reworked material and fine siliciclastics is also common in deeper and open water areas. Although rates of carbonate precipitation are high, sediment rates are low, and in basinal areas sedimentation is controlled by lake dynamics (Platt and Wright, 1991). In shallow or polymictic lakes, oxygenated bottom waters results in bioturbation of bottom sediments, leading to their oxidation (Platt and Wright, 1991; Gierlowski-Kordesch, 2010).

**Low-energy bench margin:** The littoral zone is one of high productivity due to submerged plants, resulting in building-up of the shore and progradation into the lake (Fig. 2.3). They present a dipping bench slope. Resedimentation and downslope transport may also occur due by tubiditic currents. The sedimentary succession shows a coarsening upwards trend, from microcrystalline carbonate with biogens (profundal and sublittoral zones) to bioclastic sands and gravel dominated by oncoids and pisoids (littoral zone). Peat deposits border subaerial areas of the lake.

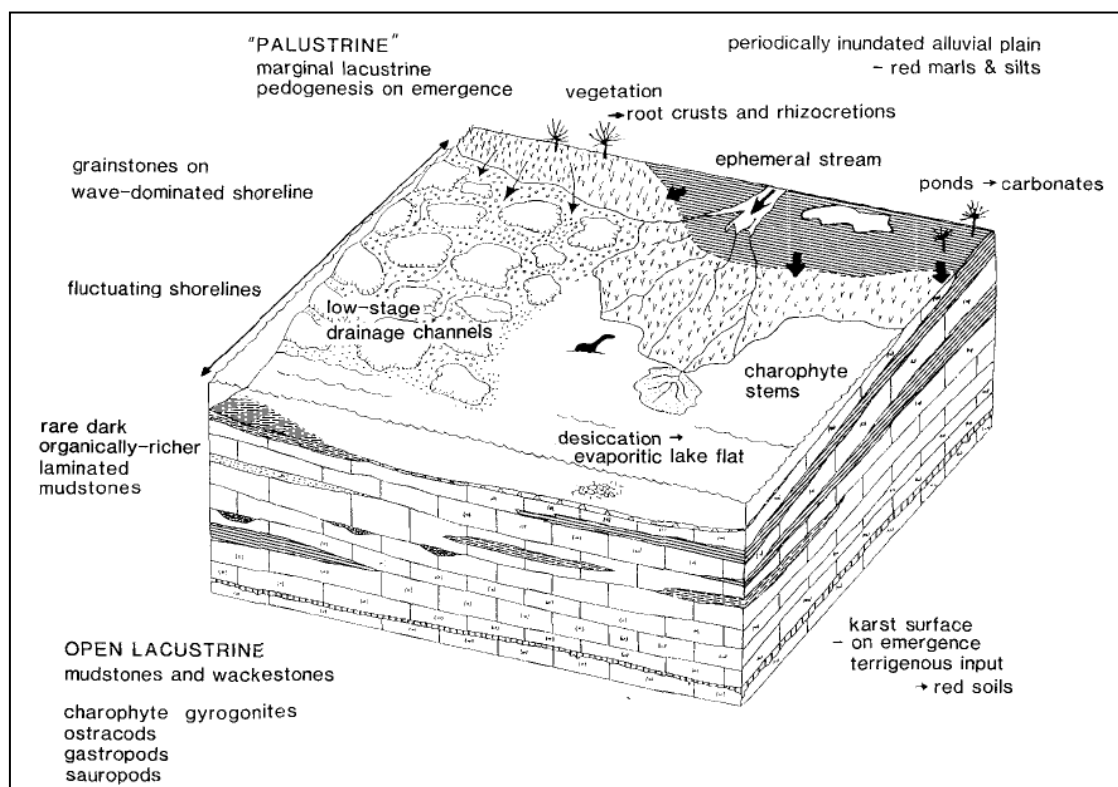
**High-energy wave dominated bench:** In this type of lake margin, wave effects produce facies asymmetry, and usually contain packstone and grainstone textures. In areas exposed to wave activity coarse-grained calcarenites, cross-bedded oolites, and shelly lags may occur, and also poorly develop bioherms. Strong permanent currents are absent in lakes, however, wind driven currents may affect lake water surface, and depending their velocity redistribute fine grained sediment (Nichols, 2004). Hilton (1985) states that turbulence caused by wave action may redeposit sediment in deep waters, however slumping and sliding may cause more effective turbidity currents that reach deep waters in lake basins.



**Figure 2.3.** Low energy bench type lake margin (from Platt and Wright, 1991, after Murphy and Wilkinson, 1980).

**Low-energy ramp margins** are common in shallow and oligotrophic lakes (Fig.2.4). The sedimentary succession is mud-dominated, rich in charophyte bioclasts, bioherms, mudstone and wackestone textures with some oolitic packstones, and low detrital contents, probably due to clastic filtering by marginal marsh zones. Minor evaporite and fine alluvial deposits are common. The tops of regressive episodes are commonly subjected to subaerial exposure, and pedogenesis (Freytet and Verrecchia, 2002; Wright and Platt, 1995; Alonso-Zarza and Wright, 2010). This type of succession is characteristic of shallow playas and palustrine environments (Cohen, 2003).

**High energy, wave dominated ramp:** Highly wave influenced, with low margins containing winnowed grainstones dominate deposits with some nearshore bars. Evaporites, (trona, halite) oil shales, and stromatolitic structures may also be present.

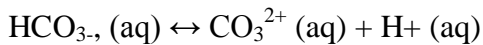
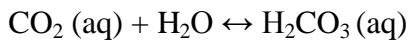
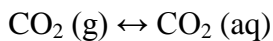


**Figure 2.4-** Low energy ramp type lake margin (Platt, 1989).

## 2.5 Carbonate sedimentology: some chemical considerations

Carbonates are qualitatively important component of lake sediments, and in areas with calcareous bedrock, they might constitute a significant fraction (Håkanson and Jansson, 1983)

Lake water ionic content is usually dominated by the cations  $\text{Ca}^{2+}$ ,  $\text{Mg}^{2+}$ ,  $\text{Na}^+$  and the anions  $\text{HCO}_3^-$ ,  $\text{CO}_3^{2-}$ ,  $\text{SO}_4^{2-}$  and  $\text{Cl}^-$ . Other ions also occur in lower concentrations ( $\text{PO}_4^{3-}$ ,  $\text{S}^{2-}$ ,  $\text{Fe}^{2+}$ ,  $\text{NO}_3^-$ ,  $\text{Na}^+$  and  $\text{Si}^+$ ). Commonly  $\text{Ca}^{2+}$ ,  $\text{Mg}^{2+}$  and  $\text{HCO}_3^-$ , arrive in solution via surface or groundwater inflow (Platt and Wright, 1991). Precipitation of calcium carbonate results from: evasion/invasion of  $\text{CO}_2$ ; reactions involving  $\text{OH}^-$ ; and increase in  $\text{Ca}^{2+}$ . In the geochemistry of the sedimentary carbonates the anion  $\text{CO}_3^{2-}$  takes part of a complex chemical system in natural waters known as the carbonic acid system, represented by a sequence of reactions (Morse and Mackenzie, 1990):



$\text{H}^+$  ion plays a major role in influencing the pH and buffer capacity of natural waters. If ground waters rich in calcium mix with alkaline surface water, hydroxyl ions in the lake water react with bicarbonate to form carbonate, followed by precipitation of calcium carbonate:

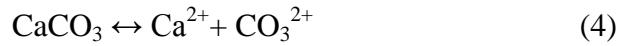
Dissolution or precipitation of  $\text{CaCO}_3$  in water is controlled by the invasion or evasion of  $\text{CO}_2$  through a series of equilibrium reactions (Bathurst, 1971):



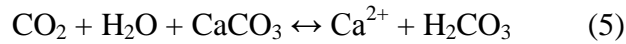
If dissolution contains free  $\text{CO}_3^{2-}$ , then the proton released in reaction 2 reacts with the carbonate ion to give more carbonate:



At the interface between the solution and solid  $\text{CaCO}_3$  the equilibrium is:

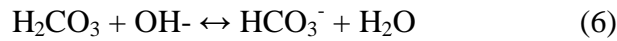


If these equilibria move to the right both  $\text{CO}_2$  and  $\text{CaCO}_3$  are dissolved. If they move to the left, as a result of evaporation or photosynthesis,  $\text{CO}_2$  is removed and  $\text{CaCO}_3$  is precipitated. The net result can be summarized as:



The restricted reversibility of this last reaction in sea water or any solution with  $\text{Mg}^{2+}/\text{Ca}^{2+}$  ratio is of prime importance in carbonate equilibrium.

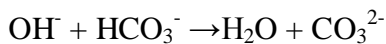
Reaction 1 is relatively slow, but is followed by the instantaneous reaction:



Although it has been suggested that widespread and spontaneous inorganic calcification should be expected according to the equation:

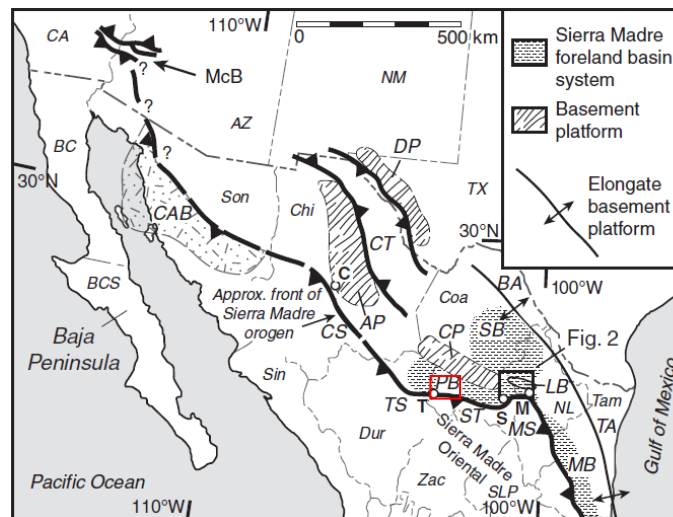


This has nowhere been unequivocally demonstrated, maybe because abundant ionic species are present and tend to cluster around  $\text{Ca}^{2+}$  and  $\text{CO}_3^{2-}$  forming complexes that prevent the ions coming together to precipitate (Altermann et al., 2006). According to Altermann et al. (2006), only when pH is increased due to production of hydroxyl ions ( $\text{OH}^-$ ), typically either by photosynthesis or by bacterial sulphate reduction, does the buffering capacity of seawater generate an increase in the concentration and availability of carbonate ions, available for carbonate precipitation:



## 2.6 Geology of the Mayrán Formation

The Mayrán Formation (late Neogene) was deposited unconformably in a series of sub-basins (the Mayrán Basin system) that erosionally overlie Late Campanian to Early Maastrichtian rocks within the Parras foreland fold-and-thrust belt in northeast México (Fig. 1 and 2.6). The deformed Cretaceous bedrock consists of marine siliciclastic mudstones (Parras Formation), and marine to continental deltaic siliciclastic mudstones and sandstones (Cerro del Pueblo and Cerro Huerta formations) of the Difunta Group (Weidie and Murray, 1967; McBride et al., 1974; Soegaard et al., 2003). The southern margin of the Mayrán Basin System comprises deformed Upper Jurassic-Cretaceous carbonate and subordinate siliciclastic rocks of the Parras Range (part of the Sierra Madre Oriental orogenic belt)



**Fig. 2.5** Locations of geological and geographical context of northeast Mexico. The Parras foreland and fold-thrust belt (PB), Coahuila Block (CP), red square indicate location of the Mayrán Basin system. Modified after Lawton et al. (2009).

Throughout the Late Cretaceous to Eocene, the sedimentary rocks within the orogenic belt and foreland area were affected by Laramide deformation (McBride et al., 1974; Gray et al., 2001; Lawton et al., 2009). The sedimentary cover in the Parras Foreland detached on the siliciclastic mudstones of the Parras Formation (Tardy et al., 1975) creating a series of WNW-ESE-striking folds and NE-SW-striking tear faults. The Laramide-age folds in the study area are stepped, and present their lowest structural level towards the Coahuila Block at the north (Fig.2.5). The Basement blocks exerted a paleogeographical control in the sedimentation (Goldhammer and Johnson, 1999) and the regional Laramide-style deformation (Chávez, 2005).

In the study area, the Laramide foreland folds are typically tight and parallel, with slightly asymmetric box-fold geometry. They range from 6 to >45 km in length and have a wavelength between 250 m and 2 km. The fold hinges are gently to moderately, doubly plunging, and bifurcate along strike giving rise to broad culminations and depressions along the strike of the fold and thrust belt. The vergence of the folds and thrust faults indicates that the main direction of tectonic transport was towards the north/northeast (Eguiluz et al., 2000). The Laramide deformation in the Sierra Madre Oriental ended in the Eocene, approximately ~46 to ~41 Ma (Gray et al., 2001; Molina et al., 2008). Subsequent post-Eocene uplift of northeastern México resulted in the differential erosion of up to 2 km of strata from the foreland region in the Parras area (Gray et al., 2001). This differential erosion constructed the landscape upon which the Mayrán Formation was deposited. Thus the undeformed Mayrán Formation overlies the rocks of the Parras Foreland along a prominent angular unconformity. Plutonic and volcanic activity occurred intermittently during Paleogene and Neogene in northeast Mexico (Aranda et al., 2005; Demant and Robin, 1975), and no volcanic ash marker beds have been reported from the study area.

Originally the Mayrán Formation was defined by Imlay in 1936, as “*a series of well cemented conglomerates and interbedded tufaceous deposits, capping the mesas at the eastern side of Parras Municipality, and northwards to the Saltillo-Torreón highway*”. The formation was described as containing a succession of well-cemented conglomerates composed by pebbles of Lower Cretaceous limestone, with minor amounts of tufaceous deposits containing some plant moulds that occur as beds or locally thick masses. The Mayrán Formation ranges in thickness from 61m to 30m and varies in colour from greyish-yellow to yellowish-brown (Imlay, 1936). Imlay (1936) proposed a probable Pleistocene age based on a report of “elephant-like bones” found in tufa deposits approximately 32 km east of Parras. Rogers et al. (1961) also assigned a Pleistocene age to the Mayrán Formation, based on a report of fossil molars of *Equus excelsus* Leidi collected 7 km northwest of the of Parras village. Because of the geographic location where these fossils were found, it is however, very unlikely that they were collected in the Mayrán Formation. Instead it is possible, that these fossils were deposited in post-Mayrán tufas (Fig. 2.6)

Except for recent Holocene studies carried out in palaeosols (see Butzer et al. 2008), there are no other published data on the post-Mayrán deposits. The study of paleosols, however, indicates that wet cycles were prominent during the early Holocene, and that excessive rain

promoted valley and slope instability causing high rates of landscape erosion (Butzer et al. 2008)

During the field seasons of this research, post-Mayrán deposits were identified deposited in deeply incised valleys that dissected the Mayrán Formation and the underlying Cretaceous bedrock (Fig 2.6 A and B). These deposits consist of both tufa and thin beds of limestones with lacustrine fauna, the later occur only in poorly preserved outcrops. Moreover these post-Mayrán carbonates are also deeply incised (Fig. 2.6B). No further research however was conducted in these deposits.



**Figure.2.6-** A. Several depositional events in the study area. Mayrán Formation, pre- and post-Mayrán Formation deposits. Cerro Huerta Formation (CH), Cretaceous. Yellow dashed line is Mayrán basal angular unconformity. White dashed line angular unconformity between Cretaceous bedrock and Post-Mayrán deposits. B. Photopanorama of deeply incised, post-Mayrán tufas and alluvial deposits at the south of Palo Alto village (see Fig. 1 for location in the basin).



## **Chapter 3**

## **Chapter 3**

# **Cascading carbonate lakes of the Mayrán Basin System, Northeast México: The interplay of inherited structural geometry, bedrock lithology and climate**

Natalia Amezcua, Rob Gawthorpe, and Joe MacQuaker

### **3.1 Abstract**

The Mayrán Formation (Late Neogene) exposed in northeast México was investigated to determine how antecedent topography, climate, sediment input, bedrock geology and primary production controlled facies architecture in this lacustrine-dominated succession. The succession was deposited in four, broadly coeval lake sub-basins (Mayrán Basin System) developed at different elevations. The sub-basins are separated by Cretaceous bedrock ridges and infilled by differing proportions of siliciclastic and carbonate deposits. Adjacent sub-basins are connected by spillover points. To investigate how these factors controlled overall facies architecture we generated a structural and stratigraphic framework for each sub-basin. In the most proximal sub-basin (I), alluvial sediments consisting of nonchannelized and channelized conglomerates, pebbly sandstones, calcareous sandy, and siliciclastic mudstones change laterally into horizontally bedded lacustrine limestones, calcareous mudstones, and evaporites. Vertically, these lithofacies are organized into shallowing upward cycles. The more distal sub-basins (II - IV) are predominantly filled by lacustrine limestones. Striking aggradational and progradational tufa topsets and clinofolds are present at the spillover points (waterfalls) between sub-basins. These tufas interfinger up- and down-dip with the lacustrine limestones.

The distribution of clastic facies was mainly controlled by their proximity to the major sediment input in the south, and to the Cretaceous bedrock ridges. Primary production within each sub-basin was controlled by a combination of lake level, accommodation availability, and solute inputs. Overall, while autogenic processes likely controlled facies distribution within the basin, climate was the overall driver of large scale facies variability.

## 3.2 Introduction

Lake deposits can provide high resolution paleoclimate records and may also contain resources of economic interest. In order to exploit the information preserved within the lake stratigraphy it is vital to understand the key controls on their facies architecture. The development of a lake is controlled by the interaction of tectonic and climatic processes, including the availability of accommodation, nature of sediment input, and hydrological regime (Kelts, 1988; Lambiase, 1990; Olsen, 1990; Sladen, 1994, Katz, 1995; Carroll and Bohacs, 1999, 2001; Bohacs et al., 2000a; Gawthorpe and Leeder, 2000; Carroll et al., 2006). Unraveling the influence of these various controls on the style of basin fill of an individual lake basin is often difficult because facies typically change rapidly in space and time (Blatt et al., 1991; Bohacs et al., 2003; Gierlowski-Kordesch et al., 2008; Gierlowski-Kordesch, 2010).

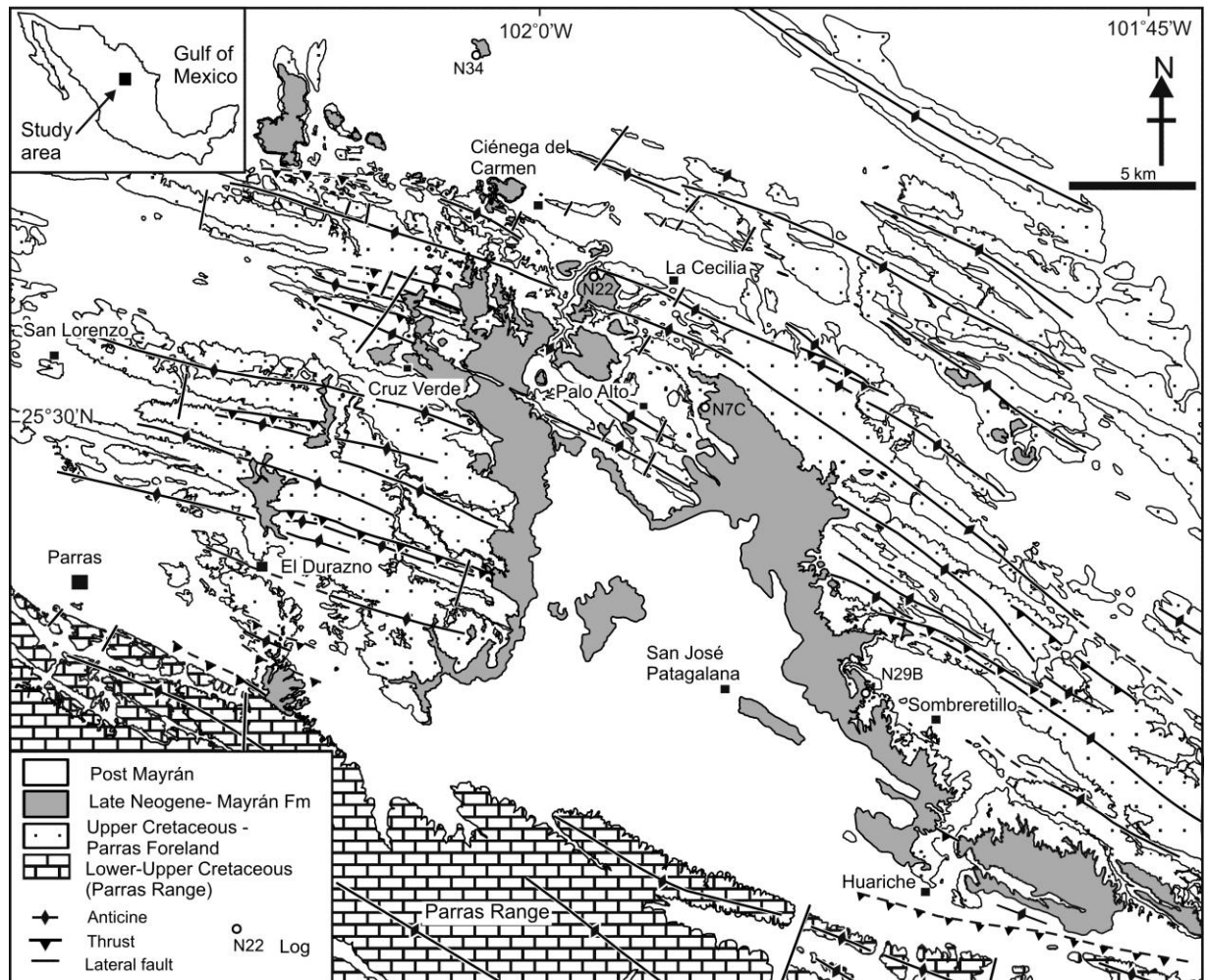
This study investigates the relative roles of inherited structural geometry, bedrock lithology, sediment production, and basin hydrology as key controls on fluvio-lacustrine facies in the Mayrán Formation (Imlay, 1936, 1937), northeast México. The Mayrán Formation is regionally well exposed and undeformed, allowing structural, geomorphological and stratigraphic relationships between the sub-basins to be established. We outline the structural and stratigraphic framework of sub-basins, here named the Mayrán Basin System, the coeval facies present in each sub-basin, and the facies and paleogeomorphic linkages between the different sub-basins. With these data, the differing fill architectures of each of the sub-basins could be compared and the relative effects of different sediment production and dispersal mechanisms on facies geometries determined. Our results show that non-tectonic lake basins can have a complex geomorphology due to the underlying inherited structural framework and variations in bedrock lithology. Furthermore, we show that the Mayrán Formation comprises a cascading series of hydrologically linked, shallow carbonate lake sub-basins that formed at different elevations spanning approximately 500m. Critical to the recognition of this type of lake basin geomorphology in the ancient rock record is the identification of spill-point deposits, in this case lobate tufa clinoform bodies.

### 3.3 Geologic setting

The Mayrán Formation (late Neogene) was deposited unconformably in a series of sub-basins that erosionally overlie Late Campanian to Early Maastrichtian rocks within the Parras Foreland Basin in northeast México (Fig. 3.1). The deformed Cretaceous bedrock consists of marine siliciclastic mudstones (Parras Formation), and marine to continental deltaic siliciclastic mudstones and sandstones (Cerro del Pueblo and Cerro Huerta formations) of the Difunta Group (Weidie and Murray, 1967; McBride et al., 1974; Soegaard et al., 2003). Deformed Upper Jurassic–Cretaceous carbonate and subordinate siliciclastic rocks of the Parras Range (part of the Sierra Madre Oriental orogenic belt) form the southern margin of the Mayrán Basin System.

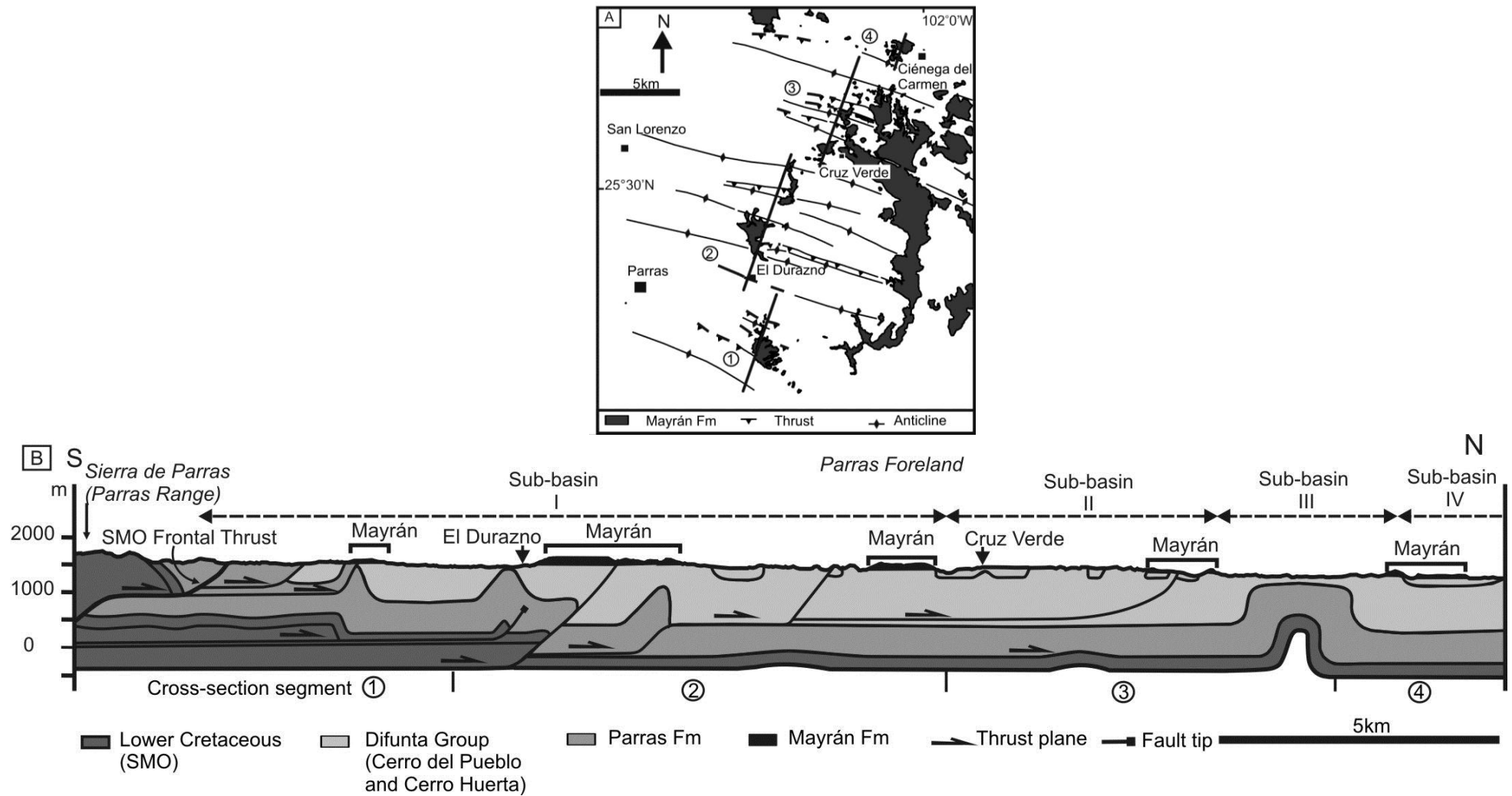
Throughout the Late Cretaceous to Eocene, the sedimentary rocks within the orogenic belt and foreland area were affected by Laramide deformation (McBride et al., 1974; Gray et al., 2001; Lawton et al., 2009). The sedimentary cover in the Parras Foreland detached on the siliciclastic mudstones of the Parras Formation (Tardy et al., 1975) creating a series of WNW-ESE-striking folds and NE-SW-striking tear faults (Fig. 3.1). In the study area, the Laramide foreland folds are typically tight and parallel, with a slightly asymmetric box-fold geometry (Fig. 3.2). They range from 6 to >45 km in length and have a wavelength between 250 m and 2 km. The fold hinges are gently to moderately, doubly plunging, and bifurcate along their length, giving rise to broad culminations and depressions along the strike of the fold and thrust belt. The vergence of the folds and thrust faults indicate that the main direction of tectonic transport was towards the north to northeast (Eguiluz et al., 2000). Thrusting increased the regional structural level, with more elevated Cretaceous bedrock in the south near the orogenic wedge and a northward down-stepping pattern of Laramide folds towards the foreland (Figs. 3.2 and 3.3).

The Laramide deformation in the Sierra Madre Oriental ended in the Eocene, approximately ~46 to ~41 Ma (Gray et al., 2001; Molina et al., 2008). Subsequent post-Eocene uplift of northeastern México resulted in the differential erosion of up to 2 km of strata from the foreland region in the Parras area (Gray et al., 2001). This differential erosion constructed the landscape upon which the Mayrán Formation was deposited. Thus the undeformed Mayrán Formation overlies the rocks of the Parras Foreland along a prominent angular unconformity (Fig. 3.4).



**Figure 3.1-** Geologic map of study area. Nondeformed Mayrán Formation overlies the Upper Cretaceous Perras foreland with angular unconformity. The thrust belt (Perras Range) of the Sierra Madre Oriental (SMO) lies along the south of the study area and forms the southern basin margin to the Mayrán Formation. Locations of stratigraphic sections (e.g., N7C) are indicated.

Several incision and aggradation events occurred after the Mayrán Formation was deposited. The incision events are characterized by the formation of incised alluvial valleys, dissecting both the Mayrán Formation and the underlying deformed Cretaceous formations. Post-Mayrán deposits within these incised valleys include tufas and limestones with lacustrine fauna. It is uncertain if these deposits were also originally considered as part of the Mayrán Formation by Imlay (1936, 1937).

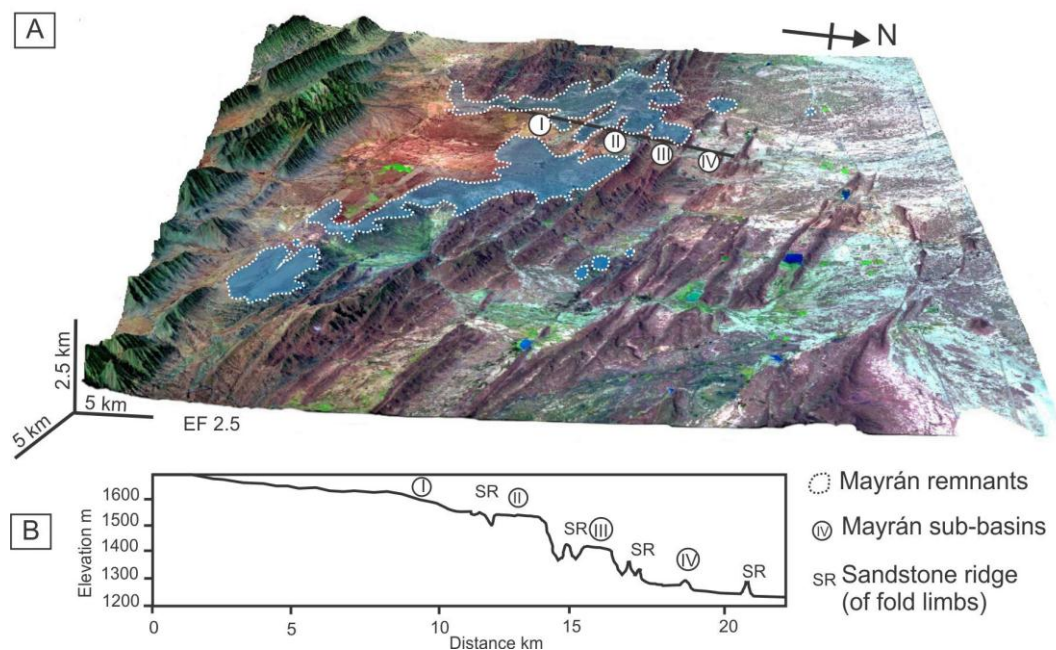


**Figure 3.2-** Simplified structure and N-S cross section across the study area. **(A)** Location of cross section and simplified structure. **(B)** Cross section showing the orogenic wedge (Parras Range) in the south and major thrust faults and folds of the Parras foreland. The Mayrán Formation (vertically exaggerated) unconformably overlies the deformed foreland succession. Note the decreasing elevation of subbasins I to IV from south to north. SMO—Sierra Madre Oriental.

### 3.4 The Mayrán Basin system

#### 3.4.1 Geomorphology

Exposures of the Mayrán Formation cover an area of approximately 2,000 km<sup>2</sup>. The formation occurs in four major sub-basins (I-IV) that range from 2 to >15 km wide in a NE-SW-direction, and are over 40 km long in a NW-SE-direction, parallel to the strike of the underlying Laramide folds. The sub-basins occur at different, discrete elevations, ranging from 1700 m in sub-basin I in the south to 1250 m in sub-basin IV in the north (Fig. 3.3). The sub-basins are most clearly defined where there are major changes in elevation between them, for example between sub-basin II and III where there is a 90 m difference in elevation (Fig. 3.3). These elevation changes between sub-basins are typically associated with elongated topographic ridges along the basal unconformity of the Mayrán Formation, where thick, erosionally resistant Cretaceous sandstones in the Laramide fold limbs underlay the unconformity (Fig. 3.3). In contrast to the elongate ridge-like morphology of the basal unconformity along the sub-basin boundaries, the basal unconformity within the sub-basins is sub-horizontal with local irregularities related to variations in the erodibility of the underlying Cretaceous bedrock.



**Figure 3.3-** The Mayrán Basin system. (A) Digital elevation model draped with Landsat image showing basin topography and the distribution of the Mayrán deposits in the eastern and central sectors of the study area. Doubly plunging Late Cretaceous foreland folds form prominent E-W to WNW-ESE ridges. Major subbasins are labeled I–IV; EF—vertical exaggeration. (B) Present-day topographic profile showing typical mesa morphology produced by Mayrán horizontally bedded limestones and prominent sandstone ridges. Note terrace-like subbasins downstepping northward.

### 3.4.2 Facies associations

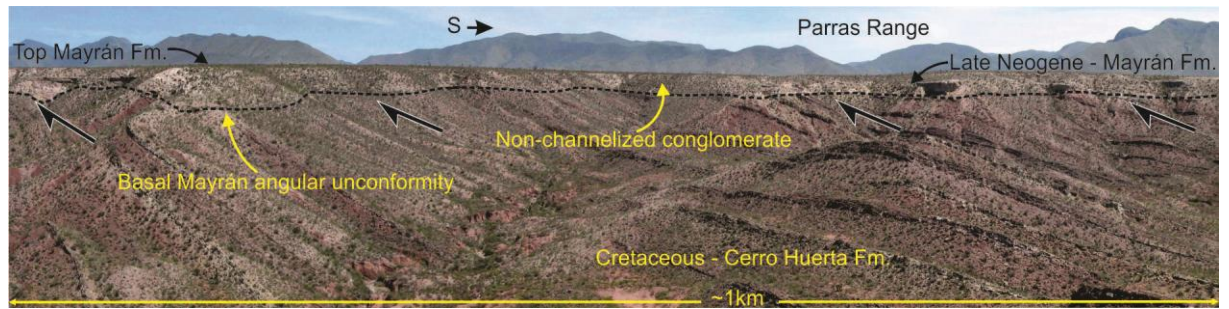
Over most of the study area the Mayrán Formation consists of coarse-grained clastic deposits at the base and carbonate-dominated units towards its top. The clastic deposits contain variable proportions of carbonate, siliciclastic grains and rock fragments. We use the term *siliciclastic* here to emphasize clastic rocks that are predominantly composed of non-carbonate detritus (i.e. silicate mineral grains and non-carbonate rock fragments). These deposits include nonchannelized conglomerates, channelized conglomerates and pebbly sandstones, and calcareous sandy and siliciclastic mudstones. The carbonate deposits include a variety of limestone facies that can be mapped as two main types, laterally extensive and sheet-like horizontally bedded limestones and more localized tufa clinoform deposits. All the sub-basins contain calcretized and/or pedogenically modified mudstones as well as rare evaporites. Descriptions of each facies association are provided in the following paragraphs.

#### 3.4.2.1 *Nonchannelized conglomerates*

Nonchannelized, crudely bedded conglomerates are laterally extensive and interfinger northwards with channelized conglomerates on a scale of tens of meters, and with sandstones and mudstones on scales of hundreds of meters. The nonchannelized conglomerates are predominantly found in sub-basin I, are poorly sorted and contain sub-rounded cobble- to boulder-size clasts that are predominantly composed of reworked Cretaceous limestone (>80%), sandstone, and subordinate chert. The conglomerates rarely contain any sedimentary structures and are weakly matrix- to framework-supported. Locally, however, pebble imbrication is visible and the paleocurrents measured from these fabrics indicate a dominant northwest-directed paleoflow (Fig. 3.5).

A second type of nonchannelized conglomerate can be distinguished based on clast composition. They occur locally within sub-basins II-IV forming laterally discontinuous deposits over tens of meters to less than one kilometer, and are composed of boulder- to cobble-size clasts of reworked sandstone and siltstone derived from the local Cretaceous bedrock highs between the sub-basins (Figs. 3.6A and 3.7A).

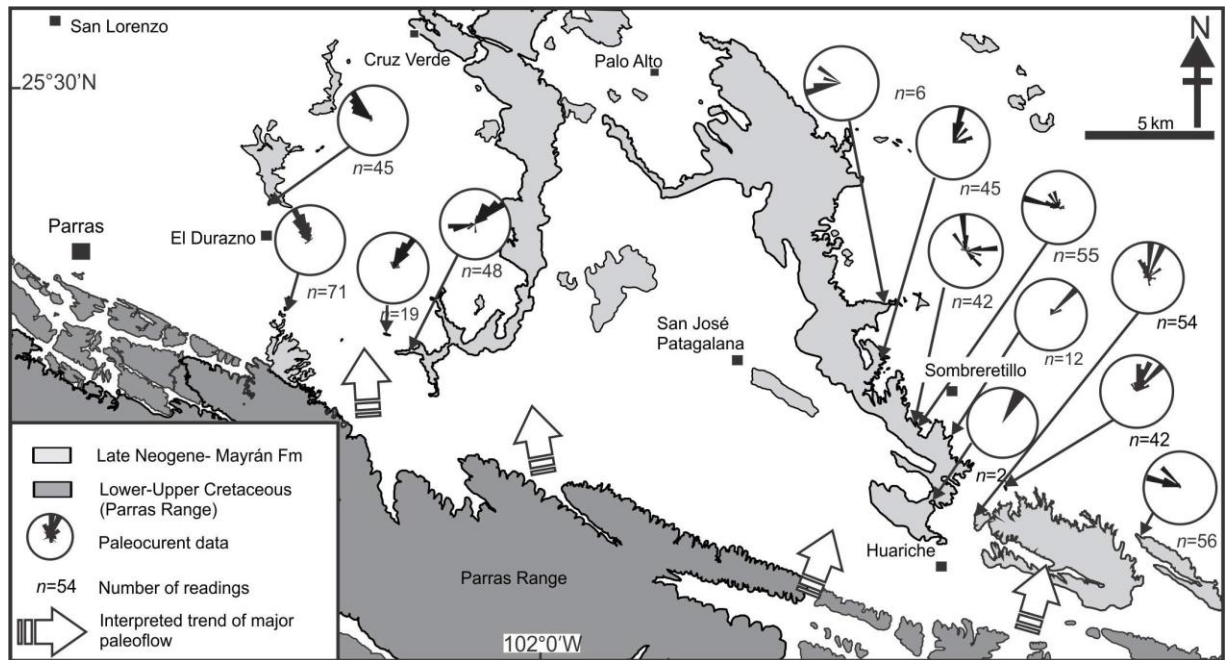




**Figure 3.4-** Panorama view to the south showing the Mayrán Formation resting with angular unconformity on deformed Cretaceous bedrock. Note the largely planar nature of the angular unconformity. The Parras Range, the major source of clastic detritus, is in the distance.

#### 3.4.2.2 *Channelized conglomerates and pebbly sandstones*

These conglomerates comprise channels with an erosional relief up to 1 m and are also well represented in the sub-basin I (Fig.3.7 B). Individual beds range in thickness from 0.3 to 1.5 m and amalgamate to form units up to 8 m thick (Fig. 3.6 B). These units can be traced laterally for several kilometers and are interbedded with nonchannelized conglomerates in the proximal regions. The channelized conglomerates are poorly to moderately sorted, vary from matrix- to framework-supported, and comprise rounded to sub-angular clasts. Locally, in sub-basin I they grade northward into pebbly sandstones that are up to 0.3 m thick and may form stacked units up to 0.5 m thick (Fig. 3.7 C). The clasts within the conglomerates are mainly pebbles and coarse cobbles, with rare small boulders (0.25 to 0.50 m long) and are predominantly composed of Cretaceous limestone (>80%) with subordinate sandstone and chert. Internally, individual beds exhibit both normal and inverse grading. Low-angle planar cross bedding and imbrication fabrics are developed locally and indicate that the main paleoflow was to the north and in a radial pattern (Fig. 3.5). These conglomerates and pebbly sandstones incise into siliciclastic and calcareous sandy mudstones (Fig.3.7B).



**Figure 3.5-** Paleocurrent measurements ( $n = 497$ ) from clast imbrication for the nonchannelized and channelized conglomerates in subbasin I. The dominant paleoflow directions are interpreted as being associated with alluvial fans and related stream channels coming from the Parras Range immediately south of the Mayrán depocentre.

### 3.4.2.3 *Calcareous sandy mudstones and siliciclastic mudstones*

Calcareous sandy mudstones of grey to dull pink or dull yellow colour typically form tabular homogenous units (0.5 m to 2.5 m thick) that are interbedded with grey to dark brown clay-rich siliciclastic mudstones (0.1 to 0.3 m thick) (Fig. 3.7B). Together, these facies form units up to 15 m thick within sub-basin I (Figs. 3.1, 3.6 and 3.8). The siliciclastic mudstones contain detrital clay minerals, silt, and up to 10 % fine sand and carbonate grains (derived from reworking of Cretaceous limestones and sandstones in the Parras Range). They are variably cemented by sparry and microsparry calcite. The mudstones are bioturbated and contain root traces (commonly defined by green to grey halos) and *microcodium*. Shelly fossil molds and scattered ostracodes also occur in this facies. Prominent fenestral pores (<0.5 m) occur locally in the calcareous sandy mudstones. These pores are organized into vertical pipes and horizontally aligned vugs. The vugs are partially to completely occluded by calcite spar and/or reddish-brown clay minerals, and gypsum.

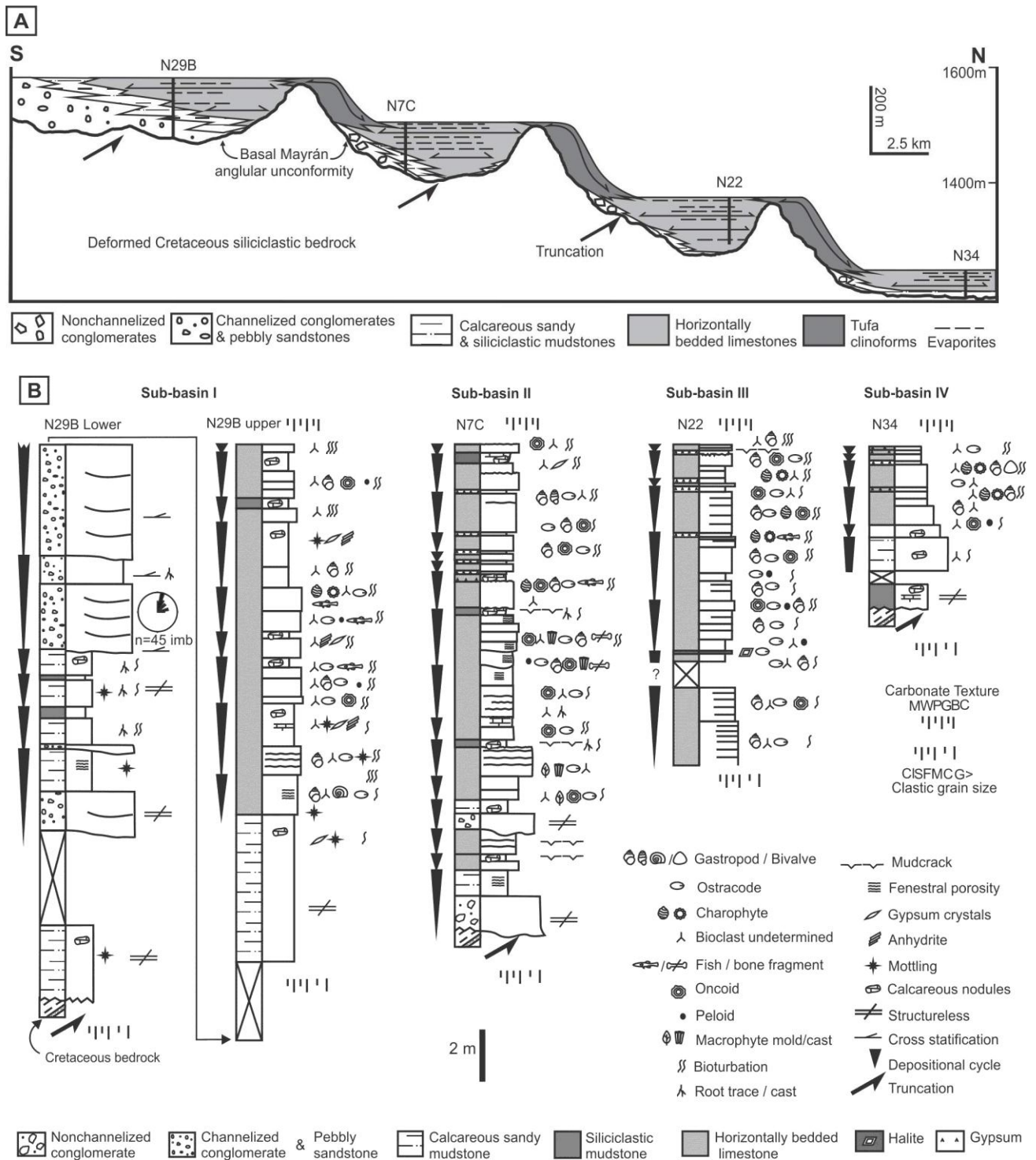
Siliciclastic mudstones of a different type occur interbedded with horizontally bedded limestones. They are green to dull gray in color, and form laterally continuous, poorly cemented, structureless units, 0.3 to 3 m thick. They consist of silt-sized sub-angular quartz, clay minerals, and a range of detrital grains, including rutile, zircon and suspected vitric volcanic grains. These grey green siliciclastic mudstones also contain gypsum aggregates, calcareous nodules, and root casts (Fig. 3.7 D). The grey green siliciclastic mudstones occur in all the subbasins.

#### 3.4.2.4 *Horizontally bedded limestones*

Horizontally bedded limestones occur as amalgamated units up to 13 m thick and form prominent cliffs that can be traced across entire sub-basins (Figs. 3.6 and 3.8). These amalgamated units are composed of beds 0.03 to 1 m thick (3.7 E), which are laterally extensive over meters to kilometers. Bedding planes are mainly parallel and wavy, but are locally erosional with shallow scours.

The horizontally bedded limestones mostly exhibit a wackestone to packstone texture; however, sub-ordinate mudstones, boundstones, grainstones, and crystalline carbonates are also present. The beds are sparsely to highly bioturbated by infauna and roots. Discontinuous, parallel-wavy laminae are preserved in some beds. Certain horizons within the limestones contain fenestral pores, tepee-like structures, oversized vuggy pores, karren structures, and *microcodium*. V-shaped cracks filled with calcite spar or silt-sized carbonates occur locally in these limestones.

The framework fossil content in the limestones includes ostracodes, molluscs (gastropods and bivalves), charophytes and other calcareous algae, and phosphatized skeletal components (millimeter-size fish remains). In addition, peloids, oncoids, stromatolites, intraclasts, phytocasts, calcified macrophytes, and amorphous organic matter appear in the limestones (Fig. 3.6 B). The matrix consists of either microcrystalline calcite or calcite spar and may contain up to 15% silt-size siliciclastic detritus.



**Figure 3.6-** (A) Simplified N-S cross section across the Mayrán Basin system illustrating the down-stepping northward pattern, basal angular unconformity, and overall lateral and vertical facies relationships. (B) Examples of sedimentary logs from subbasins I to IV. The sections illustrate the facies and depositional cycles interpreted to have occurred in each subbasin. Carbonate textures: M—mudstone, W—wackestone, P—packstone, C—crystalline, B—boundstone. Clastic grain size: Cl—clay, S—silt, Vf—very fine grained, F—fine grained, C—coarse grained, G—gravel and coarser. See Figure 1 for log locations

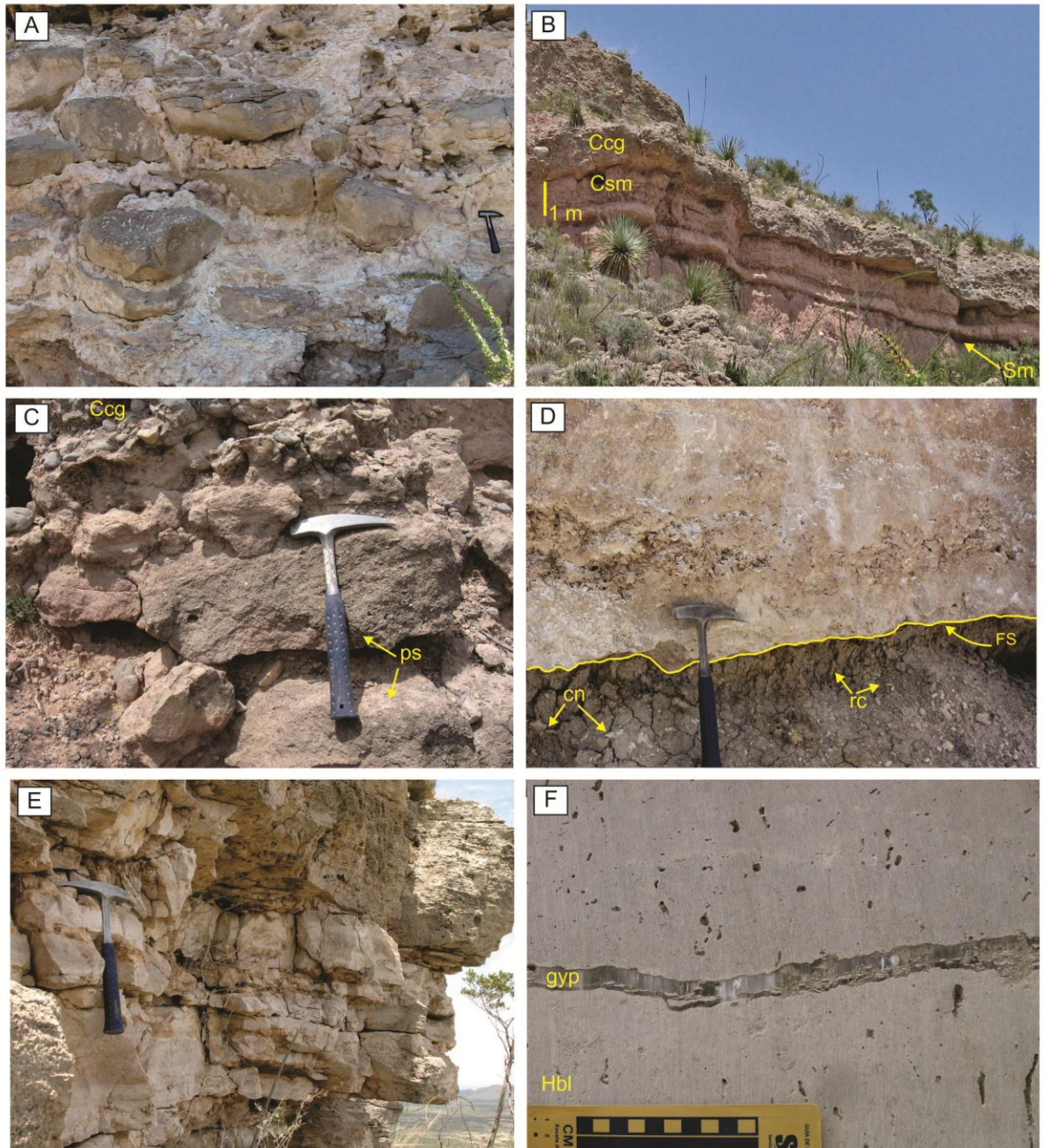
Petrographically, the horizontally bedded limestones are similar, but subtle differences in the relative proportions of the components, grain-size, and texture allow us to make the subdivisions and to identify facies, facies stacking patterns, lateral facies variations, and cyclicity. The main facies recognized are: ostracode mudstone-wackestones, clotted boundstones, gastropod wackestone-packstones, charophyte wackestone-packstones, macrophyte boundstones, oncoid wackestone-packstones, stromatolites, and marlstone.

The cycles recognized in the horizontally bedded limestones are asymmetric and vary between 0.3 and 2.5 m thick. An ideal cycle comprises ostracode mudstone-wackestones at the base, overlain successively by gastropod wackestone-packstones, oncoid wackestones-packstones and, towards the top of the cycles, charophyte wackestone-packstones and macrophyte boundstones (Fig. 3.6 B). Cycle boundaries are typically capped by evaporites or mudstones that contain V-shaped cracks. Flooding surfaces are marked by irregular basal contacts and contain commonly freshwater components (e.g. molluscs, charophytes, fish remains, and ostracodes) or intraclasts reworked from underlying beds (Fig. 3.7 D).

#### 3.4.2.5 *Tufa clinofoms*

This facies is locally developed and forms discrete large-scale sedimentary bodies that have a 'lobe-like' geometry (Fig. 3.9 A) and are tens to hundreds of meters in diameter and up to 40 m thick. The tufa clinofoms are very distinctive deposits that comprise prominent, 10 - 60° dipping beds with prograding, sigmoidal to oblique geometries (Fig. 3.9 B and C). Subhorizontal topsets of horizontally bedded tufas may also be developed along the proximal (southern) margins of the clinofoms. More typically the clinofoms can be traced up-dip and down-dip into the horizontally bedded limestone facies with which they are interbedded (Fig. 3.6A, 3.10 and 3.11).

The most common texture in these tufas is boundstone, in which calcified macrophyte and microbial communities occur. Internally, they have very complex fabrics and porosities, with abundant geopetal and botryoidal cements. The typical components in these tufas are calcareous encrustations of plants stems and leaves, bryophytes, calcified microbial laminations and ostracodes. These components are commonly oriented parallel to the dip of the clinofoms.



**Figure 3.7-** Examples of clastic and carbonate facies in the Mayrán Formation. **(A)** Nonchannelized conglomerate occurring in subbasins II to IV. Note matrix-supported cobble- to boulder-sized sandstone clasts. Hammer for scale (35 cm) at right side of image. **(B)** Channelized conglomerate (Ccg) erosively overlying calcareous sandy mudstone (Csm), and siliciclastic mudstones (darker color beds). **(C)** Pebbly sandstone (ps) overlain by matrix-supported channelized conglomerate (Ccg). **(D)** Horizontally bedded limestones overlying siliciclastic mudstone containing pedogenic features (e.g., calcareous nodules [cn] and root cast [rc]). FS marks the flooding surface at the base of the horizontally bedded limestones. **(E)** Amalgamated beds of horizontally bedded limestone (mudstone and wackestone texture). **(F)** Interbedded gypsum (gyp) in horizontally bedded limestone (Hbl).

#### 3.4.2.6 *Evaporites*

The evaporite mineral-rich units are typically thinly bedded (10 to 100 mm thick), and internally are either homogenous or exhibit lamination (Fig.3.7E). They are relatively rare within the Mayrán Formation, forming <10% of the succession. The minerals present include sulfates (both gypsum and anhydrite) and halite. In some strata gypsum forms crusts associated with the widespread development of V-shaped cracks. These cracks have a polygonal planform on bedding planes, penetrate the sediment to a depth of 20 mm, have raised edges, and are infilled either by gypsum (gypsite) or calcite cements. Gypsum also occurs as discrete nodules up to 20 mm in diameter that have grown displacively in the sediment and are associated with a brecciated fabric. Anhydrite is less abundant and commonly present as isolated lath-shaped crystals (typically 250  $\mu\text{m}$  in size) and centimeter-sized nodules. Halite is uncommon, its fabric poorly preserved, and is only observed in sub-basin III, forming thin, orange-weathering beds up to 10 mm thick within the horizontally bedded limestones.

#### 3.4.3 Spatial distribution of facies

The general stratigraphy of the Mayrán Formation comprises a lower coarse clastic unit dominated by nonchannelized conglomerates, channelized conglomerates, and pebbly sandstones that grade into finer-grained clastic rocks (calcareous sandy and siliciclastic mudstones). In contrast, the upper part of the Mayrán Formation succession is dominated by the horizontally bedded limestones. However, the relative proportions of the lower clastic unit and the upper carbonate-dominated unit vary from sub-basin I, the southern sub-basin adjacent to the Parras Range, to the more distal sub-basins (II-IV) to the north. There are also internal lateral and vertical facies variations within the individual sub-basins superposed on this larger-scale spatial variation in facies (Fig. 3.6A).

Sub-basin I is located immediately north of the Parras Range (Fig.3. 3) and comprises more than 50% clastic deposits (nonchannelized and channelized conglomerates, pebbly sandstones, calcareous sandy mudstones and siliciclastic mudstones). The clastic facies are particularly abundant immediately adjacent to the Parras Range (Fig. 3.4). Here, laterally continuous nonchannelized conglomerates interfinger basinward, over 2 to 4 km, with channelized conglomerates. Northwards, approximately 5

to 8 km from the range front, the channelized conglomerates interfinger with and incise into pebbly sandstones. Further north still (8 to 12 km from the range front) these pebbly sandstones in turn grade into calcareous sandy and siliciclastic mudstones. Stacked beds of these dominantly fine-grained siliciclastic units amalgamate forming successions up to 15 m thick, which are capped by the horizontally bedded limestones (Fig. 3.8).



**Figure 3.8-** Laterally continuous horizontally bedded limestones overlying stacked beds (~15 m thick) of calcareous sandy mudstones (Csm) and siliciclastic mudstones (Sm) in subbasin II, north of Cruz Verde Village (see Fig. 1 for location). Note the angular unconformity at the base of the Mayrán Formation (truncation indicated by arrows).

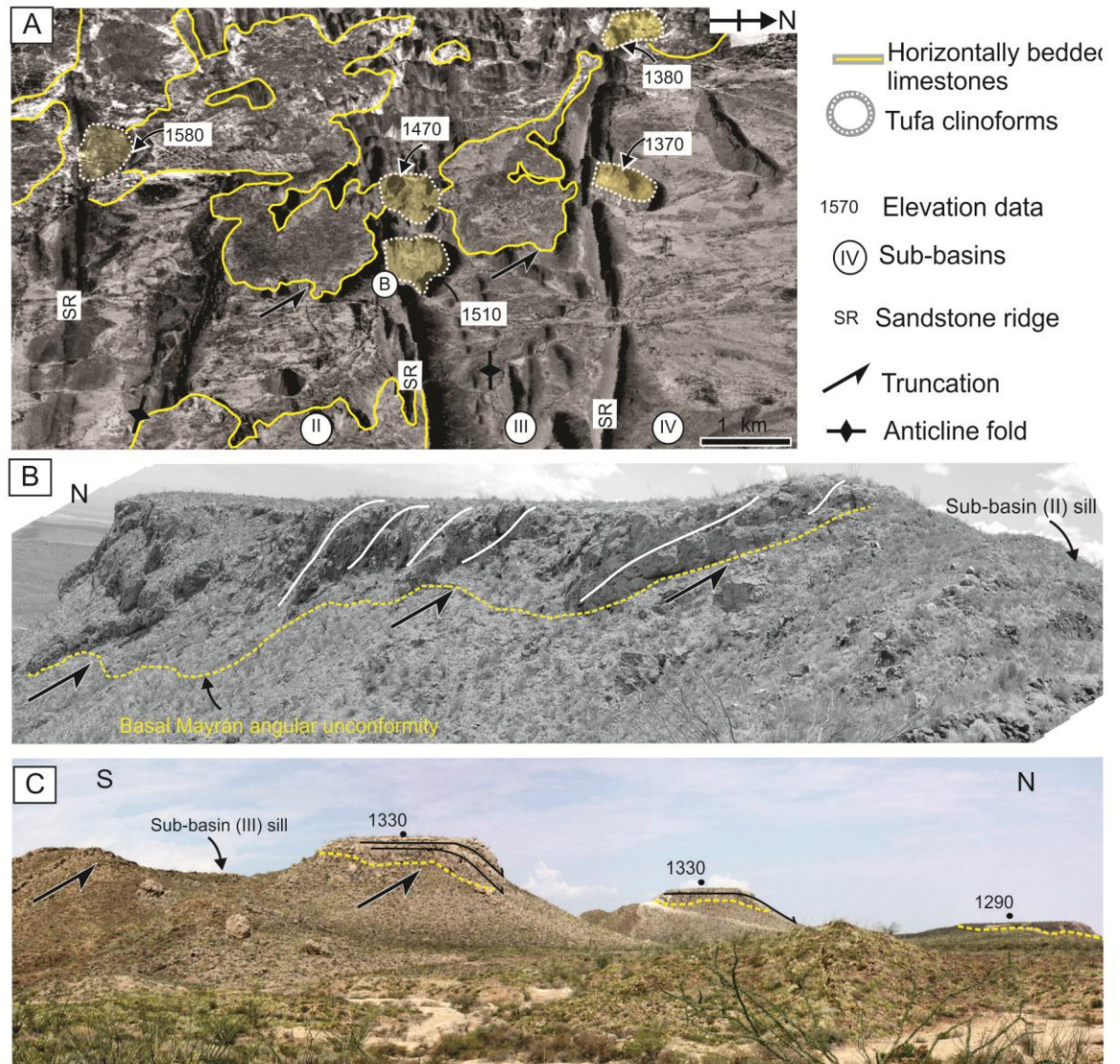
In the northern part of sub-basin I, horizontally bedded limestones dominate the upper part of the succession and comprise >35% of the total Mayrán thickness (for example log N29B; Fig. 3.6B). Scattered evaporite nodules occur in both the calcareous sandy and siliciclastic mudstones and horizontally bedded limestones. However, these evaporites are very rare and, in contrast to the sub-basins to the north, do not form well-defined beds.

At the northern edge of sub-basin I, the horizontally bedded limestones lap onto Cretaceous sandstone bedrock ridges, and locally grade laterally into tufa topsets and clinofolds. These tufa clinofolds only occur immediately basinward (north) of valley-like topographic lows along the bedrock ridge that separates sub-basins I and II, and form large ‘lobe-like’ bodies with a radius of up to 700 m and a clinofold height of up to 40 m. The toes of the tufa clinofolds interfinger with the horizontally bedded limestones at the



southern edge of the topographically lower, sub-basin II. Similar facies relationships occur along the northern edge of sub-basins II and III (Fig. 3.6A and 3.9). In these more northerly sub-basins, tufa clinoform bodies have radii of up to 1 km and clinoform heights of between 50 and 90 m.

In sub-basins II to IV, horizontally bedded limestones dominate the Mayrán succession and comprise over 70% of their thicknesses (Fig. 3.6B, e.g. logs 3N7C, N22 and N34). Nonchannelized conglomerates occur at the base of the succession in sub-basins II-IV (Fig. 3.7 A), and grade into pebbly sandstones and calcareous sandy mudstones over a distance of less than 500 m. These conglomerates were deposited immediately adjacent to the bedrock sandstone ridges that separate the sub-basins. In addition, discrete intervals of calcareous sandy and siliciclastic mudstones occur in the northerly sub-basins. These mudstones are widespread and commonly appear overlying cycle boundaries within the horizontally bedded limestones. The fill of the middle and upper parts of sub-basins (II-IV) consist dominantly of horizontally bedded limestones, with discrete intervals of siliciclastic mudstone and evaporites. In contrast to sub-basin I, the evaporites form discrete beds that cap the cycles within the horizontally bedded limestones. The cycles within the horizontally bedded limestones are laterally extensive and can be traced along most of the sub-basins width and strike, at least as far as the exposures allow. The cycles can also be traced into the tufa clinoforms, but it is not possible to trace individual cycles unequivocally through the tufa clinoform bodies from one sub-basin to the next.



**Figure 3.9-** (A) Digital elevation model draped with aerial photographs showing preserved Mayrán horizontally bedded limestones (highlighted by solid yellow lines) in subbasins II–IV, separated by prominent sandstone ridges of Cretaceous bedrock (SR), and the main tufa clinoform deposits developed at spillways (dotted lines). Note northward decrease in the elevation of the subbasins; numbers indicate elevation (in m) above sea-level. (B) Field photograph of tufa clinoform deposits, north of Palo Alto Village. Position is indicated in A. Tufa clinoforms prograde downslope. (C) Stratal geometries and stacking patterns within the tufa clinoforms at the spillway between subbasins III and IV. Dashed yellow line is the basal unconformity.

### 3.4.4 Facies interpretation and paleogeography

The range of clast composition in the conglomerates within sub-basin I is similar to the bedrock in the Perras Range. The proximity of the nonchannelized conglomerates to the range front, their immaturity, the fact that they are both matrix- and framework-supported, and the northwest-directed flow directions indicate that they were likely deposited as unconfined debris flows on the proximal portions of alluvial fans developed adjacent to the Perras Range (e.g. Bull, 1977; McPherson et al., 1987; Fraser and DeCelles, 1992; Blair and McPherson, 1994, 2007). The existence of channelized conglomerates that exhibit crude graded bedding and imbricate fabrics, locally with radial flow directions oriented broadly to the northwest (Fig. 3.5), implies that some channelized flow also occurred on these fans (McPherson et al., 1987; Blair and McPherson, 2007; Nichols and Fisher, 2007).

In sub-basin I, away from areas immediately adjacent to the Perras Range, the channelized conglomerates typically incise pebbly sandstone sheets and calcareous sandy and siliciclastic mudstones. Here the fine-grained sediments are typically organized into stacked successions of normally graded beds that have sheet like geometries. The lack of other diagnostic sedimentary structures in these units, as well as their overall geometry, suggests that these finer-grained siliciclastic units were deposited from waning sheet flows at the distal portions of alluvial fans (Blair and McPherson, 1994; Bridge, 2003). The presence of scattered aquatic fossil molds, bioturbation, calcareous nodules and rooted horizons in the calcareous sandy mudstones and siliciclastic mudstones indicates that these fans transitioned into a marginal lacustrine setting where soils were forming (e.g., Gierlowski-Kordesch, 1998; Freydet and Verrecchia, 2002). The high carbonate contents of the soils suggests that, during pedogenesis, evaporation exceeded precipitation (e.g. Tucker and Wright, 1990; Wright and Tucker, 1991; Alonso-Zarza and Wright, 2010) forming calcic paleosols (e.g. Mack et al., 1993).

Down-dip, these pedogenized mudstones typically interfinger with the horizontally bedded limestones. The fossils present in these limestones (gastropods, bivalves, ostracodes, calcareous algae), as well as calcified microbial filaments, peloids, oncoids, phytocasts and stromatolites, indicate that the sub-basins were occupied by high productivity lakes with temporal variation between both fresh and saline compositions (c.f. Kelts and Hsü, 1978; Dean and Fouch, 1983; Cohen, 2003; Gierlowski-Kordesch, 2010). The presence of so much carbonate in these lakes coupled with their associated mudstone, boundstone and packstone textures indicates that much of the primary production occurred

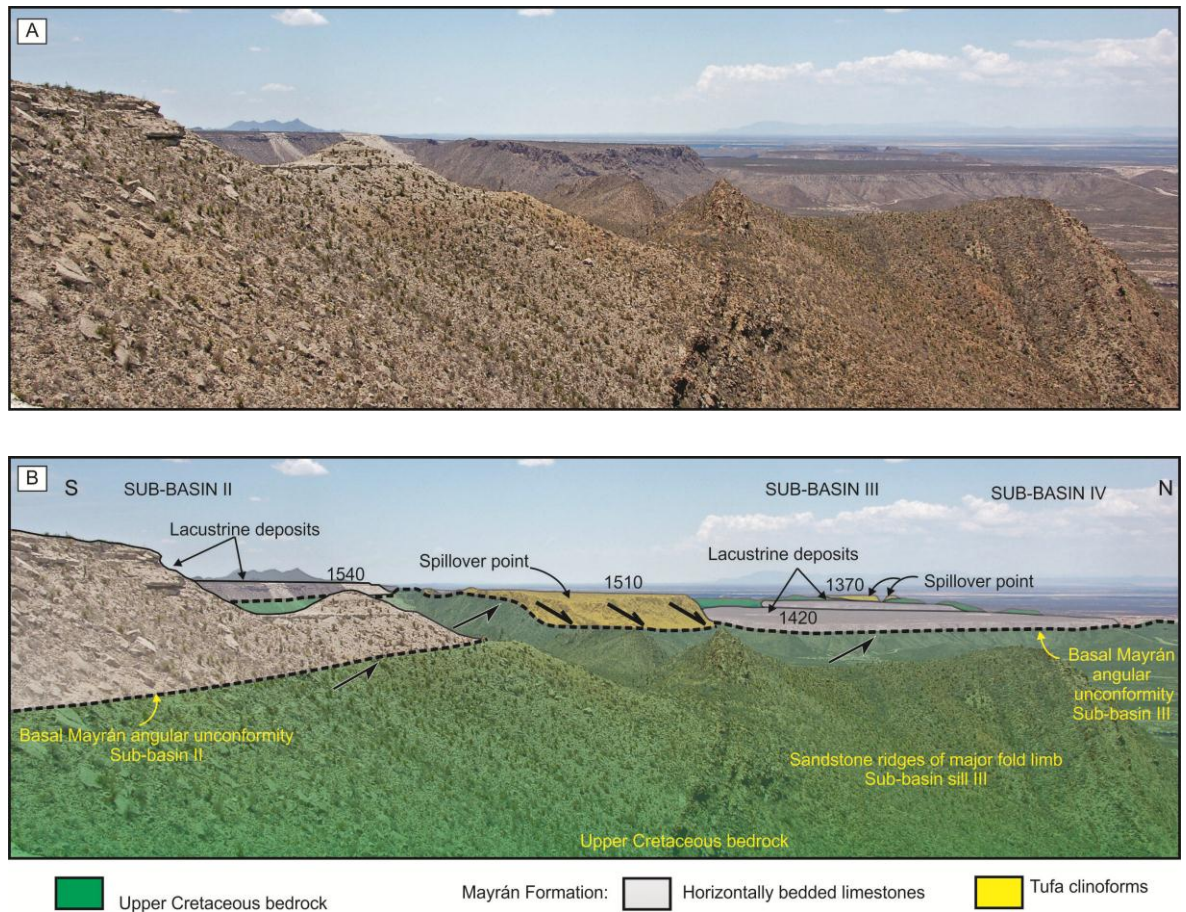
*in situ* with the necessary nutrients being supplied by detrital inputs to the basin (e.g. Gierlowski-Kordesch, 2010).

The cyclic facies stacking patterns in the horizontally bedded limestones, and their spatial variability attest to the fact that depositional environments and the composition of the lakes were variable. The presence of evaporites and polygonal desiccation cracks indicates that the sub-basins episodically became hypersaline, and that the basin floors became exposed so that playa conditions developed. During phases of drawdown thin evaporite units (e.g. halite or laminated bedded gypsum) were likely deposited subaqueously. In contrast, the abrupt change from either exposure surfaces or evaporites back to horizontally bedded limestones with a fresh-water fauna indicates rapid flooding and lake expansion.

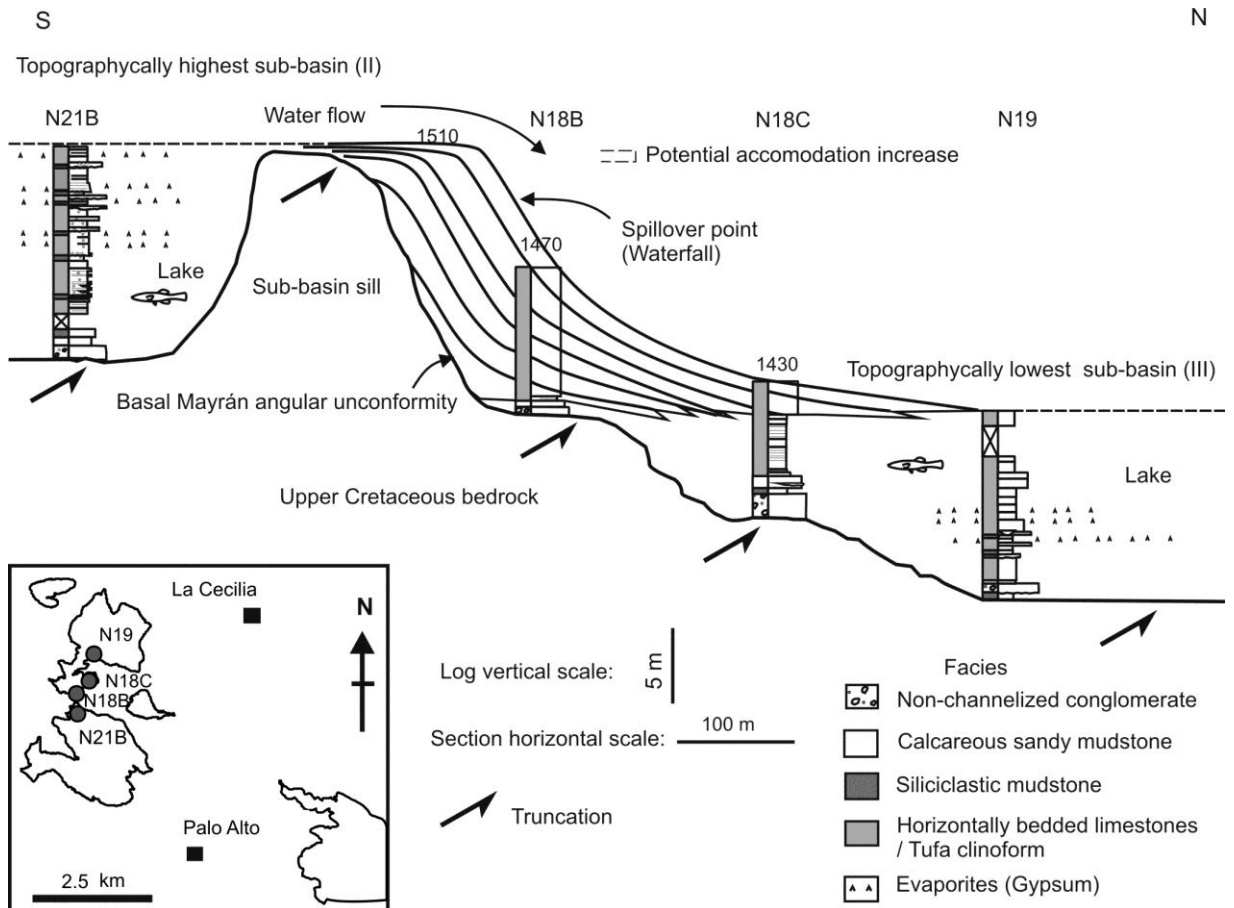
The presence of localized tufa clinoforms on the northern side of the sandstone bedrock ridges that separate the sub-basins indicates that outflow occurred during periods of high lake level. The large size of these tufa clinoform bodies and the differences in elevation between successive sub-basins, suggest that large constructional waterfalls dominated the drainage patterns between the sub-basins (Figs. 3.10, 3.11 and 3.12). A peculiarity of these waterfalls is that they are progradational features, rather than incisional features associated with headward knickpoint retreat (see Lamb and Dietrich, 2009; Crosby and Whipple, 2006). Carbonate sediment precipitation in topset tufa beds led to spillway aggradation, increasing the height of the spillway. It is inferred that the process of topset aggradation was a significant contributor to the overall aggradation of the horizontally bedded limestones in the up-dip sub-basin.

Although there are certainly variations in the carbonate facies present, there are no significant differences that can be easily attributed to widely varying bathymetries within and between the sub-basins (Fig. 3.6A and B). All the horizontally bedded limestone facies suggest deposition in the photic zone (e.g. Kelts 1988; Talbot, 1988; Anadón et al., 1989; Cohen, 2003). Based on spillway elevation and the thickness of the succession in each sub-basin, it is inferred that the lakes were no deeper than 20 m and probably much shallower, as individual horizontally bedded limestone cycles are <3 m thick. Lithofacies with wide distribution such as the gastropod wackestone-packstones, and subordinately the charophyte wackestone-packstones, support the interpretation of shallow lake systems. Thus as the sub-basins span an elevation range of some 500 m, each lake sub-basin must have

had its own lake level, and the Mayrán Basin System as a whole is interpreted to have formed a northerly down-stepping array of isolated lake depocentres (Fig. 3.12).



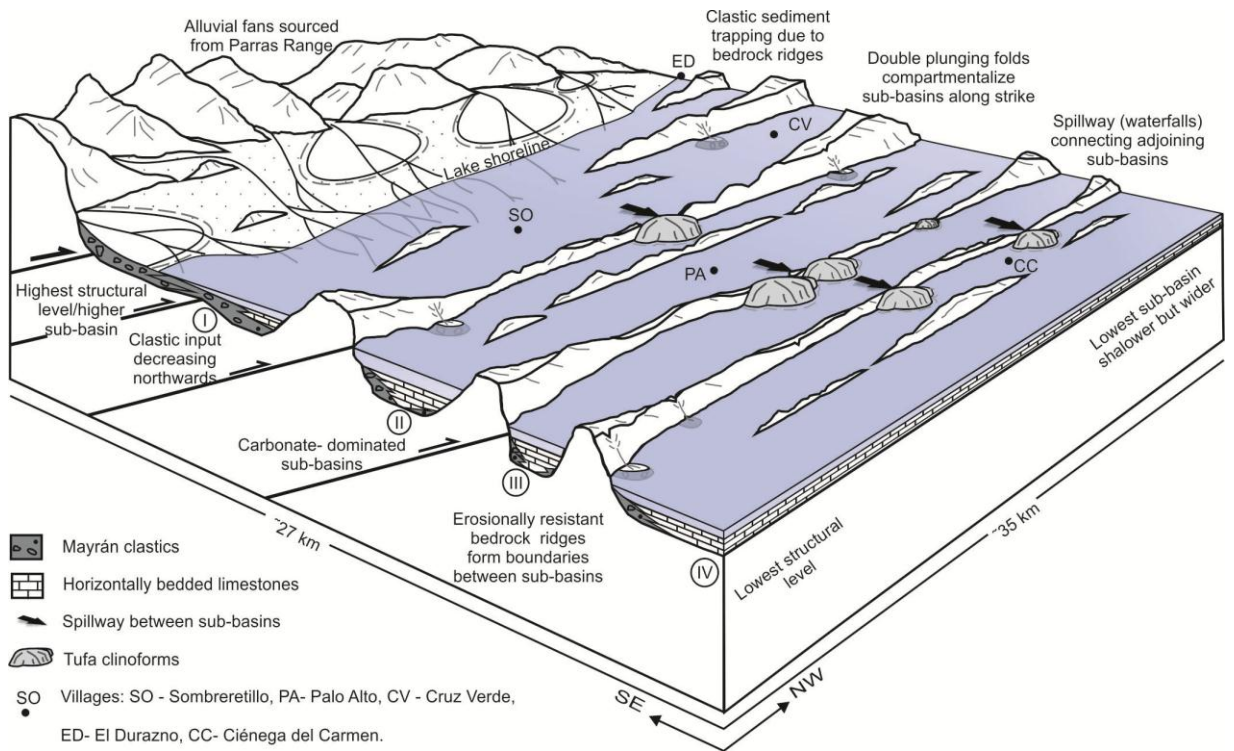
**Figure 3.10-** (A) Photopanorama and (B) interpretation of the subbasins II, III, and IV showing: (1) northward down-stepping of the subbasins, (2) bedrock sandstone ridges separating the subbasins, (3) tufa clinoforms (waterfalls) in the spillover areas between adjacent subbasins, and (4) the prominent subhorizontal top of Mayrán horizontally bedded limestones. Dashed line is the basal unconformity; numbers indicate elevation (in m) above sea-level.



**Figure 3.11-** N-S transect across the boundary between subbasins II and III showing relationships between the lacustrine, horizontally bedded limestones deposited in the subbasins and the tufa cliniforms deposited at the basin spillways. Inset shows section location; numbers above logs indicate elevation (in m) above sea-level.

### 3.5 Discussion

The Mayrán Formation is dominated by widespread lacustrine carbonates with a more clastic-rich succession along the southern basin margin (Parras Range), characterized by alluvial fan to muddy lake shoreline deposits. Although the formation post-dates Laramide deformation and is undeformed, the basin physiography is complex, comprising four sub-basins (the Mayrán Basin System), each at a discrete elevation, that form a northward down-stepping array. This basin morphology has a pronounced impact on the spatial distribution of facies, but it cannot explain all aspects of the Mayrán sedimentology and stratigraphy. In the following section we discuss the main controls on the basin geomorphology, sediment sources and partitioning, and the role of autogenic and allogenic controls on facies and cyclicity. Consideration of these controls enables us to understand more clearly the dynamics and complexity of other lacustrine depositional systems.



**Figure 3.12-** Model of the Mayrán Basin system during high lake-level stages when the subbasins were hydrologically linked by flow through spillways creating tufa clinoforms. Note partitioning of facies, with clastics largely restricted to subbasin I, adjacent to the main clastic source area (Parras Range), whereas subbasins II to IV are characterized by widespread deposition of horizontally bedded limestones. Also note the northward down-stepping of the subbasins and the prominent ridges (composed of resistant sandstone bedrock) separating the subbasins.

### 3.5.1 Basin geomorphology

The importance of bedrock topography and geomorphic controls on continental basin infill has been documented by several authors (e.g. Pietras and Carroll, 2006; Carroll et al., 2006, 2010; Davis et al., 2009; Duchesne et al., 2010; Chetel and Carroll, 2010). The overall configuration of the Mayrán Basin System is strongly influenced by the folding and lithology of the Cretaceous-aged subcrop (Figs. 3.2 and 3.12). The individual sub-basins are underlain by the basal Mayrán unconformity which has a sub-horizontal and overall planar morphology. In each sub-basin this unconformity overlies easily eroded Cretaceous siliciclastic mudstones and thin to thick bedded sandstones. In contrast, the sub-basins are separated by NW-SE-trending bedrock ridges of erosionally resistant Cretaceous sandstones which represent the eroded limbs of the Laramide folds. These ridges are several tens of meters to 100 m above the height of the adjacent sub-basins. Variations in

the erodibility of the local bedrock geology therefore had a major impact on the spatial distribution of the sub-basins.

On a larger scale, the overall geometry of the Mayrán Basin System is influenced by two major factors that affect the 3D geometry of the fold and thrust belt. First, the northward decrease in structural elevation from the orogen in the south to the foreland in the north controlled the progressive northward down-stepping of the Mayrán sub-basins. Second, the doubly-plunging and segmented nature of the folds and thrusts created significant along-strike variations in structural elevation in the form of culminations and depressions. The Mayrán Basin System as a whole is located at a major depression in the fold and thrust belt, with the adjacent culminations acting as lateral confinement to the lake system.

It is important to emphasize that, while the Mayrán Basin System is morphologically similar to a series of isolated piggyback basins in a foreland basin setting (e.g. Lawton et al., 1994; DeCelles and Giles, 1996), it is not a syn-tectonic geomorphological feature. Its complex basin morphology results instead from differential erosion of a pre-existing Laramide-aged fold belt and consequently it has a post-tectonic origin. In this setting, a combination of pre-existing structural geometry and variations in the erodibility of the different lithologies, within the fold and thrust belt, were the dominant controls on the geomorphology of the Mayrán Basin System.

### **3.5.2 Sediment sources and partitioning**

The coarse-grained detrital components sourced from the Parras Range comprise more than 80% limestone clasts, and are a significant component of the fill in sub-basin I. By contrast, the neighboring sub-basins to the north contain only local coarse clastic deposits adjacent to the bounding sandstone bedrock ridges. The restriction of coarse clastic facies may have, in part, been a product of waning flow away from the Parras Range. The physical topographic barrier formed by the sandstone bedrock ridges along the distal, northern margin of sub-basin I, however, were also likely a major factor limiting the dispersal of clastic sediment to the more northerly sub-basins (Fig. 3.12). Sub-basin I therefore acted as a clastic sediment sink to the system.



Crucially, discharge from Parras Range drainage catchments not only supplied detrital sediment to sub-basin I, but likely also supplied calcium, magnesium, and bicarbonate ions in solution via surface water flow to fuel carbonate production in all the lake sub-basins. These nutrients could not easily have been derived from the underlying bedrock which is dominated by siliciclastic sediments, but may in part have been introduced via fault-related springs from carbonate-rich aquifers at depth, as occurs today in the Cuatro Ciénegas lakes some 150 km north of the study area (see Winsborough et al., 1994; Johannesson et al., 2004).

### 3.5.3 Allogenic vs. autogenic controls on sediment stacking patterns

The sedimentary succession of the Mayrán Formation records a combination of clastic and chemical sediments (carbonates with minor evaporites) deposited in shallow lakes subject to varying water levels. All the Mayrán sub-basins exhibit similar laterally extensive shallow lacustrine carbonate deposits containing thin evaporitic intervals, together with subaerial exposure surfaces and well expressed flooding surfaces (Fig.3.6B). The widespread occurrence of these facies implies that conditions in the sub-basins, when the lakes were present, were relatively stable. The aggradational stacking patterns of the carbonates and the presence of subordinate evaporites suggest that basin hydrology (water supply and precipitation/evaporation ratios) had an important influence on facies architecture and cyclicity (e.g. Carroll and Bohacs, 1999, 2001).

During high lake levels, overflow from one sub-basin to the next occurred as water reached the height of spillover point along the lowest point of a sandstone bedrock ridge. Progradational to aggradational tufa clinoform bodies formed at these spillover points (Fig. 3.9 C, and 3.11). Aggradation at the lip of the spillway, in response to tufa precipitation, created some additional accommodation in the up-dip lake basin, and allowed the lacustrine carbonates to aggrade higher than the initial height of the bedrock at the spillway. Accommodation within each of the sub-basins, however, was largely inherited from the differential erosion of the foreland fold and thrust belt. It was mainly controlled by the difference in elevation of the basal unconformity along the sub-basin floor and the lowest point along the sandstone bedrock ridge bounding the northern margin of the sub-basin.

The presence of evaporites (mainly gypsum), and the widespread lacustrine carbonates containing pedogenic features and exposure surfaces in all the sub-basins indicates that the individual sub-basins became isolated from time to time and occasionally dried out. The precipitation of evaporites in the sub-basins is likely to have been enhanced by closed drainage conditions within the small sub-basins and low precipitation/high evaporation ratios (e.g. Carroll and Bohacs, 1999; Bohacs et al., 2003, Pietras and Carroll, 2006).

Although cycle-to-cycle correlation between the different sub-basins cannot be demonstrated unequivocally, the similarity of facies in the sub-basins and the interfingering of the tufa cliniform facies with the lacustrine limestones in the adjacent sub-basins indicate that hydrologically all the sub-basins were linked, at least when outflow was occurring into a coeval depositional system. The similarity of facies and cyclicity across the sub-basins suggests a regional, allogenic control on the Mayrán Formation that, given the basin location and lack of active tectonic influence, is most likely to have been climatic.

### **3.6 CONCLUSION**

Analysis of the Mayrán Basin system provides evidence of a large Neogene-age lake system covering approximately 2,000 km<sup>2</sup>. The excellent field exposures of the Mayrán Basin System reveal a complex series of cascading lakes that were present in four down-stepping sub-basins. Sub-basin geomorphology was determined by the inherited topography of the exhumed and differentially eroded foreland fold and thrust belt. The sub-basins overlie a basal unconformity developed on deformed Cretaceous rocks and are separated by bedrock ridges formed from erosionally resistant Cretaceous sandstones.

The sedimentary infill of the sub-basins comprises alluvial conglomerates, pebbly sandstones and mudstones in proximal settings, and carbonate production-derived components, in the form of horizontally bedded lacustrine limestones, in more distal settings. Away from the southern basin margin, the sediments are organized into upward fining packages capped by soil deposits and evaporites. The limited lateral facies variability in the horizontally bedded limestones and the thickness of the succession in each sub-basin suggest that lake waters were no deeper than 20 m and probably much shallower. As the sub-basins span an elevation range of 500 m, each sub-basin must have

had its own lake level, and the Mayrán Basin System as a whole is interpreted to have formed a northerly down-stepping array of lake depocenters. Aggradational to progradational tufa clinofolds are present at spillways connecting the sub-basins and were formed by large constructive waterfalls.

Proximity to clastic sediment sources, primary carbonate production and accommodation availability largely controlled facies variations within each sub-basin. Nutrients to fuelling carbonate production were likely derived from inputs of carbonate clastic detritus (Cretaceous limestones), and most carbonate accumulation occurred when the basins were either overfilled or balanced-filled. The tufa clinofolds represent important hydrologic connections between the individual sub-basins.

While accommodation availability in each sub-basin was mainly controlled by the pre-existing erosional relief of resistant sandstone ridges, tufa cement precipitation at the spillways added small volumes of accommodation in the sub-basins up-dip of the spillover points. During periods of relative low lake levels when evaporation became dominant, lake contraction occurred, soils developed on the basin margin, and evaporites precipitated within the sub-basins. It is not possible to correlate individual cycles unequivocally between the different sub-basins but the overall synchronicity in deposition across the Mayrán Basin System suggests that external (allogenic) factors, most likely climate, controlled initiation, evolution and termination of the Mayrán Formation deposition.

This study suggests that without the excellent exposure and tectonically unaffected nature of the Mayrán deposits, the stratal geometries and northward down-stepping character of the sub-basins would have been very difficult to identify and reconstruct. The stratigraphic architecture and nature of vertical and lateral facies changes occurring at the spillways, in particular the tufa clinofolds, provide evidence for the compartmentalization into sub-basins, and quantify the elevation change between them. Thus, in the stratigraphic record, identifying tufa clinofolds would be a critical step in correctly interpreting a down-stepping basin geometry. The compartmentalization of a lake basin into a series of sub-basins of different elevation linked by spillover points is relatively rare in post-tectonic (or pre-tectonic) phases of basin evolution. The observations made here on the cascading lakes of the Mayrán Basin System may therefore be more applicable to syn-tectonic lake basins where compartmentalization by active structures can readily lead to sub-basin formation, each with its own base level.

**3.7 ACKNOWLEDGMENTS**

This contribution represents a portion of Amezcua's doctoral dissertation at the University of Manchester. Support for this project was provided by the Mexican Geological Survey (SGM). Funding was provided by the National Council of Science and Technology (CONACYT) for the studentship grant to N. Amezcua. We acknowledge R. Rainbird (Associate Editor) and the anonymous reviewers for their constructive comments on the manuscript. Discussion and assistance in the field by S. Eguiluz, and proof reading by C. Hunt and M. Palacios-Fest is also acknowledged.

## **Chapter 4**

## Chapter 4

### **Prograding tufa clinofoms in cascading lake basins**

Natalia Amezcua, Robert Gawthorpe, and Joe MacQuaker

#### **4.1 Abstract**

A series of large scale lobes of amalgamated tufa clinofoms are herein interpreted as prograding tufa clinofoms. These large scale carbonate bodies are located at northerly subbasin boundaries in the late Neogene Mayrán Basin system. The tufa clinofoms were deposited onto Cretaceous sandstone ridges that confined coeval, cascading carbonate-dominated lacustrine subbasins. To investigate what controlled their distribution and deposition their basin wide locations were mapped and their stratigraphic and sedimentologic attributes described. The prograding tufa clinofoms radiate broadly northwards. Overall they comprise a main tufa body that may build off subordinate coalesced lobes that bifurcate from the main lobe. Basin wide, the distribution of the tufa lobes was mainly controlled by the preceding topography at the subbasin sill, and by the local base level of the topographically higher lake. The large prograding tufa lobes generally have a subhorizontal top and a steep relief down-dip. Internally, they are composed of a main tufa body with a horizontal top and steeply dipping forests. The tufas comprise macrophyte boundstone lithofacies, that contain abundant calcareous encrustations of plants, bryophytes, algae and calcified microbial laminations. Their depositional dips are preferentially oriented northwards, indicating paleowater flow direction. Pendant and other vadose botryoidal cements in vug or mouldic pores are common in the macrophyte boundstones. Deposition of the tufa clinofoms was controlled by both inorganic and biogenic carbonate precipitation by waters flowing down-dip to the topographically lower subbasin. Basin hydrology influenced lake levels and consequently tufa clinofom formation was likely climatically controlled. These are the first well-preserved, exposed examples of a large scale prograding tufa clinofoms described in the literature.

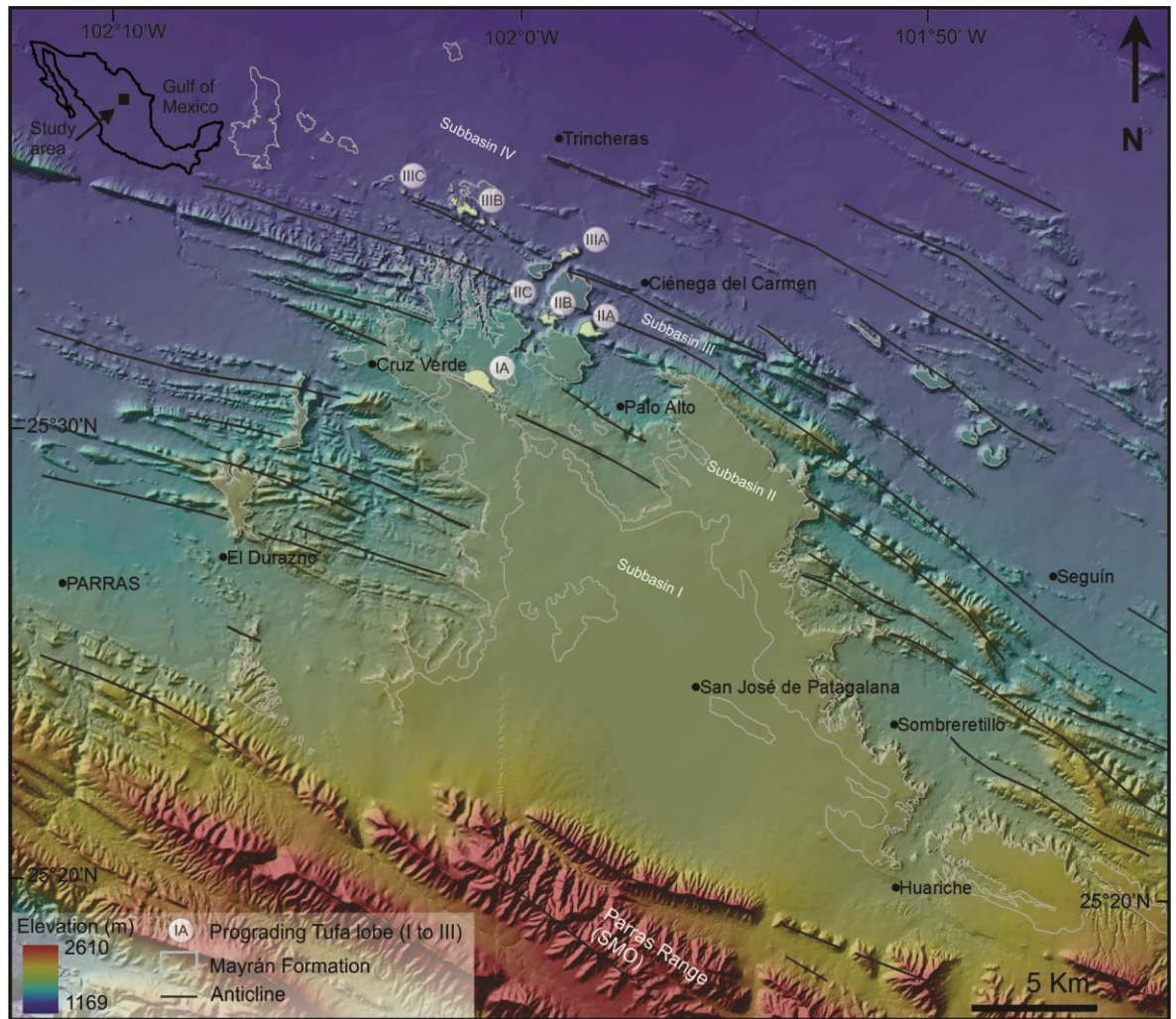
## 4.2 Introduction

Tufa deposition occurs in a variety of continental settings. They commonly form barrages along fluvial systems (Gregory 1911; Pedley, 1990; Pentecost, 1995; Markowska, 2004; Arenas et al., 2010; Vázquez-Urbez et al., 2010), amalgamated deposits at the edge (nickpoint) of waterfalls (Pedley, 1990), irregular beds at lake margins (Pedley, 1990; Benson et al. 1995) and mounds associated with springs in both sublacustrine (Council and Bennett, 1993) and subaerial settings (Pedley, 1990; Ford and Pedley, 1996; Merz-Preiß and Riding, 1999, Pedley et al 2003). Their occurrence and deposition results from a complex interaction between hydrological (availability and volume of water, and water chemical composition), geological (bedrock rock type and tectonics), geomorphological (topography and relief) factors, and biological (nucleation sites and photosynthetically induced calcite precipitation) processes. The large scale geometries of tufa deposits are rarely fully preserved in well exposed lateral and vertical continuous outcrops. Consequently information regarding their large scale morphological attributes and depositional aspects remain sketchy (Pedley et al., 2003). Here are described some large-scale tufa lobes composed of amalgamated tufa clinofolds that prograde down-dip into a lake margin, that is exposed in the Mayrán Basin system. In order to determine the origin of these large scale tufa lobes more fully, their location was analyzed, together with their geometry, stratigraphy, sedimentology, and potential links to lakes hydrology. Finally these large scale tufa lobes were compared with similar sedimentologic features reported in the literature.

### 4.3 Geologic setting

The Late Neogene Mayrán Formation was deposited in four major subbasins collectively named the Mayrán Basin system. The Formation unconformably overlies Cretaceous (Late Campanian to Early Maastrichtian) rocks of the Parras foreland thrustbelt in northeast México (Fig. 4.1) (Amezcuca et al., 2012). The Cretaceous bedrock comprises marine siliciclastic mudstones of the Parras Formation, and marine to continental deltaic siliciclastic mudstones and sandstones of the Cerro del Pueblo and Cerro Huerta formations, Difunta Group (Weidie and Murray, 1967; McBride et al., 1974; Soegaard et al., 2003). The southern margin of the Mayrán Basin system is bounded by Upper Jurassic – Cretaceous carbonate (and subordinate siliciclastic) rocks that form the Parras Range (NW sector of the Sierra Madre Oriental Orogenic Belt). The sedimentary rocks within the foreland and the orogenic belt were affected by the Laramide (Hidalgoan) deformation throughout the Late Cretaceous to Eocene (McBride et al., 1974; Gray et al., 2001; Lawton et al., 2009), creating a series of WNW-ESE-striking, tight, parallel, folds with slightly asymmetric box-fold geometry; and NE-SW-striking tear faults. Thrusting created an overall northward-decreasing structural level, with the highest structural level at the south, near the orogenic wedge, associated with a northward down-stepping pattern of Laramide folds in the Parras foreland (Amezcuca et al., 2012). The Laramide deformation in the Sierra Madre Oriental ended in the Eocene, approximately ~46 to ~41 Ma (Gray et al., 2001; Molina et al., 2008). Subsequent post-Eocene uplift of northeast México resulted in the differential erosion of up to 2 km of strata from the foreland region in the Parras area (Gray et al., 2001). This uneven erosion constructed the landscape upon which the Mayrán Formation deposited. Thus the undeformed Mayrán Formation overlies the rocks of the Parras foreland along a prominent angular unconformity.





**Figure 4.1.**-The Mayrán Basin system location indicating position of relicts of large scale prograding tufa clinoform lobes.

The Mayrán Formation consists of an upward-fining succession that comprises coarse, clastic continental deposits at the base and carbonate-dominated lacustrine units towards the top, which form shallowing-upward cycles, with an overall aggradational stacking pattern. The cycles are capped by evaporites or pedogenized lacustrine carbonate, and are defined by surfaces that can be traced among most of the subbasins (Amezcuca et al., 2012). Clastic deposits include channelized and nonchannelized conglomerates, pebbly sandstones, and calcareous sandy and siliciclastic mudstones. The carbonate deposits include horizontally bedded limestones, evaporite units, and more localized tufa clinoform deposits, the latter being subject of this paper. Post-Maryán deposits include tufas and limestones with lacustrine fauna, deposited in valleys that incised both the Mayrán

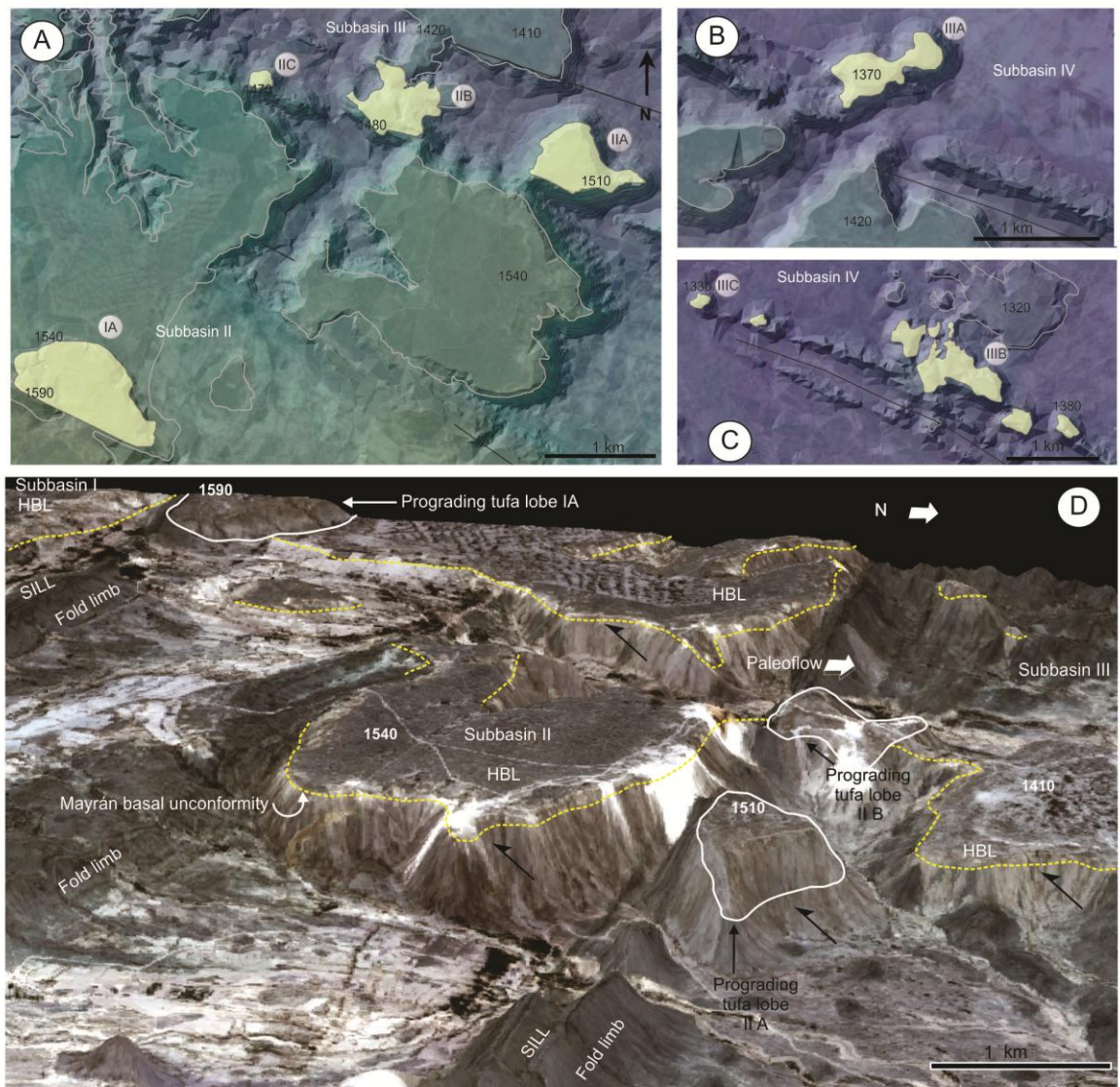
Formation and the Cretaceous bedrock. Some of the tufas were deposited on valley sides. Present day tufa precipitates near springs and stream channels, and locally springs resurge in zones where the Cretaceous rocks are affected by left lateral fault displacement.

Deposits of the Mayrán Formation are found over an area of approximately 2,000 km<sup>2</sup>. They were deposited in four major subbasins (I to IV), that have variable dimensions (2 to >15 km wide to overall 40 km long), but all are parallel to the strike of the underlying Laramide folds. The subbasins occur at different, discrete elevations, ranging from 1700 m in subbasin I in the south, to 1250 m in sub-basin IV in the north. The elevation changes among the subbasins are associated with elongated prominent topographic ridges formed by erosionally resistant Cretaceous sandstones that form the limbs of Laramide folds (Amezcuca et al., 2012).

#### **4.4 The Mayrán Basin system Prograding Tufa Lobes**

##### **4.4.1 Spatial distribution and external form**

Preserved tufa lobes are located at the north-central sector of the Mayrán Basin system. They occur immediately north of the boundaries between subbasins (Fig. 4.1 and 4.2) on topographic changes onto the sandstone bedrock ridges that separate topographically upper from topographically lower lake subbasins. The overall geometry of the tufa lobes, as seen in plan view, is lobe-like, with radial growth broadly to the north (Fig. 4.2). More than one tufa lobe may be present between adjoining subbasins along strike, these may be separated from one and another by up to 2.7 km.



**Figure 4.2-** Large scale prograding tufa clinoform lobes in the Mayrán Basin system. (A, B and C) Digital elevation model integrated with satellite Landsat image, and QuickBird image (D). Numbers indicate elevation in meters. DEM elevation curves (in pale gray colour) every 10 m. Elevation (e.g. 1590) in meters. Prograding tufa clinoforms located at the northern ridge among adjoining subbasins: (A) Prograding tufa clinoform IA, among subbasin I and II, and prograding tufa clinoform bodies II A, B and C among subbasin II and III, and (B and C) Prograding tufa clinoform bodies III A, B, and C among subbasin III and IV. Scale of each body shown in figure A. For basin scale location see figure 4.1. (D) 3D view showing the relations between lake subbasins and the prograding tufa clinoform IA, IIA and IIB. Yellow dashed line underlining basal Mayrán angular unconformity. HBL: Horizontally bedded (lacustrine) limestone. Prograding tufa clinoforms locate on the sills formed by prominent sandstone ridges of fold limbs that compartmentalize the subbasins.

In cross section, the main tufa bodies typically exhibit sub-horizontal top sets and steep relief on the down-dip foresets. Subordinate coalesced lobes that bifurcate from the main lobe may also be present. Individually they possess variable dimensions and subtle lower meter-scale elevation differences with respect to the main lobe (Fig.4.1, Table 4.I). Elevation ranges are estimated based on the height of the tufa top sets with respect to the height of tufa bottom sets that downlap and interfinger with the lacustrine carbonates. In the rest of the subbasins up to three main tufa bodies occur. No evidence of incising channel features connecting the subbasins was identified.

Subbasin	Prograding tufa lobe	Elevation range (m)	Radius (m)
I	IA	1590-1540	700
II	IIA	1510-1420	~1000
II	IIB	1480-1420	700
II	IIC	1480- 1420	150
III	IIIA	1370-1340	820
III	IIIB	1380-1340	160
III	IIIC	1330- 1310	200

**Table 4.I.** Comparative table showing dimensions of major prograding tufa clinofold bodies.

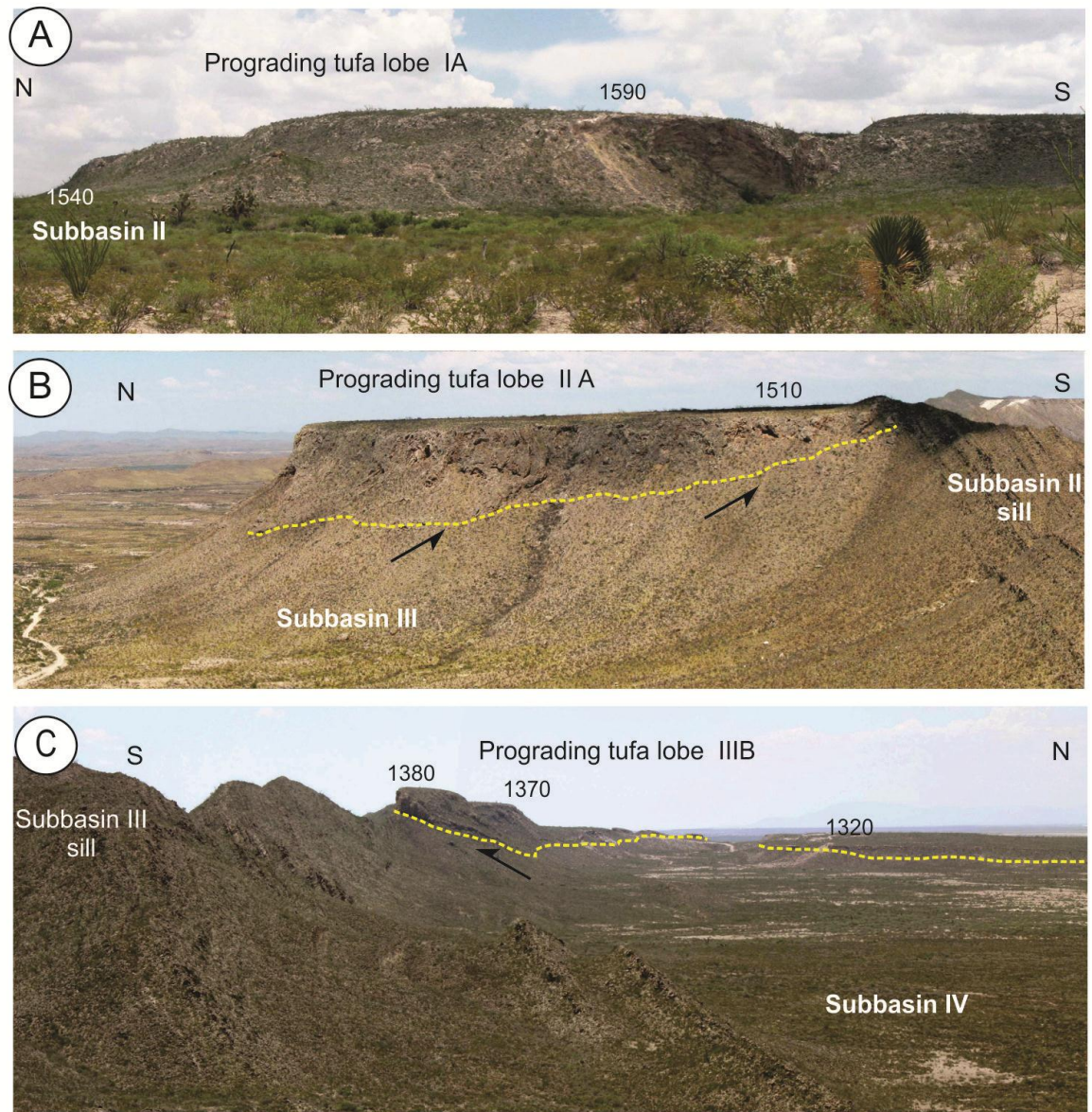
Subbasins I and II connect by one (IA) tufa lobe (Figs. 4.2A and 4.23A). Subbasins II and III, are connected by three major lobes the IIA and IIB, IIC (Figs. 4.I and 4.2A and D) and IIIA, IIIB, IIIC respectively (Figs. 4.2B and C, and 4.3C). The overall range of elevation of the tufa lobe from 30 m up to 90 m (Table 1), however does not represent the total thickness of the tufa lobe itself. Rather, they indicate the elevation range covered by the tufa clinofolds. This is because the tufa clinofolds mantle the steeply dipping topography inherited from the Cretaceous bedrock.

#### 4.4.2 Stratigraphy and Sedimentology

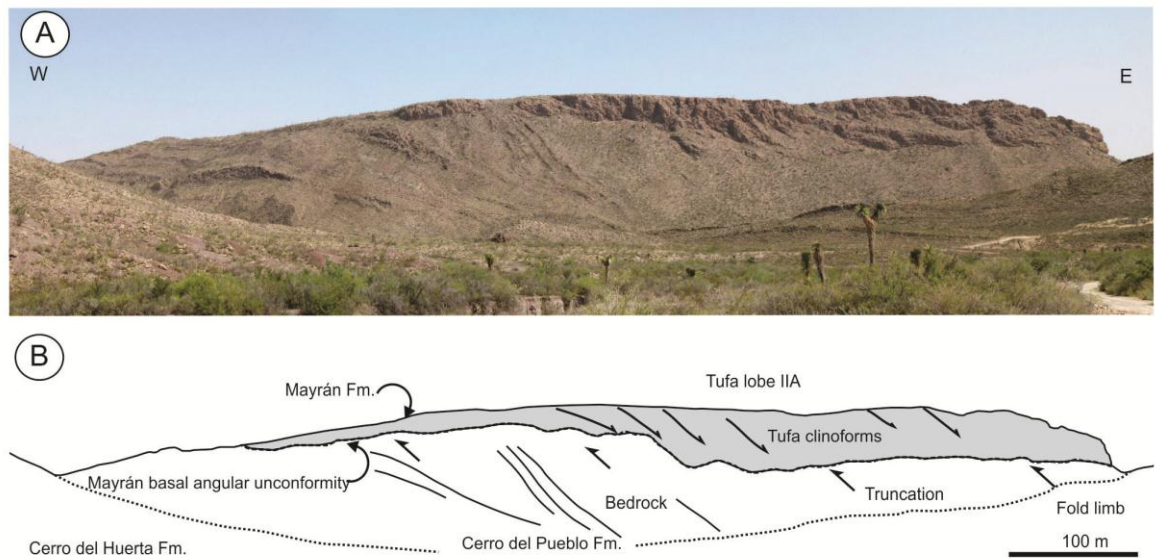
In cross section the large scale tufa lobes consist of spectacular prograding clinofolds. Typically the tufa clinofolds dip between 10° and 60°, and have sigmoidal to oblique geometries (Fig. 4.4). The tufa clinofolds are heterogeneous and their length and thickness vary from 0.1 up to 2 m thick. Irregular surfaces with erosion and dissolution of pre-deposited calcium carbonate coated macrophytes locally affect tops of clinofolds. These surfaces can be traced laterally up to 10 m. Along the up-dip proximal (southern) margins, the clinofolds are composed of subhorizontal tufa top sets which extend laterally for approximately 30 m, and comprise stacked beds up to 1m thick (e.g. locality IIC, Fig.4.2). The toes of the clinofolds downlap onto steeply dipping beds that form the Cretaceous fold limbs (Fig. 4.4), and are interbedded with the horizontally bedded lacustrine limestones (e.g. locality IIB and IIIB, Figs. 4.2 and 4.3 C).

Elevations of the tufa deposits relative to the up-dip horizontally bedded limestones are either broadly similar (e.g. between subbasin I and the tufa lobe IA), or present greater elevation differences, varying up to 40 m. Moreover more than one tufa lobe formed at the northern margin of the same subbasin, and some have different elevation. Here average elevation differences between lobes are from 10 to 20 m.

Sediment sorting is observed from proximal to distal sectors of the prograding tufa clinofold. The tufa clinofold bottom sets deposited immediately on the sandstone ridges contain <10% of very poorly sorted pebble to block size (1 m) angular to subangular clasts of Cretaceous sandstone and siltstone (Fig. 4.5 A and B). Occasionally angular blocks (up to 0.7 m) of tufa are found in some locations near the base of clinofolds, together with dissolution and collapse features (e.g. locality IIB). The sandstone and tufa clasts are either oriented randomly or dipping slightly northwards, supported by the carbonate matrix and cemented either by calcite spar or aragonite (Fig. 4.5 B). Down-dip, the tufa lobes are dominated by calcareous encrustations. Here, boundstone (by both macrophyte and microbial) is the most common depositional texture. Included within these are calcareous encrustations of plants stems and leaves, bryophytes (mosses), algae, calcified microbial laminations and ostracodes (Fig. 4.5).

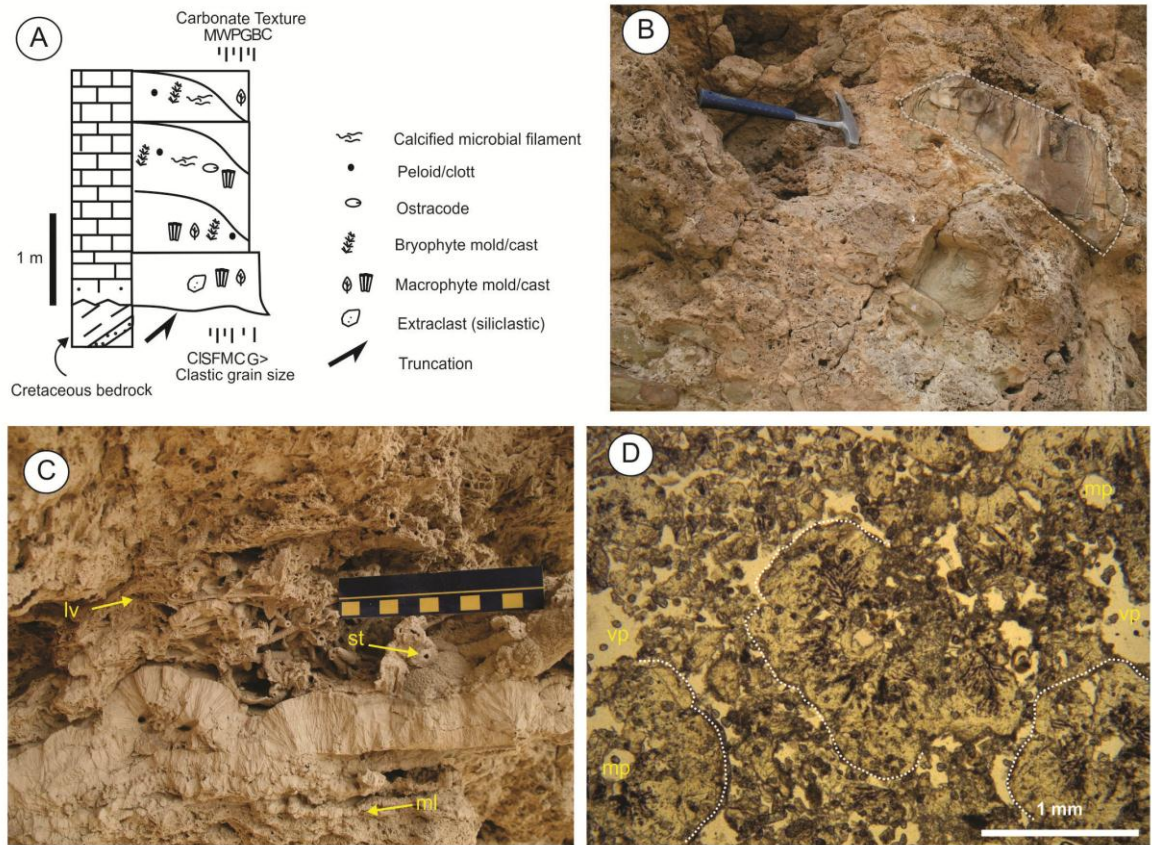


**Figure 4.3-** Field exposure of the large scale prograding tufa clinoform lobes showing their large scale dimensions (radius: IA=700 m; IIA= ~1km; IIB= ~820 m) and position with respect to the sandstone ridges that form the subbasin sill. (A) Subbasin I, (B) Subbasin II; (C) Subbasin III. For basin scale location see Fig. 4.1. Yellow dashed line mark basal angular unconformity.

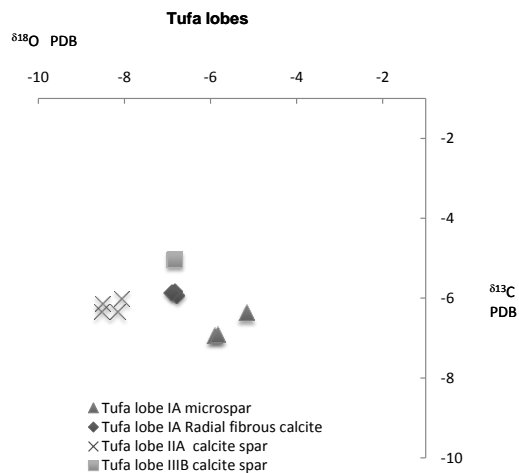


**Figure 4.4–** (A) Detail of prograding tufa clinofolds in tufa lobe IIA. (B) Interpretation of image A, showing clinofold dipping with prograding pattern, radially northwards.

These calcified biogenic components are either randomly or preferentially oriented parallel to the dip of the clinofolds. Due to the rock fabric the tufas contain abundant pores (>20%). Pore types include a combination of growth-framework, shelter, interparticle, intraparticle, fenestral, intercrystal and mouldic porosity (cf. Choquete and Pray, 1970). Together with non-fabric selective vuggy pores which have sizes up to 0.40 m width. Geopetal structures and botryoidal cement fabrics are common. Cements are heterogeneous and consist of isopachous rims of coarsely crystalline bladed crystals some with fan-shape, micrite (average values of  $\delta^{18}\text{O}_{\text{calcite}}$  -6.74 ‰ and  $\delta^{13}\text{C}_{\text{calcite}}$  -5.64‰ in tufa lobe IA, Fig. 4.6) peloid cements, micrometre-sized crystalline equant calcite spar crystals (average values of  $\delta^{18}\text{O}_{\text{calcite}}$  -6.85‰ and  $\delta^{13}\text{C}_{\text{calcite}}$  -5.87 ‰ in tufa lobe IA), and radial fibrous calcite spar (average values of  $\delta^{18}\text{O}_{\text{calcite}}$  -6.83‰ and  $\delta^{13}\text{C}_{\text{calcite}}$  -5.83 ‰ in tufa lobe IIIB, and average values of  $\delta^{18}\text{O}_{\text{calcite}}$  -8.31 ‰ and  $\delta^{13}\text{C}_{\text{calcite}}$  -6.20 ‰ in tufa lobe IIA).



**Figure 4.5.-** (A) Idealized stratigraphic log of the proximal part of the prograding tufa lobe. Large macrophyte components are less common towards the top of the tufa clinoform, and bryophyte and laminar encrustations become more common. Carbonate textures: M-mudstone, W-wackestone, P-packstone, C-crystalline, B-boundstone. Clastic grain size: Cl- clay, S-silt, Vf-very fine grained, F-fine grained, C-coarse grained, G-gravel and coarser. (B) Detail of large Cretaceous sandstone blocks (underlined by dotted line). Hammer (35cm) for scale. Distal tufa clinoforms lack of sandstone extraclasts. (C) Close up to tufa fabric, note diversity of calcified components such as leaves (lv), stems (st), microbial laminations (ml) forming the tufa clinoform. (D) Coarse calcite crystals calcifying bryophyte? Note abundant vug pores (vp) and mouldic pores (mp).



**Figure 4.6.** Stable isotope plot of calcite cements from the tufa lobes. Total of analyzed samples  $n=12$ .



## 4.5 Discussion

In the tufa lobes, vegetation colonized both the Cretaceous bedrock and active water flowing areas on the pre-existing tufas. The presence of calcified (coated), well preserved macrophyte and bryophyte moulds, together with microbial laminations (biofilms), and geopetal cements, indicate that these biological components formed suitable nucleation sites for both inorganic and biogenic calcite precipitation (Fig. 4.7).

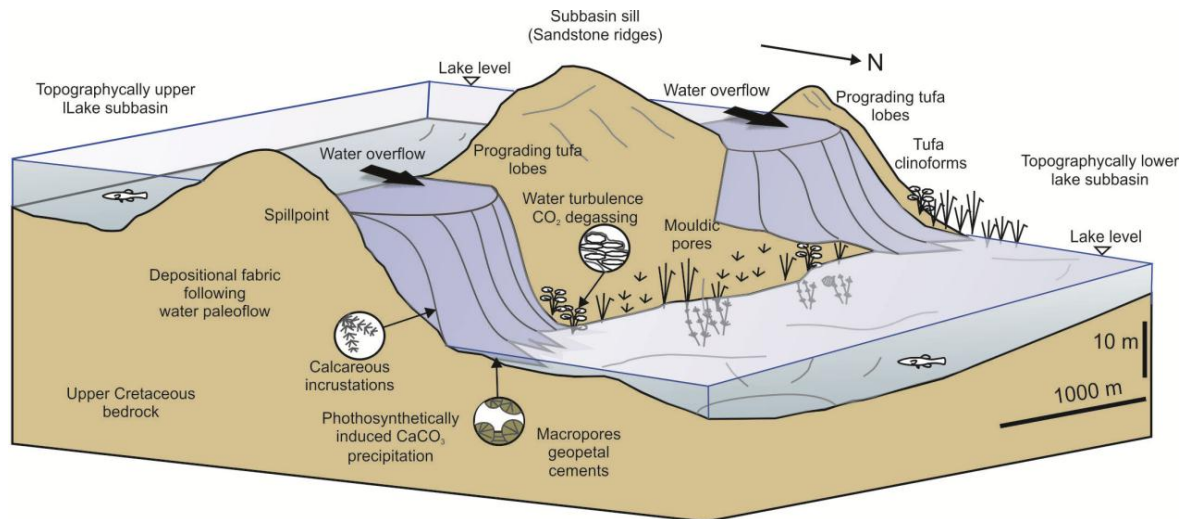
The tufa clinofold bodies are dominated by calcareous encrustations where macrophyte moulds are preserved together with several calcified microbial morphotypes, and fabrics indicative of microbial and biogenic activity. These biogenic components imply that biomediation processes promoted calcite precipitation. Biogenically mediated calcite precipitation involves both, constructive and destructive mechanisms, that include *in situ* microbial calcification, trapping and binding of carbonate particles, and microbially induced calcification; while destructive processes include substrate destruction by dissolution, boring, and production of residual micrite (Jones, 2010).

To achieve calcium carbonate precipitation in these settings, water commonly requires supersaturation (5 to 10 times) with respect to calcite (Chen et al., 2004). This saturation is caused by  $\text{Ca}^{2+}_{(\text{aq})}$  and  $\text{CO}_3^{2-}_{(\text{aq})}$  ionic activity and delivery rate, together with metabolic uptake of  $\text{CO}_2$  by photosynthetic biota, as water velocity and turbulence directly affect biofilm photosynthetic activities (Pedley and Rogerson, 2010). The biofilm contains exopolymeric substances (EPS) that consist of organic substances, mostly polysaccharides, organic acids, proteins, lipids and nucleic acids (Nichols and Nichols, 2008). The EPS helps of microorganisms to attach on different substrates, and acts in trapping, binding  $\text{Ca}^{2+}$ , immobilizing water and precipitation of  $\text{CaCO}_3$  sediment (Turner and Jones, 2005; Dietrich and Sibling, 2010).

The tufa clinofoms are all located on the northern side of the sandstone bedrock ridges that separate subbasins with different elevation, and are overall distributed in the north-central sector of the Mayrán Basin system (Fig. 4.1). They formed at slight topographic depressions occurring in the sandstone bedrock ridges. The tufa clinofoms deposited here can be traced up-dip and down-dip into coeval horizontally bedded lacustrine carbonate facies (Fig. 4.7). Therefore their locations appear to be controlled by the preceding topography of the subbasin sills, and by the local base level of the topographically higher lake. As a result they indicate subbasin spillways of water flowing onto the sill, from the topographically upper to the topographically lower lake subbasin, as demonstrated by the paleoflow directions of the tufa clinofoms which dip broadly northwards. Tufa clinofoms continued to form onto pre-existing tufa, and progressively stacked one upon another. Therefore, they are constructive progradational features overall. The presence of sub-horizontal topsets in the tufa lobes also indicates that locally aggradation occurred while they were forming.

There is no evidence of channels connecting the subbasins, thus, the main source of water to form the tufa clinofoms came directly from the topographically upper lake. It is therefore likely that high lake level fluctuations in the level of the topographically upper lake strongly controlled the development of the tufa bodies at the sill. Frequent to intermittent lake overflow conditions, occur in the spillways of overflow and balance filled lakes (see Carroll and Bohacs, 1999; 2001, Carroll et al., 2010). These lake conditions were determined for the Mayrán lakes (Amezcuca et al., 2012). It is therefore suggested that basin scale hydrology strongly controlled the development of the prominent tufa clinofom lobes when the lakes were hydrologically open.

Basin scale evidence of episodes of lake desiccation and subsequent flooding are documented in the lacustrine lithofacies, by the presence of evaporite crusts and pedogenically overprinted lacustrine carbonates (e.g. Amezcuca et al., 2012). In the tufa clinofoms, these events are recorded by major irregular surfaces that truncate older clinofoms, which are followed by reactivation surfaces where ripped up angular tufa blocks were redeposited at the base of younger clinofoms. It is uncertain if the subaerial exposure surfaces present in the horizontally bedded lacustrine carbonates, are related with the surfaces that truncate the tufa clinofoms.



**Figure 4.7.-** Idealized model for large scale prograding tufa clinoforms formation in the lobes. Water from the topographically upper lake basin spilled over the sill where the tufa clinoforms formed while water flow downslope to the topographically lower lake subbasin.

Two major implications arise from the distribution of the prograding tufa clinoforms in the Mayrán basin system. The first implication relates to their down dip (south to north) distribution in the basin and the second to their position along strike of the sandstone ridges, in individual subbasins. Based on their down dip deposition, and considering their stratigraphic relations (e.g. distal tufa clinoform toes interfinger with the lacustrine carbonate lithofacies in all the subbasins), it is uncertain if the southernmost tufa bodies are older than those deposited in the subbasins northwards. Considering their along strike distribution, we speculate that tufa lobes formed along the same ridge are approximately coeval, and those with lower elevation were likely produced by subordinate lobe shifts. This possibly resulted during progradation of tufas caused by changes in direction of water flow.

Similar sedimentological features forming tufa lobes on hill slopes are known as spring line tufas. These tufas develop from spring or stream resurgence, and deposit on valley sides, forming lobate or multilobate, convex to flat surface deposits, thickening away from the source creating a wedge like profile (Pedley, 1990; Ford and Pedley, 1996). Tufa lobes in the Mayrán Basin system share some distinctive characteristics with perched springline tufas, such as: deposition on valley sides/ basin sills, forming discrete lobes, having wedge shaped profiles, and flat tops, their distal slope is steep, with tufa breccias and speleothem cements (e.g. Pedley, 1990; Ford and Pedley, 1996; Pedley et al 2003).

An important difference, however is that; the perched spring-line tufas form at spring resurgence points (e.g. Ford and Pedley, 1996), while the prograding tufa clinofolds form associated to direct overflow of lake waters.

Because overflow of the lake waters influences prograding tufa deposition, the resulting  $\delta^{18}\text{O}$  values of the tufas could give information about isotopic values of the waters involved in the tufa carbonate precipitation (e.g. Jansen et al., 1999), in this case those of the topographically upper lake. Oxygen isotopes are more sensitive to physical changes in the lake systems (e.g. Andrews et al., 2000), because of local effects such as evaporation/ precipitation ratios and water residence time that ultimately effect the individual isotopic composition of the lake waters (see Leng and Marshall, 2004).

Isotopic variability of calcite cements in the tufas forming the prograding lobes, was likely influenced by the isotopic composition of the lake water, local production, and vadose diagenesis. Isotopic  $\delta^{18}\text{O}_{\text{calcite}}$  values of calcite spar cements in the tufa lobe IA (-6.8‰ average), and the radial fibrous calcite cements in IIIA (-6.8‰ average) are less negative, compared to those in the calcite spar cements in IIA (-8.31‰ average). Compared to the  $\delta^{18}\text{O}_{\text{calcite}}$  isotopic values, the  $\delta^{13}\text{C}_{\text{calcite}}$  values (-5.85‰ average) are less negative. This relative enrichment is considered to be produced during cyanobacterial photosynthesis as  $^{12}\text{CO}_2$  is extracted preferentially, either by photosynthetic pathways or degassing by flow turbulence, causing supersaturation of calcite in the microenvironment around the cyanobacterial cells, resulting in precipitation of dissolved inorganic carbon preferentially enriched in  $^{13}\text{C}$  (e.g. Merz, 1992, Andrews et al., 1997, and 2000). Isotopic data, however, are not conclusive to discriminate the potential input of spring waters which requires further studies. See chapter 5 for further reference on isotopic analysis of lacustrine carbonates.

## 4.6 Conclusions

The tufa lobes in the Mayrán Basin system contain tufa clinofoms that dip broadly northwards, downlapping onto the sandstone ridges that once confined the lake subbasins with different elevations. Up-dip, proximal to the topographically upper lake, and down-dip to the topographically lower lake, the tufa clinofoms interbedded with horizontally bedded lacustrine limestones. The former presece of these stratigraphic relations, strongly suggest that tufa clinofom development was controlled by episodes of standing water in the topographically upper lake. They acted as spillpoints forming constructive waterfalls that connected coeval lake subbasins. Mayrán lakes were relatively shallow (<20 m), and their bathymetry was partially controlled by the height of the sill.

Tufa deposits differ from those in the lakes as they form not under subaqueous but in subaerial conditions. The tufas comprise macrophyte boundstones formed by encrustations and cast of plants, mosses, algae and microbial filaments. They were produced by calcium carbonate precipitation by both phothosyntetically-induced and inorganically by CO<sub>2</sub> degassing, as water flowed down dip to the lower subbasin. Stacked beds of these tufas form both aggradational but mainly progradational large scale features. Fluctuations of water supply over the tufa clinofoms controlled their development, by stopping or promoting their deposition. Further re-establishment of water supply onto preceding tufa clinofoms may either have caused the continued build-up of the main prograding tufa lobe, or will form a different subordinated lobe. This study suggests that subbasins with a common hydrology can be connected by constructive progradational features developed at the subbasin sill. The observations made here on the prograding tufa clinofoms, may therefore be used as valuable proxy indicators of hydrological links between subbasins, but also as indicators of former individual paleobase levels of compartmentalized lake subbasins.

## **Chapter 5**

## Chapter 5

### Lacustrine carbonate lithofacies in the Mayrán Formation

Amezcuca, N., Macquaker, J. H. S, Gawthorpe, R., and Marshall, J.M.

#### 5.1 Abstract

Lithofacies analyses were undertaken on a suite of well-exposed carbonate deposits from the (late Neogene) Mayrán Formation, in the Mayrán Basin system, northeast Mexico to investigate the controls on carbonate lithofacies variability in a series of linked lacustrine subbasins, with a common hydrology yet very different inputs. The rocks in the four subbasins were investigated utilising field observations, coupled with geochemical (carbon and oxygen stable isotopes, whole rock XRD, and TOC) and petrographic techniques (optical, and electron optical methods).

The lacustrine carbonates contain variable proportions of production-derived components, with subordinate proportions of detrital and early diagenetic components. The lithofacies contain, inorganic and organic calcite (average 91% CaCO<sub>3</sub>), and organic matter (10.5% to 13.8 % average 12.6 % TOC), together with minor detrital quartz, feldspar and clay. Nine sub-facies were identified: ostracode mudstone-wackestone, clotted boundstones, gastropod wackestone-packstones, oncoid wackestone-packstones, charophyte wackestone-packstones, stromatolites and associated evaporite minerals. Isotopic composition of specific components such as micritic laminations in stromatolites ( $\delta^{13}\text{C}_{\text{calcite}}$  -6.3‰ and  $\delta^{18}\text{O}_{\text{calcite}}$  -8.0 ‰), and micritic matrix from samples in all the subbasins,  $\delta^{13}\text{C}_{\text{calcite}}$  -5.7 ‰ and  $\delta^{18}\text{O}_{\text{calcite}}$  -7.8 ‰), indicate that overall calcite deposition occurred in freshwater lakes. Non (e.g. charophytes) to orange dull luminescence (micrite) strongly suggest that *in situ* carbonate production occurred, and that most of these particles were delivered either by suspension settling through the water column or by *in-situ* disaggregation of larger particles on the lake floor. Together these processes contributed to the local production of lime mud. Rare microtextural evidence of scour surfaces however, indicates that occasionally the sediment was eroded and transported laterally.

Intense to moderate bioturbation (BI 1 to 4), indicates that deposition took place under predominantly oxic conditions. Moreover, significant organic matter was preserved in these lacustrine rocks (12.6 % TOC). Moderate sedimentation rate and moderate production rate is likely to have controlled organic matter preservation.

The lacustrine lithofacies were deposited in proximal and distal lacustrine settings. Stratal stacking patterns are organized into shallowing upwards cycles (0.3-2.5 m thick), which are capped either by evaporites or beds with a pedogenic overprint. Their stacking patterns reflect lake level variations which can be recognized in all the subbasins. The lithofacies architecture within each subbasin forms parasequences that overall exhibit aggradational geometries. The lithofacies and their large scale geometries also indicate deposition occurred in a series of relatively shallow (<10 m), lake systems with ramp-like margins. The aggradational stacking patterns of the carbonates and the presence of subordinate evaporites suggest that basin hydrology (water supply and precipitation/evaporation ratios) had an important influence on facies architecture and cyclicity. The Mayrán Formation was likely deposited under overfilled to balance-filled lake conditions; although balance-filled conditions with an open hydrology were more likely.

Overall, facies variability in the lacustrine carbonate lithofacies was controlled by accommodation, basin inherited geomorphology, and basin hydrology, which ultimately controlled clastic trapping, solute inputs, water chemistry, primary production, and lake level changes. We interpret that all these controls were largely driven by climate.

## 5.2 Introduction

The fill of lake basins is controlled by a complex interaction of forcing mechanisms including, regional climate, basin hydrology, basin geology, geomorphology and tectonics (Glen and Kelts, 1991; Sarg, 2001). These forcing mechanisms ultimately control: i) accommodation, ii) lake level variations, iii) type of sediment yield iv) water chemical composition; v) and lithofacies variability (Eugster and Hardie, 1975; Talbot and Livingstone, 1989; Smoot and Lowenstein, 1991, Bohacs et al., 2000a, Carroll and Bohacs, 1999 and 2001, Gierlowski-Kordesch 2010)



Lacustrine successions commonly contain varying proportions of clastic and carbonate sediments, sedimentary organic matter, sulfates, chlorides, and clay minerals (Eugster and Hardie, 1975; Lowenstein and Hardie, 1985; Rosen and Warren, 1990; Armenteros et al., 2010; Cohen, 2003). These components occur as products of clastic inputs of detrital carbonate to the basin, primary production and/or chemical precipitation within the lake, combined with diagenetic alteration of the lake sediments once they had been deposited.

Carbonate lakes develop on both siliciclastic and carbonate bedrock, particularly where the inputs of siliciclastic detritus are either episodic or restricted (e.g. Cohen, 1989 and 2003; Gierlowski-Kordesch et al., 1998; Gierlowski-Kordesch 2010). Precipitation of carbonates in lakes is largely dependent upon how much carbonate detritus enters the lake and how much dissolved carbonate is present in the water (Gierlowski-Kordesch, 1998, and 2010).

Recognizing the processes involved in sediment production (of both carbonate and organic matter), processes of deposition and type of sediment yield, and potential diagenetic pathways that affect these sediments, can help us to understand the controls on facies variability in a carbonate dominated lakes.

This study aims to investigate how primary production, variable inputs of clastic detritus and diagenesis controlled carbonate lithofacies variability, and stacking patterns in a series of lacustrine carbonate subbasins.

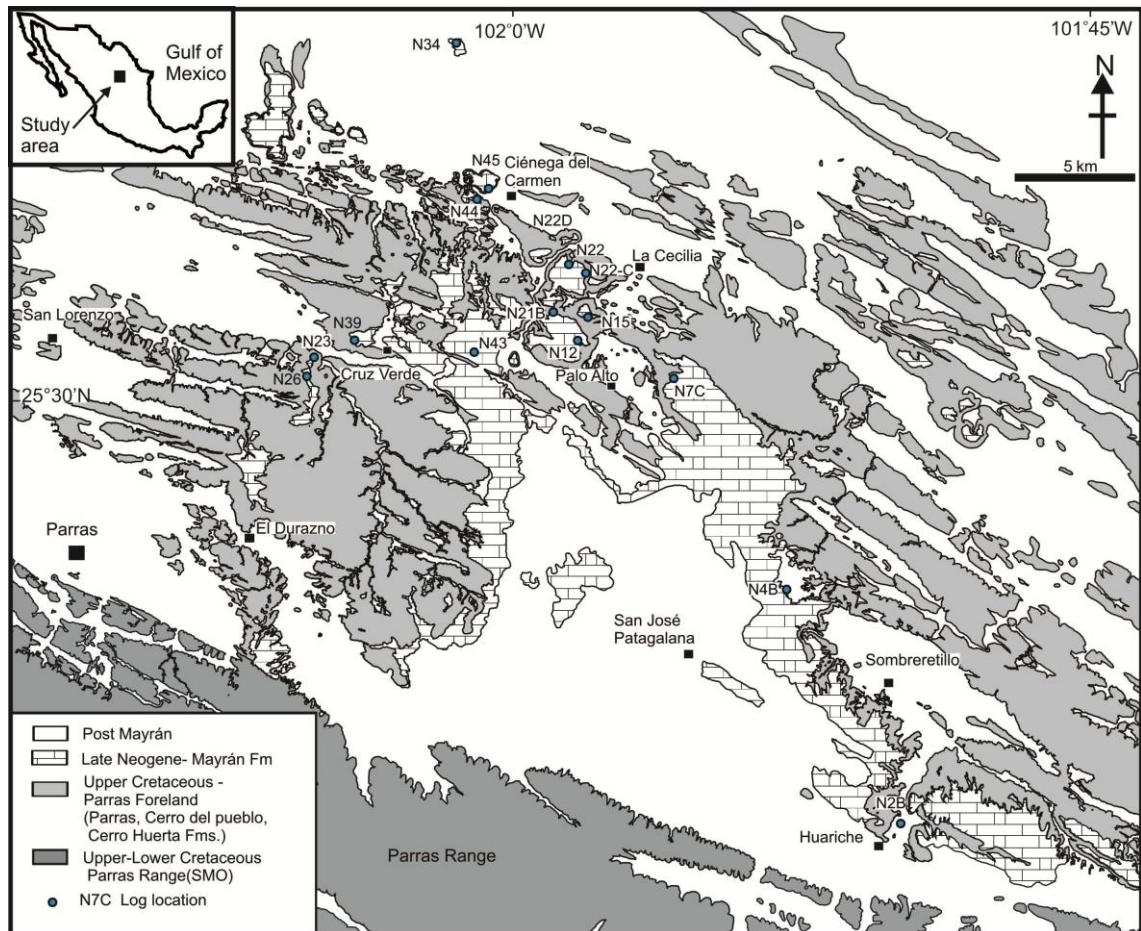
The Late Neogene Mayrán Basin system in northeast México was selected for this study and comprises four coeval carbonate-dominated lacustrine subbasins, each containing varying proportions of clastic sediment, and yet were hydrologically linked (Amezcuca et al., 2012). The Mayrán Basin system is a particularly suitable natural laboratory because: i) the succession is preserved in excellent exposures that have neither been subject to neither significant burial nor deformation, ii) the infill is carbonate dominated, iii) clastic detritus was mainly trapped in the southernmost subbasin, iv) and overall the other forcing mechanisms (e.g. climate, hydrology, and basin geomorphology) controlling deposition were kept broadly constant.

In order to meet these aims (A) the background geology of the Mayrán Basin system is provided, (B) the lithofacies architecture within each subbasin were mapped, (C) the lithofacies present are described and characterized using petrographic and geochemical techniques, (D) the controls on the lithofacies variability were investigated, and (E) the overall controls accommodation in the subbasins discussed.

### 5.3 Geologic Setting

The late Neogene Mayrán Formation (see Imlay, 1936 and 1937) is a fluvio-lacustrine succession that was deposited unconformably, in a series of subbasins (The Mayrán Basin system), that unconformably overlie Late Campanian to Early Maastrichtian rocks within the Parras foreland fold-and-thrust belt in northeast México (Fig. 5.1) (Amezcuca et al., 2012). The Cretaceous bedrock consists of marine siliciclastic mudstones (Parras Formation), and marine to continental deltaic siliciclastic mudstones and sandstones (Cerro del Pueblo and Cerro Huerta formations) of the Difunta Group (Weidie and Murray, 1967; McBride et al., 1974; Soegaard et al., 2003). Upper Jurassic–Cretaceous aged carbonate and subordinate siliciclastic rocks of the Parras Range (part of the Sierra Madre Oriental orogenic belt) form the southern margin of the Mayrán Basin system.

The Mayrán Basin system comprises four major subbasins that occur at different elevations, ranging from 1700 m (southern subbasin I) to 1250 m (northern subbasin IV). Subbasin fills vary from south to north. Subbasin I contains coarse-grained detrital components yield from the Parras Range, which consist of more than 80% limestone clasts. The rest of the subbasins in contrast contain only clastic material derived from the bounding sandstone bedrock ridges (Amezcuca et al., 2012).



**Figure 5.1.-**Simplified map with location and distribution of the Mayrán Formation. Stratigraphic log location indicated.

Overall, the Mayrán Formation stratigraphy comprises by coarse clastics at the base (non-channelized conglomerates, channelized conglomerates, and pebbly sandstones) that grades into finer-grained clastic rocks (calcareous sandy and siliciclastic mudstones). In contrast, the upper part of the Mayrán Formation is dominated by the horizontally bedded limestones with discrete intervals of siliciclastic mudstone and evaporites. Large tufa clinofolds forming lobe-like (up to kilometre scale) features deposited onto the sandstone ridges at the subs basin sills also associate to the Mayrán Formation (Amezcuca et al., 2012).

## 5.4 Methods

In order to identify the lithofacies present and the effects of lithofacies variability in the subbasins of the Mayrán Basin System, fifty-five sections were measured and logged. The locations of these logs were chosen specifically so that both regions where clastic inputs were dominant and regions where carbonate production was dominant were well-documented. Some of the logged locations are shown in Figure 5.1, and representative logs are shown in Figure 5.2.

The lithofacies present were studied using petrographic and whole rock geochemical techniques. A total of 195 thin-sections were described then scanned using a flat-bed scanner (Epson1250). Optical and electron optical (plane light, BSE, cold CL microscopy) analyses were performed on regular (48 x 26 mm) and large (75 x 48 mm), unusually thin (*circa.* 20  $\mu\text{m}$ ) sections to determine mineralogy and micro-fabric relations. Photomicrographs were taken using a Nikon Labophot Pol petrographic microscope (at x2, x4, x10, and x20 magnifications), and a Jeol 6400 scanning electron microscope (SEM), equipped with Link 4-quadrant, solid state backscattered electron detector, Oxford Instruments energy dispersive X-ray detector, and Link eXL microcomputer running ZAF-4 analytical software, were used to gather the data. The SEM was operated at 20 kV and 0.2 mA at a working distance of 15.0 mm, to produce images where individual minerals can be identified on the basis of their different backscattered coefficients ( $\eta$ ). Cathodoluminescence (CL) of 24 samples was achieved using a CITL, (model CCL8200 MkIII) cold cathode luminoscope, with operating conditions of 10-120 kV accelerating voltage, gun current of 250-300  $\mu\text{A}$  and 0.2 Torr vacuum.

The mineralogy of the sediment (122 samples) was also investigated using X-Ray diffraction (XRD) to determine the bulk rock mineralogy, and electron microprobe analyses to determine specific cement composition, using a Philips PW1730 X-ray diffractometer was used and 20 mA, utilising a copper  $\text{K}(\alpha)$  radiation with a step size and time constant of  $0.01^\circ$  and 2.00. Calcite staining with a solution of dilute hydrochloric acid containing alizarin red and potassium ferricyanide was carried out in selected samples (20) to assess the characterization of carbonate types (e.g. Dickson, 1965, 1966). Bioturbation Index criteria of Taylor and Golding (1993) after Reineck (1963) is used here to identify the grade and degree of bioturbation.

The nomenclature of Campbell (1967) was used to characterize and describe geometries of bed and lamina. Porosity classification is based on Choquette and Pray (1970) criteria. Identification of microporosity, and presence of baryte and celestine cements was determined under BSE examination.

Fifty three  $\delta^{18}\text{O}$  and  $\delta^{13}\text{C}$  stable isotope analyses were performed on 2 specific carbonate components present in samples from subbasin I to IV to constrain the origins of these components. The two components were: i) micrite present in matrix, coated grains, and other microbial laminations, and ii) calcite spar cement occluding pore space in both matrix and allochems. About 2 to 5 mg of these components were obtained by microdrilling selected areas of polished slabs, under petrographic microscope observation. The measurement of carbon and oxygen isotope ratios was analyzed on an automated VG SIRA 12 mass spectrometer at the University of Liverpool. Carbon and oxygen isotope data are reported in conventional delta ( $\delta$ ) notation in “parts per mil” (‰) relative to V-PDB (Pee Dee Belemnite Standard). Accuracy and reproducibility of the isotopic analyses was assessed by replicate analysis of BCS2 (internal calcite standard) against NBS-19 and two internal calcite standards.

Thirty samples from three stratigraphic sections in subbasin II were also selected to perform TOC and  $\delta^{13}\text{C}_{\text{organic}}$  analyses to evaluate the proportions of organic matter and potential origins. The samples were prepared by decarbonating whole rock powder with 1N HCl, rinsed in distilled water and dried for 24 hours at 50°C, and analyzed with a Carlo Erba NA1500 Series II Elemental Analyzer, coupled to a ThermoElectronDeltaVPlus Mass Spectrometer, at the Stable Isotope Laboratory of Memorial University of Newfoundland, Canada.

#### 5.4.1 Nomenclature of Mayrán carbonates

In carbonate depositional environments, hydrodynamic, biogenic and diagenetic processes determine rock fabric and texture (Dunham, 1962; Tucker and Wright, 1990). Continental carbonates are characterized by particles derived from a wide variety of origins (both from within the basin and derived from inputs to the basin) and exhibit a wide range of microfabrics. For practical purposes, the classification scheme of Dunham (1962) is used here to describe the carbonate lithofacies texture, whereas the terminology for crystal textures and fabrics is based on the classification scheme redefined by Friedman (1965).

Lithofacies names are initially based on the main fossiliferous or diagenetic components and these are suffixed by a description of rock texture. Overall the components are derived from; a) *in situ* production, b) from detrital inputs and c) from subsequent diagenesis. The **production**-derived components (autochthonous) comprises allochemical (either direct ‘bioclastic’ or biogenically induced) materials including shell debris, calcareous algae, vertebrate remains, oncoids, peloids, and stromatolites as well as organic carbon related to primary production within the subbasins. The **detrital** (or allochthonous) component is derived from local non-carbonate sources and consist of clay minerals and silt-grade quartz and other siliciclastic minerals. Finally, the **diagenetic** components include cement components, and consist of authigenic minerals such as sulfates, halite, silica, and carbonate cements.

‘Micrite’ is used here in a non-genetic sense for carbonate particles <4 µm (Milliman et al., 1985; Jones, 1989; Jones and Renault, 2010), regardless of the mechanism that underpins its formation. Many researchers (e.g. Folk, 1959; Dunham, 1962; Friedman, 1985; Milliman et al., 1985; and Jones and Renault, 2010) have discussed the various processes likely responsible for the formation of micrite and the use of this term. Dense microcrystalline to cryptocrystalline calcite are then here considered part of the finer (<4 µm) fraction of carbonate particles. Finally the term ‘mudstone’ is used as a non-genetic and non-mineralogic sense to describe fine grained sedimentary rocks of both carbonate and siliciclastic composition with average grain size less than 62.5 µm (see Macquaker and Adams 2003; for further references).

## 5.5 Lithofacies Analyses

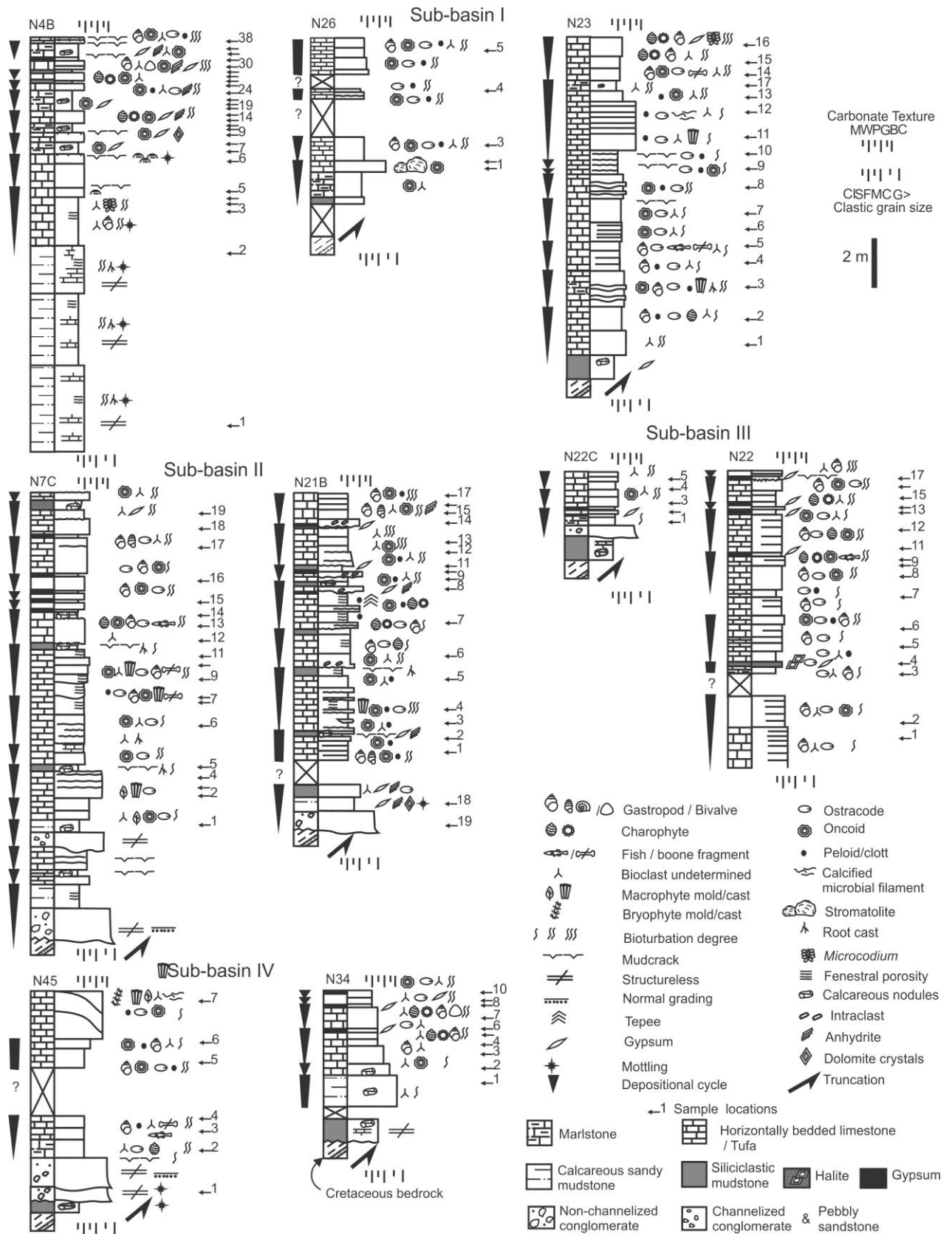
Overall six major lithofacies composed of both clastic and carbonate rocks form the sedimentary fill of the Mayrán Basin system (Table 5.1). Clastic lithofacies comprises non-channelized and channelized conglomerates, and pebbly sandstones that grade into finer-grained clastic rocks (calcareous sandy and siliciclastic mudstones) that change laterally into horizontally bedded limestones and evaporites. This section focuses only on the carbonate and evaporite lacustrine deposits of the Mayrán Formation.

The horizontally bedded limestones are widely distributed in the Mayrán Basin system subbasins, where they form prominent, laterally continuous, erosion resistant exposures, up to 13 m thick. The horizontally bedded limestones are subdivided into 9 lithofacies based on detailed field and petrographic analyses, mainly by their differences in their microfabrics, and fossil content (see Table 5.1 for summary). Descriptions of each sub-facies are given below. These descriptions are presented in the stratigraphic order in which they occur at most localities.

Summary of lithofacies types of the Mayrán Formation								
ID	Lithofacies	Texture & components (Description)	Bed Geometry	Sedimentary / Biosedimentary structures	Biological components	Bioturbation	Interpretation	Associated lithofacies
1	<b>Horizontally bedded limestones</b>							
1a	<b>Ostracod Md-Wk</b>	Md, Wk	Tabular, laminated	Peloids, oncoids	Ostracods mainly articulated, subordinate allochems, undetermined globose calcareous algae?	poorly bioturbated, cryptic bioturbation	Nearshore-offshore/ open lake	Peloid Md-Wk, gastropod Wk-Pk
1b	<b>Clotted Boundstone</b>	Boundstone, Wk- Pk	Tabular, laminated	Thinly bedded/ Peloids, oncoids	Ostracods, oncoids, gastropods, phytocast	Criptic bioturbation	Nearshore-offshore/ open lake	Oncoid Wk-Ru, ostracod Md-wk, Macrophyte and microbial boundstone
1c	<b>Gastropod Wk-Pk</b>	Md, Wk, Pk	Tabular, laminated	Peloids, oncoids, undifferentiated calcified structures (calcareous allochems)	Limnaeidae, Physidae and Planorbidae types, ostracods, possible bivalves, fish remains, charophyte.	Moderately to highly bioturbated	Littoral and nearshore-sub-littoral	Ostracod Wk, Charophyte Wk-Pk, Oncoid wk-Bou, Macrophyte Bou.
1d	<b>Oncoid Wk-Pk</b>	Wk-Pk	Tabular, irregular	Internally laminated,	ostracods	Moderately bioturbated	littoral (Nearshore)	Gastropod Wk-Pk, Peloid Wk-Bou.
1e	<b>Stromatolite</b>	Boundstone	Irregular distribution along bed surfaces	Internally laminated	ostracods, calcified microbial filaments (cyanobacteria sheaths)		Littoral (nearshore)	Siliciclastic mudstone, Calcareous sandy mudstone, Marlstone
1f	<b>Charophyte Wk-Pk</b>	Wk, Pk	Tabular	Peloids, oncoids, undifferentiated calcified structures	Gastropods, ostracods, fish remains	Moderately to highly bioturbated	Littoral (nearshore), sub-littoral	Gastropod Wk-Pk, Marlstone
1g	<b>Macrophyte boundstone</b>	Boundstone, Wk- Pk-Gr	Tabular and lenticular	Macrophyte calcareous encrustations (phytcasts), peloids, oncoids. Very prone to karstification	Ostracods, calcified microbial filaments	Poorly bioturbated, to moderately bioturbated	Shore, littoral (nearshore)	Allochem Wk-Pk, Clotted Bd
1h	<b>Marlstone</b>	Wackestone-Packstone, Gr, breccia	Irregular	Intraclasts, nodular, may be affected by displavive gypsum	bioclasts	Moderately bioturbated	Shore and littoral (nearshore) sediment reworking, flooding episode in shallow lake	Evaporites, Charophyte Wk-Pk, Gastropod Wk-Pk, Oncoid Wk-Pk, Calcareous sandy and Siliciclastic mds.
1i	<b>Crstalline Carbonate</b>	Microspar, sparite cement dominated, microcrystalline calcitized dolomite (dedolomite)		ocasionally circumgranular cracks			Pedogenized lime mud, also calcitized finely-crystalline dolomite-dolosparite-groundwater calcrete	Calcareous sandy and siliciclastic mudstones, Charophyte Wk-Pk.
2	<b>Tufa Clinofoms</b>	Boundstone (flowstone), Breccia with carbonate intraclasts and sandstone extraclasts	Cliniform (large scale: lobe-like)	Macrophyte calcareous encrustations (phytcasts), peloids, oncoids,	Ostracods, calcified microbial filaments (cyanobacteria sheaths)		Constructive waterfall deposits (Spillover points)	Marlstone, Charophyte Wk-Pk, Gastropod Wk-Pk, Calcareous sandy & Silic. Md.
3	<b>Evaporites (Sulphates and Halite)</b>	Sulphates (Gypsum, Anhydrite, Barite, Celestite) and Halite.	Bedded irregular, laminated, nodular, isolated	Gypsite and gypsarenite, isolated crystals or aggregates (rossetes or nodules), Displavive, Breccia	Ostracods		littoral and sub-littoral and basinal deposition. Synsedimentary or secondary cements	May occur as well defined thin beds or lamina or as a discrete component in all the other
4	<b>Calcareous sandy mudstones and siliciclastic mudstones</b>	Structureless	Tabular	Vertical and horizontal vug pores, <i>Microcodium</i> , gypsum /calcareous nodules		Poorly bioturbaed	Waning sheet flows in distal portions of alluvial fans, transitional to marginal lacustrine	Horizontally bedded limestones, siliciclastic mudstones and channelized conglomerates
5	<b>Channelized conglomerates and Pebbly Sandstones</b>	Conglomerates. Subrounded to sub-angular pebbles-cobbles	Channelized with erosional relief	Low-angle plannar cross bedding. Imbricated, poorly to moderately sorted, matrix to framework supported, normal and inverse grading			Channels on distal alluvial fan sectors	Non-channelized conglomerates, calcareous sandy, and siliciclastic mudstones
6	<b>Non-channelized conglomerates</b>	Conglomerates. Cobble-boulder, subrounded, limestone (>80%), and other siliciclastic clasts	Crudelly bedded	Structureless, weakly matrix-to framework supported. Rare clast imbrication			Unconfined debris flows formed in alluvian fans	Channelized conglomerates, Pebbly sandstones and siliciclastic mudstones

**Table 5.1-** Summary of lithofacies types in the Mayrán Formation. Abbreviations: Mudstone (Md), Wackestone (Wk), Packstone (Pk), Grainstone (Gr), Bondstone (Bd), Siliciclastic (Silic.). A synthesized description of clastic facies, is included for reference, for more detail see chapter 3.





**Figure 5.2.-** Stratigraphic logs of the Mayrán Formation illustrating stacking patterns and lithofacies in the lacustrine setting from proximal to distal in sub-basins I to IV. Logs 7C, N22 and 34 modified from Amezcua et al., 2012. Carbonate textures: M-mudstone, W-wackestone, P-packstone, C-crystalline, B-boundstone. Clastic grain size: Cl- clay, S-silt, Vf-very fine grained sandstone, F- fine grained sandstone, C-coarse grained sandstone, G-gravel and coarser. See Figure 5.1 for log locations.

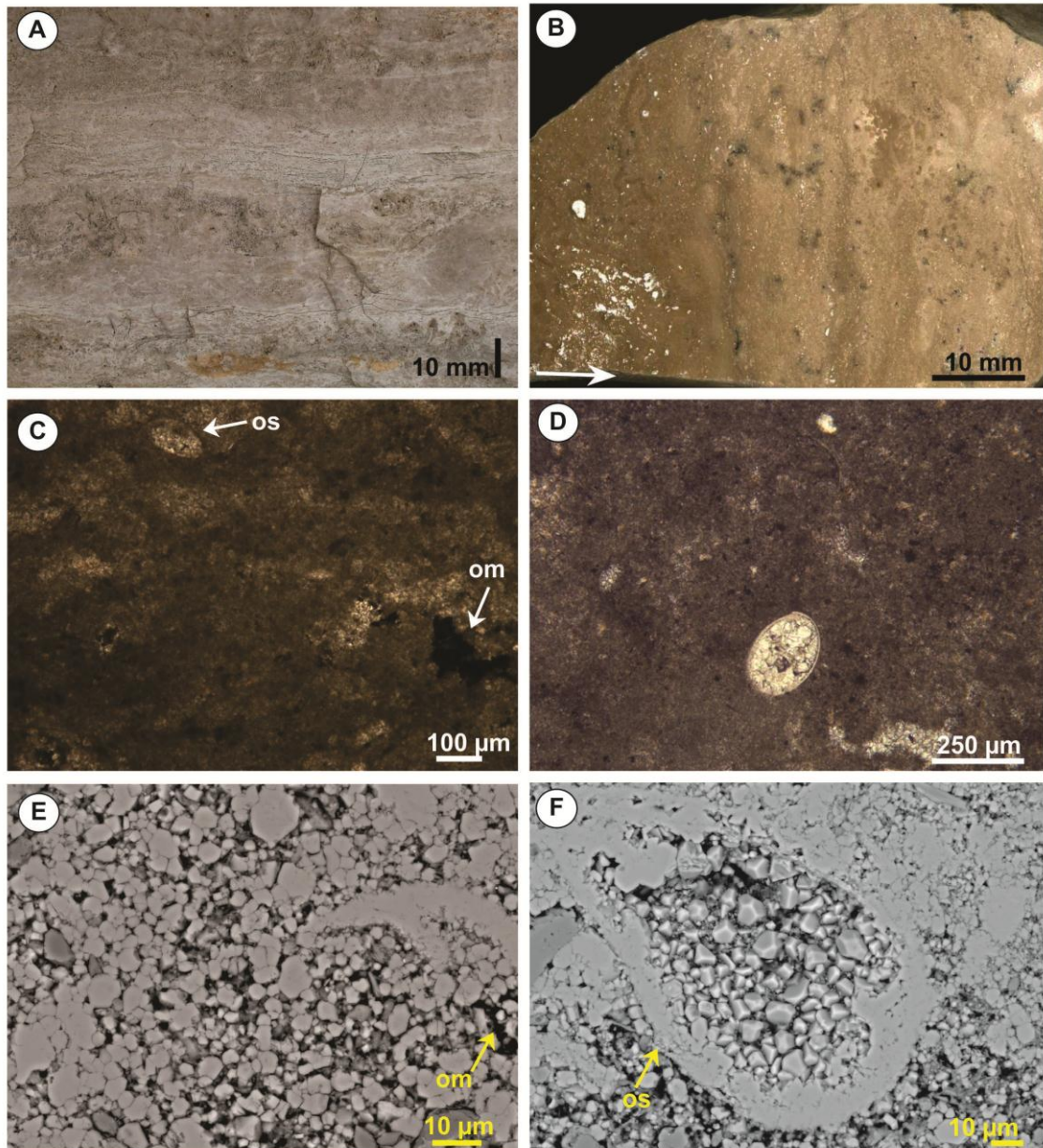
### 5.5.1 Ostracode mudstone-wackestone (Table 5.1, Figs. 5.2 and 5.3)

**Description.**-Ostracode mudstone-wackestones are present in the all the subbasins with the exception of subbasin IV. These lithofacies are typically organised into thin, brownish coloured-beds, that have even parallel geometries and even to wavy basal contacts. Internally some of these units are laminated (Fig. 5.3 A and B), most, however, have had their internal primary fabrics disrupted by the burrowing activities of a diminutive infauna (mm sized burrows) causing them to exhibit a sparse to moderate bioturbation (bioturbation index: BI1). Individual beds are organised into stacked bed-sets (up to 0.3 m thick) (Fig 5.3, log N22) that can be traced laterally for tens of meters. These units contain (up to 10 %) articulated and very well preserved ostracodes (Fig. 5.3 C and D), this being the main fossil present with subordinated peloids, and calcareous spheres (<200 $\mu$ m). Less commonly (< 5%) coarse silt-sized (40 to 60  $\mu$ m) detrital quartz grains are present.

Carbonate mudstone (*sensu* Dunham, 1962) is the dominant texture but wackestones are also present. Optical and electron optical imagery reveals that the matrix in these units is formed of dense microcrystalline calcite. The matrix comprises both anhedral and subhedral calcite crystals that range in size from <4  $\mu$ m (Fig. 5.3 E) to 20  $\mu$ m, that have dull orange luminescence. These microcrystalline calcites have stable isotopic values that average  $\delta^{13}\text{C}_{\text{calcite}}$  -5.8 ‰ and  $\delta^{18}\text{O}_{\text{calcite}}$  -7.6 (Table 5.2 and Fig.5.4). Amorphous black-brownish aggregates are present in the matrix (Fig. 5.3 C), from which 12.4% TOC and  $\delta^{13}\text{C}_{\text{organic}}$  -6.6 ‰ values were obtained (Table 5.3 and Fig.5.5). Most of the porosity in this lithofacies is intergranular, however subordinate intragranular, mouldic, shelter porosity, intercrystalline and vuggy porosity is present locally. Fine grained, <63  $\mu$ m subhedral calcite cements occlude intrafossil pores, vuggy pores and shelter porosity (Fig. 5.3 F). In addition to carbonate cements, sulfates (gypsum, baryte and celestine), iron oxides and limonite are also present. Rarely chlorite and siderite cements, may occur in vuggy pores, intergranular and intercrystalline porosity.

**Environment of deposition-** The predominant mudstone texture, together with the well preserved articulated ostracode shells, and calcareous spheres resembling free-floating calcareous algae, may indicate that the ostracode mudstone-wackestone lithofacies are open lake carbonates, deposited in offshore lake settings (Fig. 5.14). Because of the lack of clastic detritus, deposition of this lithofacies occurred in settings protected from clastic input. The minor degree of bioturbation (BI 1) suggests that possibly low oxygen

conditions occurred in profundal (offshore) areas that diminished the effects of diminutive ichnofauna, resulting in preservation of some lamination (cf. Macquaker and Gawthorpe, 1993; Macquaker et al., 2007, Gingras et al., 2011). The high TOC content (12.4%) of this facies probably resulted from a combined effect of the oxic- -dysoxic conditions, moderate to high primary production and sedimentation rate (cf. Meyers and Ishiwatary, 1993)



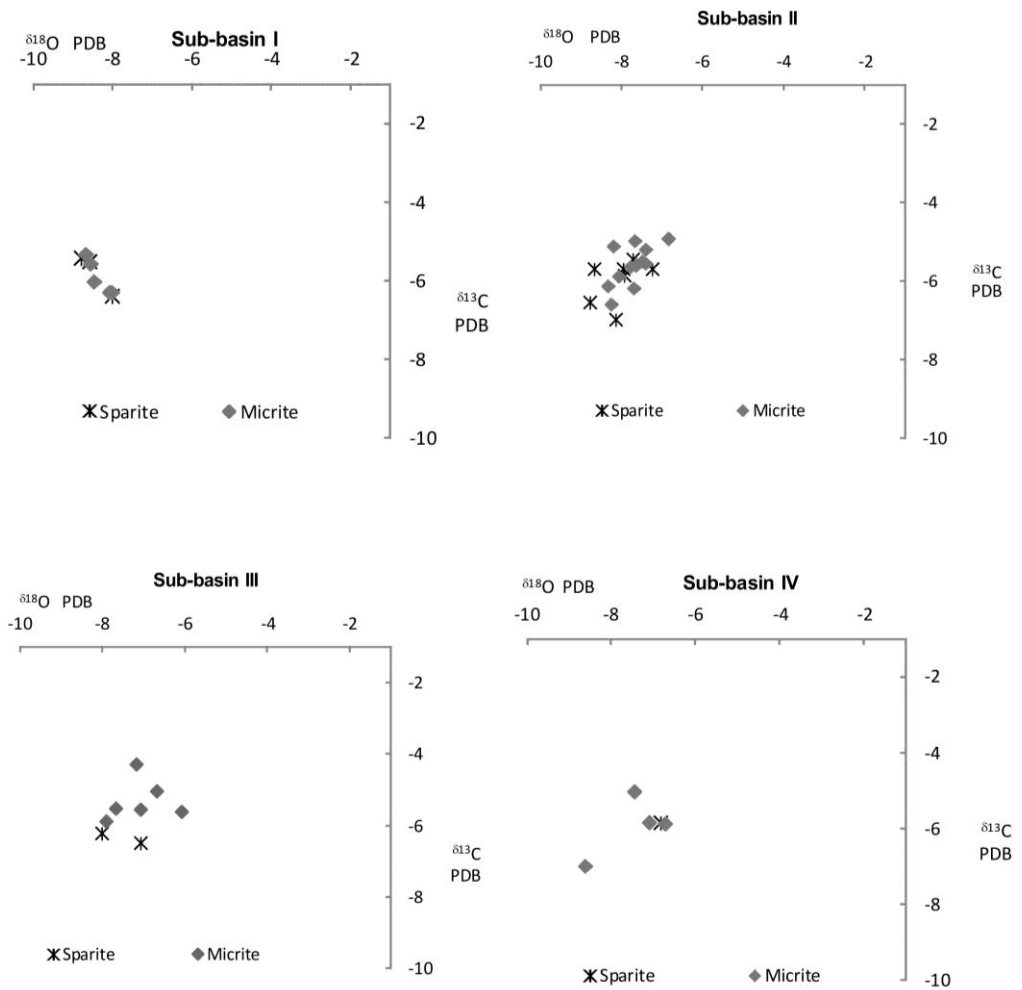
**Figure 5.3.-** Ostracod mudstone-wackestone (A, B and C). (A) Field exposure showing laminations. (B) Polished slab with wavy-like laminations taken from exposure in A. Solid white arrow indicates orientation towards top of sample. (C) Organic matter (om) occurring as amorphous black aggregates, disperse in the micrite matrix. (D) Completely occluded ostracodes by calcite spar cement. (E and F) Fine grained texture under BSE examination, showing effects of recrystallization of micrite (larger, subhedral crystals and crystal aggregates. Intragrain microporosity cemented by <10 micron rhombic calcite cement. Ostracode (os). Note intercrystal microporosity between calcite crystals within ostracode, and the microcrystalline calcite matrix.

Log-interval	$\delta^{13}\text{C PDB}$	$\delta^{18}\text{O PDB}$	Component	Lithofacies	Location
N37-7	-6.04	-8.45	Sparite in vug pore	Oncoid wackestone/packstone	Sub-basin I
N37-8	-6.31	-7.99	Sparite in vug pore	Gastropod wackestone/packstone	Sub-basin I
N37-9	-5.42	-8.77	Sparite in vug pore	Clotted boundstone	Sub-basin I
N37-12	-5.52	-8.58	Sparite in vug pore	Gastropod wackestone/packstone	Sub-basin I
N37-22	-5.58	-8.54	Micrite in matrix	Gastropod wackestone/packstone	Sub-basin I
N37-14	-5.32	-8.65	Micrite oncolid laminations	Oncoid wackestone/packstone	Sub-basin I
N6-5	-6.98	-8.15	Sparite in vug pore	Gastropod wackestone/packstone	Sub-basin II
N6-9	-4.94	-6.83	Micrite in matrix	Marlstone	Sub-basin II
N6-13	-5.66	-7.75	Micrite oncolid laminations	Oncoid wackestone/packstone	Sub-basin II
N6-18	-5.87	-7.92	Sparite in vug pore	Macrophyte boundstone	Sub-basin II
N6-24	-5.70	-7.96	Sparite in vug pore	Macrophyte boundstone	Sub-basin II
N6-25	-5.64	-7.77	Micrite in matrix	Ostracode mudstone/wackestone	Sub-basin II
N6-27	-5.90	-8.05	Micrite oncolid laminations	Gastropod wackestone/packstone	Sub-basin II
N6-31	-5.46	-7.70	Sparite in vug pore	Macrophyte boundstone	Sub-basin II
N6-34	-6.13	-8.32	Micrite oncolid laminations	Oncoid wackestone/packstone	Sub-basin II
N6-40	-5.60	-7.60	Micrite in matrix	Ostracode mudstone/wackestone	Sub-basin II
N6-41	-5.62	-7.63	Micrite oncolid laminations	Marlstone	Sub-basin II
N6-46	-4.27	-6.35	Sparite in vug pore	Oncoid wackestone/packstone	Sub-basin II
N7-i	-5.70	-8.65	Sparite in vug pore	Clotted boundstone	Sub-basin II
N8-3ii	-6.56	-8.76	Sparite in vug pore	Clotted boundstone	Sub-basin II
N12-7	-6.20	-7.68	Micrite in matrix	Ostracode mudstone/wackestone	Sub-basin II
N26-1a	-6.38	-8.00	Micrite in stromatolite laminae	Stromatolite	Sub-basin II
N26-1b	-6.31	-8.08	Micrite in stromatolite laminae	Stromatolite	Sub-basin II
N21B-7	-5.00	-7.66	Micrite in matrix	Charophyte wackestone/packstone	Sub-basin II
N21B-8	-6.60	-8.24	Micrite in matrix	Oncoid wackestone/packstone	Sub-basin II
N21B-9	-5.51	-7.48	Micrite oncolid laminations	Oncoid wackestone/packstone	Sub-basin II
N21B-11	-5.56	-7.40	Micrite in matrix	Oncoid wackestone/packstone	Sub-basin II
N21B-12	-5.13	-8.18	Micrite in matrix	Oncoid wackestone/packstone	Sub-basin II
N21B-15	-5.22	-7.40	Micrite oncolid laminations	Gastropod wackestone/packstone	Sub-basin II
N22-1	-6.49	-7.06	Sparite in vug pore	Gastropod wackestone/packstone	Sub-basin III
N22-5	-5.90	-7.90	Micrite in matrix	Gastropod wackestone/packstone	Sub-basin III
N22-6	-6.22	-8.02	Sparite in vug pore	Gastropod wackestone/packstone	Sub-basin III
N22-8	-5.52	-7.67	Micrite oncolid laminations	Gastropod wackestone/packstone	Sub-basin III
N22-9	-4.29	-7.18	Micrite in matrix	Charophyte wackestone/packstone	Sub-basin III
N22-11	-5.57	-7.06	Micrite in matrix	Gastropod wackestone/packstone	Sub-basin III
N22-13	-5.05	-6.67	Micrite in matrix	Oncoid wackestone/packstone	Sub-basin III
N22-15	-5.61	-6.07	Micrite in matrix	Charophyte wackestone/packstone	Sub-basin III
N34-9	-5.03	-7.45	Micrite in matrix	Oncoid wackestone/packstone	Sub-basin IV
N45-4	-5.84	-7.10	Micrite oncolid laminations	Gastropod wackestone/packstone	Sub-basin IV
N45-5	-5.88	-6.71	Micrite in matrix	Gastropod wackestone/packstone	Sub-basin IV
N45-6	-7.00	-8.61	Micrite in matrix	Oncoid wackestone/packstone	Sub-basin IV
N43-1	-5.17	-6.37	Microspar in laminae	Tufa clinoform	Spillover point I
N43-2	-5.83	-6.78	Radial fibrous calcite in laminae	Tufa clinoform	Spillover point I
N43-3	-5.91	-6.94	Microspar in laminae	Tufa clinoform	Spillover point I
N43-4	-5.93	-6.90	Radial fibrous calcite in laminae	Tufa clinoform	Spillover point I
N43-5	-5.84	-6.91	Microspar in laminae	Tufa clinoform	Spillover point I
N43-6	-5.86	-6.88	Radial fibrous calcite in laminae	Tufa clinoform	Spillover point I
N15-1a	-6.34	-8.52	Sparite	Tufa clinoform	Spillover point II
N15-1b	-6.34	-8.15	Sparite	Tufa clinoform	Spillover point II
N15-1c	-6.00	-8.06	Sparite	Tufa clinoform	Spillover point II
N15-1d	-6.13	-8.50	Sparite	Tufa clinoform	Spillover point II
N44	-5.03	-6.83	Sparite	Tufa clinoform	Spillover point III
N45-7	-5.86	-6.82	Sparite occluding vug pores	Tufa clinoform	Spillover point III

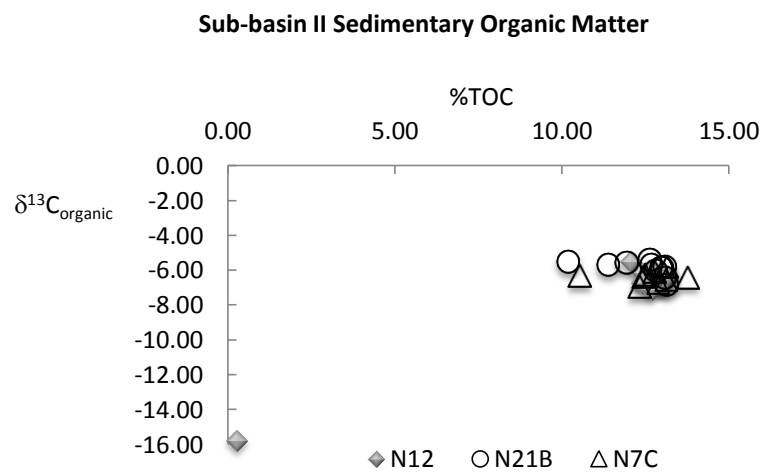
**Table 5.2.** Stable oxygen and carbon isotopes from lacustrine limestone samples in the Mayrán Formation. Whole rock average values:  $\delta^{13}\text{C}_{\text{calcite}} -5.71$  ‰ and  $\delta^{18}\text{O}_{\text{calcite}} -7.52$ .

Log-Interval	$\delta^{13}\text{C}_{\text{org}}$ PDB	TOC	Lithofacies
N12-3	-6.28	13.01	Gastropod wackestone/packstone
N12-4	-6.61	12.97	Gastropod wackestone/packstone
N12-5	-6.15	12.40	Gastropod wackestone/packstone
N12-6	-6.38	12.88	Gastropod wackestone/packstone
N12-7	-6.69	12.40	Ostracode mudstone/wackestone
N12-10	-7.10	12.70	Gastropod wackestone/packstone
N12-11	-6.44	13.14	Clotted boundstone
N12-12	-6.34	13.20	Macrophyte boundstone
N12-14	-5.49	12.08	Gastropod wackestone/packstone
N12-15	-5.94	12.72	Gastropod wackestone/packstone
N21B-1	-6.00	12.81	Gastropod wackestone/packstone
N21B-2	-5.39	12.64	Oncoid wackestone/packstone
N21B-4	-6.82	13.15	Macrophyte boundstone
N21B-5	-5.54	11.95	Oncoid wackestone/packstone
N21B-6	-5.84	12.99	Charophyte wackestone/packstone
N21B-7	-5.66	12.68	Charophyte wackestone/packstone
N21B-9	-5.68	11.39	Oncoid wackestone/packstone
N21B-12	-5.83	12.97	Oncoid wackestone/packstone
N21B-13	-5.50	10.19	Oncoid wackestone/packstone
N21B-15	-5.78	13.07	Gastropod wackestone/packstone
N21B-17	-6.42	13.08	Gastropod wackestone/packstone
N7C-4	-6.94	12.33	Clotted mudstone/packstone
N7C-6	-6.40	13.77	Oncoid wackestone/packstone
N7C-7	-6.06	12.78	Clotted boundstone
N7C-7	-6.24	12.49	Clotted boundstone
N7C-9	-5.77	13.16	Oncoid wackestone/packstone
N7C-12	-6.29	10.55	Marlstone
N7C-14	-6.73	12.89	Gastropod wackestone/packstone
N7C-15	-6.36	12.45	Gastropod wackestone/packstone
N7C-16	-6.56	13.13	Gastropod wackestone/packstone

**Table 5.3.** Total organic carbon and stable isotopes of organic carbon from lacustrine limestone samples in the Mayrán Formation sub-basin II.



**Figure 5.4.-** Isotope plot of micrite and calcite spar of the lacustrine carbonates in the sub-basins.



**Figure 5.5.-** Plot of Total organic carbon (TOC) and organic carbon stable isotopes values of the lacustrine carbonates (Gastropod wackestone-packstone, Clotted boundstone, Macrophyte boundstone, Oncoid wackestone-packstone, Charophyte wackestone-packstone, and Marlstone).

### 5.5.2 *Clotted boundstones (Table 5.1, Fig. 5.6)*

**Description.**-Clotted boundstones have been identified in subbasins I, II and III. In these locations they form irregular beds that can be traced laterally for 10's meters. In the field this lithofacies is very prone to karstification. Clotted boundstones are interbedded either with gastropod or oncoid wackestone-packstone and bounded by subaerially exposed surfaces (Fig. 5.2). Tepee-like structures, interbedded with centimetre-thick gypsum units and isolated patches of calcified vertical macrophyte stem moulds of 10's mm scale, occur in some localities (e.g. Fig. 5.2, log N21B).

Individual bed thicknesses in the clotted boundstones are difficult to define precisely, because bed contacts are typically gradational and discontinuous (Fig. 5.6 A). Based on incipient bedding fabrics, however, individual units vary from being thin-bedded (10 mm thick) to medium bedded (0.30 m thick). Stacked successions of these beds form units up to 2 m thick. This lithofacies commonly exhibits a clotted boundstone texture; locally however, wackestone and packstone textures are present.

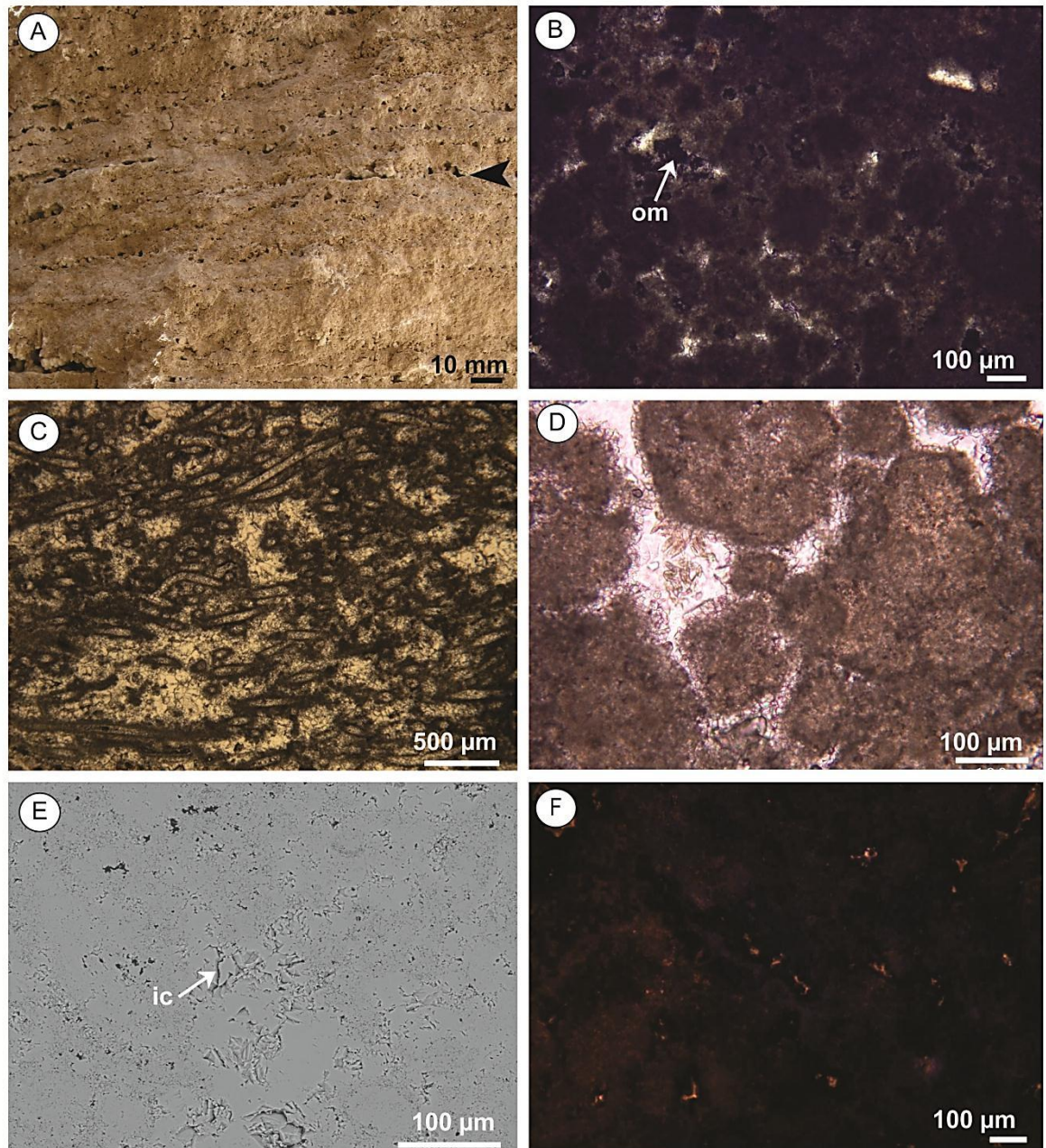
Clotted boundstones are predominantly composed of calcite (>99% CaCO<sub>3</sub>), with rare clastic detritus (<1%). Neither siliciclastic nor organic matter rich beds are interbedded with this facies. In thin section the clotted fabric is well defined, with clots formed by spheroidal masses composed of dense micro to crypto-crystalline calcite with a very-dull orange luminescence (Fig. 5.6). Less common are clots of fibrous aragonite that form 'microspherulites'. Well-preserved elongated tubes of micrite are locally present (Figs. 5.6 C), together with peloids and articulated ostracodes, but are not ubiquitous. As in the other carbonate lithofacies, organic matter occurs as black-brownish amorphous aggregates (Fig. 5.6 B), with mean TOC values of 12.8 % and  $\delta^{13}\text{C}_{\text{organic}}$  values of -6.2 ‰ (Table 5.3 and Fig. 5.5). Vuggy pores and fenestral pores are characteristics of this lithofacies. Non fabric selective vuggy megapores (up to 0.2 m diameter) crosscut horizontal fenestral porosity, and are filled by euhedral, scalenohedral calcite crystals forming aggregates up to 10 mm long. This calcite cement has an average stable isotope value of  $\delta^{13}\text{C}_{\text{calcite}}$  -5.8 ‰ and  $\delta^{18}\text{O}_{\text{calcite}}$  -7.7 ‰ (Table 5.2 and Fig. 5.4). The fenestral pores are irregular, laterally discontinuous, a few millimetres wide to centimetres long and partially occluded by botryoidal calcite cements, and isopachous rims of bladed calcite. Intercrystalline porosity is observed under BSE examination (Fig. 5.6 E), some of this porosity is occasionally cemented by iron oxide aggregates.

**Environment of deposition.**- The presence of clots, microbial morphotypes, and the entire calcitic composition (>99% CaCO<sub>3</sub>) in this lithofacies indicates biogenically mediated precipitation.. The presence of fine purely calcitic beds, preserving microbial morphotypes, tepee-like features, and lacking clastic detritus, suggest that they may have formed in protected shallow lake settings, in relatively 'distal' lake areas, well protected of clastic input. Such conditions may have occurred in either distal basinal areas or nearshore (littoral) lake areas likely fringed by macrophyte boundstones (Fig. 5.14). The presence of isolated macrophyte moulds in the clotted boundstones, also suggest that their deposition occurred in relatively shallow waters, possibly less than 2 m deep (Fig. 5.14). The interpretation of shallow water conditions is supported by the presence of tepee-like features, and gypsum units, which also suggest that saline episodes and occasionally subaerial exposure affected this lithofacies.

The presence of fenestral pores and the discontinuity of the thin-beds indicate that carbonate deposition might have occurred mediated by microbial communities (e.g. biofilms). This interpretation is supported by the presence of calcified microbial morphotypes, although, the former are not ubiquitous. The lack of lamination also suggests that during deposition the sediment/water interface was likely oxic, allowing ichnofaunal activities to homogenize the sediment (cf. Gingras et al., 2011).

Low stable oxygen isotope values (-8.7‰ average) of the euhedral calcite spar cements in vug porespace this lithofacies, suggest that they might have derived from dissolution and re-precipitation of the preceding carbonate. This type of cement and its isotopic signal also suggests precipitation in meteoric vadose to meteoric phreatic environments (e.g. James and Choquette, 1989; Moore, 2001), and probably relates to regional post-depositional paleowater table changes, as subaerial exposure of the lake sediment occurred. Particularly the cement in vug pores of clotted boundstones formed by bladed calcite with euhedral terminations, commonly exhibits concentric zonation with non-luminescent-dull luminescent and bright luminescent patterns. The presence of an orange zone between the yellow and black has been interpreted to indicate a higher Fe<sup>2+</sup> content than in the preceding yellow zone or a decrease in Mn<sup>2+</sup> concentrated while iron content increase is related to non-luminescent response (e.g. Horbury and Adams, 1996). Absence of significant (200 ppm, Machel, 1985) detectable Fe<sup>2+</sup> in non-luminescent zones (black) of the overgrowths represent high Eh conditions (Horbury and Adams, 1996) of the cementing fluids.





**Figure 5.6.-** Clotted boundstone. **(A)** Facies fabric exposed in field exposure with fenestral pores (dark arrow). **(B)** Thin section showing clotted aggregates composed of microcrystalline-cryptocrystalline calcite, and organic matter (om-arrowed). **(C)** Elongated tubes without partitions or branching of microbial origin (microbial sheath mould), preserved microcrystalline calcite around filament sheaths, note cement-filled mould composed of equant calcite spar. This microbial morphotype is similar to present day *Oscillatoriaceae* and ancient *Girvanella*. **(D)** Diagenetic overprint in clots producing peloidal fabrics. Isopachous, circumgranular calcite cements partially around clots **(E)** BSE image showing, intercrystalline microporosity (arrowed ic). **(F)** CL response of clotted calcite (dull orange), and calcite spar cement (non to bright orange luminescence) occluding porespace.

### 5.5.3 *Gastropod Wackestone-Packstone (Table 5.1, Fig. 5.7)*

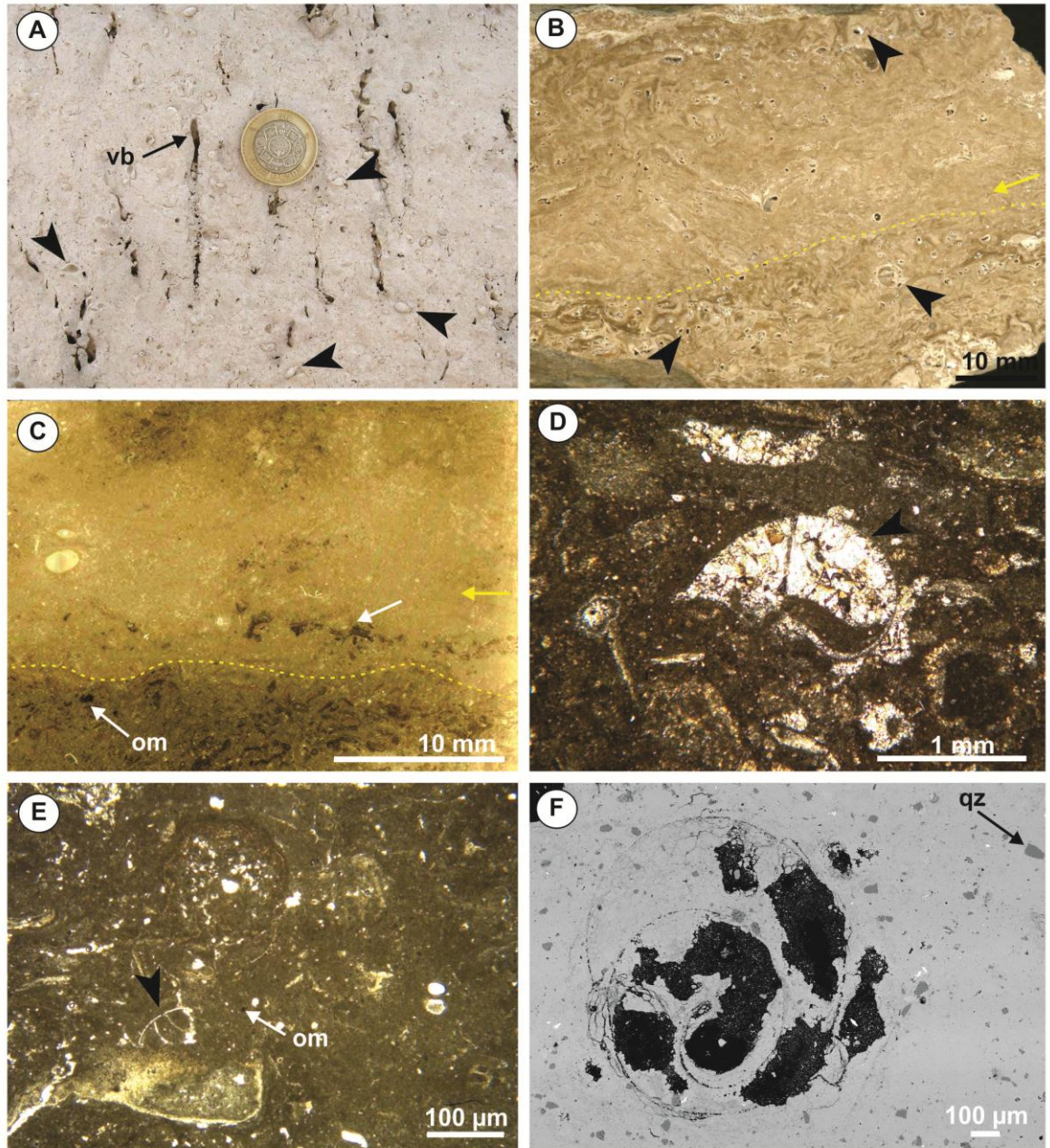
**Description.**-This lithofacies is very well represented in all the subbasins. It forms laterally continuous beds that range in thickness from 0.05 to 0.50 m, that are organised into bedsets up to 1.5 m thick. Individual beds are tabular, largely lack internal structure (although wavy lamina, erosional surfaces, and normal grading are rare), and weather variously cream, light grey to brown. The beds are burrowed and moderately to highly bioturbated (BI 3-4). Two populations of burrows are present, the first consist of centimetre scale, vertically oriented, cylindrical, non-tapering burrows (Fig. 5.7A) and the second comprise smaller millimetre scale, cylindrical randomly oriented burrows.

Gastropod wackestone-packstones overlie either ostracodes mudstones or clotted mudstone-packstone and commonly underlie either oncoid wackestone-packstones, or macrophyte boundstones. The most distinctive feature of this lithofacies is the presence of gastropod moulds that are either infilled by equant calcite spar or micrite cements (Fig. 5.7 D to F). The gastropods are less than 10 mm in size, and include: coiled elongated oval shells (attributed to Limnaeidae and Physidae types), coiled planispiral shells (Planorbidae type) (Fig. 5.7 A-D), and other undetermined forms (Fig. 5.7 E). The gastropods typically occur in monospecific assemblages although rarely more than one morphotype is present in the same bed. No coquina layers were identified. Other allochemical components include ostracodes, bivalves (e.g. log N34, Fig. 5.2), charophyte fragments, fish scales and rare millimetre size phosphatised bone fragments, amorphous and algae-like organic matter, as well as peloids (composed of either micrite or mixtures of micrite and silt-sized quartz), micro-oncoids and calcareous fragments of uncertain origin. This facies typically contain minor proportions (1.3-3.5 %) of silt-size clastic detritus, dispersed in the micritic matrix.

Texturally this lithofacies are mainly wackestones and packstones although sometimes mudstone textures are present. The matrix is composed of micrite with mean stable isotopic values of  $\delta^{13}\text{C}_{\text{calcite}}$  -5.6 ‰ and  $\delta^{18}\text{O}_{\text{calcite}}$  -7.5 ‰, with very dull orange luminescence. Gastropod wackestone-packstones contain average 12.7 % TOC, with  $\delta^{13}\text{C}_{\text{organic}}$  6.2‰ mean values.

Vuggy pores of millimetre to centimetre size are either partially or completely occluded by subhedral calcite spar, and microcrystalline calcite with average isotopic values of  $\delta^{13}\text{C}_{\text{calcite}}$  -6.3 ‰ and  $\delta^{18}\text{O}_{\text{calcite}}$  -7.9 ‰. Orange brown amorphous iron oxides, and rare baryte and siderite cements are also present. Siderite composed by sub-micrometer-sized

irregular crystal aggregates (seen only in BSE examination) are formed in porespace in the matrix together with calcite spar.



**Figure 5.7-** Gastropod mudstone-packstone. **(A)** Field exposure showing gastropod moulds (arrowed) with dextral coiled spiral shell (*Lymnaeidae*-type), and cylindrical vertical burrows (vb). Coin diameter is 2.7 cm. **(B)** Polished slab showing gastropod mould pores (black arrow), erosional surface (dashed line), interpreted flow direction indicated by yellow arrow. **(C)** Thin section scan of B, showing detail of scour surface caused by lateral sediment transport. Note grain size change above bioclast lag (white arrow). Organic matter (arrowed om). **(D)** Gastropod shell replaced with geopetal cement made of micrite and calcite spar (arrowed). **(E)** Gastropod mould, and organic matter. **(F)** BSE image of gastropod mould, note fine grained microcrystalline calcite matrix and cement within gastropod mould. Note scattered baryte cement showing high  $\eta$  coefficient, and silt size quartz (qz) grains with intermediate  $\eta$  coefficient.

**Environment of deposition.**- The wackestone-packstone texture in this lithofacies, and the presence of subordinated allochems such as ostracode valves, fragments of oncoids charophytes, and algae like fragments that commonly inhabit low water depth conditions, indicate that deposition and high productivity occurred in nearshore lake areas (cf. Flügel, 2004) (Fig. 5.14).

The low clastic detritus in this lithofacies may imply that, either insufficient detrital input delivery into the lake basin margins, baffled effects in the lake margins, or that lakes had overall low relief affecting sediment transport basinward. However, locally, rare microtextural evidence of scour surfaces, indicates that occasionally the sediment was laterally transported offshore (Fig. 5.7C).

In this lithofacies, moderate to high bioturbation degree (BI 3-4) by a variable set of vertically and randomly oriented burrows indicates, that enough oxygen was available in the sediment /water interface to sustain benthonic and endobenthonic activity. This is important because, gastropods inhabit mainly littoral and sublittoral to profundal environments, that are well oxygenated (Gierlowski-Kordesch, 2010). Although enough oxygen existed during deposition of this lithofacies, considerable amounts of organic matter were preserved. This might have been achieved by moderate rates of sediment production and deposition that ultimately preserved organic matter rich sediments (Meyers and Ishiwatary, 1993). Productivity is also inferred by the presence of Lymnaeidae-type gastropods indicated oligotrophic conditions, and presumably meso- to eutrophic conditions, when Physidae? forms were present (cf. Miller and Tevesz, 2001; Ložek, 1986).

Selective carbonate dissolution is common in the gastropod wackestone-packstone lithofacies. Here, early diagenesis and dissolution of metastable aragonitic gastropod shell, produced intraparticle (mouldic) porosity. This likely occurred early after deposition, as some calcite spar cements partially occlude intraparticle pores.

#### 5.5.4 *Oncoid Wackestone-Packstone (Table 5.1, Fig. 5. 8)*

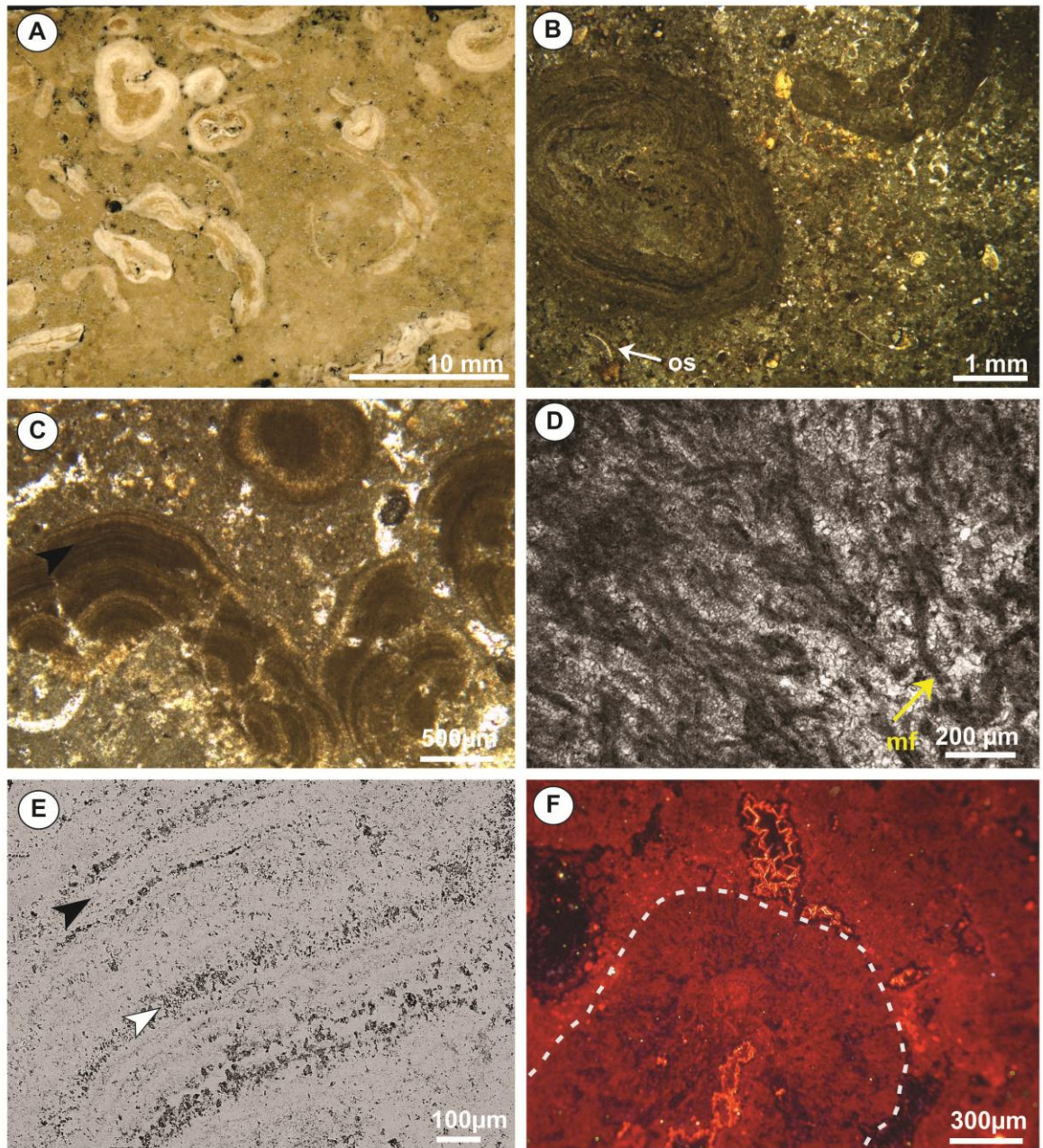
**Description.**-Oncoid wackestone-packstone facies occur in all the subbasins of the Mayrán Basin system. They are interbedded with gastropod wackestone-packstone, charophyte wackestone-packstones, stromatolites, macrophyte boundstone and marlstone lithofacies. Bed thicknesses, vary from 0.1 to 0.5 m, and extend laterally from a few meters up to hundreds of meters. The oncoids have an irregular shape and range in size from sub-millimetre to 10s of millimetres (Fig. 5.8). They are supported by a matrix composed of dull orange luminescent microcrystalline calcite.

Oncoids nuclei are either made of clotted micrite, or coarse equant calcite spar with a drusy mosaic but rarely by undifferentiated calcified structures (macrophyte cast?). Nuclei are rimed by irregular concentric laminations and / or micritic filaments that are either branching or straight (Fig. 5.8 D and F). The alternating laminae are composed of dense microcrystalline (micritic) calcite, microspar, and radial fibrous calcite (aragonite cement). The average stable isotope values of both laminations and matrix are of  $\delta^{13}\text{C}_{\text{calcite}} -5.8 \text{ ‰}$  and  $\delta^{18}\text{O}_{\text{calcite}} -7.7 \text{ ‰}$ . Articulated and disarticulated ostracods, and millimetre-sized peloids composed of microcrystalline cement are ubiquitous. In this facies organic carbon occurs as sparse brownish-black amorphous aggregates in the micritic matrix and average TOC contents of 12.2 %, with  $\delta^{13}\text{C}_{\text{organic}} -5.7 \text{ ‰}$  (average) organic carbon.

Detrital components in this lithofacies comprise silt-size quartz (average 3.3 range 0.8 - 15 %), minor proportions (<1%) of feldspar, and rare muscovite. Pore-filling cements are predominantly composed of calcite spar, with subordinate iron oxides and limonite. Baryte cements occur rarely in vug porespace, and comprise lath shaped/ crystals with tabular habit or as crystal aggregates (~200  $\mu\text{m}$ ).

**Environment of deposition.**- Oncoids and stromatolites commonly occur in nearshore litoral lacustrine settings (see Dean and Fouch, 1983; Garber and Friedman, 1983; Cohen and Thouin, 1987; Guierlowski-Kordesch, 2010) (Fig. 5.14), under both, high (e.g. Carozzi, 1964) and low hydrodynamic conditions (e.g. Peryt, 1981; Arenas et al., 2010). The Mayrán oncoids are irregular in shape, and because of their asymmetry, are considered characteristic of deposition in low-energy shallow parts of the lakes (cf. Nickel, 1983; Leinfelder and Hartkopf-Fröder 1990; Smith and Mason 1991), and probably were not reworked during their growth (e.g. Schäfer and Stapf, 1978). Locally, millimetre size, fragmented oncoids together with intraclasts occur in poorly cemented erosion-based beds

composed of calcareous silt. These units occur in channels that locally incise the gastropod wackestone-packstones.



**Figure 5.8-** Oncoid wackestone-packstone. (A) Polished slab with oncooids and oncooid fragments with asymmetric shape. B to E Photomicrographs. (B) Detail of image A. Oncoid nucleus with clots of micrite calcite, note irregular irregular laminations, and ostracod fragment (os). (C) Oncoid with irregular laminations some peloid cement, calcified filament arrowed. (D) Calcified microbial filaments of elongate shape occurring in some oncooids. (E) BSE image of oncooid laminations, note alternating laminae of dense microcrystalline calcite (black arrow) and calcite spar with abundant pores (white arrow), (F) Cathodoluminescence, oncooid underlined by dashed line.

### 5.5.5 *Stromatolites (Table 1, Fig. 5.9)*

**Description.**- Stromatolites were identified in the middle and northern sectors of subbasin I and in the northern sector of subbasin II (Fig. 5.9 A). They are irregular in shape and size and are sporadically distributed on specific horizons, extending discontinuously for 1 to 10s m on these surfaces. They occur overlying loose calcareous clay and silt, calcareous sandy mudstones and marlstones. They may be associated with irregular, relatively spheroidal oncolites up to 30 millimeters in diameter, with hollow nuclei that resemble macrophyte moulds (Fig. 5.2 log N26).

The stromatolites display two main fabric types: Type 1 and Type 2. Type 1 exhibits irregular shape, with a ‘cauliflower like’ external morphology, that ranges in size from centimetres to decimetres. Internally they contain multiple nucleation sites (Figs. 5.7 C) that enclose irregular concentric laminae (<100  $\mu\text{m}$  thick), with alternating compositions, that grow from a clotted micrite nucleus (Figs. 5.9 D and E). Individual lamina are variously composed of dense microcrystalline calcite, and light microcrystalline spar (Fig. 5.9 E), exhibit non, dull and bright orange luminescence, and have stable average isotope values of  $\delta^{13}\text{C}_{\text{calcite}} -6.3 \text{‰}$  and  $\delta^{18}\text{O}_{\text{calcite}} -8.0\text{‰}$ . Equant calcite cement in pore spaces, however, exhibits a concentric zoning pattern with non to bright and dull to bright orange luminescence (Fig. 5.9 F). Type 2 stromatolites form dome-like mounds (<0.2 m diameter) that are, particularly present at the transition between calcareous sandy mudstones and marlstones. Their internal fabric is poorly preserved. They, however, do contain irregular discontinuous fenestral crinkly pores up to 50 mm long, that are rimmed by microspar cements (Fig. 5.9 B). Fenestrae may be either completely or partially occluded by calcite cement, and rarely contain silt-size quartz and clay.

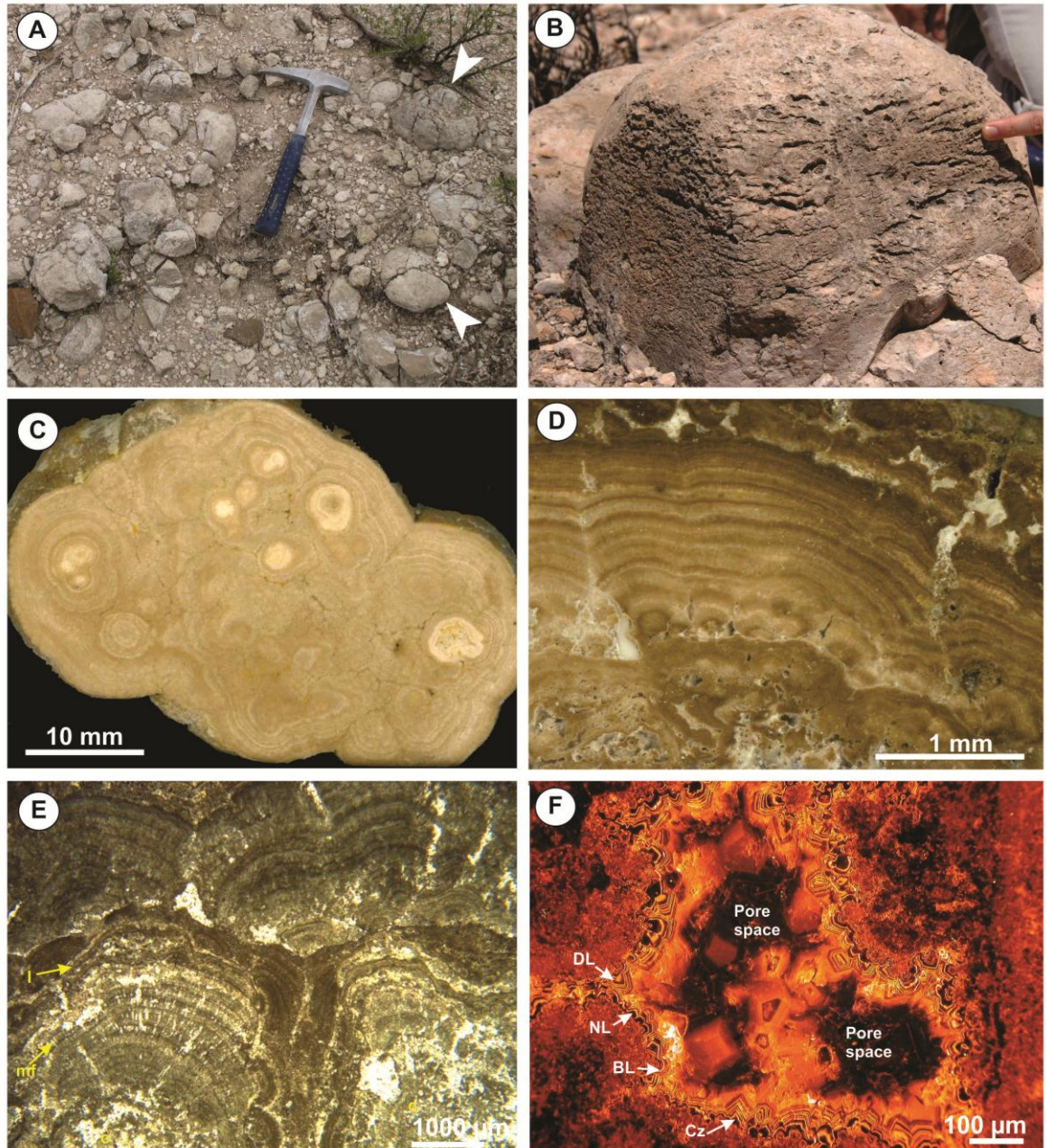
**Environment of deposition.**- Based on their morphology and preservation of internal laminations, together with diagenetic overprint and stratigraphic relations, it is suggested that type I stromatolites formed under standing water conditions, and in areas of protected from clastic input. Stromatolite type 2, instead, is more affected by diagenetic overprint, and formed in areas with relatively more significant clastic input and subjected to episodic subaerial exposure conditions. Stromatolites formed in littoral lake areas (cf. Dean and Fouch, 1983; Garber and Friedman, 1983; Cohen and Thouin, 1987; Guierlowski-Kordesch, 2010), and were deposited along surfaces where there sedimentation rates were very slow (Fig. 5.14). Low stable isotope values and the luminescent response of the

calcite spar cements in the stromatolites type I, indicates episodically the stromatolites may have been partially subaerially exposed and affected by of meteoric diagenesis.

The presence of elongated tubes (Fig. 5.6 C) similar to those of ‘*Girvanella*’ group (see Riding, 1977) in the clotted mudstones-packstones and macrophyte boundstones commonly form by *in vivo* calcification of cyanobacteria sheaths during photosynthesis (e.g. Riding 1977, 2006; Chafetz and Buczinsky, 1992; Merz-Preiß, 2000). The micrite forming the sheaths is produced by epicellular calcification, rather than being formed as a later ‘micritic envelope’ (Awramik, 1971; Monty, 1981; Pentecost, 1987; Merz, 1992; Robbins and Blackwelder, 1992; Winsborough et al., 1994; Arp et al., 1999; Merz-Preiß, 2000; Riding, 2000; Dupraz et al., 2008).

The microbial morphotypes formed by micritic laminations and filaments that may have branching or radial straight clusters in Mayrán oncoids and stromatolites are similar to those found in the Holocene lacustrine stromatolites and oncolites in the Cuatro Ciénegas spring-lakes (e.g. Winsborough et al., 1994), located at 150 km northwest of the Mayrán Basin system. In these spring-lakes cyanobacteria genus *Homeotrix* and *Schizotrix* are responsible for producing the rhythmical depositional pattern in the fabric of both oncolites and stromatolites (Winsborough et al., 1994). Moreover, the micritic laminations (e.g. Fig. 5.8B and 5.9 E) are considered to be produced by superimposed compacted filaments of *Schizotrix* (Monty, 1981). In the type 2 stromatolites (Fig. 5.9 B) microbial morphotypes are not preserved, however the presence of distinctively stacked fenestral pores formed by discontinuous wavy parallel laminae, likely produced by organic matter oxidation in the microbial mat are also suggestive of microbially induced structures (see Monty, 1976, Abell et al., 1982; Schieber, 1999; Nofke et al., 2001; Allwood et al., 2009).





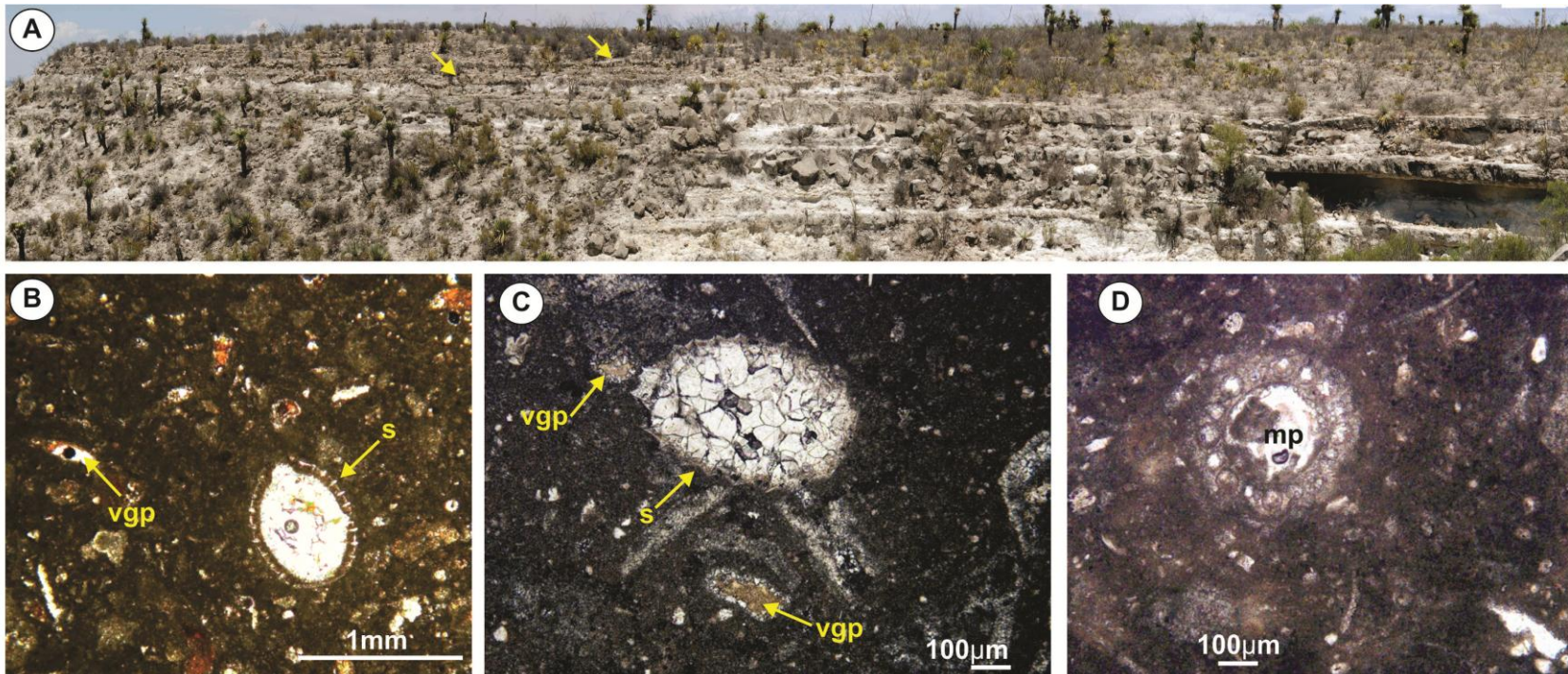
**Figure 5.9-** Stomatalites. (A) Field exposure of type 1 stromatolites (arrowed) in subbasin II. Hammer (35 cm) for scale. (B) Type 2 stromatolite forming dome-like mounds, discontinuous fenestral pores pointed (in subbasin I). (C) Polished longitudinal section of small type 1 stromatolite with merged multiple nucleation sites. (D) Polished slab of type 1 stromatolite, superposed, irregularly alternating, concentric laminations (l) made of dense micrite and microspar, growing away from an irregular micritic clotted nucleus (from log N26, Fig. 3). (E) Thin section from stromatolite in figure D. Clotted nucleus (c), microbial filaments (mf). (F) CL image of internal fabric of stromatolite in figure D and E. Diagenetic phases in cement filled void: NL- non luminescent, DL- dull luminescent, BL - bright luminescent.

### 5.5.6 Charophyte Wackestone -Packstone (Table 5.1, Fig. 5.10)

**Description.**-Charophyte bearing strata occur as greyish-brown coloured (Fig. 5.10 A), structureless beds of 0.1 to 0.30 m, that form bedsets up to 1 m thick (Fig. 5.2), that grade laterally to gastropod or oncoïd wackestone-packstone facies and locally to macrophyte boundstones. These units are variably bioturbated (BI 1 to 4) by millimetre-diameter vertical and horizontal burrows. In thin section, charophyte oogonia (gyrogonites) have a variable number of spirals (from 7 to 10), and range in size from 340 to 720  $\mu\text{m}$  long, and 240 to 550  $\mu\text{m}$  wide (Fig. 5.10 B and C). Both charophyte oogonia and 'stem' (internodia) fragments (Fig. 5.10 D) occur associated with ostracode valves, rare gastropod moulds and micro-oncoïd fragments, together with disseminated amorphous organic matter (12.8 % TOC with  $\delta^{13}\text{C}_{\text{organic}} -5.7\text{‰}$  average values). Remains of carbonized organic matter rarely occur in some root traces. The allochemical components are supported by a dull orange luminescent micritic matrix, conversely charophyte oogonia and oogonia fragments are non-luminescent. Average stable isotope values of the micritic matrix are  $\delta^{13}\text{C}_{\text{calcite}} -5.3 \text{‰}$  and  $\delta^{18}\text{O}_{\text{calcite}} -6.8 \text{‰}$ .

Charophyte wackestone-packstones contain some silt-size quartz grains (average 8, range 3-14%) and detrital clay. In addition, they contain silt- to fine sand- sized rounded extraclasts composed of both reworked Cretaceous bedrock and Cretaceous foraminifera, the latter occur exclusively in subbasin I. Separated vuggy pores, and minor intraparticle pores, have partially or completely filled by calcite spar. Amorphous clay and iron oxide aggregates are subordinate cements (Fig. 5.10 C). Scattered subhedral prismatic gypsum and lath-shaped anhydrite crystals occasionally (1%) occur within this facies as pore-filling cements.

**Environment of deposition.**-Charophytes generally colonize the photic zone of alkaline oligotrophic lakes (e.g. Dean and Fouch, 1983; Tucker and Wright, 1990; Gierlowski-Kordesch, 2010) and occur at depths from 0 to 10 m (Cohen and Thouin, 1987). The wackestone-packstone textures and the considerable proportions (average 8%), of clastic detritus, including reworked silt-to sand-size extraclasts carbonate particles; in this lithofacies indicate that they occupy littoral lake areas. They may have colonized lake zones with moderate to low energy, causing *in situ* disaggregation and deposition of their calcified structures (stems and oogonia). However, advective transport in the lake margins is suggested by the presence of extraclastic detritus.



**Figure 5.10-** Charophyte wackestone-pakstone. **(A)** Photopanorama, charophyte facies (arrowed). Gastropod units are the most prominent thicker beds, while marlstone form the most weathered intervals. Image form sub-basin I, north of San José Patagalana (see Fig. 1 for village location). **(B and C)** Thin section images of cross- and oblique sections of charophyte oogonia (gyrogonites). Note variable number of spirals (labelled ‘s’ in figure C) and calcite spar occluding intrafossil porespace. **(C)** Vuggy pores (vgp) both rimed by calcite spar and occluded by limonite cement indicated by thick white arrow. **(D)** Cross section across calcified ‘stem’ (‘internodia’); also showing the intraparticle (intrafossil-mouldic) porosity (md).

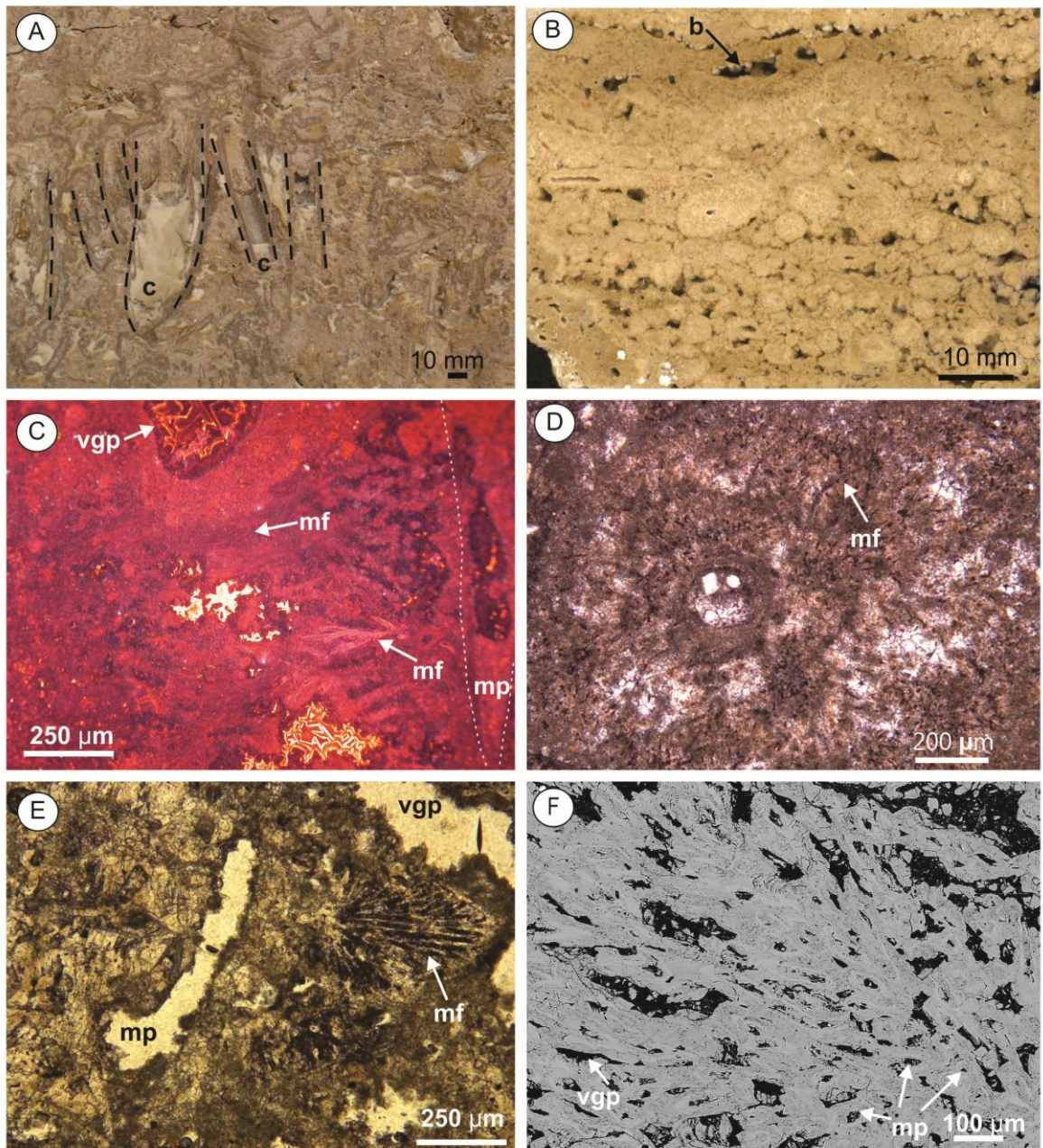
### 5.5.7 *Macrophyte Boundstone (Table 5.1, Fig. 5.11)*

**Description.**- Macrophyte boundstone facies occur in all subbasins, forming laterally discontinuous, irregular metre-scale masses. Boundstone is the dominant texture, although subordinate packstone and grainstones are also present. Rare (<3%) silt-sized quartz grains are found at most localities, however, in subbasin I this facies (e.g. log N2B, Fig. 5.1) contains sand- to pebble-size clasts. Macrophyte components predominantly comprise calcite coated plant stems and leaves (casts), and other undetermined calcified vegetal structures (Fig. 5.11 A to F), together with amorphous organic matter, ostracodes, peloids, oncoids and subordinate gastropods. These components are supported by a matrix composed of dull orange luminescent micrite; a similar luminescence response is emitted by the coated allochems. In some calcareous coatings, calcified filaments are present, composed of either micrite or coarser plate-like calcite crystals (Fig. 5.11 C, E and F). This lithofacies contain 13.1% (average) TOC, with  $\delta^{13}\text{C}_{\text{organic}} = -6.5 \text{ ‰}$  (average) isotopic values.

Porosity in these units is both fabric (mouldic, fenestral and shelter) and non-fabric selective (vug pores) (Fig. 5.11 B). The latter have irregular shapes, and range in size from <0.01 to 0.4 m long, and are commonly partially infilled by geopetal cements (Figs. 5.11 A and B). These cements are composed of either calcite or limonite, that forms microspar and dense microcrystalline masses. Calcite cements also include calcite spar that forms isopachous rims around allochems, fibrous, radiaxial bladed and fibrous calcite. Calcite spar cements exhibit mainly a dull to bright to dull luminescence (Fig. 5.11 C). These cements have average isotopic values of  $\delta^{13}\text{C}_{\text{calcite}} = -5.6 \text{ ‰}$  and  $\delta^{18}\text{O}_{\text{calcite}} = -7.8 \text{ ‰}$ .

**Environment of deposition.**- Generally the calcified component of the macrophytes is the plant 'stem'. This partial preservation indicates that the rest of the plant was subaerially exposed, and the calcified segment was that submerged in the lake water, acting as a marker likely indicating water depth near lake margin (cf. Pedley, 1990). Macrophyte boundstones commonly acted as a baffle, evidence of this action is the presence of coarse sand and pebble-size clasts of Cretaceous limestone found in some localities. Macrophyte boundstones have been referred as phytoherms by other authors (e.g. Pedley, 1990; Arenas et al., 2010), and are the most shoreward lithofacies deposited under normal freshwater lacustrine conditions. Occasionally, the macrophytes are found submerged in distal sub-

littoral lake areas, generally at depths of less than 1 to 2 m (Gasith and Hoyer, 1998). This may explain why some macrophyte patches occur in the clotted boundstone lithofacies.



**Figure 5.11.-** Macrophyte Boundstone. (A) Note vertical calcified plant stems partially filled by calcite spar (c) and microcrystalline calcite forming geopetal cements. Macro and macrophyte casts and coatings partially preserving morphology, indicated by dashed line. (B) Polished slab. Vuggy pores with millimetre size botryoids (b) indicated by the arrow. (C) Cold CL image, variable concentric zoning in vug pores, and relatively homogeneous dull orange luminescence in matrix and encrustation. Calcified microbial filaments (mf), mouldic pore (mp), and vug pore (vgp). (D and E) Different types of calcified microbial filaments and mouldic pores (E). (F) BSE image of calcified undetermined macrophyte. Note moulds and vug pores of non-fabric selective origin. Black background is porespace.

### 5.5.8 Marlstone (Table 5.1, Fig. 5.12)

**Description.**-Marlstones form tabular, irregular beds 0.10 to 0.8 m thick, with pale brownish-grey to greenish- white colour, nodular fabric and variable weathering profile (Figs. 5.10 A and 5.12 A). They are underlain by either fine-grained clastic lithofacies such as the calcareous sandy mudstones, by charophyte wackestone-packstone, or oncoid wackestone-packstones. The marlstones are predominantly composed of detrital fine grained clay and silt size particles (<25%) made of quartz and feldspar cemented by microcrystalline calcite in variable proportions (Fig. 5.12 B and C). Some horizons contain both a few fragmented oncoids, and ostracode valves. Stable isotope analysis of both matrix and oncoids in this lithofacies has average values of  $\delta^{13}\text{C}_{\text{calcite}} -5.2 \text{‰}$  and  $\delta^{18}\text{O}_{\text{calcite}} -7.2 \text{‰}$ . The marlstones are depleted in organic carbon relative to the other lithofacies although results from one interval yield up to 10.5 % TOC and organic carbon stable isotopic values of  $\delta^{13}\text{C}_{\text{organic}} -6.2 \text{‰}$ . In addition intraclasts, carbonate and evaporite nodules, lenticular gypsum crystals, together with circumgranular cracks (Fig. 5.12 B) and *microcodium* with its typical “corn-on-the-cob fabric” surrounded by amorphous clay coatings (Fig. 12 D) are present.

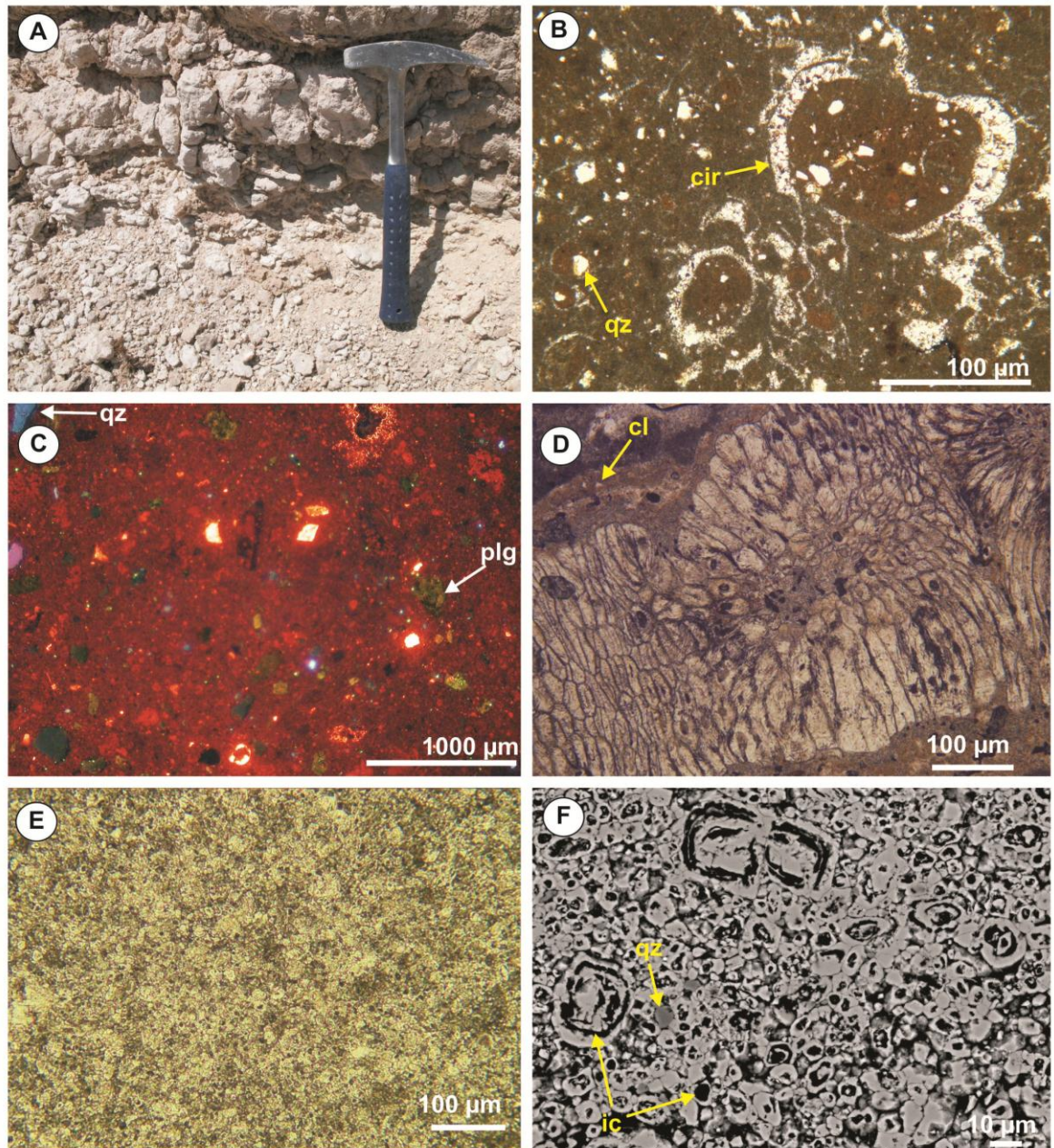
**Environment of deposition.**- The marlstones contain relatively higher proportions of clastic detritus, when compared with the rest of the carbonate lithofacies. The presence of a nodular fabric, intraclasts, bioclast fragments with rare articulated skeletal components together with circumgranular cracking, and *microcodium* features indicate deposition of marlstones took place in lake shore areas subjected to subaerial exposure and variable proportions of clastic input (Fig. 5.14). *Microcodium* is a structure related to either calcification of roots (e.g. Klappa, 1979; Freytet and Plaziat, 1982; Košir, 2004), or fungal mycelia (e.g. Kabanov et al., 2008), and together with the circumgranular cracks support the interpretation that the lacustrine carbonate mud was subaerially exposed and subjected to pedogenic overprint. Intraclasts in this facies also indicates penecontemporaneous sediment reworking from underlying sediment, occurred during subsequent flooding, when clastic detrital input was delivered in the lake margins.

### 5.5.9 Crystalline carbonate (Table 5.1, Fig. 5.12)

**Description.**-Crystalline carbonate is subdivided into microspar-dominated crystalline calcite, and finely-crystalline calcitized dolomite. Proportionally it is the least abundant lithofacies in the Mayrán Basin system. It forms thin (centimetre scale) irregular, structureless, laterally discontinuous deposits, some with a nodular fabric that can be traced laterally for several meters in outcrop in all the subbasins. They occur at the base of the fine grained deposits of the Mayran Formation and at the base of the top of the shallowing upward cycles. Gypsum crystals and nodules occur associated with these deposits.

These units are dominantly cemented by micro-crystalline carbonate composed of non-ferroan calcite spar with anhedral crystals that have of xenotopic fabric. Cemented by this fine grained carbonate there are variable proportions (5 to 25%) of silt-sized detrital grains, mainly quartz, and subordinated feldspars and muscovite. The finely crystalline calcitized dolomite fabric however, is composed of subhedral, equigranular, hypidiotopic crystals of less than 40  $\mu\text{m}$  (Figs. 5.12 E and F). BSE examination of these crystals shows partially “leached” cores (Fig. 5.12 F).

**Environment of deposition.**- Crystalline carbonates forming irregular aggregates rich in calcite spar and microspar were observed in the lake margins (Fig. 5.14 B). Their sedimentological characteristics and position within the sedimentary succession, suggest they are mainly calcrete deposits. Indeed they are similar to the alpha calcrete facies (e.g. Wright and Tucker, 1991). Assuming this to be the case, then they were precipitated from carbonate rich groundwater in the capillary fringe zone or below the water table due to  $\text{CO}_2$  degassing and evaporation (Wright and Tucker, 1991, Alonso-Zarza and Wright, 2010). Additionally calcitized dolomites, formed in the lake margins, and are deposited in the mixing zone of dense concentrated lake brines with groundwaters, during episodes of intense evaporation (Colson and Cojan, 1996).



**Figure 5.12.-** Marlstone (A to D) and crystalline carbonates (E and F). (A) Field exposure showing variable degree of cementation, and weathering in this facies unit starting below base to top of hammer. (B) Thin section in plain light showing circumgranular crack fabric (cir) rimed by equant calcite spar, detrital grains (quartz -qz), microcrystalline calcite and clay, with scattered ostracode (os) valves. (C) CL response showing variable detrital content made of quartz, and plagioclase (plg), micrite matrix with homogenous orange response and cements with brighter orange luminescence. (D) Typical corn-cob aggregates of *Microcodium* with clay coatings (cl). (E and F) Finely crystalline calcitized dolomite crystals, note hollow (black) zones forming intracrystalline porespace (ic) within crystals, pointed by the arrow.



### 5.5.10 Evaporites (Table 5.1, Fig. 5.13)

**Description.**-Gypsum is the most common evaporite mineral in the Mayrán in the Mayrán Basin system, although halite and traces of anhydrite, baryte and celestine are present. Overall they are relative rare and contribute <10% of the succession. Where present, however, gypsum and halite form thin bedded (10 to 100 mm thick) units that internally are either homogenous or exhibit lamination. Gypsum beds occur interbedded with the charophyte wackestone-packstone, gastropod wackestone-packstone, ostracode mudstone-wackestone, and marlstones.

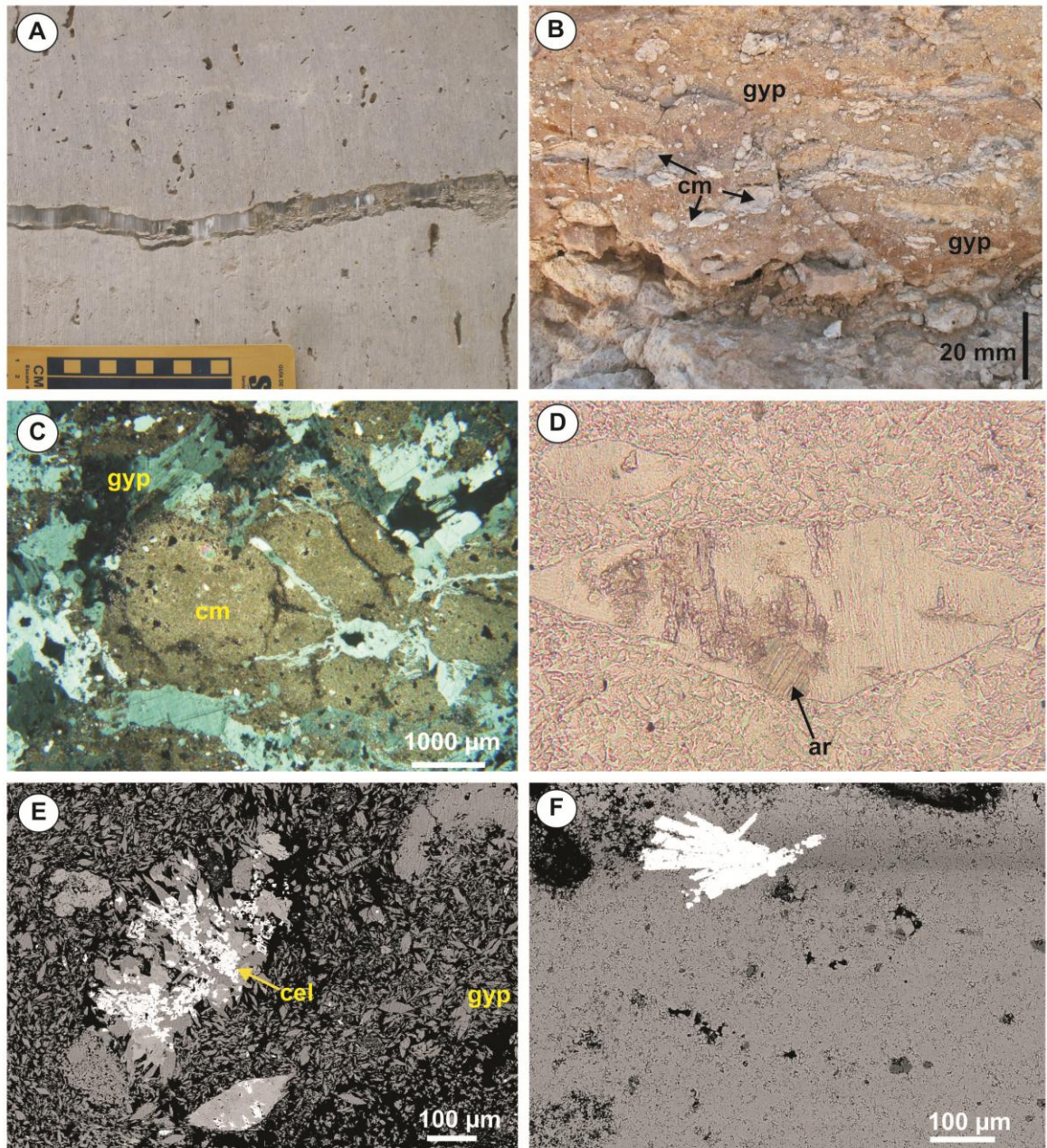
Gypsum forms crusts that are closely associated with mud cracks developed on bedding planes. These cracks have a polygonal planform, penetrate the sediment to a depth of 20 mm, have raised edges and are infilled by gypsum and calcite cements. Gypsum also occurs as discrete selenite nodules, up to 20 mm in diameter that have grown displacively in the sediment and are associated with a brecciated fabric. Large gypsum crystals (up to 1000  $\mu\text{m}$ ) have grown enclosing carbonate mud, and abundant carbonate inclusions are preserved within the crystals (Fig. 5.13 C). Gypsum crystal fabric is lensoid, needle like, prismatic, prismatic lenticular. Some silt-sized lenticular gypsum crystals are partially replaced by fibrous aragonite and sparry calcite cements (Fig. 5.13 D).

Halite is interbedded between ostracodes mudstones (e.g subbasin III, Fig. 5.2 log N22). It forms an orange-weathering unit up to 10 mm thick. Its fabric is poorly preserved. Well preserved and articulated ostracodes occur associated to the halite interval.

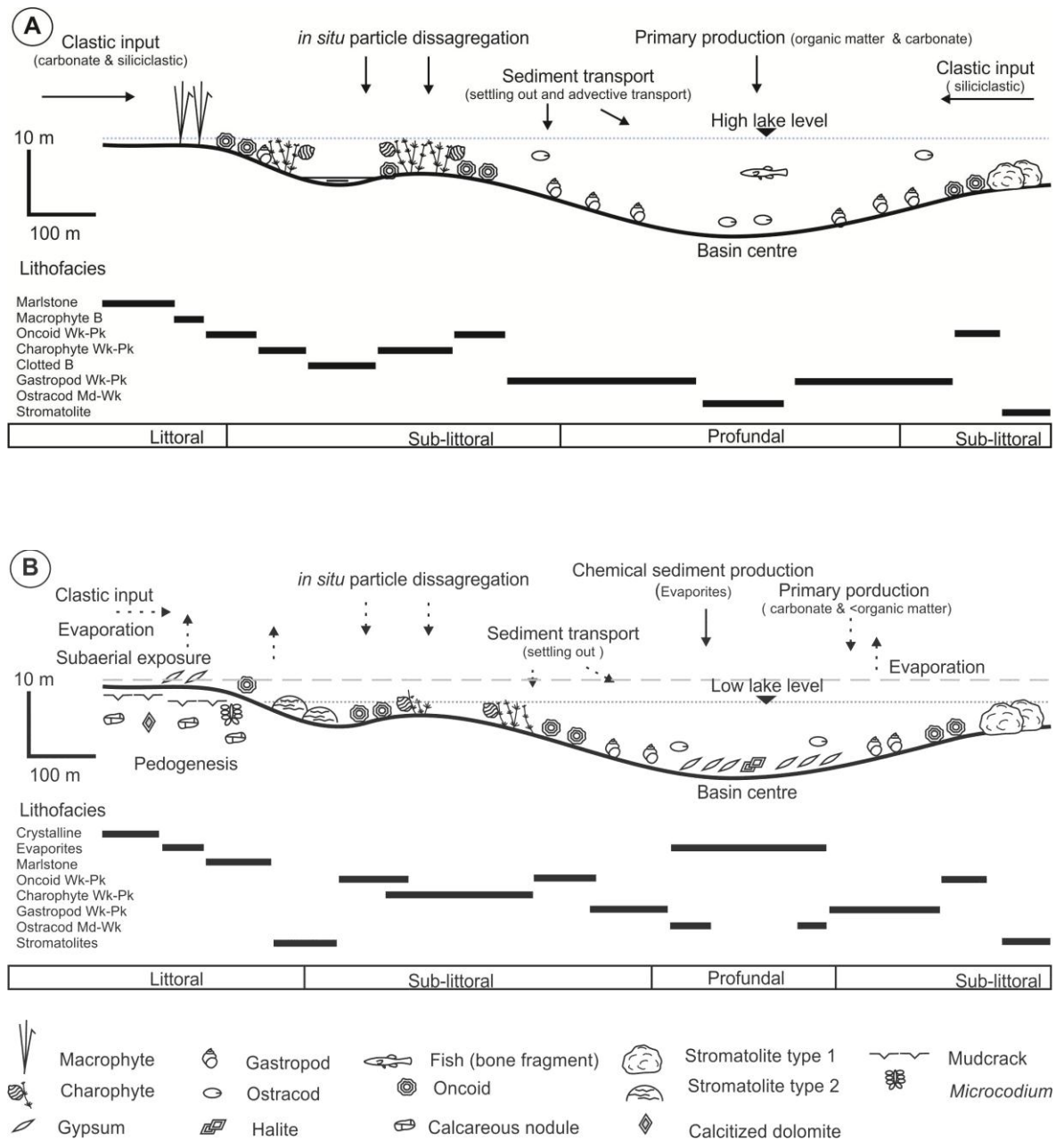
Less abundant evaporite minerals such as anhydrite are present as isolated lath shaped crystals (250  $\mu\text{m}$ ) and as centimetre-sized irregular nodules. Baryte and celestine were determined only under BSE examination (Fig. 5.13 E and F). They form either pore filling cements partially replacing gypsum, or isolated crystals supported in the matrix of the charophyte wackestone-packstone and gastropod wackestone-packstone facies. Baryte occurs as lath shaped crystals with tabular habit or as crystal aggregates (~200  $\mu\text{m}$ ). Celestine occurs as anhedral crystals (<10  $\mu\text{m}$ ) that form aggregates of micrometre size.

**Environment of deposition.**- The presence of gypsum beds interbedded with lithofacies containing freshwater lacustrine components (e.g. gastropod or oncoïd wackestone-packstones) indicate that episodes of saline conditions occurred. Evaporite minerals occur variably in most of the lithofacies, in the form of primary precipitates or cements.

Evaporite precipitation in the lakes resulted from the increase of salinity in lake waters, causing chemical precipitation due to evaporative concentration, when the lakes were hydrologically closed (see Murray, 1964; Hardie, 1991; Hardie and Lowenstein, 2004; Warren, 2010) (Fig. 5.14). Gypsum and halite occur in thin beds, and deposited in the most saline phases of the Mayrán lakes. The record of one critical saline phase occurred in an interval of subbasin II, where the thin halite unit indicate hypersaline conditions occurred (>35,000 ‰), when at least 85-90 % of the lake water was already lost by evaporation (Warren, 2006). These conditions commonly relate to terminal stages of lake desiccation (e.g. Pietras, et al. 2003). Moreover gypsum and anhydrite crystals also formed scattered pore filling evaporitic cements suggesting deposition within previous existing pores, that were once occupied by water, a situation that occurred when lacustrine carbonate mud underwent subaerial exposure effects.



**Figure 5.13**-Sulphates and Halite. **(A)** Gypsum beds interbedded with gastropod wackestone-packstones. **(B)** Bedded gypsum (gyp) with displacive fabrics affecting carbonate mud (cm). **(C)** Large gypsum crystals (gyp) which have grown within the enclosing carbonate mud (cm). Note the carbonate mud inclusions within the crystals. **(D)** silt-sized lenticular gypsum locally pseudomorphed by calcite and aragonite (ar) indicated by the arrow. **(E)** BSE image showing gypsum crystal fabrics and presence of Celestine (cel) in bright  $\eta$  coefficient, partially replacing gypsum. **(F)** Baryte cements in bright  $\eta$  coefficient after gypsum, within a micrite carbonate matrix.



**Figure 5.14.-** A and B.- Schematic lateral distribution of microfacies types in the lacustrine setting and their depositional processes during high lake level (A) and low (B) lake level.

## 5.6 Discussion

Petrographic and geochemical characterization of the Mayrán carbonate lithofacies indicates that they contain variable proportions of detrital components, production derived components, and post depositional early diagenetic components; deposited in proximal and distal lacustrine settings.

### 5.6.1 Detritus derived components

The depositional context of the Mayrán Formation indicates that the major source of water and clastic detrital components was the Parras Range, localized at the south of the basin system (Fig. 5.1). Subordinate sources of siliciclastic detritus were locally derived from the sandstone bedrock ridges that confine the lake subbasins (Amezcuca et al., 2012). The sediments sourced were predominantly composed of limestone clasts (80%), and the coarse clastic particles were trapped in the most proximal subbasin (I). Their mechanical and chemical disaggregation, coupled with down-dip sorting, supplied sand- to mud- size detrital particles to the lakes. Allochthonous carbonate particles found in the carbonate lithofacies include fine sand to mud size grains, including reworked Cretaceous foraminifera, that were sedimented by the baffling effects of the macrophytes living in the margins of the lakes (e.g. Macrophyte boundstones in locality N2B, Fig. 5.1 and Appendix 6), while the rest dispersed offshore. Overall the amount of detrital derived components in the lacustrine limestones is variable, yet it represents only a minor proportion (< 25%) when compared to the dominant production-derived components. Siliciclastic particles commonly consist of silt-sized quartz and subordinate feldspars. More importantly detrital inputs into the lakes were likely insufficient to cause significant carbonate dilution (Gierlowski-Kordesch, 1988). Additionally, the predominant input of solutes from surficial and groundwater sources into the Mayrán lakes, likely provided dissolved solutes required for calcium carbonate precipitation in the lakes (e.g. Ca;  $\text{SO}_4^{2-}$ ,  $\text{HCO}_3^-$ ;  $\text{HCO}_3^-$ -Na,  $\text{SO}_4^{2-}$ -Cl-Na). Moreover, the deposition of lacustrine limestones here was partially influenced by the input of the clastic carbonate sediment yield to the subbasin I. Similar sedimentological response of carbonate lacustrine successions has been documented from shallow lakes from the Jurassic, Newark Supergroup (e.g. Gierlowski-Kordesch, 1998).

### 5.6.2 Locally produced components

Biogenic and non-biogenic processes occurring within the lake water column were responsible of autochthonous primary production of carbonate sediment and organic matter, including some early diagenetic components.

The lithofacies revealed that primary production of biogenic components was by organisms with calcareous skeletons such as ostracodes, gastropods, calcareous algae (charophytes and unicellular algae), and calcifying microbial communities. The mineralogical composition of their skeletons was either calcite or aragonite, and occasionally phosphate (e.g. teeth and bone fragments). This carbonate production took place in the water column and in the sediment water interface.

Important carbonate producers in the Mayrán Basin lakes were the charophytes. Their in situ disaggregation contributed to the local lime mud production in the lake littoral zone, where they supply up to several hundred grams per square meter per year (cf. Murphy and Wilkinson, 1980; Dean, 1981).

Fine-grained carbonate particles determined in most of the lithofacies under BSE observation include euhedral to subhedral crystals of less than 20  $\mu\text{m}$  size (Fig. 5.3E and F). Their origin may relate to the episodic oligotrophic conditions that occurred in the water column of Mayrán lakes, as indicated by the presence of the Lymnaeidae-type gastropods (e.g. Lőzek, 1986; Miller and Tevesz, 2001) (Fig. 5.7A). Under oligotrophic limnic conditions non-biogenic authigenic calcite crystals can also precipitate, producing larger (10 to 20  $\mu\text{m}$  size) calcite crystals with well-defined exagonal and platy morphologies (Leng et al, 2010), because they form by rapid precipitation in waters with low magnesium content (Folk, 1974; Leng et al., 2010).

Assuming that in the water column of the Mayrán lakes oligotrophic conditions took place, fine-grained calcium carbonate particles may have also precipitated via photosynthetically induced processes promoted by free-floating cyanobacteria picoplankton (e.g. *Synechococcus*) and algal blooms during whitening events (Kelts and Hsü, 1978, Thompson and Ferris, 1990; Thompson et al., 1997; Thompson, 2000; Dittrich et al., 2004; Riding, 2006). In these conditions precipitation takes place both in the water column due to alkalinitization processes derived from the uptake of  $\text{CO}_2$  during photosynthesis (Kelts and Hsü, 1978; Stabel, 1986) as well as in the vicinity of the picoplankton cell

(Thompson et al., 1997). The produced carbonate particles are commonly  $<5\mu\text{m}$  in size (Thompson et al., 1997), and are typically composed of calcite (e.g. Shinn, et al., 1989; Robbins and Blackwelder, 1992).

Primary production in the water column also produced high amounts of organic matter (ranging from 10.19 to 13.20%, average 12.60). The little variation in TOC content observed in the lacustrine lithofacies suggests that, overall similar processes of organic matter production and conditions for its preservation occurred in both proximal and distal lake settings. Whole rock organic carbon isotope values yielded from the sedimentary organic matter (ranging from  $\delta^{13}\text{C}_{\text{organic}}$  -5.8 to -18.1‰, average -6.4‰) are however, similar to those obtained from the green algae *Potamogeton* in the Quaternary lakes in the Qinghai-Tibet Plateau (see Aichner et al., 2010), and from cyanobacteria communities (-5.4 ‰ mean values) from microbial mats in the Solar Lake (e.g. Schidlowski 2000). Input of land plant material (e.g.  $\delta^{13}\text{C}_{\text{organic}}$  -20 to -32‰), is not demonstrated from the organic carbon isotopic data. Alternatively, the relative enrichment of the isotopic values, could relate to fractionation occurring during oxidation of the organic matter (Talbot and Livingstone, 1989). Petrographic evidence together with the organic carbon isotope values, however, suggests that organic matter was autochthonous and likely produced in both the water column (by algae and cyanobacteria), and by benthonic organisms, including microbial communities. A subordinate contribution by aquatic fauna is not established, although millimetre sized phosphatized fragments were observed under petrographic examination.

Although high carbonate production occurred in the Mayrán lakes, autochthonous carbonate sediment production was not sufficiently enough to dilute the organic matter. Moreover, the fine grained micritic matrix of the lacustrine sediments may have aided in the preservation of considerable amounts of organic matter (cf. Thompson and Eglinton, 1978). As a result, a moderate sedimentation rate and moderate production rate is likely to have controlled organic matter preservation (cf. Bohacs et al., 2005) in Mayrán lake basins. These processes may have also coped with the infauna and microbial processes that degrade the available organic matter (see Coleman et al., 1979, Kelts, 1988, Katz, 2001). Therefore, the accumulation of organic matter-rich lacustrine carbonates is a complex interaction of processes such as rates of production, destruction, and dilution of the organic matter (Kelts, 1988; Bohacs et al., 2005).

Intense to moderate bioturbation (BI 1 to 4) in most of the lithofacies, indicates that sufficient oxygen was likely available in the water column to sustain biological activity. Deposition of the lacustrine lithofacies occurred under predominantly oxic conditions. Under oxic conditions, a positive correlation exists between the sedimentation rates of organic matter preservation, quantity and quality (Kelts, 1988; Canfield, 1994, Katz, 2001). Despite considerable oxidation occurred below the oxygen penetration zone (cf. Canfield, 1994), significant organic matter was preserved. This probably occurred because of the relatively rapid isolation of the organic matter from the oxidizing conditions in the water column, without causing significant dilution, as it deposited in the fine grained micritic matrix (e.g. Arthur and Sageman, 1994; Meyers and Ishiwatari, 1993). Consequently, organic matter preservation here was a function of moderately high primary production linked to optimizing rates of sediment accumulation (cf. Bohacs et al., 2000a; Carroll and Bohacs, 2001), and inherent characteristics of the fine grained carbonate matrix.

### 5.6.3 Early diagenesis

The early diagenetic transformations that carbonate sediments and rocks undergo in these environments include physical, chemical and biologically mediated processes occurring either after deposition or precipitation of a particle in the water column, at the sediment-water interface and until the rock enters into metamorphic domains (cf. Berner, 1980; Morrow and McIlreath, 1990). Diagenesis in continental carbonates encompasses a range of processes occurring in the lacustrine, meteoric, and subsurface environment (e.g. James and Choquette, 1989; Moore, 2001). Common diagenetic processes observed in the Mayrán carbonate lithofacies include calcite cementation, selective dissolution, 'micritization', mineral replacement, oxidation of organic matter and evaporite mineralization. Most of these changes span processes driven by physicochemical conditions caused by lake level variations. Overall diagenetic features include: isopachous fringes of equant calcite, together with radiaxial fibrous, acicular calcite, precipitation of calcite spar and microspar filling porespace including burrows, *microcodium* features, circumgranular cracking, dissolution of aragonite allochems and cementation of equant calcite spar, and gypsum calcitization. As observed in all the lithofacies, early diagenetic components may occur either as 'primary' or replacing cements, and are either authigenic or detrital in origin. The most ubiquitous cement identified petrographically was calcite, although subordinate aragonite and calcium sulfates also occur.



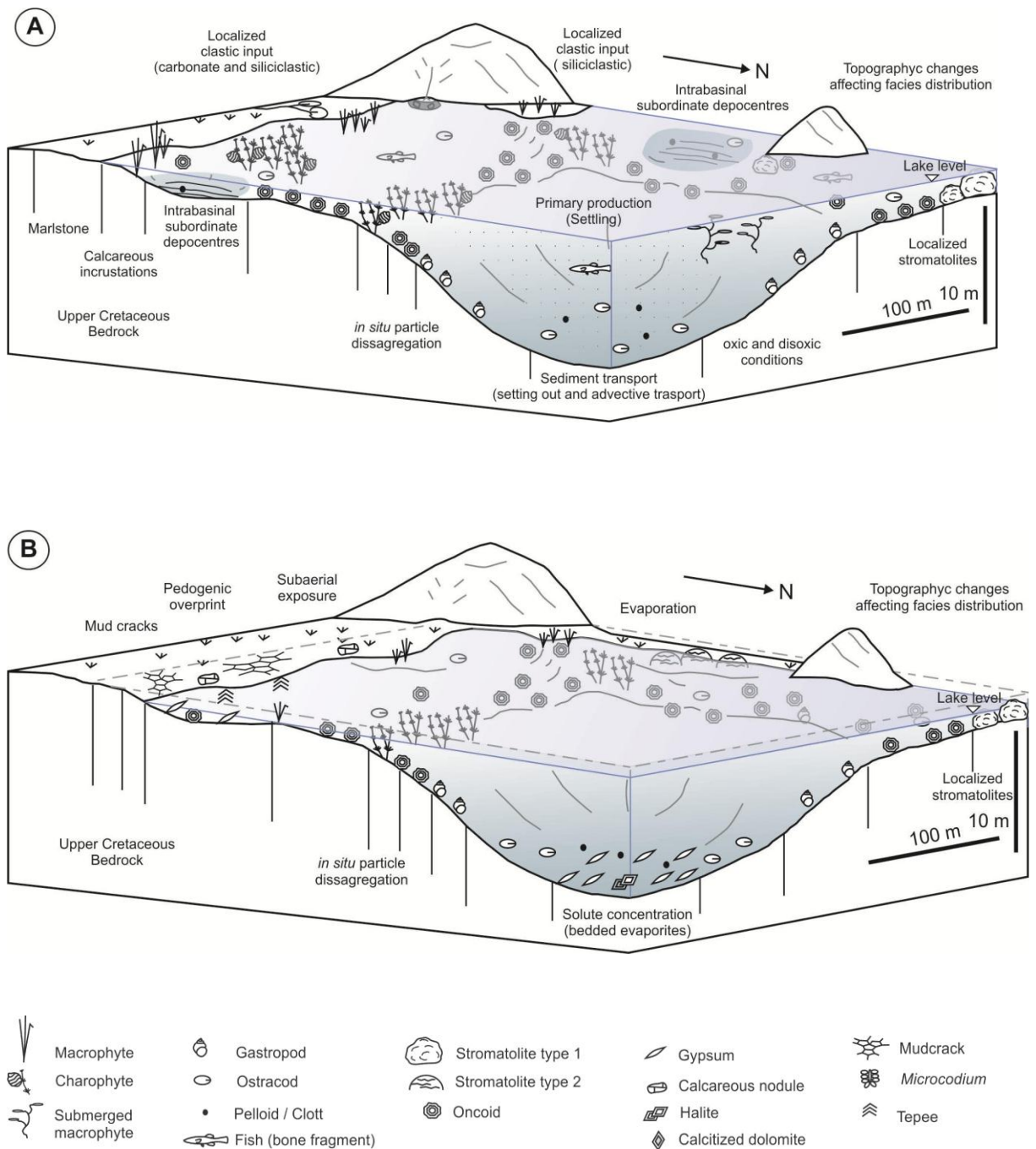
Early diagenetic processes might have been dominated by microbial redox reactions, which oxidize organic matter, in the presence of oxygen, iron oxides and sulfates (cf. Berner, 1985). Subsequently successive reactions mediated by sulfate reducing bacteria and microbial methanogenesis generate by-products such as carbonate, sulfide and reduced iron that can precipitate as early diagenetic minerals such as calcite, gypsum, dolomite, siderite, ferroan calcite and pyrite (e.g. Coleman 1985; Raiswell and Canfield, 1998).

The relative little differentiation between the stable isotope values of both oxygen (ranging from  $\delta^{18}\text{O}_{\text{calcite}}$  -6.3 to -8.6 ‰, average -7.6 ‰) and carbon (ranging from  $\delta^{13}\text{C}_{\text{calcite}}$  -4.2 to -7.0‰, average -5.7 ‰) of micrite and calcite spar cement could reflect the difficulty of microsampling the samples. Alternatively, and based on the euhedral morphology of the microcrystalline calcite observed in the BSE examination suggest that there has been recrystallization and likely isotopic resetting of much of the Mayrán Formation carbonates by post-depositional flux of rainwater. Some pore filling calcite cements, show a characteristic meteoric phreatic non luminescent-bright luminescent concentric zonation in CL examination, clearly indicating being post-depositional meteoric diagenesis.

Several evaporite mineral intervals are found in the Mayrán succession. Sulfate may have been sourced from oxidation of elemental sulphur present in the waters that drained into the lakes, and calcium sulfate saturated solutions formed during stages of lake contraction, due to high evaporation rates (Fig. 5.14 B and 5.15 B). Abiotic and biogenic processes may have removed sulphate from the water. Sulphide microbial oxidation results in the precipitation of gypsum (Thompson and Ferris, 1990) and Baryte (Raven and Knoll, 2010) and even halite (Castanier, et al., 1999). Nodules of gypsum (and anhydrite) displacively affect the carbonate mud are closely associated with mud cracks and pedogenic deposited in lake shore areas, subjected to subaerial exposure (Fig. 13B). They may have resulted from groundwater saturation with respect to gypsum recharged around lake margins (cf. Rosen and Warren, 1990).

Mineral replacement obliterated the original fabric in some lithofacies. For example, calcite and aragonite pseudomorphs formed in silt-sized lenticular gypsum in some intervals. Aragonite replacement of gypsum has been related to bacterial sulfate reduction, where carbonate carbon was supplied by oxidation of organic matter (e.g. Anadón et al., 1992). Siderite cements found in the ostracodes mudstones and gastropod

wackestones-packstones, are authigenic cements. Microbially mediated redox reactions occurring during organic matter oxidation likely caused iron reduction under low dissolved sulfide promoting siderite cement precipitation (e.g. Coleman, 1985; Rajan et al., 1996). Methanogenic siderite origin (e.g. Curtis and Spears, 1968) is not considered, because isotopic  $\delta^{13}\text{C}_{\text{organic}}$  (average -6.4 ‰) values are not depleted enough to indicate this process.



**Figure 5.15-** Idealized paleoenvironmental reconstruction Mayrán lakes. Sedimentary facies distribution and depositional processes in the lacustrine setting, during high lake level stage (A), and during low lake level stage (B).

#### 5.6.4 Spatiotemporal facies variation within the carbonate lithofacies

Primary sedimentary structures, fossil content, together with relative proportions of detrital, autochthonous, and diagenetic components, indicate the lithofacies deposited in proximal (littoral) and distal offshore (profundal) lake settings (Fig. 5.14 and 5.15). Strata stacking patterns organize in shallowing upwards cycles (0.3-2.5 m thick), which are capped by either evaporites or beds with pedogenic overprint. These characteristics reflect lake level variations, which can be recognized in all the subbasins. The lithofacies architectures within each subbasin forms parasequences that overall exhibit aggradational geometries. The lithofacies present and their large scale geometries also indicate deposition occurred in a series of relatively shallow (<10 m), lake systems with ramp-like margins (Fig.5.15) (cf. Platt and Wright, 1991). The aggradational stacking patterns of the carbonates and the presence of subordinate evaporites suggest that basin hydrology (water supply and precipitation/evaporation ratios) had an important influence on facies architecture and cyclicity (e.g., Carroll and Bohacs, 1999, 2001).

Interestingly at the top most of the lacustrine carbonate successions in all the subbasins, occur thin beds (10 cm) of either gastropod wackestone-packstones, charophyte wackestone-packstones, or oncolid wackestone-packstones occur, some of which may form bed duplets (e.g. log N4B-subbasin I, N21B-subbasin II, N22-subbasin III, and N34-subbasin IV, see Figure 5.2 and Appendix 6, 7, 11, 12, and 16). Based on this observation it is inferred that the thinning upward bed pattern observed at the top of the carbonate successions in all the subbasins, possibly relates to the lack accommodation availability in the lake depocentres (see Bohacs et al., 2000a). Finally, organic carbon rich sediments commonly deposit in aggrading successions of balance filled lake basins (e.g. Bohacs, et al 2000a).

This is possible because accommodation in the lake depocentres was geomorphically controlled by the inherited topography, and because the Mayrán Basin system initiation, fill and termination occurred during tectonically quiescent conditions (e.g. Amezcua et al., 2012). –The Mayrán Basin system lakes, likely developed during a relatively humid period with episodic hidrological basin closure. The lake level changes controlling facies architecture were consequently the product of allocyclic climatic mechanisms that controlled water supply.

## 5.7 Concluding comments

Carbonate deposits of the Mayrán Basin system were investigated using field observations, geochemical, and petrographic analysis to determine controls on their spatial and lithofacies variability. Using these techniques nine sub-facies were identified in the horizontally bedded limestones facies, based on their textural attributes and identifying their production derived components, detrital components, and diagenetic overprint. The sub-facies are: ostracode mudstone-wackestone, clotted mudstone-packstone, gastropod wackestone-packstone, oncolite wackestone-packstone, stromatolites, macrophyte boundstone, marlstone, and crystalline carbonate, together with evaporites. These facies deposited in the lacustrine setting and commonly interbedded with evaporites. Proximal lake areas in subbasin I, were highly influenced by carbonate clastic input, while open lake areas protected from this input were dominated by chemical and biochemical sedimentation processes that formed the limestones. Proximal areas in the rest of the subbasins (II-IV) have also subordinated clastic (siliciclastic) input and are dominated by lacustrine limestones.

Depositional controls indicated by rock texture, fossil content, geochemistry and primary and secondary sedimentary structures, indicates that the lakes were relatively shallow (<10m), and that overall oxic conditions prevailed in the water column. Intense primary productivity is revealed by the high volume of carbonate sediment deposited in all the subbasins and by the high content of sedimentary organic matter preserved in the carbonate facies.

Wide distribution of some lithofacies (e.g. gastropod wackestone-packstones) suggests that overall the lake subbasins had low relief, and had ramp like margins. The spatio-temporal distribution of the lacustrine facies, also reveal that intense aggradation of the sedimentary lacustrine succession occurred in response to lake level variations. Stacked limestone beds indicate that overall the succession comprises a series of shallowing upward cycles. Carbonate dissolution, desiccation cracks, evaporite nodules, calcretization and pedogenic features affecting the top of the shallowing upward cycles, indicate that wide lake areas were subaerially exposed during low lake level stages. Subsequent flooding episodes are marked by irregular erosional surfaces overlaid by lithofacies containing freshwater dominated fauna (e.g. charophyte wackestone-packstones, oncolite wackestone-packstones and occasionally gastropod wackestone-packstone), indicate the reestablishment of normal lacustrine conditions as the lake expanded likely during high

lake level stages. Overall cyclic variations occurring in all the subbasins, although not unequivocally correlated suggest that climate controlled basin hydrology and individual lake level variations. The lake subbasins, in spite of being formed onto siliciclastic bedrock, were filled by considerable volumes of carbonate sediments. This happened because enough calcium (both detrital and dissolved) and likely input of groundwater enriched in calcium ions drained the subbasins, together with the local physico-chemical, and biological processes that acted to induced carbonate precipitation and organic matter production.

In conclusion, the identification of the relative proportions of primary production derived components, detrital components and early diagenetic processes in these lacustrine lithofacies, allowed construction of a model that illustrates the facies lithofacies variability in carbonate dominated lakes.

## **5.8 Acknowledgements**

This contribution represents a portion of Amezcua's doctoral dissertation at the University of Manchester. Support for this project was provided by the Mexican Geological Survey (SGM). Funding was provided by the National Council of Science and Technology of Mexico (CONACYT) for the studentship grant to N. Amezcua. Thanks to Jim Bell who performed stable isotope analyses at the Liverpool University; to Stephen Stockley and Harry Williams of the thin-section Laboratory at Manchester University; and to Allyson Pye for performing the TOC and organic carbon isotope analyses at the Isotope Laboratory at Memorial University of Newfoundland, Canada.

## **Chapter 6**

## Chapter 6

# U-Pb Dating of carbonates in the Mayrán Formation, Northeast México

N. Amezcua, D.J. Condon, and R. Gawthorpe, J.H.S. Macquaker

### 6.1 Abstract

Originally a Pleistocene age was suggested for the Mayrán Formation when it was first described by Imlay (1936 and 1937). Stratigraphically the Formation overlies on angular unconformity onto Cretaceous (Campanian-Maastrichtian) rocks deformed by the Laramide tectonic event, which ended in the Eocene. The formation occurs in four adjoining carbonate-dominated subbasins product of the erosional topography of the Parras foreland-thrust-belt. Present exposures of the Mayrán formation are deeply incised, and contain post-Mayrán deposits containing Pleistocene to Holocene fauna.

The U-Pb dating technique was implemented on continental carbonates, in order to obtain an absolute age of the Mayrán Formation. The samples were carefully selected based on detailed petrographic analyses. These samples include botryoidal calcite cements filling voids in the tufa formed at lake spillover points IA and IIA, oncoids and laminations in stromatolites deposited in the lacustrine setting of subbasins I and II.

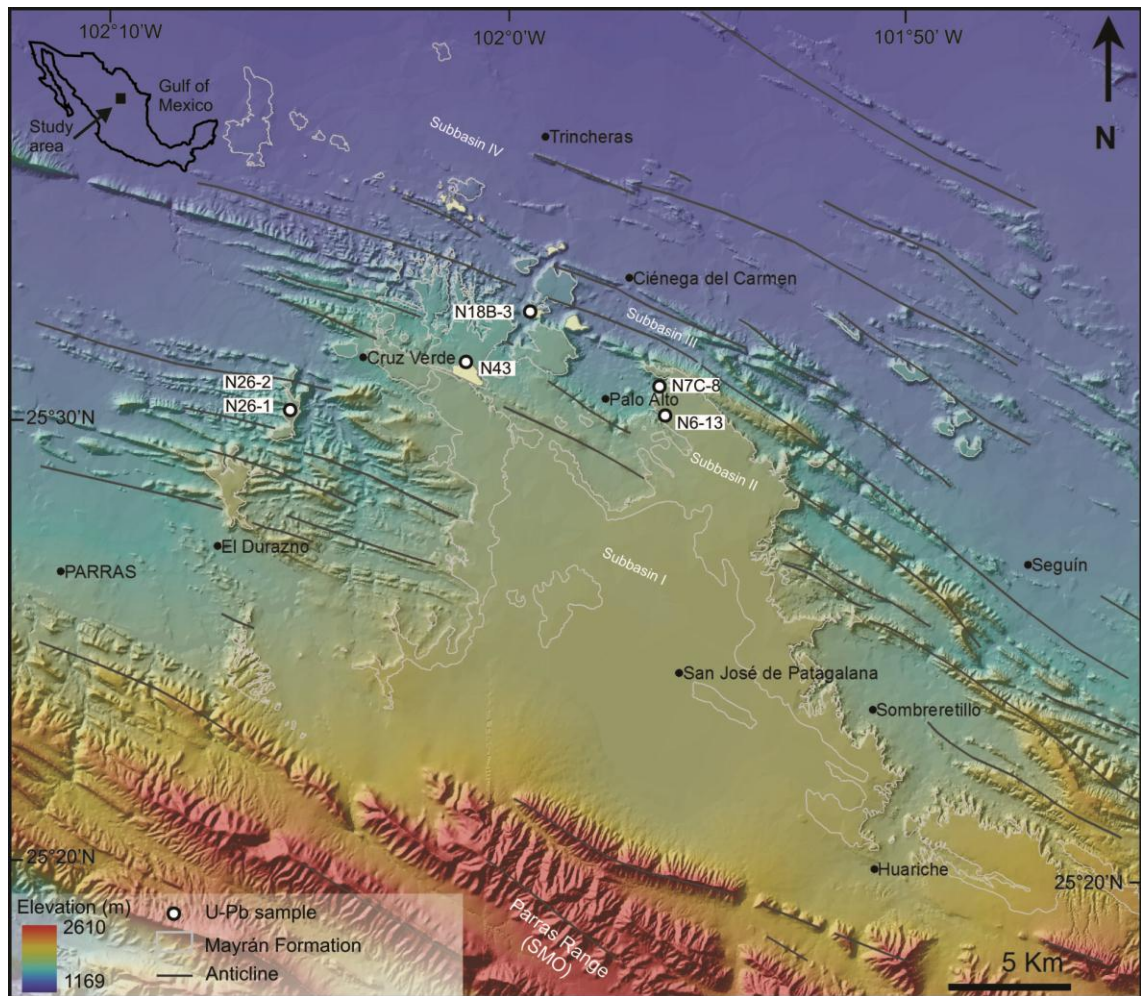
An accurate Pliocene age ( $3.06 \pm 0.21$  Ma) was obtained for the Mayrán Formation based on uranium-lead dating on botryoidal calcite speleothem cements from the tufa delta lobe IIA. The results indicates that U-Pb dating can provide good age constraints, when suitable samples are selected. Moreover, this dating technique is particularly useful when other dating methods are not applicable.

## 6.2 Introduction

In continental settings, carbonates commonly form in lakes, caves and calcrete deposits. Determining the age of continental carbonate successions is complicated, because they commonly lack diagnostic fossils. This is even more difficult when volcanic ash marker beds or siliciclastic deposits containing either pollen or microfossils are not present. U-Pb dating of continental carbonates has been proven to provide reliable ages and is therefore useful to constraint timing of their deposition (e.g. Richards et al., 1998; Richards and Dorale, 2003; Cole et al., 2004, 2005; Woodhead et al., 2006; Polyak et al., 2008, and Rasbury and Cole, 2009). Lacustrine carbonates, tufas and speleothems are good candidates for U-Pb dating because they are relatively abundant; they are generally composed of stable low magnesium calcite, and may have a considerable amount of uranium due to complexation with organic matter (e.g. Idiz et al., 1986; Cole et al., 2005, Rasbury and Cole, 2009). Furthermore, in alkaline settings, U is enriched because elevated dissolved carbonate increases U concentrations in both the precipitated carbonate and water (Simpson et al., 1989; Richards and Dorale, 2003; Cole et al., 2005; Rasbury and Cole, 2009).

Determining the age of the Mayrán Formation is important because it can help to constrain the age of a pluvial event that created a series of coeval lake subbasins. The effects of these climatic conditions likely extended to other areas of northeast Mexico (e.g. Providencia Formation see Rodríguez and Werner, 1993) and south USA (e.g. Goliad Formation, see Page et al., 2005), where fluvio lacustrine successions of late Neogene age deposited. Moreover dating of carbonates in the Mayrán Formation can help to solve the ambiguous and poorly constrained Pleistocene age based on stratigraphic relations that involve considerable time intervals. The Mayrán Formation contains a succession dominated by continental carbonates deposited in lacustrine and giant progradational tufa lobes, formed at the subbasin sills. The Mayrán Formation is younger than the underlying Campanian-Maastrichtian rocks, but older than both the tufa and lacustrine carbonates containing Pleistocene fauna, and Holocene sediments. These post-Mayrán carbonates deposited were in deeply incised valleys that cut into the Mayrán Formation (e.g. Subbasin II, Amezcua et al., 2012), and the Cretaceous bedrock. There are neither diagnostic vertebrate nor microfossils to constraint a biostratigraphic age, nor volcanic ash deposits upon which other radioactive dating techniques can be applied.





**Figure 6.1-** Map showing location of the Mayrán Basin system, its sub-basins, and U-Pb sample locations: lacustrine stromatolites (N26-1, and N26-2), oncolites (N7C-8, N6-13), calcite with dendrite-like crystals (N43); and botryoidal calcite cement (N18B-3). Sierra Madre Oriental (SMO) geological province.

The Mayrán Formation continental carbonates contains pristine carbonate deposits appropriate for U-Pb isotopic analysis. These include stromatolites, and oncolites deposited in a lacustrine setting, and botryoidal calcite (speleothem) cements deposited in the prograding tufa clinofolds (spillover points). Whilst there have been an increased application of the U-Pb method to date authigenic carbonates formed in a variety of depositional settings, successful application requires that several criteria being met, primarily that U is incorporated into the calcite during crystallization, are the incorporation of Pb is limited and that a spread in U/Pb can be sampled so that an array in U-Pb isotope space can be generated and an age calculated based upon that linear array (see Rasbury and

Cole., 2009 for a recent review). Other significant requirements include that U and Pb are not mobile and are not lost or added to the sample. Given these selective criteria we have used *in situ* sampling methodologies to screen a number of samples in order to assess their suitability for isotope dilution analyses to provide accurate U-Pb data. With the U-Pb dating the age of the Mayrán Formation can be constrained. Moreover, overall climatic conditions can be suggested based on the yield age when compared with other proxy data of north Mexico and south USA.

### 6.3 Geologic Setting

The Mayrán Formation is a post-Cretaceous fluvio-lacustrine succession exposed in the erosional remnants of the Parras Basin, Northeast Mexico (Fig. 6.1). It is undeformed and overlies on angular unconformity onto Cretaceous (Campanian-Maastrichtian) siliciclastic rocks of the Difunta Group (Cerro Huerta and Cerro del Pueblo Formations), and Parras Formation (Amezcuca et al., 2012), that were deformed during the Laramide deformation (McBride et al., 1974; Gray et al., 2001). The clastic and carbonate rocks that form the Mayrán Formation were deposited in four down northwards stepping, carbonate-dominated, coeval lacustrine subbasins, that comprise the Mayrán Basin system (Amezcuca et al., 2012).

The Mayrán Formation consists of fluvial to lake shore clastics (nonchannelized- and channelized conglomerates, and pebbly sandstones, calcareous sandy and siliciclastic mudstones), widely distributed lacustrine carbonates and localized tufa clinoform deposits. The lacustrine carbonates comprise ostracode mudstones, clotted mudstone-packstones, gastropod wackestone-packstones, oncoid wackestone-packstones, charophyte wackestone-packstone, macrophyte boundstone, marlstones, crystalline carbonate, and evaporites. Vertically these lithofacies is organized into shallowing upward cycles, forming overall aggrading stacking patterns. Relatively similar facies and cycles are observed in the four subbasins. The tufa clinoforms are located at the spillower points between the subbasins and form prominent lobes. Commonly in these tufas, pore space (up to cavernous vugs) is filled by speleothems often with a botryoidal (mammillary) fabric.

The Mayrán Formation has been considered of Pleistocene age (Imlay 1936, 1937), based on stratigraphic relations, as it overlies onto an angular unconformity to the

Campanian-Maastrichtian rocks and is overlaid by recent (Holocene) deposits (Fig. 6.2). Moreover, post-Mayrán rocks consisting of limestones with lacustrine fauna and tufa deposits (associated with springs and lake margins) occupy deeply incised valleys that cross cut the Mayrán Formation and the Cretaceous bedrock. Consequently, the age of the Mayrán Formation based on stratigraphic relations is still rather ambiguous.

Era / Period / Epoch			Age (Ma)	Study area	
				Imlay (1936)	This work
Cenozoic	Quaternary	Holocene	0.011		Undetermined
		Pleistocene			Post Mayrán
	Neogene	Pliocene	2.588	Mayrán Fm.	Mayrán Fm.
			5.332		
		Miocene			
		Oligocene	23.03		
	Paleogene	Eocene	33.9±0.1		
			55.8±0.2		
		Paleocene			
	Cretaceous	Upper	65.5±0.3	Difunta Group* & Parras Fm	Difunta Group* & Parras Fm (Foreland)
Lower		99.6±0.9			
Jur.	Upper	145.5±4.0	Parras Range (SMO)	Parras Range (SMO)	

**Figure 6.2-** Generalized stratigraphic section of the Mayrán Formation and Cretaceous bedrock (\*Cerro Huerta and Cerro del Pueblo Formations of the Difunta Group), and Jurassic rocks of the Parras Range, Sierra Madre Oriental (SMO) geological province. Listed numerical ages are taken from the Geologic Time Scale from Gradstein et al., 2004.

Age diagnostic fossils have not been found in the fluvial or lacustrine deposits of Mayrán formation, although molluscs, charophytes and some fish remains occur in the lacustrine carbonate lithofacies. The relative Pleistocene age assigned to the Mayrán deposits, however seems very unlikely, since fossils of horses (*Equus excelsus* Leidy) were found by Rogers et al. (1961), in the post-Mayrán deposits. *Equus excelsus* is synonymous

of *Equus scotti* (Azzaroli, 1998), and reports of these species of horses in other localities of north Mexico indicate a middle Pleistocene (~1.6 Ma) age (Carranza-Castaneda and Roldán-Quintana, 2007).

### 6.3.1 Stromatolites, oncoids and botryoidal cements

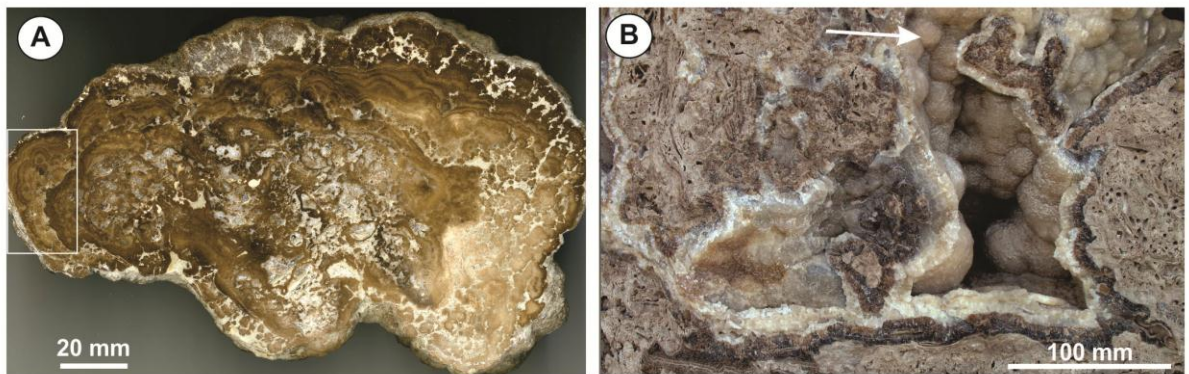
Specific components, such as stromatolites, oncoids and calcite cements with bedded radial fibrous and botryoidal fabric, were selected for the analysis. Six samples comprising stromatolites (N26-1 and N26-2), oncolites (N7C-8, N6-13), bedded dendrite-like (N43) and botryoidal calcite cement (N18B-3) were selected for U/Pb dating based on petrographic analysis. Stromatolites and were collected from close to the base (at 1.5 m) of the lacustrine succession (of ~2.5 m thick) deposited at a distal northerly sector of subbasin I (Figure 1). Oncolites were taken from the middle part of the lacustrine succession in subbasin II. The bedded dendrite-like cement was collected from about 2 m below the top, at the middle sector of the prograding tufa lobe IA. The botryoidal (mammillary) cement was taken from the middle sector of the prograding tufa lobe IIB, near (1.5 m) the contact with the Mayrán basal angular unconformity (See Figure 4.2D, in Chapter 4).

Samples were initially analysed using optical and electron optical (plane light, BSE, cold CL) microscopy analyses performed on regular (48 x 26 mm) and large (75 x 48 mm), unusually thin (*circa.* 20 µm) sections. Samples were investigated using X-Ray diffraction (XRD) to determine the bulk rock mineralogy. In order to carry out U-Pb analyses of samples those contained least clastic detritus were targeted. The selected samples consist entirely of calcite and do not contain other detritus. The same slabs used for thin section making were cut into blocks of 5x10 mm and polished to perform U-Pb dating.

The oncoids (samples N7C-8 and N6-13) are of irregular shape and size, ranging from sub-millimetre to tens of millimetres in diameter, and occur within the beds of well-cemented microcrystalline calcite matrix. Their internal fabrics consist of a clotted micritic nucleus rimmed by either concentric micritic laminations or microsparitic laminations. The stromatolites (samples N26-1 and N26-2) from the northern sector of sub-basin I (Fig.6.1) have an irregular shape, and exhibit diverse nucleation sites. Their internal fabric consists of superposed, concentric irregular laminations, growing away from a micritic clotted

nucleus. The lamina are less than 100 micrometers, and consists of dense microcrystalline calcite, or light microcrystalline spar (Fig. 6.3 A). Small irregular vug pores commonly occur in the internal structure of the stromatolite, and are filled by equant calcite spar cements. Cathodoluminescence examination of the stromatolites indicates that the clotted nucleus and laminations have a dull orange luminescence. Equant calcite cement in pore spaces however exhibits a concentric zoning pattern with non to bright and dull to bright orange luminescence. For this study only the laminated fabric was sampled to perform U-Pb analyses.

The fabric of the tufa clinofolds is very complex (e.g. Chapter II). For the U-Pb analyses, samples were isolated from thin (10 mm) beds of crystalline calcite with dendrite-like crystal fabric (sample N43) deposited in the lobe IA (Fig. 6.1), and calcite botryoidal cements, also known as mammillary calcite (sample N18B-3, Figs. 6.1 and 6.3B), from a cavity in the lobe IIB (Fig. 6.1). Internally in sample N18B-3 the botryoid is formed by large radiaxial calcite crystals; that have euhedral terminations. No CL data are available for this sample, but XRD analysis indicates calcite composition.



**Figure 6.3.-** Carbonate samples of the Late Neogene Mayrán Formation. **(A)** Lacustrine stromatolite (polished) sample N26-1. Thin section and polished slab taken from the area indicated by the square. **(B)** Botryoidal calcite cement sample N18B-3, formed in a cavity in the tufa clinofold lithofacies at spillover point II.

## 6.4 Analytical Techniques

The complexities of U-Pb dating applied to carbonates require a combination of petrographic screening and micro-sampling for isotopic analyses. In order to effectively tackle this suite of samples we employed a two-stage U-Pb analytical program: (1) in-situ analyses using laser ablation inductively coupled plasma multiple collector mass spectrometer (LA-ICP-MC-MS) to rapidly assess U and Pb concentrations, U/Pb ratios and their variation related to the petrography, followed by (2) isotope dilution (ID) isotope ratio mass spectrometry on select samples for which the LA-ICP-MS results indicated potential for geochronologically useful data.

For the in-situ screening stage, samples were analysed by LA-ICP-MC-MS at National Environmental Research Council (NERC) Isotope Geoscience Laboratory (NIGL), British Geological Survey in Keyworth, UK. Samples were ablated using a New Wave Research UP193FX (193 nm) excimer laser ablation system coupled to a Nu HR MC-ICP-MS. The laser sampling protocol employed ablation with a spot size of 100 $\mu$ m, a dwell time of 15 seconds, and a fluence at 10Hz at  $\sim 6.7\text{J}/\text{cm}^2$ . NIST 614 glass was used as an ablation standard monitor for approximate quantification, with the Mayrán carbonate samples normalized to NIST 614 according to the deviation of the measured average session values using the concentrations and isotopic composition measured for NIST 614 relative to the expected ratios for NIST 614 (Woodhead and Hergt, 2001).

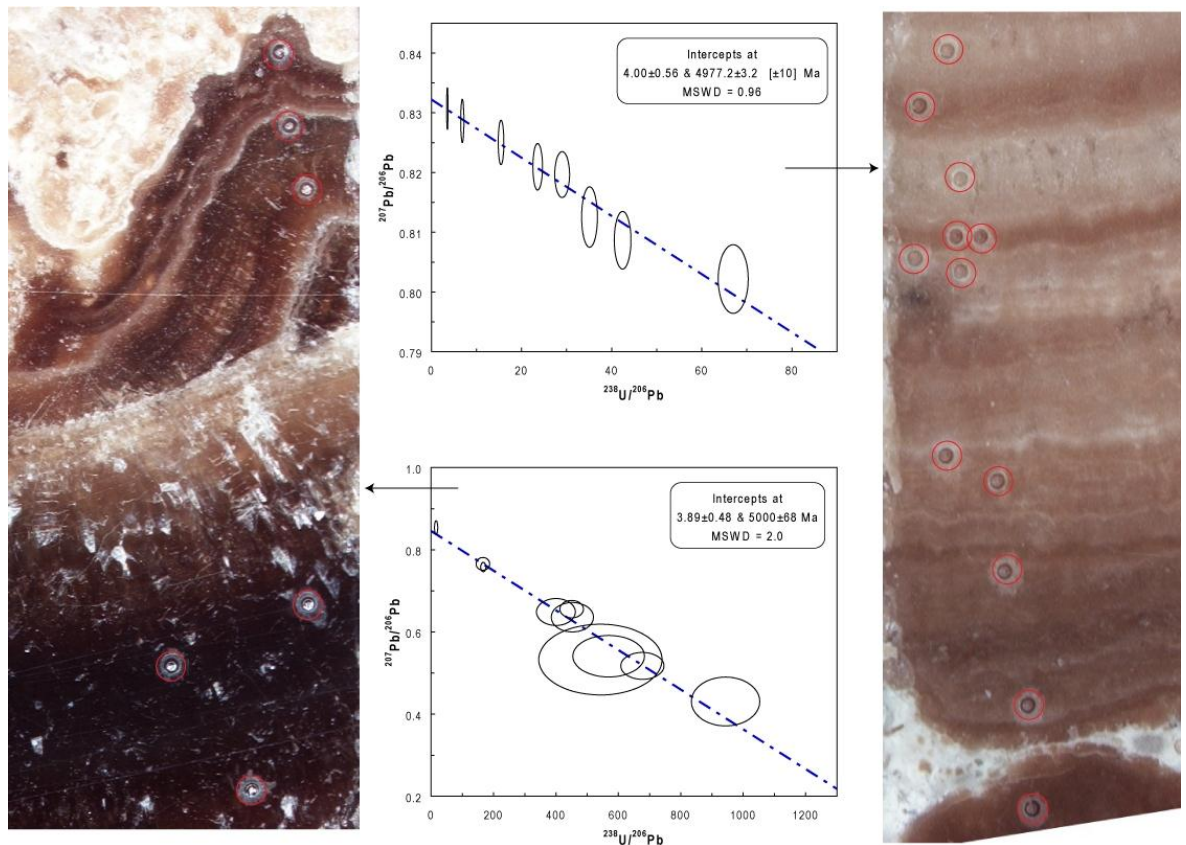
For isotope dilution analyses U was measured by MC-ICP-MS in wet plasma mode with static detection using a multiple collector Faraday cup array whereas Pb was measured using a Thermo Triton TIMS instrument fitted with an axial secondary electron multiplier (SEM) allowing the small Pb signal to be detected in dynamic single-collector mode on the SEM. Pb and U standards SRM 981 (TIMS) and U500 (MC-ICP-MS) were analysed to monitor mass spectrometer performance. For details of mass spectrometry and column chemistry see Slama et al (2008). Moles of Pb and U, and the U/Pb ratio were determined using a mixed  $^{205}\text{Pb}$ -( $^{230}\text{Th}$ )- $^{233}\text{U}$ - $^{235}\text{U}$  double spike with a U/Pb ratio of  $\sim 110$  which was calibrated against a metals derived (NBS 982 Pb and CRM 112a natural U) gravimetric shelf solution with the error in the U/Pb ratio estimated to be  $\sim 0.1\%$ . Data reduction, error propagation and plotting were carried out using customized data reduction spreadsheets based on Schmitz and Schoene U-Pb ID-TIMS data reduction Excel

workbook (Schmitz and Schoene, 2007) and Isoplot version 3.00 (Ludwig, 1991). The decay constants used were those proposed by Jaffey et al. (1971).

## 6.5 Results

The initial data obtained from LA-ICP-MS screening indicated that the samples contain variable proportion of U ranging from ~0.1 to ~5.4 ppm (Table 6.1) and that the range in  $^{238}\text{U}/^{206}\text{Pb}$  was <100 for five of the six samples, with one sample (N18B-3) recording  $^{238}\text{U}/^{206}\text{Pb}$  up to ~900. Because no matrix-matched carbonate standard was available it is difficult to quantify the accuracy of the LA-ICP-MS U-Pb data and it is only to be used as a guide. This is compounded by the fact that the Mayrán carbonate samples themselves have variable textures which result in a differential response to laser ablation. Deeper laser ablation holes resulted in the more porous textured samples (e.g. N43), while less deeper holes were drilled by the laser in samples where calcite is denser (Fig. 6.4, N18B and N26-1). This textural effect resulted in variation in down-hole fractionation difference between calcites. Given the wide-range of possible ages for the Mayrán carbonates (post-Cretaceous to pre-Pleistocene) lower intercept (Terra-Wasserburg, T-W) ages were calculated as a broad indication of age (Fig. 6.5). These ages are suggestive of post-Miocene age for the Mayrán carbonates however the large analytical uncertainty, combined with issues of accuracy related to normalisation.

The botryoidal cement sample (N18-B) records a greater spread in  $^{238}\text{U}/^{206}\text{Pb}$  ratios with values ranging up to 900 (Table 1 and Figure 5) and yield a T-W lower intercept date of  $3.82 \pm 0.29$  Ma (MSWD = 2.5) (relative to NIST 614 glass). This sample was selected for isotope dilution analyses in order to obtain accurate U/Pb ratios. The prograding tufa lobe where N18B was collected locates at the central part of the Mayrán Basin system (Fig. 6.1). Sample N26-1 yielded a similar T-W lower intercept date of  $3.99 \pm 57$  Ma (MSWD = 0.95) indicating that both the stromatolite (N26-1) and the botryoidal cement (N18B-3) are broadly similar in age (at the 0.5 Myr level). Considering its distribution within the basin, sample N26-1 locates near the base (at 1.5 m) of a lacustrine succession of ~2.5 m, at a distal sector of subbasin I (Fig. 6.1).



**Figure 6.4.** Laser ablation on samples N18B-3 and N26-1.

Eight aliquots of carbonate were isolated from sample N18B-3, weighing between 8 and 33 mg. U/Pb ID analyses by combined TIMS ICP-MS was also carried out in this sample, and yields an age of  $3.06 \pm 0.21$  Ma (MSWD = 346) (Table 6.2 and Figure 6.5), assuming an initial  $[^{234}\text{U}/^{238}\text{U} = 1]$ . The high MSWD for this regression indicates excess scatter is calculated as a ‘Model 2’ regression (Ludwig, 1991) where the assumption of a Gaussian distribution about the regression line is made.

Although the uncertainty on the lower intercept is calculated from the observed scatter of the points and is not weighted by the analytical errors, it does not take into account any potential bias. Excess scatter could reflect variation in the isotopic composition of Pb within the sample and or open-system behaviour of U and/or Pb after calcite precipitation (see Rasbury and Cole for a review of U-Pb systematic in carbonates). A further complication comes from correcting for the initial  $[^{234}\text{U}/^{238}\text{U}]$ , we make no correction for elevated  $^{234}\text{U}$  due to lack of any other age constraints, and the fact that  $^{234}\text{U}$  with its half life of  $\sim 246,000$  years approximately twelve half lives have passed making



detection of any initial excess  $^{234}\text{U}$  analytically challenging. If initial  $[\text{}^{234}\text{U}/\text{}^{238}\text{U}]$  was greater than unity then our calculated T-W lower intercept date would be too old. Considering some of the most elevated initial  $[\text{}^{234}\text{U}/\text{}^{238}\text{U}]$  known for potentially analogous systems (e.g., Walker et al., 2006) this correction could be on the order of ~600 kyrs. Given these uncertainties we consider the T-W lower intercept date of  $3.06 \pm 0.21$  Ma to be a maximum age for deposition of the speleothems carbonate however it is not likely to be younger than ca. 2.5 Ma therefore we are confident in assigning a Pliocene age to the dated material of the Mayrán Formation.

Sample	$^{206}\text{Pb}$ mV	$^{207}\text{Pb}$ mV	$^{238}\text{U}$ mV	Pb ppm	Uppm	$\frac{^{207}\text{Pb}}{^{206}\text{Pb}}$	% err	$\frac{^{206}\text{Pb}}{^{238}\text{U}}$	% err	corr. coef.
N26-1-1	3.21	2.21	25.92	2.3	4.0	0.8287	0.18	6.86	2.1	1.00
N26-1-2	5.36	3.67	22.57	3.9	3.5	0.8307	0.17	3.55	1.9	1.00
N26-1-3	1.39	0.94	25.09	1.0	3.9	0.8250	0.19	15.44	1.7	0.99
N26-1-4	0.70	0.47	23.33	0.5	3.6	0.8197	0.19	29.01	2.3	1.00
N26-1-5	0.60	0.40	16.58	0.4	2.6	0.8210	0.20	23.58	1.8	0.99
N26-1-6	0.48	0.32	23.71	0.4	3.7	0.8087	0.25	42.43	1.8	0.99
N26-1-7	0.63	0.43	11.90	0.5	1.8	0.8182	0.22	15.87	1.8	0.99
N26-1-8	0.34	0.23	27.26	0.2	4.2	0.8022	0.29	66.97	2.0	0.99
N26-1-9	0.49	0.33	16.37	0.4	2.5	0.8122	0.20	27.65	2.6	1.00
N26-1-10	0.43	0.29	17.72	0.3	2.7	0.8125	0.26	35.10	2.1	0.99
N43-1	0.28	0.19	4.51	0.2	0.7	0.8358	0.26	13.73	2.4	0.99
N43-2	0.10	0.07	5.22	0.1	0.8	0.8456	0.42	39.23	6.7	1.00
N43-3	0.07	0.05	4.58	0.1	0.7	0.8378	0.73	54.37	13.0	1.00
N43-4	0.11	0.08	3.96	0.1	0.6	0.8489	0.45	29.64	8.6	1.00
N43-5	0.31	0.22	4.12	0.2	0.6	0.8552	0.34	11.14	7.7	1.00
N43-6	0.07	0.05	4.61	0.1	0.7	0.8460	0.34	53.79	9.7	1.00
N43-7	0.15	0.11	3.80	0.1	0.6	0.8464	0.54	21.01	7.4	1.00
N43-8	0.04	0.03	5.04	0.0	0.8	0.8170	1.11	101.8	12.2	1.00
N43-9	0.10	0.07	5.19	0.1	0.8	0.8267	0.55	43.44	7.9	1.00
N43-10	0.13	0.09	3.13	0.1	0.5	0.8466	0.43	20.58	10.6	1.00
N26-2-1	5.87	4.01	11.12	4.3	1.7	0.8293	0.18	1.60	1.9	1.00
N26-2-2	6.39	4.37	11.63	4.7	1.8	0.8294	0.17	1.54	1.7	0.99
N26-2-3	3.86	2.63	12.70	2.8	2.0	0.8283	0.17	2.76	1.7	1.00
N26-2-4	3.59	2.45	11.56	2.6	1.8	0.8267	0.17	2.70	2.0	1.00
N26-2-5	3.44	2.34	13.83	2.5	2.1	0.8260	0.18	3.38	2.2	1.00
N18B-3-1	0.38	0.26	7.19	0.3	1.1	0.8233	0.21	15.83	2.0	0.99
N18B-3-2	0.11	0.07	9.11	0.1	1.4	0.8003	0.29	69.12	2.1	0.99
N18B-3-3	0.19	0.13	6.41	0.1	1.0	0.8207	0.28	28.44	1.9	0.99
N18B-3-4	0.10	0.06	9.54	0.1	1.5	0.7933	0.49	82.74	2.3	0.98
N18B-3-5	0.10	0.07	9.09	0.1	1.4	0.7917	0.36	74.94	3.0	0.99
N18B-3-6	0.05	0.03	8.17	0.0	1.3	0.7783	1.20	138.2	5.6	0.98
N18B-3-7	0.08	0.05	15.57	0.1	2.4	0.7656	0.82	166.0	5.4	0.99
N18B-3-8	0.08	0.05	14.26	0.1	2.2	0.7579	0.60	167.3	2.1	0.96
N18B-3-9	0.03	0.02	13.73	0.0	2.1	0.6485	2.06	400.0	6.4	0.95
N18B-3-10	0.07	0.04	34.92	0.1	5.4	0.6358	2.30	452.5	6.1	0.94
N18B-3-11	0.03	0.01	16.88	0.0	2.6	0.5327	6.60	542.5	14.9	0.91
N18B-3-12	0.02	0.01	14.81	0.0	2.3	0.5174	2.58	676.9	4.2	0.85
N18B-3-13	0.02	0.01	13.92	0.0	2.2	0.5409	3.82	569.0	8.2	0.91
N18B-3-14	0.02	0.01	17.50	0.0	2.7	0.4307	5.63	943.4	4.7	0.64
N18B-3-15	0.04	0.02	20.39	0.0	3.2	0.6555	1.32	450.2	3.4	0.93
N18B-3-16	0.03	0.02	0.63	0.0	0.1	0.8539	0.80	16.05	13.0	1.00

**Table 6.1.** Summary of LA-ICP-MS U-Pb results used for screening carbonate samples for U and Pb concentrations and spread in U/Pb ratio and their variation related to petrography. U and Pb data are normalised to NIST glass 614.

Sample	$^{206}\text{Pb}$ mV	$^{207}\text{Pb}$ mV	$^{238}\text{U}$ mV	Pb ppm	Uppm	$\frac{^{207}\text{Pb}}{^{206}\text{Pb}}$	% err	$\frac{^{206}\text{Pb}}{^{238}\text{U}}$	% err	Corr. coef.
N6-13_1	0.25	0.17	5.74	0.2	0.9	0.8210	0.28	19.20	1.7	0.99
N6-13_2	0.13	0.09	3.64	0.1	0.6	0.8157	0.29	23.08	1.7	0.99
N6-13_3	0.05	0.03	2.68	0.0	0.4	0.8038	0.53	49.37	2.3	0.97
N6-13_4	0.22	0.15	4.81	0.2	0.7	0.8242	0.31	18.46	1.8	0.99
N6-13_5	0.14	0.09	4.24	0.1	0.7	0.8157	0.27	26.02	2.0	0.99
N6-13_6	0.05	0.04	2.93	0.0	0.5	0.8053	0.48	45.68	1.9	0.97
N7C-8-1	0.21	0.15	2.63	0.2	0.4	0.8286	0.23	10.35	4.0	1.00
N7C-8-2	0.35	0.24	3.23	0.3	0.5	0.8247	0.22	8.18	3.8	1.00
N7C-8-3	0.24	0.17	2.96	0.2	0.5	0.8253	0.28	10.15	2.2	0.99
N7C-8-4	0.65	0.44	2.36	0.5	0.4	0.8272	0.22	3.10	1.8	0.99
N7C-8-5	0.30	0.20	3.24	0.2	0.5	0.8256	0.26	8.96	2.0	0.99
N7C-8-6	0.24	0.17	3.44	0.2	0.5	0.8226	0.35	12.09	3.4	0.99

**Table 6.1.- Continue.** Summary of LA-ICP-MS U-Pb results used for screening carbonate samples for U and Pb concentrations and spread in U/Pb ratio and their variation related to petrography. U and Pb data are normalised to NIST glass 614.

## 6.6 Discussion

The Pleistocene age originally assigned to the Mayrán Formation by Imlay (1936; 1937), was inferred based on relative stratigraphic relations (Fig. 6.2). A Pleistocene age for the Mayrán Formation, however, is not entirely consistent, rocks deposited in highly incised valleys dissected both the Mayrán Formation and the Cretaceous bedrock, contain Pleistocene fauna (see Rogers, 1961).

Overall the U-Pb laser ablation ages yield from a suite of lacustrine and botryoidal speleothem cements span from the Lower Pleistocene (N7C-8 =  $1.2 \pm 1.2$ ; N43  $1.6 \pm 4.7$  Ma), Lower Pliocene (N18B-3=  $3.82 \pm 0.29$  Ma: and N26-1=  $3.99 \pm 0.57$  Ma), Upper Miocene (N6-13=  $5.5 \pm 1.8$  Ma), down to the Lower Miocene (N26-2=  $14 \pm$ Ma). These preliminary U-Pb laser ablation ages are imprecise, particularly N26-2 and N6-13 are the most controversial. This is because not all the samples contain enough U, but have lots of initial Pb, that resulted in a little spread in the U-Pb ratios (Table 1, Figure 4). Consequently based on their U-Pb ratios, samples N26-2, N43, N7C-8, and N6-13, were not suitable to perform further isotopic dilution to obtain a precise age. Therefore the overall age range from Lower Miocene to Lower Pleistocene is not considered a conclusive age for the Mayrán Formation.

Sample	Compositional Parameters							Sample (Radiogenic + Initial Pb) Isotope Ratios								
	Wt.	U	$\frac{\text{Th}}{\text{U}}$	Pb	$^{206}\text{Pb}^*$	mol %	$\frac{^{206}\text{Pb}}{^{204}\text{Pb}}$	$\frac{^{238}\text{U}}{^{206}\text{Pb}}$	%	$\frac{^{207}\text{Pb}}{^{206}\text{Pb}}$	%	$\frac{^{204}\text{Pb}}{^{206}\text{Pb}}$	%	corr. coef.	corr. coef.	corr. coef.
	mg	ppm	(d)	(c)	$\times 10^{-13}$ mol	(e)	(f)	(j)	(h)	(j)	(h)	(j)	(h)	8/6-7/6	8/6-4/6	7/6-4/6
<b>N18B-3</b>																
A	32.77	0.6	1.221	0.018	0.5343	7.00%	19.42	109.21	0.16	0.8047	0.12	0.05149	0.19	-0.373	0.432	-0.581
B1	15.46	0.6	0.414	0.011	0.2192	10.08%	20.09	170.76	0.31	0.7803	0.09	0.04976	0.17	-0.500	0.121	-0.783
C1	16.45	0.8	0.281	0.020	0.3525	8.44%	19.73	125.30	0.18	0.7941	0.08	0.05068	0.17	-0.538	0.394	-0.896
C2	8.66	0.8	0.327	0.004	0.1519	30.10%	25.86	597.45	1.25	0.6087	0.52	0.03829	0.57	-0.924	-0.831	0.865
G1	31.39	1.1	0.119	0.005	0.7232	28.82%	25.38	598.42	0.26	0.6238	0.13	0.03933	0.20	-0.797	-0.146	-0.133
E	18.86	0.1	1.509	0.016	0.1915	5.08%	19.03	28.20	0.19	0.8232	0.08	0.05255	0.16	-0.482	0.410	-0.962
F1	25.77	0.7	0.478	0.006	0.4069	19.95%	22.57	365.32	0.34	0.6961	0.13	0.04426	0.31	-0.588	-0.061	-0.194
G2	19.99	1.2	0.084	0.013	0.5323	15.51%	21.38	296.73	0.20	0.7355	0.08	0.04675	0.17	-0.653	0.250	-0.808

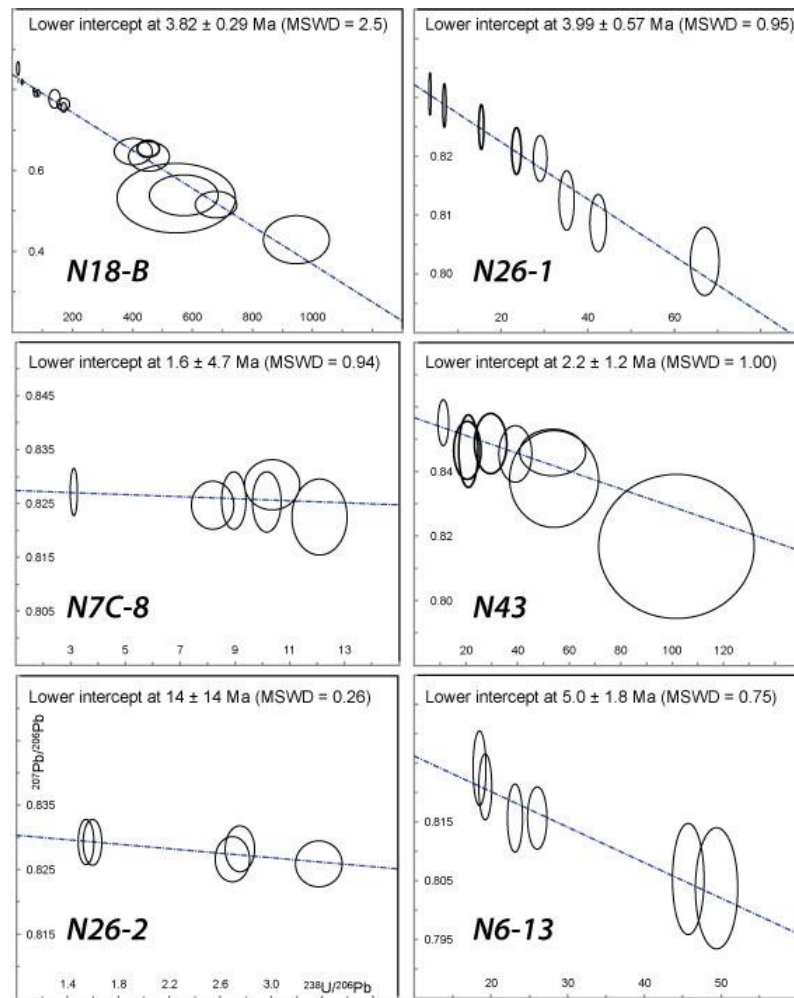
(e) Pb\* and Pbc represent radiogenic and common Pb, respectively; mol %  $^{206}\text{Pb}^*$  with respect to radiogenic, blank and initial common Pb.

(f) Measured ratio corrected for spike and fractionation only.

(h) Errors are 2-sigma, propagated using the algorithms of Schmitz and Schoene (2007) and Crowley et al. (2007).

(j) Corrected for fractionation, spike, and blank Pb only.

**Table 6.2.** U-Th-Pb isotopic data for sample N18B-3.

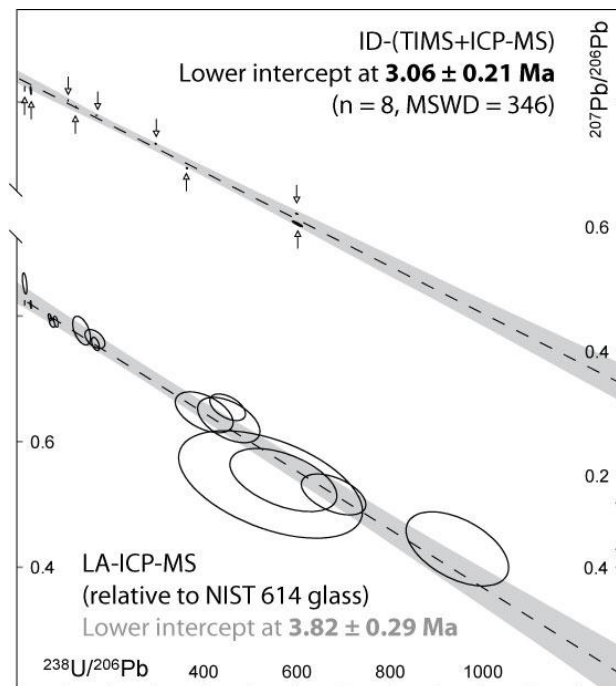


**Figure 6.5-** Terra-Wasserburg Concordia plots showing results of LA-ICP-MS screening analyses. Note – Lower Intercept ages are shown to illustrate the ‘approximate age’ of a sample and the magnitude of the age uncertainty as a result of the spread in U-Pb ratios.

The analysed samples were taken from: subbasin I (N26-1 and N26-2), subbasin II (N43, N7C-8, N6-13), and subbasin III (N18B-3) (Fig. 6.1). The depositional environments of these samples include the lacustrine setting (N26-1, N26-2, N7C-8 and N6-13), and the prograding tufa lobes (N43 and N18B-3). The preliminary laser ablation results show that the ‘oldest’ lacustrine samples are N26 2 and N6-13. In the prograding tufa lobes, the oldest age resulted from the botryoidal cement in samples from N18B-3, located near the base, in the middle sector of the tufa lobe IIB, while a younger age was yield by N43 that deposited near the top (~2m) of the prograding tufa lobe IA. Comparing the stratigraphic position of the samples and the results, we observe that some are not congruent. For example, an older age of  $14 \pm 14$  Ma resulted from a sample (N26-2) that is stratigraphically younger, than the underlying N26-1 ( $3.99 \pm$  Ma).

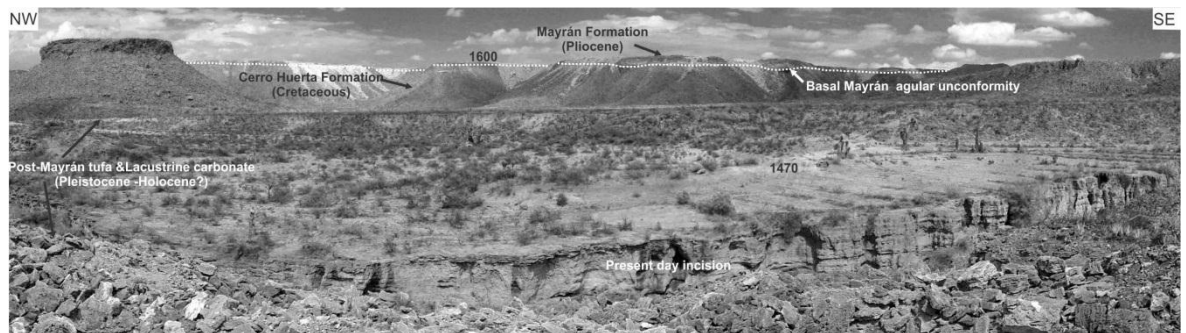
Nevertheless, the laser ablation ages obtained from N26-1 in subbasin I ( $3.99 \pm 0.57$  Ma) and N18B-3 in subbasin III ( $3.82 \pm 0.29$  Ma) are almost the same, despite they deposited in different settings and have different locations, within the Mayrán Basin system. The N26-1 is a lacustrine stromatolite, and N18B-3 consists of a botryoidal calcite cement formed in the prograding tufa lobe. The prograding tufa lobes formed by water overflow from the topographically upper to the topographically lower lake (Amezcuca et al., 2012). These water flows trigger the process of carbonate precipitation in the tufas, and the botryoidal speleothem cements within. Particularly, the botryoidal speleothem cements (N18B-3) commonly form in cavities at the water table levels (e.g. Poliak et al., 2008), and closely relate to local base level changes (Pearthree et al., 2008). The basin wide depositional context of these samples indicate that overall the entire lake subbasins of the Mayrán Basin system were hydrologically linked by the spillover points.

Preliminary laser ablation data from the botryoidal cement (N18B-3), indicate that this sample was the most suitable to perform further isotope dilution analyses, because it contained high enough U-Pb ratios. The results yield a precise U-Pb age of  $3.06 \pm 0.21$  Ma (Fig. 6.6), and indicate a Pliocene age for the Mayrán Formation.



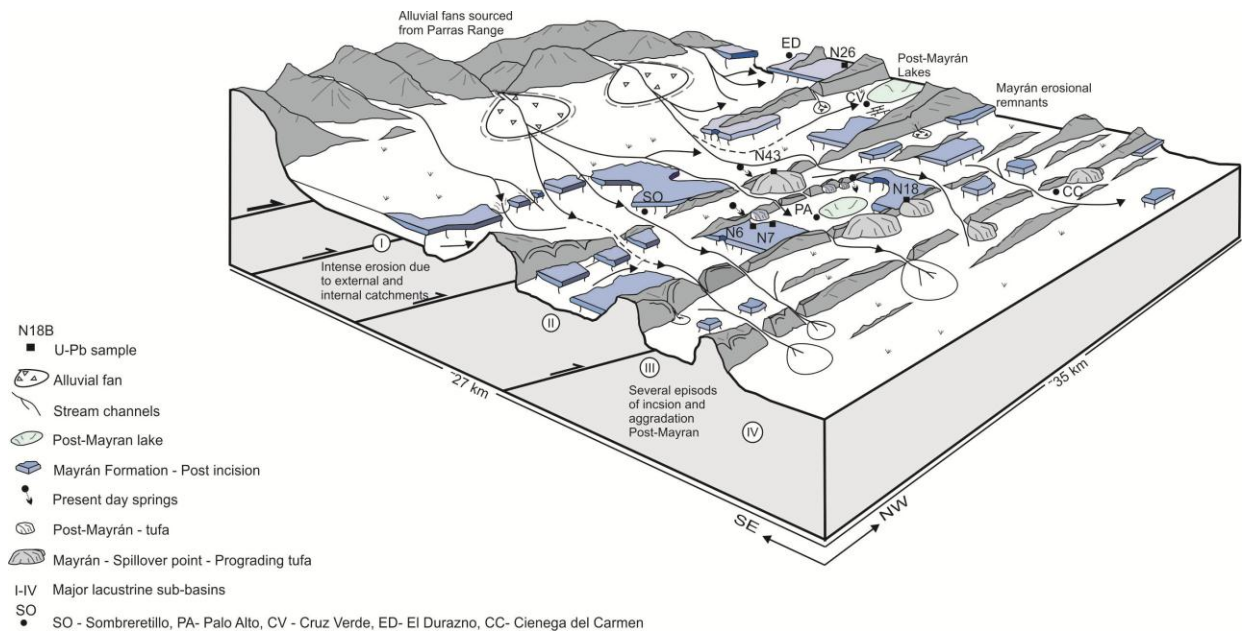
**Figure 6.6-** Composite Terra-Wasserburg Concordia diagram for sample N18B-3 showing isotope dilution (upper regression) and laser ablation lower regression) U-Pb data. Note – the LA-ICP-MS data are normalised to NIST 614 Glass and no attempt has been made to account for the differential impact the glass matrix has on the U/Pb normalisation. Vertical arrows demark the error ellipses

Originally a Pleistocene age was suggested for the Mayrán Formation (e.g. Imlay, 1936 and 1937), and also some laser ablation samples indicate this age. Therefore the age range of the Mayrán Formation possibly spans the Pliocene to Lower Pleistocene. Moreover, post-Mayrán lacustrine carbonates and tufas are deposited in deeply incised valleys that incise both the Mayrán Formation and the Cretaceous bedrock (Amezcuca et al, 2012) (Fig. 6.7 and 6.8). Post-Mayrán stream incision events occurred during both Pleistocene and Holocene times. Holocene palaeosols formed in valleys that erode the post-Mayrán deposits are reported from the study area (see Butzer et al., 2008). The Holocene palaeosols resulted from alternating ‘wet’ cycles that cause excessive rains, and produced high rates of landscape erosion (Butzer et al 2008) (Fig. 6.7).



**Figure 6.7-** Pliocene Mayrán Formation overlying on angular unconformity onto Cretaceous (Campanian-Maastrichtian) bedrock (view from Subbasin II at Palo Alto area-PA in Fig. 1), and post-Mayrán Pleistocene-Holocene tufas, lacustrine limestones and soils deposited in stream incised valleys that deeply eroded Mayrán and Cretaceous rocks. Numbers indicate elevation in meters.

The Pliocene age of the Mayrán Formation can be used to relate similar ‘pluvial’ climate stages that are consistent with carbonate lakes development in both the northeast Mexico (e.g. the Providencia Fm., see Rodriguez and Werner, 1993), and south USA (e.g. Goliad Fm., see Page et al., 2005). This is important for the understanding of the Pliocene geology and stratigraphy of this region. Finally the U-Pb dating in lacustrine carbonates and botryoidal spellothem cements, proved to be a key tool to provide age constraints that aided to correlate complex continental successions.



**Figure 6.8-** Present day model of the Mayrán Basin system, illustrating the Campanian-Maastrichtian bedrock, the post-Eocene erosional surface is underlying the horizontal beds (and tufa clinofolds) of the Pliocene age Mayrán Formation, post-Mayrán (Pleistocene-Holocene?), deposits and recent Holocene deposits.

## 6.7 Conclusion

U-Pb dating of the Mayrán lacustrine carbonates and speleothems has proven to be an important tool for obtaining dates in a carbonate-dominated stratigraphic succession where neither key volcanic ash beds nor diagnostic fossils have been identified. An age of  $3.06 \pm 0.21$  Ma was obtained from speleothem carbonate, indicating a Pliocene age for this dated interval of the Mayrán Formation. A similar age, obtained from a stromatolite confirms this result and offers an opportunity to test correlations among coeval carbonate deposits belonging to different lithofacies in the same continental carbonate dominated basin system. The U-Pb age obtained from carbonates in the Mayrán Formation also bring new constraints to understand the Neogene geological evolution of Northeast Mexico and gives new insights for the correlation with geological events in the southeast USA.



## **6.8 Acknowledgements**

The U-Pb dating was supported by the NERC-NIGL, British Geological Survey. Special thanks to S. Noble and Randall Parrish at NIGL for their support during U-Pb analysis and discussion of the results. This contribution represents a portion of Amezcua's doctoral dissertation at the University of Manchester. Support for this project was provided by the Mexican Geological Survey (SGM). Funding was provided by the National Council of Science and Technology (CONACYT) for the studentship grant to N. Amezcua.

## **SECTION THREE**

### **Chapter 7**

## **Chapter 7**

### **Synthesis, Discussion, Conclusions and Further work**

#### **7.1 Introduction**

An investigation of the controls on the facies variability in carbonate lake basins has been undertaken using the Mayrán Basin system and the Mayrán Formation as a natural laboratory. The basin and its deposits are suitable subject matter, because they are carbonate-dominated and their depositional geometries and sedimentary successions are well-preserved in excellent exposures.

The basin has not been previously investigated, and for this reason, a multi-scale and multi-proxy approach was implemented to integrate outcrop and detailed laboratory analyses to meet the goals of this research. These analyses included: field-based geologic and structural mapping, stratigraphic sections logging and sampling, petrographic analyses using combined optical (transmitted light microscopy, backscattered electron imagery and cathodoluminescence techniques), together with geochemical analysis of the units present to identify and characterise lithofacies present.

#### **7.2 Synthesis and Discussion**

The aim of this final section is to: 1) summarize the observations results and conclusions of the individually themed research Chapters (Chapters Three to Six respectively). Here the reasons for the differing scales of facies variability as expressed in stratigraphic and lithofacies variability preserved with the Pliocene Mayrán Lacustrine Basin system, are reviewed 2) the main outcomes and implications of this research derived from the research chapters, 3) present key conclusions of the thesis, and 4) suggest directions for further work.

##### **7.2.1 Cascading carbonate lakes of the Mayrán Basin system, the interplay of inherited structural geometry, bedrock lithology, and climate.**

Chapter Three provides a basin-scale introduction on the Mayrán Basin system. It focused on identifying the relative roles of inherited structural geometry, bedrock lithology sediment supply and production, together with and basin hydrology, as key controls on the fluvio-lacustrine facies in the Mayrán Formation. For this purpose the structural and

stratigraphic framework of the subbasins was outlined. With this context in place the lithofacies in each subbasin were mapped and the lithofacies and paleogeomorphic linkages between subbasins identified.

It was demonstrated that the Mayrán Formation was deposited in four, broadly coeval, hydrologically linked, carbonate-dominated lake subbasins that formed at different elevations spanning ~500 m. In this thesis were named these adjoining lake basins ‘The Mayrán Basin system’ (Fig. 7.1). The subbasins are separated by Cretaceous bedrock ridges, connected by spillover points, and infilled by variably proportions of siliciclastic and carbonate deposits. The fill of the most proximal subbasin (I), consist of nonchannelized and channelized conglomerates, pebbly sandstones, and calcareous sandy and siliciclastic mudstones change laterally into horizontally bedded lacustrine limestones, calcareous mudstones, and evaporites. Vertically, these lithofacies are organized into shallowing-upward cycles. The fill of the more distal northerly subbasins (II–IV) is predominantly by lacustrine limestones with subordinated siliciclastics. Prominent aggradational and progradational tufa topsets and clinofolds are present at the spillover points between the subbasins (Chapter 4). These tufas interfinger up- and down dip with the lacustrine limestones (Chapters 4 and 5).

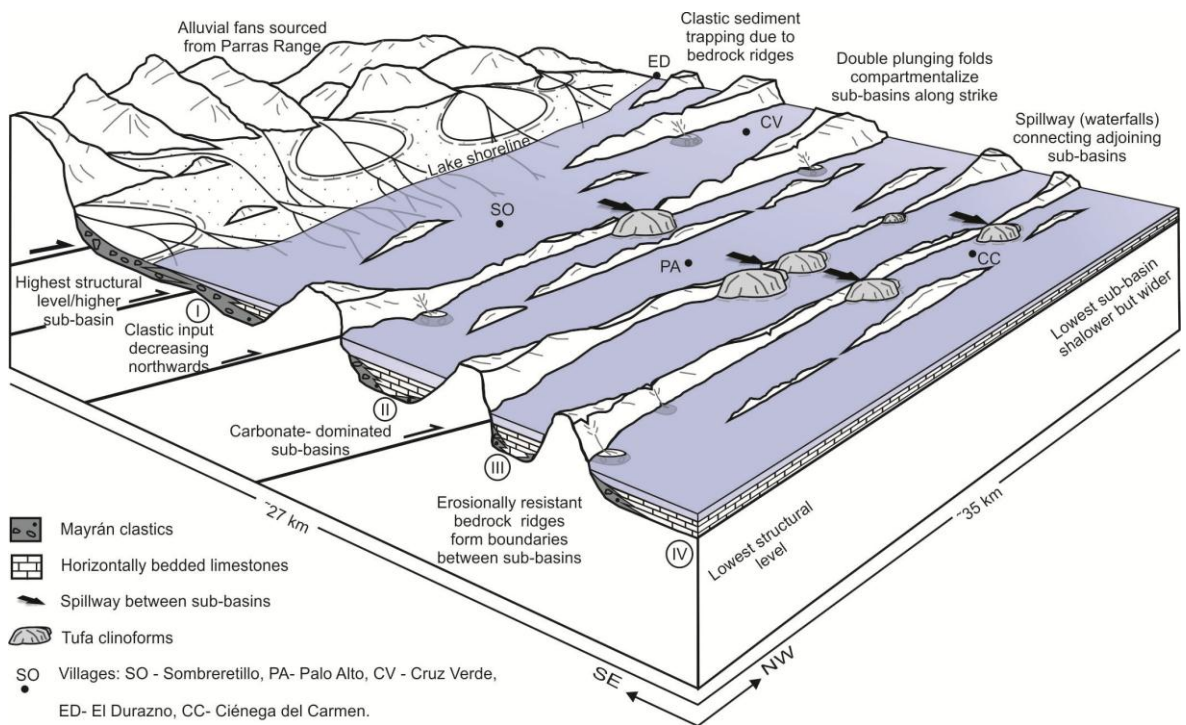
The distribution of clastic facies was mainly controlled by their proximity to the major sediment input in the south (The Parras Range) and to the Cretaceous bedrock ridges dividing the subbasins. This is important because typically the existence of carbonate lakes is interpreted to indicate low siliclastic input (e.g. DeWet et al.,1998, 2002; Gierlowski-Kordesch, 2010). Crucially, discharge from Parras Range drainage catchments not only supplied detrital sediment to subbasin I, but likely also supplied solutes (calcium, magnesium, and bicarbonate ions) to fuel carbonate production in all the lake subbasins (Chapter 5).

Most of the carbonate accumulation occurred when the lakes were either overfilled or balance filled (e.g. Carroll and Bohacs, 1999; Bohacs et al 2000a, 2003). Such conditions have been identified in several basins such as the Greater Green River Basin (Carroll et al., 2008; Davies et al., 2008; 2009). My contribution is consistent with generic conceptual models of these lake types, and particularly illustrates an example of carbonate dominated basins. Stratal stacking patterns in all the Mayrán subbasins the lake successions show

overall aggradational geometries. Accommodation within each of the subbasins, however, was largely inherited from the differential erosion of the Parras foreland fold-and thrust belt. This is particularly important and contrasts to lacustrine settings where accommodation continuously created by tectonic subsidence (e.g. Carroll and Bohacs, 1999; Pietras et al., 2003). Because inherited accommodation in the Mayrán Basin system was a function of sediment supply + sediment production + hydrology, factors that were all broadly climatically controlled, it can be used as an analogue for reservoir prediction in overfilled to balance filled carbonate basins.

The Mayrán Basin system is morphologically similar to a series of isolated piggyback basins in a foreland basin setting (e.g., Lawton et al., 1994; DeCelles and Giles, 1996), but it is not a syntectonic geomorphological feature. The compartmentalization of a lake basin into a series of subbasins of different elevations linked by spillover points is rare in both pre-tectonic and post-tectonic phases of basin evolution. The observations made here for the cascading lakes of the Mayrán Basin system may therefore be more applicable to syntectonic lake basins, where compartmentalization by active structures can readily lead to subbasin formation, each with its own base level.

The main outcomes of this research were to demonstrate that in carbonate lake system autogenic processes likely controlled facies distribution within the basin, whereas climate was the overall driver of initiation, driving and termination of the development of the formation. The results of this chapter show that nontectonic lake basins can have complex geomorphology, and sedimentary fill, due to the underlying inherited structural framework, varying sediment inputs and basin hydrology. They also show that identification of spillover points is a key aspect to recognize adjoining lake basins in the ancient rock record.



**Figure 7.1.** Model of the Mayrán Basin system during high lake-level stages when the subbasins were hydrologically linked by flow through spillways creating the tufa clinoforms.

### 7.2.2 Prograding tufa clinoforms in cascading lake basins

Once the background to this study had been introduced in Chapter Three, here Chapter Four documents the large-scale tufa lobes that occur at the drainage points between the various subbasins in the Mayrán Basin system. These crucial deposits provide information about how the subbasins were hydrologically linked and how these linkages changed through time. In order to address this problem the locations, geometry, stratigraphy and sedimentological attributes of these units were described. In addition the sedimentological features of similar deposits preserved elsewhere in the stratigraphic record were reported and the tufa masses described here were compared with these related units

The large scale tufa lobes preserved within the Mayrán Basin consist of amalgamated steeply dipping tufa clinoforms that prograde broadly northwards. They were deposited onto the Cretaceous sandstone ridges that confine coeval cascading carbonate-dominated lake subbasins. Overall they comprise a main tufa body that generally have a subhorizontal top and a steep relief down-dip, and may build off subordinated coalesced lobes that bifurcate from the major one. Up-dip proximal to the topographically upper lake, and

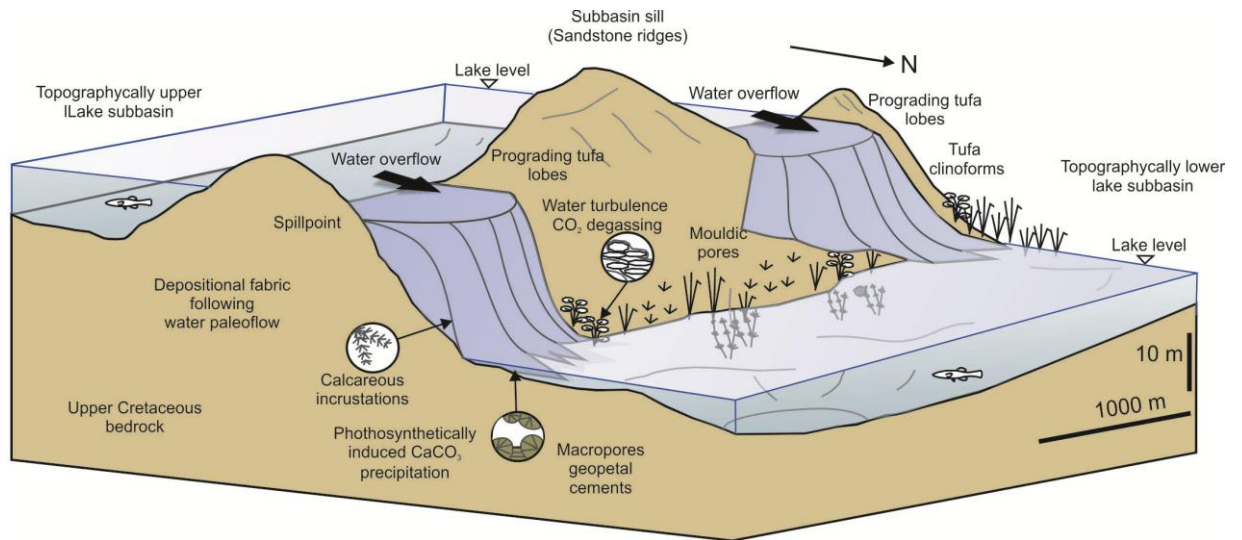
down-dip to the topographically lower lake, the tufa clinofoms are interbedded with horizontally bedded lacustrine limestones. The tufas comprise macrophyte boundstone lithofacies that contain abundant calcareous encrustations of plants, bryophytes, algae and calcified microbial laminations. Mouldic pores, pendant and other vadose botryoidal cements in vug pores are common in the macrophyte boundstones. The tufas formed by inorganic calcite precipitation resulting from CO<sub>2</sub> outgassing in fast flowing waters and by biogenic calcite precipitation (Fig. 7.2) during metabolic uptake of CO<sub>2</sub> by the photosynthetic biota (Chafetz and Folk, 1984; Viles and Goudie, 1990; Janssen et al., 1999), as carbonate saturated waters, flowing down-dip from the upper to the topographically lower subbasin.

Because of continuous carbonate precipitation, tufa clinofoms continue forming onto pre-existing tufa, progressively stacking as water flowed down slope from the topographically upper to the lower subbasin. Geometrically they are constructive progradational geomorphological features. The presence of sub-horizontal topsets on these clinofoms also indicates that locally aggradation occurred. The fact that they are progradational and subordinated aggradational feature, also suggest that despite water frequently overflowing the sill, while the lakes were hydrologically open, overflow did not cause significant erosion in the previously deposited, well-cemented tufas.

The distribution of the tufa clinofom lobes is predominantly controlled by the preceding topography at the subbasin sill, and by the local base level of the topographically higher lake. The prominent tufa lobes are key sedimentological features, unusually preserved in the rock record, which can be related to either frequent or intermittent lake overflow conditions, as occur in the spillways of overfill and balance filled lakes ( see Carroll and Bohacs, 1999, 2001; Bohacs et al., 2003), as initially documented in Chapter 3.

Similar sedimentological features forming tufa lobes on hill slopes are known as spring line tufas. These tufas developed from spring or stream resurgence, and deposit on valley sides, forming lobate or mutilobate, convex to flat surface deposits, with wedge like profile, thickening away from the source creating a wedge like profile (Pedley, 1990; Ford and Pedley, 1996). Unlike the perched spring-line tufas, the prograding tufa clinofoms form associated to direct overflow of lake waters. As a result basin hydrology influencing lake levels and consequently overflows played a crucial role for the tufa clinofoms formation.

These are the first well-preserved, exposed examples of a large scale prograding tufa bodies. The results of this chapter: 1) reinforce interpretations of Chapter 3 related to the climatic influences on deposition of the prograding tufa clinofolds, and basin hydrological connections that influenced lacustrine basin deposition (Chapter 5, and 3) demonstrate that lakes at different elevations had their own lake level.



**Figure 7.2-** Idealized model for large scale prograding tufa clinofolds formation.

### 7.2.3 Lacustrine carbonate lithofacies in the Late Neogene Mayrán Formation

Chapter Five examined the controls on stratigraphy of the carbonate-dominated lake subbasins described in the previous chapters, and incorporates detailed sedimentological and geochemical analyses of the lithofacies that comprise the horizontally bedded limestones (lacustrine carbonates). Investigating the deposits within the lakes gave us new data to correlate with the processes operating at the spillover points (Chapter 4). In this chapter the controls on carbonate lithofacies variability in the Mayrán subbasins, with a common hydrology yet very different inputs were investigated.

The rocks in the four subbasins were investigated utilizing field observations, coupled with geochemical (carbon and oxygen stable isotopes, whole rock XRD, and TOC) and petrographic techniques (optical, and electron optical methods).



The data obtained here indicate that these lacustrine carbonates contain variable proportions of production-derived components, with subordinate proportions of detrital and early diagenetic components. The lithofacies contain, inorganic and organic calcite (average 91% CaCO<sub>3</sub>), and organic matter (10.5% to 13.8 % average 12.6 % TOC), together with minor detrital quartz, feldspar and clay. Nine sub-facies were identified: ostracodes mudstone-wackestone, clotted boundstones, gastropod wackestone-packstones, oncoid wackestone-packstones, charophyte wackestone-packstones, stromatolites and associated evaporite minerals. Isotopic composition of specific components such as micritic laminations in stromatolites ( $\delta^{13}\text{C}$  -6.3‰ and  $\delta^{18}\text{O}$  -8.0 ‰), and micritic matrix from samples in all the subbasins,  $\delta^{13}\text{C}$  -5.7 ‰ and  $\delta^{18}\text{O}$  -7.8 ‰), indicate that overall calcite deposition occurred in freshwater lakes (e.g. Talbot, 1990; Leng and Marshall, 2004).

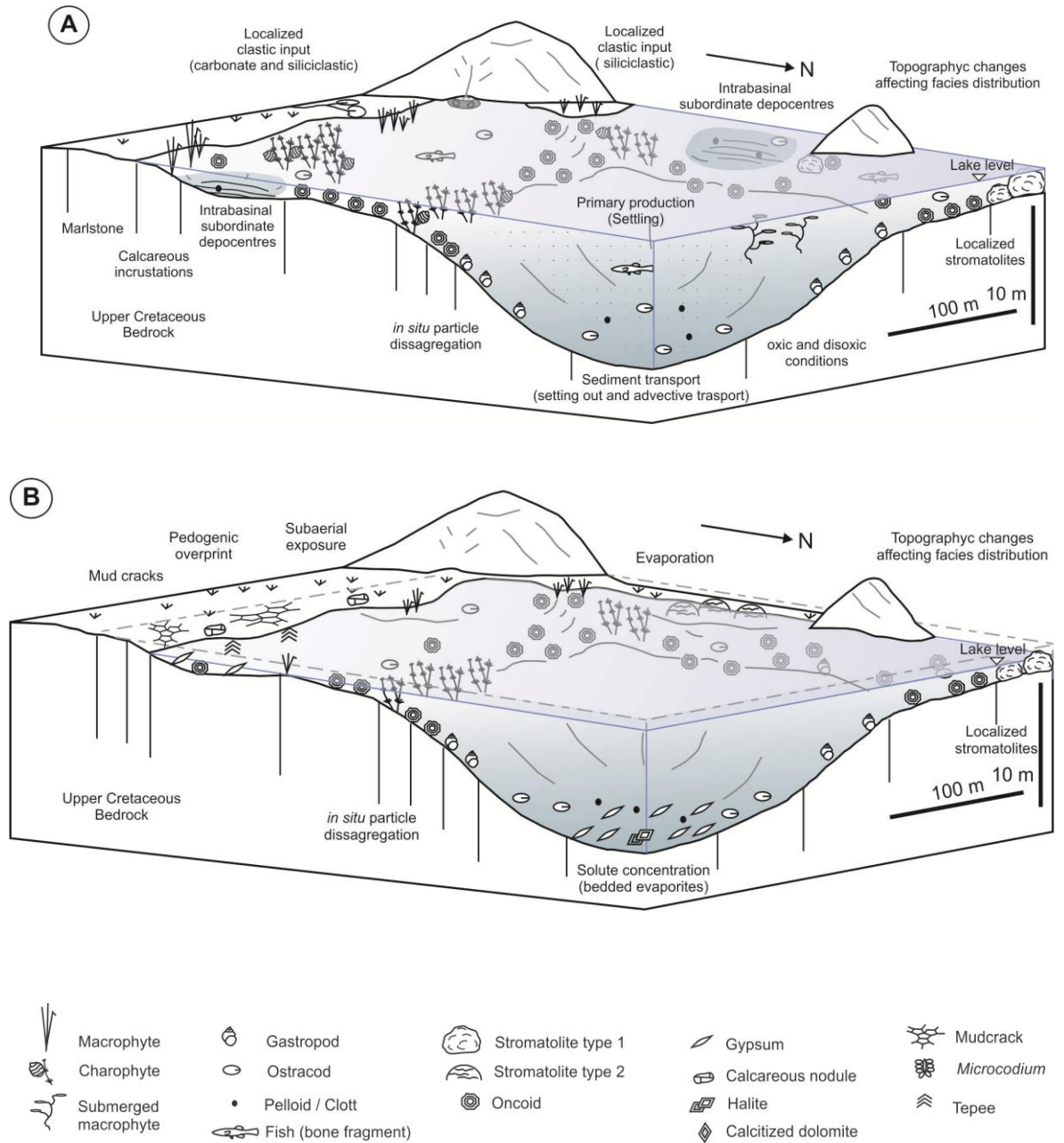
Main carbonate producers identified in these lakes include calcareous shelled molluscs, ostracodes, calcareous algae (e. g. charophyte and free floating calcifying cyanobacteria), and microbial carbonates (e.g. stromatolites and oncolites) (Fig. 7.3). In particular the gastropod morphotypes indicate that lakes underwent oligotrophic and presumably meso- to eu-trophic, the later particularly when Physidae? forms are present (e.g. Miller and Tevesz, 2001; Ložek, 1986). Non (e.g. charophytes) to orange dull luminescent response (micrite) strongly suggest that *in situ* carbonate production occurred, and that most of these particles were delivered either by suspension settling through the water column or by *in-situ* disaggregation of larger particles on the lake floor. Together these processes contributed to the local production of lime mud.

Rare microtextural evidence of scour surfaces (e.g. in gastropod wackestone-packstones), however, indicates that occasionally the sediment was eroded and transported laterally. Intense to moderate bioturbation (BI 1 to 4), indicates that deposition took place under predominantly oxic conditions. Moreover, significant organic matter was preserved in these lacustrine rocks (12.6 % TOC). This can be achieved by isolating the organic matter from the oxidizing water column, without causing significant dilution, as it deposited in the fine grained matrix (e.g. Arthur and Sageman, 1994; Meyers and Ishiwatari, 1993). Moreover detrital inputs into the lakes were insufficient to cause significant carbonate dilution (Gierlowski-Kordesch, 1988). Moderate sedimentation rate and moderate production rate is likely to have controlled organic matter preservation. The accumulation of organic matter rich lacustrine carbonates is then a complex interaction of

processes such as rates of production, destruction, and dilution of the organic matter (Kelts, 1988; Bohacs et al., 2005).

The lacustrine lithofacies deposited in proximal and distal lacustrine settings. Strata stacking patterns organize in shallowing upwards cycles (0.3-2.5 m thick), which are capped by either evaporites or beds with pedogenic overprint. Their stacking patterns reflect lake level variations which can be recognized in all the subbasins. The lithofacies architectures within each subbasin forms parasequences that overall exhibit aggradational geometries. The lithofacies present and their large scale geometries also indicate deposition occur in a series of relatively shallow (<10 m), lake systems with ramp-like margins. The aggradational stacking patterns of the carbonates and the presence of subordinate evaporites suggest that basin hydrology (water supply and precipitation/evaporation ratios) had an important influence on facies architecture and cyclicity (e.g., Carroll and Bohacs, 1999, 2001). As described in Chapter 3 and 5, Mayrán carbonates were likely deposited under overfilled to balance filled conditions; although balance filled conditions with open hydrology were more likely. The succession here can be compared with other ancient analogues, that also are rich in lacustrine limestone (see Bohacs et al., 2001; Gierlowski-Kordesch (2010) and references therein).

Preservation of these types of deposits are important because overfilled and balance filled lake basins overall present continuously open hydrology, with intermittent hydrologically closed intervals, that allows reasonably stable depositional environments (Carroll and Bohacs, 1999; Bohacs et al., 2000a). Because lakes are complex sedimentary systems, having these conditions contribute to better evaluate the potential controls on the deposition of lacustrine successions. Overall, facies variability in the lacustrine carbonate lithofacies here was controlled by accommodation, basin inherited geomorphology, and basin hydrology, which ultimately controlled clastic trapping, solute inputs, water chemistry, primary production, and lake level changes. We interpret that all these controls were largely driven by climate.



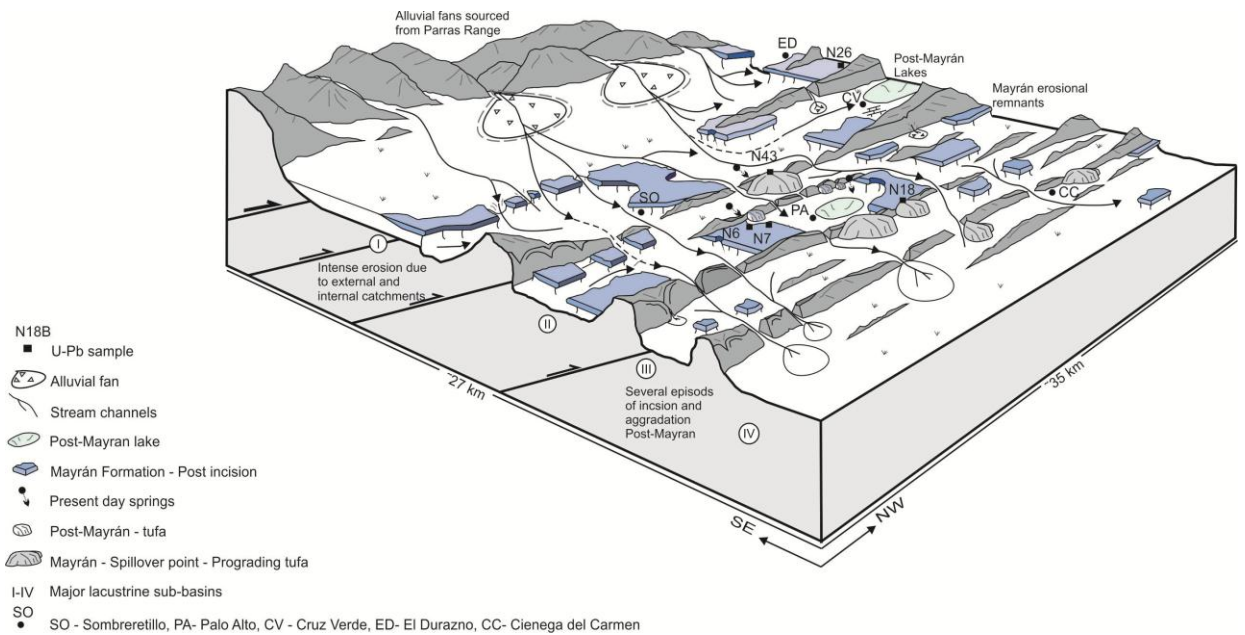
**Figure 7.3-** Idealized paleoenvironmental reconstruction and sedimentary facies distribution, and depositional processes in the lacustrine setting, during high lake level **(A)** stage and during low lake level stage **(B)**.

#### 7.2.4 U-Pb dating of carbonates in the Mayrán Formation

The Mayrán Formation carbonates are only poorly dated this means that it has been impossible to precisely place this particularly lacustrine system within a specific stratigraphic Earth System Context. Having a better constrained temporal context would be useful as the overarching control on facies variability in this basin is climate. For this reason Chapter Six focused on the application of novel U-Pb isotopic dating technique in Mayrán carbonates. This chapter is supported from previous analysis carried out in Chapters Three and Five where the basin scale context and stratigraphic position of the selected samples was firstly addressed, and then carefully selected samples resulted from detailed petrography (Chapter 5).

Originally a Pleistocene age was suggested for the Mayrán Formation when it was first described by Imlay (1936 and 1937). Stratigraphically the Formation overlies on angular unconformity onto Cretaceous (Campanian-Maastrichtian) rocks deformed by the Laramide tectonic event, which ended in the Eocene. Post-Laramide uplift exposed the Cretaceous rocks that were highly affected by intense erosion, and later, at an unconstrained time, the Mayrán Formation deposited onto the resulting erosional topography (Fig. 7.4). The U-Pb dating technique in was implemented here in order to obtain absolute age of the Mayrán Formation carbonates. Samples were carefully selected based on detailed petrographic analyses (see Chapter 5). The samples include botryoidal calcite cements filling voids in tufa formed at lake spillover points IA and IIA (discussed in Chapter 4), oncoids and laminations in stromatolites deposited in the lacustrine setting of subbasins I and II (discussed in Chapter 5).

An accurate Pliocene age ( $3.06 \pm 0.21$  Ma) was obtained based on uranium-lead dating from botryoidal calcite cements from spillover point IIA. The fact that samples were carefully selected (Chapter 5), provided essential age constraints in this continental succession. More importantly dating on continental carbonates are important tools of correlation when no other method is applicable. This is particularly important in areas with structural complexity and high facies variability (Cole et al., 2005). This new age data provide the first absolute age constrain for deposition of the Mayrán Formation, which will be the basis for further correlations to similar humid conditions that promoted the formation of lake basins in northeast México and southeast USA.



**Figure 7.4-** Present day model of the Mayrán Basin system, illustrating the Campanian-Maastrichtian bedrock, the post-Eocene erosional surface underlying the horizontal beds (and tufa clinoforms) of the Pliocene Mayrán Formation, post-Mayrán (Pleistocene-Holocene?), deposits and recent Holocene deposits.

### 7.3 Overall conclusions

The main conclusions of this research are presented below.

- The Mayrán Basin system is composed by a complex series of carbonate-dominated cascading lakes, each with its own lake level, that were present in four down-stepping subbasins that span an elevation range of 500 m.
- The Mayrán Basin system geomorphology was determined by the inherited topography of the exhumed and differentially eroded siliciclastic Cretaceous bedrock that forms the Perras foreland fold-and-thrust belt.
- Mayrán lake systems were overfilled to balance filled type, with their hydrology varied from open to intermittently open conditions.

- The sedimentary infill of the subbasins includes clastic alluvial (conglomerates, pebbly sandstones, and mudstones in proximal settings) and lacustrine carbonate lithofacies (horizontally bedded limestones), in more distal settings.
- Proximity to clastic sediment sources (e.g. the Parras Range and the Parras foreland fold thrust belt), primary carbonate production, lake level and accommodation availability largely controlled facies variations within each subbasin.
- Large hundreds of meter' scale tufa lobes were identified at the northern sectors of the subbasins and are form by prograding tufa clinoforms that steeply dip broadly to the north, down lapping onto the sandstone ridges that once confine the lake subbasins at different elevations.
- The tufa clinoforms comprise macrophyte boundstone lithofacies and are formed by by encrustations and cast of plants, mosses, algae and microbial filaments. They were produced by calcium carbonate precipitation by both photosynthetically induced and inorganically by CO<sub>2</sub> degassing as water flowed down dip to the lower subbasin. Staked beds of these tufas form both aggradational but mainly progradational large scale features.
- Up-dip proximal to the topographically upper lake, and down-dip to the topographically lower lake, the tufa clinoforms interbedded with horizontally bedded lacustrine limestones. The former present of these stratigraphic relations, strongly suggest that tufa clinoform development was controlled by episodes of standing water in the topographically upper lake. They acted as spillpoints forming constructive waterfalls that were hydrological links that connected coeval lake subbasins.
- Nine sub-facies were identified in the horizontally bedded lacustrine limestones, based on their textural attributes, and the variability of production derived components, detrital components, and diagenetic overprint. The sub-facies are: ostracode mudstone-wackestone, clotted boundstone, gastropod wackestone-packstone, oncolid wackestone-packstone, stromatolites, macrophyte boundstone, marlstone, and crystalline carbonate, together with evaporites.

- Depositional controls indicated by rock texture, fossil content, geochemistry and primary sedimentary structures, indicates that the lake contained predominantly freshwater ( $\delta^{13}\text{C}$  -5.7 ‰, and  $\delta^{18}\text{O}$  -7.6‰ average), were relatively shallow (<10m), had low relief, and that overall oxic conditions prevailed in the water column. Intense primary productivity is revealed by the high volume of both carbonate sediment deposited in all the subbasins, and by the organic matter enrichment in the carbonate lithofacies (12.6 % TOC average and  $\delta^{13}\text{C}_{\text{org}}$  -6.17‰ average).
- The spatio-temporal distribution of the lacustrine facies, also reveal that intense aggradation of the sedimentary lacustrine succession occurred in response to lake level variations. Stacked limestone beds indicate that overall the succession comprises a series of shallowing upward cycles. Carbonate dissolution, desiccation cracks, evaporites, calcretization and pedogenic features affecting the top of the shallowing upward cycles, indicate that wide lake areas were subaerially exposed during low lake level stages. Subsequent flooding episodes are marked by irregular erosional surfaces overlaid by lithofacies containing freshwater dominated fauna (e.g. charophyte wackestone-packstones, oncoid wackestone-packstones and occasionally gastropode wackestone-packstone), indicate the reestablishment of normal lacustrine conditions as the lake expanded likely during high lake level stages. Nutrients to fuel carbonate production were likely derived from inputs of carbonate clastic detritus (Cretaceous limestones), and most carbonate accumulation occurred when the basins were either overfilled or balanced-filled.
- A Pliocene age ( $3.06 \pm 0.21$  Ma) for the Mayrán Formation was constrained using U-Pb dating of speleothem carbonate, and stromatolites.
- U-Pb dating of the Mayrán lacustrine carbonates and speleothems has proven to be an important tool for obtaining precise absolute ages where neither key volcanic ash beds nor diagnostic fossils have been identified.
- As observed in the lithofacies variability in the subbasins, the dominance of limestone lithofacies with indicators of intense in situ primary production, the presence of shallowing upward cycles in the lacustrine lithofacies their stacking aggradational patterns, together with the presence of the prograding tufa clinofolds

representing hydrological connections between the subbasins, suggest that overall external allogenic factors most likely climate, controlled initiation, fill, and termination of the deposition in the Mayrán Basin system.

#### 7.4 Future work

Completion of this thesis has identified several alternative investigations that would also contribute to the overall aim of this research and the study of carbonate lake basins.

- Because it is likely that groundwater inputs to the lakes may have occurred during Mayrán times, complementary field research seeking for possible spring and sublacustrine deposits is suggested. Areas suitable for their occurrence are the left lateral faults identified during geological mapping.
- Perched springs also form tufa deposits on hillsides. The presence of subordinate lobes of prograding tufa clinoform deposits located at lower elevations may possibly relate to perched springs. Further field research seeking for detailed analysis on and the subordinated lobes are required to clarify the elevation differences among them, and potential relation to perched springs.
- High resolution studies in the prograding tufa clinoforms could aid to identify key surfaces and depositional intervals in the tufas that potentially correlate with the lake contraction phases of the lakes in the subbasins.
- TOC data from subbasin II show that considerable organic enrichment occurred in the lacustrine limestone lithofacies, and that under the suitable conditions they may have been important source rocks. Also petrographic and stable isotope data indicate that overall *in situ* primary production was high and that similar mechanisms of primary production occurred in all the subbasins. Further TOC data from the rest of the subbasins may aid to compare or identify variability with the initial results; and will provide more information on the fundamental controls on organic matter preservation and source rock potential in carbonate basins with predominantly balance filled conditions.



- To use stable  $\delta^{18}\text{O}$  isotope data of diagenetically unaltered allochems (e.g. charophyte oogonia, and stromatolite laminations) to estimate paleotemperature of calcite precipitation that occurred during the Mayrán Formation deposition.
- Palynological analyses can be carried out analyzing the siliciclastic mudstone lithofacies of the Mayrán Formation, in order to generate other multiproxy data to contribute to the knowledge of Pleistocene climatic conditions of Northeast, México.
- Although we generate a precise age from the Mayrán Formation, and this is a major step forward, systematic dating is required to constrain the duration and frequency of the cycles present within the subbasins and to allow better correlations between each subbasins to be made.
- Additional dating from the youngest post-Mayrán deposits (tufa and lacustrine carbonates) deposited in the valleys that incise the Mayrán Formation can be used to address the duration of the pluvial period where the Mayrán Basin formed and its later incision formed. Present day climatic conditions in the study area are semiarid, for this reason the research are offers varying opportunities to the study of late Neogene climate.
- Finally, the information about the age of the Mayrán formation, combined with other proxy data can be used to tie similar humid 'pluvial' climate stages that are consistent with the development of other carbonate lake basins (e.g. in northeast México and south USA) and potentially to make onshore to offshore correlations with Pliocene deposits in the Gulf of México.

## REFERENCES

- Abell, P., Awramick, S., Osborne, R. H., and Tomellini, S., 1982, Plio-Pleistocene lacustrine stromatolites from Lake Turkana, Kenya: Morphology, Stratigraphy and Stable Isotopes: *Sedimentary Geology*, v. 32, p. 1-26.
- Adams, L. K., Macquaker, J. H. S., and Marshall, J. D., 2006, Iron(III)-Reduction in a Low-Organic-Carbon Brackish-Marine System: *Journal of Sedimentary Research*, v. 76, no. 6, p. 919-925.
- Aichner, B., Herzsuh, U., and Wilkes, H., 2010, Influence of aquatic macrophytes on the stable carbon isotopic signatures of sedimentary organic matter in lakes on the Tibetan Plateau: *Organic Geochemistry*, v. 41, p. 706-718.
- Alonso-Zarza, A. M., and Wright, V. P., 2010a, Calcretes, *in* Alonso-Zarza, A. M., and Tanner, L. H., eds., *Carbonates in continental settings: facies environments and processes*. *Developments in sedimentology*, Volume 61 Elsevier p. 225-267.
- Alonso-Zarza, A. M., and Wright, V. P., 2010b, Palustrine Carbonates, *in* Alonso-Zarza, A. M., and Tanner, L. H., eds., *Carbonates in continental settings facies environments and processes*, Volume Volume 61, Elsevier, p. 103-131.
- Altermann, W., Kazmierczak, J., Oren, A., and Wright, D. T., 2006, Cyanobacteria calcification and its rock-building potential during 3.5 billion years of Earth history: *Geobiology*, v. 4, p. 147-166.
- Allwood, A. C., Grotzinger, J. P., Knoll, A. H., Burch, I. W., Anderson, M. S., Coleman, M. L., and Kanik, I., 2009, Controls on development and diversity of Early Archean stromatolites: *PNAS*, v. 106, no. 24, p. 9548-9555.
- Amezcuca, T. N., Gawthorpe, R. L., and Macquaker, J. H. S., 2012, Cascading carbonate lakes of the Mayrán Basin System, Northeast México: The interplay of inherited structural geometry, bedrock lithology and climate: *Geological Society of America Bulletin*, v. 124, no. 5-6, p. 975-988.
- Anadón, P., Cabrera, L., Julia, R., Roca, E., and Rosell, L., 1989, Lacustrine oil-shale basins in Tertiary grabens from NE Spain (Western European Rift System): *Palaeogeography, Palaeoclimatology, Palaeoecology*, v. 70, p. 7-28.
- Anadón, P., Rosell, L., and Talbot, M. R., 1992, Carbonate replacement of lacustrine gypsum deposits in two Neogene continental basins, eastern Spain: *Sedimentary Geology*, v. 78, no. 3-4, p. 201-216.
- Andrews, J. E., Pedley, M., and Dennis, P. F., 2000, Palaeoenvironmental records in Holocene Spanish tufas: a stable isotope approach in search of reliable climatic archives: *Sedimentology*, v. 47, no. 5, p. 961-978.
- Aranda, G. J. J., Luhr, J. F., Housh, T. B., Valdez, M. G., and Chavez, C. G., 2005, El vulcanismo tipo intraplaca del Cenozoico tardío en el centro y norte de México: una revisión: *Boletín de la Sociedad Geológica Mexicana*, v. Volumen Conmemorativo del Centenario - Temas selectos de Geología Mexicana, LVII, no. 3, p. 187-225.

- Arenas, A. C., Vázquez, U. M., Pardo, T. G., and Sancho, M. C., 2010, Fluvial and Associated Carbonate Deposits, *in* Alonzo-Zarza, A. M., and Tanner, L. H., eds., *Developments in Sedimentology. Carbonates in Continental Settings: Facies, Environments, and Processes*, Elsevier, p. 133-170.
- Armenteros, I., Alonzo-Zarza, A. M., and Tanner, L. H., 2010, Chapter 2 Diagenesis of Carbonates in Continental Settings, *Developments in Sedimentology, Volume Volume 62*, Elsevier, p. 61-151.
- Arp, G., Reimer, A., and Reitner, J., 1999, Calcification in cyanobacterial biofilms of alkaline salt lakes: *European Journal of Phycology*, v. 34, p. 393-403.
- , 2001, Photosynthesis-induced biofilm calcification and calcium concentrations in Phanerozoic oceans: *Science*, v. 292, p. 1701–1704.
- Arthur, M. A., and Sageman, B. B., 1994, Marine black shales: Depositional mechanisms and environments of ancient deposits: *Annu. Rev. Earth Planet. Sci.*, v. 22, p. 499–551.
- Awramik, S., 1971, Precambrian Columnar Stromatolite Diversity: Reflection of Metazoan Appearance: *Science*, v. 174, p. 825-827.
- Azzaroli, A., 1995, A Synopsis of the Quaternary species of *Equus* in North America: *Bollettino della Società Paleontologica Italiana*, v. 34, no. 2, p. 205-221.
- Bathurst, R. G. C., 1975, *Carbonate sediments and their diagenesis* Amsterdam; New York, Elsevier Scientific Developments in sedimentology, 12, 658p.
- Benson, L., Kashgarian, M., and Rubin, M., 1995, Carbonate deposition, Pyramid Lake subbasin, Nevada; 2, Lake levels and polar jet stream positions reconstructed from radiocarbon ages and elevations of carbonates (tufas) deposited in the Lahontan Basin: *Palaeogeography, Palaeoclimatology, Palaeoecology*, v. 117, no. 1-2, p. 1-30.
- Benson, L. V., Lund, S. P., Burdett, J. W., Kashgarian, M., Rose, T. P., Smoot, J. P., and Schwartz, M., 1998, Correlation of late-Pleistocene lake-level oscillations in Mono Lake, California, with North Atlantic climate events: *Quaternary Research* (New York), v. 49, no. 1, p. 1-10.
- Berner, R. A., 1980, *Early diagenesis: a theoretical approach*, Princeton University Press. 241 p.
- , 1985, Sulphate reduction, organic matter decomposition and pyrite formation: *Philosophical Transactions of the Royal Society of London, Series A: Mathematical and Physical Sciences*, v. 315, no. 1531, p. 25-38.
- Blair, T. C., and McPherson, J. G., 1994, Alluvial fans and their natural distinction from rivers based on morphology, hydraulic processes, sedimentary processes, and facies assemblages: *Journal of Sedimentary Research*, v. 64, no. 3a, p. 450-489.
- Blair, T. C., and McPherson, J. G., 2007, Quaternary sedimentology of the Rose Creek fan delta, Walker Lake, Nevada, USA, and implications to fan-delta facies models: *Sedimentology*, v. 55, no. 3, p. 579-615.

- Blatt, H., Berry, W. B. N., and Brande, S., 1991, Principles of stratigraphic analysis: Blackwell Scientific Publications, 512 p.
- Bohacs, K. M., Reservoir Prediction in Lake Systems: Complex, Contingent, and Challenging., in Proceedings Sandstone Deposition in Lacustrine Environments: Implications for Exploration and Reservoir Development, AAPG Hedberg Conference, Baku, Azerbaijan, 2003, p. 1-3.
- Bohacs, K. M., Carroll, A. R., and Neal, J. E., Chaos and order: How predictable are the character and extent of lake strata?, in Proceedings AAPG Annual Meeting, Denver, Colorado, June 3-6, 2001.
- Bohacs, K. M., Carroll, A. R., Neal, J. E., and Mankiewicz, P. J., 2000a, Lake-Basin Type, Source Potential, and Hydrocarbon Character: and Integrated Sequence-Stratigraphic-Geochemical Framework, in Gierlowski-Kordesch, E. H., and Kelts, K., eds., Lake basins through space and time, Volume 46, American Association of Petroleum Geologists, p. 3-34.
- Bohacs, K. M., Grabowski, G. J., Carroll, A. R., Mankiewicz, P. J., Miskellgerhardt, K. J., Schwalbach, J. R., Wegner, M. B., and Simo, J. A., 2005, Production, destruction, and dilution—the many paths to source-rock development, in Harris, N. B., ed., The Deposition of Organic-Carbon-Rich Sediments: Models, Mechanisms, and Consequences, SEPM, Special Publication 82, p. 61-101.
- Bohacs, K. M., Neal, J. E., Carroll, A. R., and Reynolds, D. J., 2000b, Lakes are not small oceans!- Sequence stratigraphy in lacustrine basins.: Abstracts AAPG/SEPM Annual Meeting. American Association of Petroleum Geologists, p. 14.
- Bonny, S. M., and Jones, B., 2008, Controls on the precipitation of barite (BaSO<sub>4</sub>) crystals in calcite travertine at Twitya Spring, a warm sulphur spring in Canada's Northwest Territories: Sedimentary Geology, v. 203, no. 1-2, p. 36-53.
- Bowen, B. B., and Benison, K. C., 2009, Geochemical characteristics of naturally acid and alkaline saline lakes in southern Western Australia: Applied Geochemistry, v. 24, no. 2, p. 268-284.
- Bridge, J. S., 2003, Rivers and Floodplains: Forms, Processes and Sedimentary Record, Blackwell Publishing, 491 p.
- Bull, W. B., 1977, The alluvial-fan environment: Progress in Physical Geography, v. 1, no. 222, p. 222-270.
- Burne, R. V., Bauld, J., and De Deckker, P., 1980, Saline Lake Charophytes and their geological significance: Journal of Sedimentary Petrology, v. 5, no. 1, p. 281-293.
- Butzer, K. W., Abbott, J. T., Frederick, C. D., Lehman, P. H., Cordova, C. E., and Oswald, J. F., 2008, Soil-geomorphology and “wet” cycles in the Holocene record of North-Central Mexico: Geomorphology, v. 101, no. 1-2, p. 237-277.
- Campbell, C. V., 1967, Lamina, Laminaset, Bed and Bedset: Sedimentology, v. 8, p. 7-26.
- Canfield, D. E., 1994, Factors influencing organic carbon preservation in marine sediments: Chemical Geology, v. 114, p. 315-329.

- Carozzi, A. V., 1964, Complex ooids from Triassic lake deposits, Virginia: *American Journal of Science*, v. 262, p. 231-241.
- Carranza-Castañeda, O., and Roldán-Quintana, J., 2007, Mastofaunula de la cuenca de Moctezuma, Cenozoico tardío de Sonora, México: *Revista Mexicana de Ciencias Geológicas*, v. 24, no. 1, p. 81-88.
- Carroll, A. R., and Bohacs, K. M., 1999, Stratigraphic classification of ancient lakes: Balancing tectonic and climatic controls: *Geology*, v. 27, no. 2, p. 99-102.
- , 2001 Lake-type controls on petroleum source rock potential in nonmarine basins *American Association of Petroleum Geologist*, v. 85, no. 6, p. 1033-1053.
- Carroll, A. R., Chetel, L. M., and Smith, M. E., 2006, Feast to famine: Sediment supply control on Laramide basin fill: *Geology*, v. 34, no. 3, p. 197-200.
- Carroll, A. R., Graham, S. A., and Smith, M. E., 2010, Walled Sedimentary basins of China: *Basin Research*, v. 22, p. 17-32.
- Castanier, S., Perthuisot, J. P., Matrat, M., and Morvan, J. Y., 1999, Salt ooids of Berrel salt works (Bouches du Rhone, France), The role of bacteria in salt crystallization: *Sedimentary Geology*, v. 125, p. 9-21.
- Cohen, A. S., 1989, Facies relationships and sedimentation in large rift lakes and implications for hydrocarbon exploration: examples from Lake Turkana and Tanganyika: *Palaeogeography, Palaeoclimatology, Palaeoecology*, v. 70, p. 65-80.
- , 2003, *Paleolimnology: the history and evolution of lake systems*, Oxford University Press, p. 528.
- Cohen, A. S., and Thouin, C., 1987, Nearshore carbonate deposits in Lake Tanganyika: *Geology*, v. 15, p. 414-418.
- Coleman, M. L., 1985a, Geochemistry of diagenetic non-silicate minerals: Kinetic considerations: *Royal Society (London), Philosophical Transactions*, v. 315, p. 39-56.
- , 1985b, Geochemistry of diagenetic non-silicate minerals: kinetic considerations: *Philosophical Transactions of the Royal Society of London, Series A: Mathematical and Physical Sciences*, v. 315, no. 1531, p. 39-56.
- Coleman, M. L., Curtis, C. D., and Irwin, H., 1979, Burial rate a key to source and reservoir potential: *World Oil*, v. March, p. 83-92.
- Colson, J., and Cojan, I., 1996, Groundwater dolocretes in a lake-marginal environment: an alternative model for dolocrete formation in continental settings (Danian of the Provence Basin, France): *Sedimentology*, v. 43, p. 175-188.
- Council, T. C., and Bennett, P. C., 1993, Geochemistry of ikaite formation at Mono Lake, California: Implications for the origin of tufa mounds: *Geology*, v. 21, p. 971-974.
- Crosby, B., T., and Whipple, K. X., 2006, Nickpoint initiation and distribution within fluvial networks: 236 waterfalls in the Waipaoa River, North Island, New Zealand: *Geomorphology*, v. 82, p. 16-38.

- Chafetz, H. S., and Buczynski, C., 1992, Bacterially Induced Lithification of Microbial Mats: *Palaios*, v. 7, no. 3, p. 277-293.
- Chafetz, H. S., and Folk, R. L., 1984, Travertines: Depositional morphology and the bacterially constructed constituents: *Journal of Sedimentary Petrology*, v. 54, p. 289-316.
- Chávez, C. G., Aranda, G. J. J., Molina, G. R. S., Cossio, T., Arvisu, G. I. R., and González, M. G., 2005, The San Marcos Fault a Jurassic multireactivated basement structure in northeastern Mexico: Celebrating the centenary of the Geological Society of Mexico: *Geological Society of America Bulletin*, v. Special Paper 442, p. 261-286.
- Chen, J., Zhang, D., Wang, S., Xiao, T., and Huang, R., 2004, Factors controlling tufa deposition in natural waters at waterfall sites: *Sedimentary Geology*, v. 166, p. 353-366.
- Chetel, L. M. a., and Carroll, A. R., 2010, Terminal infill of Eocene Lake Gosiute, Wyoming, U.S.A.: *Journal of Sedimentary Research* v. 80, p. 492-514.
- Choquette, P. W., and Pray, L. C., 1970, Geologic Nomenclature and Classification of Porosity in Sedimentary Carbonates: *American Association of Petroleum Geologist Bulletin*, v. 54, no. 2, p. 207-250.
- Davis, S. J., Mulch, A., Carroll, A. R., Horton, T. W., and Chamberlain, C. P., 2009, Paleogene landscape evolution of the central North American Cordillera: Developing topography and hydrology in the Laramide foreland: *Geological Society of America Bulletin*, v. 121, no. 1-2, p. 100-116.
- Davis, S. J., Wiegand, B. A., Carroll, A. R., and P., C. C., 2008, The effect of drainage reorganization on paleoaltimetry studies: An example from the Paleogene Laramide foreland: *Earth and Planetary Science Letters*, p. 258–268.
- Davis, W. M., 1882, On the Classification of Lake Basins: *Proceedings of the Boston Society of Natural History*, v. 21, p. 315-381.
- De Wet, C. B., Mora, C. I., Gore, P. J. W., Gierlowski-Kordesch, E., and Cucolo, S. J., 2002, Deposition and geochemistry of lacustrine and spring carbonates in Mesozoic rift basins, eastern North America, *in* Ashley, G. M., and Renaut, R. W., eds., *Sedimentation in Continental Rifts*. Special Publication 73, SEPM, p. 309-325.
- De Wet, C. B., Yocum, D. A., and Mora, C. I., 1998, Carbonate lakes in closed basins sensitive indicators of climate and tectonics an example from the Gettysburg Basin Triassic Pennsylvania USA, *in* Shanley, K., and McCabe, P. J., eds., *Relative Role of Eustasy Climate and Tectonism in Continental Rocks* SEPM Special Publication 59 p. 191-209.
- Dean, W. E., 1981, Carbonate minerals and organic matter in sediments of modern north temperate hard-water lakes, *in* F.G. Ethridge, and Flores, R. M., eds., *Recent and ancient nonmarine depositional environments: Models for exploration*, Society of Economic Paleontologists and Mineralogists, Special Publication 31, p. 213-231.
- Dean, W. E., and Fouch, T. D., 1983, Lacustrine environment, *in* P.A. Scholle, D.G. Bebout, and Moore, C. H., eds., *Carbonate depositional environments*, American Association of Petroleum Geologist, p. 98-130.

- DeCelles, P. G., and Giles, K. A., 1996, Foreland basin systems: *Basin Research*, v. 8, no. 2, p. 105-123.
- Delrome, L. D., 1989, *Methods in Quaternary ecology*, No. 7: Freshwater Ostracods: *Geoscience Can.*, v. 16, no. 2, p. 85-90.
- Demant, A., and Robin, C., 1975, Las fases del vulcanismo en México: una síntesis en relación con la evolución geodinámica desde el Cretácico: *Revista del Instituto de Geología*, v. 1, p. 78-83.
- Dickson, J. A. D., 1966, Carbonate identification and genesis as revealed by staining: *Journal of Sedimentary Research*, v. 36, no. 2, p. 491-505.
- Dittrich, M., Kurz, P., and Wehrli, B., 2004, The Role of autotrophic picocyanobacteria in calcite precipitation in an oligotrophic Lake: *Geomicrobiology Journal*, v. 21, p. 45-53.
- Dittrich, M., and Sibling, S., 2010, Calcium carbonate precipitation by cyanobacterial polysaccharides, *in* Pedley, M., and Rogerson, M., eds., *Tufas and Speleothems: Unravelling the Microbial and Physical Controls*, Volume 336: London, Geological Society of London, Special Publications, p. 51-63.
- Duchesne, M. J., Pinet, N., Bédard, K., St-Onge, G., Lajeunesse, P., Campbell, D. C., and Bolduc, A., 2010, Role of the bedrock topography in the quaternary filling of a giant estuarine basin: the Lower St. Lawrence Estuary, Eastern Canada: *Basin Research*, v. 22, no. 6, p. 933-951.
- Dunham, R. J., 1962, Classification of carbonate rocks according to depositional texture: *in* Ham, W.E. (Ed.), *Classification of Carbonate Rocks*: American Association of Petroleum Geologists, Memoir 1, p. 108-121.
- Dupraz, C., Reid, R. P., Braissant, O., Decho, A. W., Norman, R. S., and Visscher, P. T., 2009, Processes of carbonate precipitation in modern microbial mats: *Earth-Science Reviews*, v. 96, no. 3, p. 141-162.
- Eguiluz, d. A. S., Aranda, G. S. M., and Marrett, R. A., 2000, Tectónica de la Sierra Madre Oriental, Mexico: *Boletín de la Sociedad Geológica Mexicana*, v. 53, p. 1-26.
- Eugster, H. P., and Hardie, L. A., 1975, Sedimentation in an Ancient Playa-Lake Complex: The Wilkins Peak Member of the Green River Formation of Wyoming: *Geological Society of America Bulletin*, v. 86, p. 319-334.
- , 1978, Saline lakes, *in* Lerman, A., ed., *Lakes: Chemistry, Geology and Physics*: New York, Springer-Verlag, p. 237- 203.
- Fisher, J. A., Nichols, G. J., and Waltham, D. A., 2007, Unconfined flow deposits in distal sectors of fluvial distributary systems: examples from Miocene Luna and Huesca Systems, northern Spain: *Sedimentary Geology*, v. 195, p. 55-73.
- Flügel, E., 2004, *Microfacies of Carbonate Rocks, Analysis, Interpretation and Application*, Springer Verlag, Berlin, New York, 976 p.:
- Folk, R. L., 1959, Practical petrographic classification of limestones: *Bulletin of the American Association of Petroleum Geologists*, v. 43, no. 1, p. 1-38.

- , 1974, The natural history of crystalline calcium carbonate: effect of magnesium content and salinity *Journal of Sedimentary Petrology*, v. 44, p. 40–53.
- Ford, T. D., and Pedley, H. M., 1996, A review of tufa and travertine deposits of the world: *Earth-Science Reviews*, v. 41, no. 3-4, p. 117-175.
- Fraser, G. S., and DeCelles, P. G., 1992, Geomorphic controls on sediment accumulation at margins of foreland basins: *Basin Research*, v. 4, p. 233-252.
- Freytet, P., and Plaziat, J. C., 1982, Continental carbonate sedimentation and pedogenesis- Late Cretaceous and Early Tertiary of Southern France, *in* Purser, B. H., ed., *Contributions to Sedimentology: Stuttgart, E.Schweizerbart'sche Verlagsbuchhandlung.*
- Freytet, P., and Verrechia, E. P., 2002, Lacustrine and Palustrine carbonate petrography: an overview: *Journal of Paleolimnology*, v. 27, p. 221-237.
- Friedman, G. M., 1965, Terminology of crystallization textures and fabrics in sedimentary rocks: *Journal of Sedimentary Petrology*, v. 35, no. 3, p. 643-655.
- , 1985, The term micrite or micrite cement is a contradiction- Discussion of micritic cements in microborings is not necessarily a shallow-water indicator: *Journal of Sedimentary Petrology*, v. 55, no. 5, p. 777.
- Garber, R. A., and Friedman, G. M., 1983, Coated grains along the Dead Sea shore, *in* Peryt, T. M., ed., *Coated Grains: Berlin, Springer-Verlag*, p. 142-1153.
- Gasith, A., and Hoyer, M. V., 1998, Structuring role of macrophytes in lakes: changing influence along lake size and depth gradients, p. 381-392.
- Gawthorpe, R. L., and Leeder, M. R., 2000, Tectono sedimentary evolution of active extensional basins *Basin Research*, v. 12, p. 195 - 218.
- Gierlowski-Kordesch, E., 1998, Carbonate deposition in an ephemeral siliciclastic alluvial system: Jurassic Shuttle Meadow Formation, Newark Supergroup, Hartford Basin, USA: *Palaeogeography, Palaeoclimatology, Palaeoecology*, v. 140, no. 1-4, p. 161-184.
- , 2010, Lacustrine carbonates, *in* Alosa-Zarza, A. M., and Tanner, L. H., eds., *Carbonates in continental settings facies environments and processes, Developments in sedimentology, Volume 61, Elsevier*, p. 1-101.
- Gierlowski-Kordesch, E., Jacobson, A. D., Blum, M. D., and Valero Garcés, B. L., 2008, Watershed reconstructions of a Paleocene-Eocene lake basin using Sr isotopes in carbonate rocks: *Geological Society of America Bulletin*, v. 120, p. 85-95.
- Gierlowski-Kordesch, E., and Kelts, K., 1994, Introduction, *in* Gierlowski-Kordesch, E., and Kelts, K., eds., *Global Geological Record of Lake Basins Volume 1: New York, Cambridge University Press.*
- Gingras, M. K., MacEachern, J. A., and Dashtgard, S. E., 2011, Process ichnology and the elucidation of physico-chemical stress: *Sedimentary Geology*, v. 237, p. 115-134.



- Glenn, C. R., and Kelts, K., 1991, Sedimentary Rhythms in Lake Deposits in Einsele et al. (eds.), *Cycles and Events in Stratigraphy*, Springer-Verlag Berlin Heidelberg, p. 955.
- Goldhamer, R. K., and Johnson, C. A., 1999, Mesozoic sequence stratigraphy and paleogeographic evolution of northeast Mexico, *in* Bartolini, C., Wilson, J. L., and Lawton, T. F., eds., *Mesozoic sedimentary and tectonic history of north-central Mexico Volume Special Paper 340*: Boulder, Colorado, Geological Society of America, p. 1-58.
- Golubic, S., Seong-Joo, L., and Browne, K. M., 2000, Cyanobacteria: Architects of Sedimentary Structures: *in* *Microbial Sediments*, R.E. Riding and S.M. Awramik (Eds.), Springer Verlag Berlin Heidelberg, p. 57-67.
- Gradstein, F. M., J.G. Ogg, A.G. Smith, F.P. Agterberg, W. Bleeker, R.A. Cooper, V. Davydov, P. Gibbard, L.A. Hinnov, M.R. House (†), L. Lourens, H-P. Luterbacher, J. McArthur, M.J. Melchin, L.J. Robb, P.M. Sadler, J. Shergold, M. Villeneuve, B.R. Wardlaw, J. Ali, H. Brinkhuis, F.J. Hilgen, J. Hooker, R.J. Howarth, A.H. Knoll, J. Laskar, S. Monechi, J. Powell, K.A. Plumb, I. Raffi, U. Röhl, A. Sanfilippo, B. Schmitz, N.J. Shackleton, G.A. Shields, H. Strauss, J. Van Dam, J. Veizer, Th. Van Kolfshoten, and D. Wilson, 2004, *Geologic Time Scale 2004*, Cambridge University Press, 589 p.
- Gray, G. G., Pottorf, R. J., Yurewicz, D. A., Mahon, K. I., Pevear, D. R., and Chuchla, R. J., 2001, Thermal and chronological record of syn-to post-Laramide burial and exhumation, Sierra Madre Oriental, Mexico, *in* Bartolini, C., Buffler, R. T., and Cantu-Chapa, A., eds., *The western Gulf of Mexico basin: tectonics, sedimentary basins, and petroleum systems, Volume 75*: Tulsa, OK, United States, American Association of Petroleum Geologists, p. 159– 181.
- Gregory, J. W., 1911, Constructive waterfalls: *The Scottish Geographical Magazine*, v. 27, no. 10, p. 537-546.
- Håkanson, L., and Jansson, M., 1983, *Principles of Lake Sedimentology*: Springer Verlag, p. 316 p.
- Hardie, L. A., 1991, On the significance of evaporites: *Annual Review Earth and Planetary Science* v. 19, p. 131–168.
- Hardie, L. A., and Lowenstein, T. K., 2004, Did the Mediterranean Sea Dry Out During the Miocene? A Reassessment of the Evaporite Evidence from DSDP Legs 13 and 42A Cores: *Journal of Sedimentary Research*, v. 74, no. 4, p. 453-461.
- Hilton, J., 1985, A conceptual framework for predicting the occurrence of sediment focusing and sediment redistribution in small lakes *Limnology and Oceanography*, v. 30, no. 6, p. 1131-1143.
- Horbury, A. D., and Adams, A. E., 1996, Microfacies associations in Asbian carbonates: an example from the Urswick Limestone Formation of the southern Lake District, northern England: *Geological Society, London, Special Publications*, v. 107, p. 221-237.
- Hutchinson, G. E., 1957, *A Treatise on Limnology*, v. I, Geography, Physics, and Chemistry, New York, Wiley & Sons 1015 p.:

- Imlay, R. W., 1936, Evolution of the Coahuila Peninsula, Mexico Part IV. Geology of the Western Part of the Sierra de Parras: Bulletin of the Geological Society of America, v. 47, p. 1091-1152.
- Imlay, R. W., 1937, Geology of the middle part of the Sierra de Parras, Coahuila, Mexico: Geological Society of America Bulletin, v. 48, no. 5, p. 587-630.
- Jaffey, A. H., Flynn, K. F., Glendenin, L. E., Bentley, W. C., and Essling, A. M., 1971, Precision measurement of half-lives and specific activities of <sup>235</sup>U and <sup>238</sup>U: Physical Review, v. C4, p. 1889-1906.
- James, N. P., and Choquette, P. W., 1989, Diagenesis 9. Limestones - the meteoric diagenetic environment: Geoscience Canada, v. 11, p. 161-194.
- Janssen, A., Swennen, R., Podoor, N., and Keppens, E., 1999, Biological and diagenetic influence in Recent and fossil tufa deposits from Belgium: Sedimentary Geology, v. 126, no. 1-4, p. 75-95.
- Johannesson, K. H., Cortés, A., and Kilroy, K. C., 2004, Reconnaissance isotopic and hydrochemical study of Cuatro Ciénegas groundwater, Coahuila, México: Journal of South American Earth Sciences, v. 17, no. 2, p. 171-180.
- Jones, B. F., 1989, Calcite rafts, peloids, and micrite in cave deposits from Cayman Brac, British West Indies: Canadian Journal of Earth Sciences, v. 26, p. 654-664.
- , 2010, Microbes in caves: agents of calcite corrosion and precipitation, *in* Pedely, M., and Rogerson, M., eds., Tufas and Speleothems: Unravelling the Microbial and Physical Controls, Volume 336: London, The Geological Society of London, p. 7-30.
- Jones, B. F., and Renaut, R. W., 2010, Calcareous Spring Deposits in Continental Settings, *in* Alonso Zarza, A. M., and Tanner, L. H., eds., Carbonates in continental settings: Facies, Environments and Processes, p. 177-224.
- Kabanov, P., Anadón, P., and Krumbein, W. E., 2008, Microcodium: An extensive review and a proposed non-rhizogenic biologically induced origin for its formation: Sedimentary Geology, v. 205, p. 79-99.
- Katz, B. J., 1995, Factors controlling the development of lacustrine petroleum source rocks-An update, *in* Huc, A. Y., ed., Paleogeography, Paleoclimate, and Source Rocks. Studies in Geology Volume 40, American Association of Petroleum Geologists, p. 61-79.
- , 2001, Lacustrine basin hydrocarbon exploration - current thoughts: Journal of Paleolimnology, v. 26, no. 2, p. 161-179.
- Keighley, D., Flint, S., Howell, J., and Moscariello, A., 2003, Sequence Stratigraphy in Lacustrine Basins: A model for part of the green River Formation (Eocene), Southwest Uinta Basin, U.S.A.: Journal of Sedimentary Research, v. 73, no. 6, p. 987-1006.
- Kelts, K., 1988, Environments of deposition of lacustrine petroleum source rocks: an introduction: Geological Society, London, Special Publications, v. 40, no. 1, p. 3-26.

- Kelts, K., and Hsü, K. J., 1978, Freshwater carbonate sedimentation: *in* A. Lerman (Ed.), Lakes- chemistry, geology, physics: New York, Springer-Verlag Pub., p. 295-323.
- Klappa, C. F., 1979, Calcified filaments in Quaternary Calcretes: Organo-mineral interactions in the subaerial vadose environment: *Journal of Sedimentary Petrology*, v. 49, no. 3, p. 955-968.
- Kosir, A., 2004, Microcodium Revisited: Root Calcification Products of Terrestrial Plants on Carbonate-Rich Substrates: *Journal of Sedimentary Research*, v. 74, no. 6, p. 845-857.
- Lamb, M. P., and Dietrich, W. E., 2009, The persistence of waterfalls in fractured rock: *Geological Society of America Bulletin*, v. 121, no. 7/8, p. 1123–1134.
- Lambiase, J. J., 1990, A model for Tectonic Control of Lacustrine Stratigraphic Sequences in Continental Rift Basins., *in* Katz, B. J., ed., Lacustrine Basin Exploration-Case Studies and Modern Analogues, Volume Memoir 50, American Association of Petroleum Geologists, p. 265-276.
- Lawton, T. F., Boyer, S. E., and Schmitt, J. G., 1994, Influence of inherited taper on structural variability and conglomerate distribution, Cordilleran fold and thrust belt, western United States: *Geology*, v. 22, no. 4, p. 339-342.
- Lawton, T. F., Bradford, I. A., Vega, F. J., Gehrels, G. E., and Amato, J. M., 2009, Provenance of Upper Cretaceous - Paleogene sandstones in the foreland basin system of the Sierra Madre Oriental, northeastern Mexico, and its bearing on fluvial dispersal systems of the Mexican Laramide Province: *Geological Society of America Bulletin*, v. 121, no. 5/6, p. 820-836.
- Leinfelder, R. R., and Hartkopf-Fröder, C., 1990, In situ accretion mechanism of concavo-convex lacustrine oncoids ('swallow nests') from the Oligocene of the Mainz Basin, Rhineland, FRG: *Sedimentology*, v. 37, p. 287-301.
- Leithch, A. R., 1991, Calcification of the Charophite Oosporangium, *in* Riding, R., ed., Calcareous algae and stromatolites, Springer Verlag, p. 204-216.
- Leng, M. J., Jones, M. D., Frogley, M. R., Eastwood, W. J., Kendrick, C. P., and Roberts, C. N., 2010, Detrital carbonate influences on bulk oxygen and carbon isotope composition of lacustrine sediments from the Mediterranean: *Global and Planetary Change*, v. 71, p. 175-182.
- Leng, M. J., and Marshall, J. D., 2004, Paleoclimate interpretation of stable isotope data from lake sediment archives: *Quaternary Science Reviews* v. 23, p. 811-831.
- Lewis, D. W., and McConchie, D., 1994, Analytical sedimentology, Chapman & Hall.
- Lowenstein, T. K. a., and Hardie, L. A., 1985, Criteria for the recognition of salt-pan evaporites: *Sedimentology*, v. 32, p. 627-644.
- Ložek, V., 1986, Mollusca analysis, *in* Berglund, B. E., ed., Handbook of Holocene palaeoecology and palaeohydrology, Jhon Wiley and Sons, p. 869.
- Mack, G. H., James, W. C., and Monger, H. C., 1993, Classification of Paleosols: *Geological Society of America Bulletin*, v. 105, p. 129-136.

- Machel, H. G., 1985, Cathodoluminescence in calcite and dolomite and its chemical interpretation.: *Geoscience Canada*, v. 12, p. 139-147.
- MacQuaker, J. H. S., and Gawthorpe, R. L., 1993, Mudstone lithofacies in the Kimmeridge Clay Formation, Wessex Basin, southern England; implications for the origin and controls of the distribution of mudstones: *Journal of Sedimentary Research*, v. 63, no. 6, p. 1129-1143.
- MacQuaker, J. H. S., and Adams, A. E., 2003, Maximizing information from fine-grained sedimentary rocks: an inclusive nomenclature for mudstones: *Journal of Sedimentary Research*, v. 73, no. 5, p. 735-744.
- MacQuaker, J. H. S., Taylor, K. G., and Gawthorpe, R. L., 2007, High-Resolution Facies Analyses of Mudstones: Implications for Paleoenvironmental and Sequence Stratigraphic Interpretations of Offshore Ancient Mud-Dominated Successions: *Journal of Sedimentary Research*, v. 77, no. 4, p. 324-339.
- Markowska, J., 2004, The origins of the Plitvice Lakes (Croatia): *Miscellanea Geographica*, v. 11, p. 93-99.
- McBride, E. F., Weidie, A. E., Wolleben, J. A., and Laudon, R. C., 1974, Stratigraphy and Structure of the Parras and La Popa Basins, Northeastern Mexico: *Geological Society of America Bulletin*, v. 85, no. 10, p. 1603-1622.
- McPherson, J. G., Shanmugam, G., and Moiola, R. J., 1987, Fan deltas and braided deltas: Varieties of coarse-grained deltas: *Geological Society of America Bulletin*, v. 99, p. 331-340.
- Merz-Preiß, M., 2000, Calcification in cyanobacteria, *in* Riding, R., and Awramick, S., eds., *Microbial Sediments* Berlin, Springer-Verlag, p. 50–56.
- Merz-Preiß, M., and R., R., 1999, Cyanobacterial tufa calcification in two freshwater streams: ambient environment, chemical thresholds and biological processes: *Sedimentary Geology*, v. 126, p. 103-124.
- Merz, M. U. E., 1992, The biology of carbonate precipitation: *Facies*, v. 26, p. 81-102.
- Meyers, P. A., and R. Ishiwatari, R., 1993, Lacustrine organic geochemistry — an overview of indicators of organic matter sources and diagenesis in lake sediments: *Organic Geochemistry*, v. 20, p. 867-900.
- Miller, B. M., and Tevesz, M. J., 2001, Freshwater molluscs, *in* Smol, J. P., Birks, H. J. B., and Last, W. M., eds., *Tracking Environmental Change Using Lake Sediments. Volume 4: Zoological Indicators*: Dordrecht, The Netherlands, Kluwer Academic Publishers.
- Milligan, M. R., and Chan, M. A., 1998, Coarse-grained Gilbert Deltas: facies, sequence stratigraphy and relationships to Pleistocene climate at the eastern margin of Lake Bonneville, northern Utah., *in* Shanley, K. W., and McCabe, P. J., eds., *Relative Role of Eustasy, Climate and Tectonism in Continental Rocks*, *Society of Economic Paleontologists and Mineralogists Special Publication* 59, p. 177–189.

- Milliman, J. D., Hook, J. A., and Golubic, S., 1985, Meaning and usage of micrite cement and matrix - reply to discussion: *Journal of Sedimentary Petrology*, v. 55, no. 5, p. 777-784.
- Molina, G. R. S., Chávez, C. G., Iriondo, A., Porras, V. M. A., and Terrazas, C. G. D., 2008, Paleomagnetism, structure and  $^{40}\text{Ar}/^{39}\text{Ar}$  geochronology of the Cerro Mercado pluton, Coahuila: Implications for the timing of the Laramide orogeny in northern Mexico: *Revista Mexicana de Ciencias Geológicas*, v. 25, no. 2, p. 284-301.
- Monty, C. L. V., 1976, The origin and development of cryptalgal fabrics, in Walter, M. R., ed., *Stromatolites. Developments in Sedimentology, Volume 20: Amsterdam, Elsevier*, p. 193-249.
- Monty, C. L. V., 1981, Spongistomate vs. Porostomate stromatolites and oncolites, in Monty, C. L. V., ed., *Phanerozoic Stromatolites: Amsterdam, Elsevier*.
- Moore, C. H., 2001, Carbonate reservoirs, Porosity, Evolution and Diagenesis in Sequence Stratigraphic Framework, Elsevier, *Development in Sedimentology 55*, 444 p.:
- Morrow, D. W., and McIlreath, I. A., 1990, Diagenesis. General introduction, in McIlreath, I. A., and Morrow, D. W., eds., *Diagenesis, Geoscience Canada, Reprint Series 4*, p. 128.
- Morse, J. W., and Mackenzie, F. T., 1990, *Geochemistry of sedimentary carbonates*.
- Murphy, D. H., and Wilkinson, B. H., 1980, Carbonate deposition and facies distribution in a central Michigan marl lake: *Sedimentology*, v. 27, no. 2, p. 123-135.
- Murray, R. C., 1964, Origin and diagenesis of gypsum and anhydrite: *Journal of Sedimentary Research*, v. 34, no. 3, p. 512-523.
- Nickel, E., 1983, Environmental significance of freshwater oncoids, Eocene Guarga Formation, Southern Pyrenees, Spain, in Peryt, P. M., ed., *Coated grains: Berlin, Springer-Verlag*.
- Nichols, G., 2004, *Sedimentology and Stratigraphy Blackwell Publishing*, 355 p.:
- Nichols, G. J., and Fisher, J. A., 2007, Processes, facies and architecture of fluvial distributary system deposits: *Sedimentary Geology*, v. 195, no. 1-2, p. 75-90.
- Nichols, P. D., and Nichols, C. A. M., 2008, Microbial signature lipid profiling and exopolysaccharides: Experiences initiated with Professor David C. White and transported to Tasmania, Australia: *Microbiology Methods*, v. 74, no. 1, p. 33-46.
- Noffke, N., Gerdes, G., Klenke, T., and Krumbein, W. E., 2001, Microbially Induced Sedimentary Structures: A New Category within the Classification of Primary Sedimentary Structures: *Journal of Sedimentary Research*, v. 71, no. 5, p. 649-656.
- Olsen, P. E., 1990, Tectonic, climatic, and biotic modulation of lacustrine ecosystems—examples from the Newark Supergroup of eastern North America, in Katz, B. J., ed., *Lacustrine Exploration: Case Studies and Modern Analogues, Volume 50, American Association of Petroleum Geologists* p. 209-224.

- Page, W. R., VanSistine, D. P., and Turner, K. J., 2005, Preliminary Geologic Map of Southernmost Texas, United States, and parts of Tamaulipas and Nuevo Leon, Mexico: Environmental Health Investigations in the United States-Mexico border region: U.S. Department of the Interior, U.S. Geological Survey.
- Palacios-Fest, M., Cohen, A. S., and Anadon, P., 1994, Use of ostracodes as paleoenvironmental tools in the interpretation of ancient lacustrine records: *Revista Española de Paleontología*, v. 9, no. 2, p. 145-164.
- Pearthree, P. A., Spencer, J. E., Faulds, J. E., and House, P. K., 2008, Comment on "Age and Evolution of the Grand Canyon Revealed by U-Pb Dating of water table-Type speleothems": *Science*, v. 319, p. 1377-1380.
- Pedely, H. M., and Rogerson, M., 2010, Introduction to tufas and speleothems, *in* pedley, M., and Rogerson, M., eds., *Tufas and Speleothems: Unraveling the Microbial and Physical Controls*, Volume 336: London, The Geological Society of London, p. 1-5.
- Pedley, H. M., Hill, I., Denton, P., and Brasington, J., 2000, Three-dimensional modelling of a Holocene tufa system in the Lathkill Valley, north Derbyshire, using ground-penetrating radar: *Sedimentology*, v. 47, no. 3, p. 721-737.
- Pedley, H. M., 1990, Classification and environmental models of cool freshwater tufas: *Sedimentary Geology*, v. 68, no. 1-2, p. 143-154.
- 2003, Tufas and Travertines, *in* Middleton, G., ed., *Encyclopaedia of Sediments and Sedimentary Rocks*, Kluwer, p. 753-755.
- Pentecost, A., 1987, Growth and calcification of the freshwater cyanobacterium *Rivularia haematites*: *Proceedings of the Royal Society of London. Series B, Biological Sciences*, v. 232, no. 1266, p. 125-136.
- Pentecost, A., 1995, The Quaternary travertine deposits of Europe and Asia Minor: *Quaternary Science Reviews*, v. 14, no. 10, p. 1005-1028.
- Peryt, T. M., 1981, Phanerozoic oncoids - an overview: *Facies*, no. 4, p. 197-214.
- Pietras, J. T., Carroll, A. R., and Rhodes, M. K., 2003, Lake basin response to tectonic drainage diversion: Eocene Green River Formation, Wyoming: *Journal of Paleolimnology*, v. 30, p. 115-125.
- Pietras, J. T., and Carroll, A. R., 2006, High-resolution stratigraphy of an underfilled lake basin: Wilkins Peak Member, Eocene Green River Formation, Wyoming, U.S.A.: *Journal of Sedimentary Research*, v. 76, p. 1197-1214.
- Platt, N. H., 1989, Lacustrine carbonates and pedogenesis: sedimentology and origin of palustrine deposits from the Early Cretaceous Rupelo Formation, W Cameros Basin, N Spain: *Sedimentology*, v. 36, no. 4, p. 665-684.
- Platt, N. H., and Wright, V. P., 1991, Lacustrine carbonates: facies models, facies distribution and hydrocarbon aspects: *In* Anadon, P., L. Cabrera, and K. Kelts (Eds.), *Lacustrine Facies Analysis*. IAS spec. publ. 13. Blackwell, Oxford, p. 57-74.

- Polyak, V., Hill, C., and Asmerom, Y., 2008, Age and Evolution of the Grand Canyon Revealed by U-Pb, Dating of Water Table Type speleothems: *Science*, v. 319, p. 1377-1380.
- Raiswell, R., and Canfield, D. E., 1998, Sources of iron for pyrite formation in marine sediments: *American Journal of Science*, v. 298, p. 219-245.
- Rajan, S., Mackenzie, F. T., and Glenn, C. R., 1996, A thermodynamic model for water column precipitation of siderite in the Plio-Pleistocene Black Sea: *American Journal of Science*, v. 296, p. 506-548.
- Rasbury, E. T., and Cole, J. M., 2009, Directly dating geologic events: U-Pb dating of carbonates: *Reviews of Geophysics*, v. 47, p. RG3001 / 2009.
- Raven, J. A., and Knoll, A. H., 2010, Non-Skeletal Biomineralization by Eukaryotes: Matters of Moment and Gravity: *Geomicrobiology Journal*, v. 27, p. 572-584.
- Reineck, H. E., 1963, Sedimentgefüge im Bereich der südlichen Nordsee: *Abhandlungen der senckenbergische naturforschende Gesellschaft*, v. 505, p. 1-138.
- Richards, D. A., Bottrell, S. H., Cliff, R. A., Strohle, K., and Rowe, P. J., 1998, U-Pb dating of a speleothem of Quaternary age: *Geochimica et Cosmochimica Acta*, v. 62, no. 23-24, p. 3683-3688.
- Richards, D. A., and Dorale, J. A., 2003, U-Series chronology and environmental applications of speleothems: *Reviews in Mineralogy and Geochemistry*, v. 52, p. 407-460.
- Riding, R., 1977, Calcified *Plectonema* (blue-green algae), a Recent example of *Girvanella* from Aldabra Atoll: *Palaeontology*, v. 20, p. 33-46.
- , 2000, Microbial carbonates: the geological record of calcified bacterial-algal mats and biofilms: *Sedimentology*, v. 47, no. 1, p. 179-214.
- Riding, R., 2006, Microbial carbonate abundance compared with fluctuations in metazoan diversity over geological time: *Sedimentary Geology*, v. 185, no. 3-4, p. 229-238.
- Robbins, L. L., and Blackwelder, P. L., 1992, Biochemical and ultrastructural evidence for the origin of whittings: a biologically induced calcium carbonate precipitation mechanism: *Geology*, v. 20, p. 464-468.
- Rodríguez, F., and Werner, J., 1993, Investigación preliminar de la Formación La Providencia (Calizas Terciarias de Agua Dulce) al Este de Linares, N.L., México, *in* S., C. P., F., J. A. R., R., M. M. R., and Navarro-L., I., eds., *Actas Facultad de Ciencias de la Tierra, UANL, Volume 8: Linares*.
- Rogers, C. L., De Cserna, Z., Van-Vloten, R., Tavera-Amezcuca, E., and Ojeda, R. J., 1961, 1961, Reconocimiento geológico y depósitos de fosfatos del norte de Zacatecas y áreas adyacentes en Coahuila, Nuevo León y San Luis Potosí: *Boletín del Consejo de Recursos Naturales no Renovables*, v. 56, p. 322.
- Sarg, J. F., 2001, The sequence stratigraphy, sedimentology, and economic importance of evaporite-carbonate transitions: a review: *Sedimentary Geology*, v. 140, no. 1-2, p. 9-34.

- Schäfer, A., and Stapf, K. R. G., 1978, Permian Saar-Nahe Basin and Recent Lake Constance (Germany): two environments of lacustrine algal carbonates, *in* Matter, A., and Tucker, M. E., eds., *Modern and ancient lake sediments*. Special publication, Volume 2, International Association of Sedimentologists, p. 83-107.
- Schidlowski, M., 2000, Carbon isotopes and microbial sediments, *in* Riding, R., and Awramick, S. M., eds., *Microbial sediments*: Berlin, Springer-Verlag, p. 84-95.
- Schieber, J., 1999, Microbial Mats in Terrigenous Clastics: The Challenge of Identification in the Rock Record: *Palaios*, v. 14, p. 3-12.
- Scholz, C. A., 2001, Applications of seismic sequence stratigraphy in lacustrine basins: *in* W.M. Last and J.P. Smol. (eds.), *Tracking Environmental Change Using Lake Sediments. Volume I: Basin Analysis, Coring, and Chronological Techniques*. Kluwer Academic Publishers, Dordrecht, The Netherlands., p. 7-22.
- Shanley, K. W., and McCabe, J. B., 1994, Perspectives on Sequence Stratigraphy of Continental Strata: *American Association of Petroleum Geologist*, v. 78, no. 4, p. 544-568.
- Shinn, A. E., Steinen, R. P., Lidz, B. H., and Swart, P. K., 1989, Whittings, a sedimentologic dilemma: *Journal of Sedimentary Petrology*, v. 59, no. 1, p. 147-161.
- Sladen, C. P., 1994, Key elements during the search for hydrocarbons in lake systems, *in* Gierlowski-Kordesch, E., and Kelts, K., eds., *Global Geological Record of Lake Basins, Volume 1*: New York, Cambridge University Press, p. 3-17.
- Smith, M. A., and Mason, T. R., 1991, Pleistocene, multiple-growth, lacustrine oncoids from the Poacher's Point Formation, Etosha Pan, northern Namibia: *Sedimentology*, v. 38, p. 591-599.
- Smoot, J. P., and Lowenstein, T. K., 1991, Depositional environments of non-marine evaporites, *in* Melvin, J. L., ed., *Developments in sedimentology*, 50. *Evaporites, petroleum and mineral resources*, Elsevier, p. 189-347.
- Soegaard, K., Ye, H., Halik, N., Daniels, A. T., Arney, J., and Garrick, S., 2003, Stratigraphic evolution of latest Cretaceous to Early Tertiary Difunta Foreland Basin in Northeast Mexico: Influence of Salt withdrawal on Tectonically Induced Subsidence by the Sierra Madre Oriental Fold and Thrust Belt, *in* Bartolini, C., Bluffer, R. T., and Blickwede, J., eds., *The Circum-Gulf of Mexico and the Caribbean: Hydrocarbon habitats, basin formation, and plate tectonics*, *American Association of Petroleum Geologist*, Memoir 79, p. 364-394.
- Stabel, H. H., 1986, Calcite precipitation in Lake Constance: chemical equilibrium, sedimentation, and nucleation by algae: *Limnology and Oceanography*, v. 31, no. 5, p. 1081-1093.
- Suppe, J., 1983, Geometry and kinematics of fault-bend folding: *American Journal of Science*, v. 283, no. 7, p. 684-721.
- Suppe, J., 1985, *Principles of Structural Geology*, Englewood Cliffs, New Jersey, Prentice Hall. 537p.



- Talbot, M. R., 1988, The origins of lacustrine oil source rocks: evidence from the lakes of tropical Africa, *in* Fleets, A. J., Kelts, K., and Talbot, M. R., eds., Lacustrine petroleum source rocks Volume 40, Geological Society of London, Special Publication, p. 29-43.
- , 1990, A review of the palaeohydrological interpretation of carbon and oxygen isotopic ratios in primary lacustrine carbonates: *Chemical Geology: Isotope Geoscience section*, v. 80, no. 4, p. 261-279.
- Talbot, M. R., 1994, Sequence stratigraphy in lakes: The ups and downs of small oceans or something else?: 14th International Sedimentological Congress, Abstracts, Masescone, J.M (Chairperson), Sequence Stratigraphy, 8-S69.
- Talbot, M. R., and Livingstone, D. A., 1989, Hydrogen index and carbon isotopes of lacustrine organic matter as lake level indicators: *Palaeogeography, Palaeoclimatology, Palaeoecology*, v. 70, p. 121-137.
- Tardy, M., Longoria, J. F., Martínez-Reyes, J., Mitre, L. M., Patiño, M., Padilla y S. R., and Ramírez, C., 1975, Observaciones Generales sobre la estructura de la Sierra Madre Oriental: La aloctonía del conjunto cadena alta altiplano central, entre Torreón, Coahuila y San Luis Potosí, México: *Revista del Instituto de Geología*, v. 75, no. 1, p. 1-11.
- Taylor, A. M., and Goldring, R., 1993, Description and analysis of bioturbation and ichnofabric: *Journal of the Geological Society*, v. 150, no. 1, p. 141-148.
- Thompson, J. B., 2000, Microbial whittings: *in* R. E. Riding and S.M. Awramik (Eds.), *Microbial sediments*, Springer, p. 250-260.
- Thompson, J. B., and Ferris, F. G., 1990, Cyanobacterial precipitation of gypsum, calcite, and magnesite from natural alkaline water: *Geology*, v. 18, p. 995-998.
- Thompson, J. B., Schultze-Lam, S., Berveridge, T. J., and DesMarais, D. J., 1997, Whiting events: biogenic origin due to the photosynthetic activity of cyanobacterial picoplankton *Limnology and Oceanography*, v. 42, p. 133-141.
- Thompson, S., and Eglinton, G., 1978, The fractionation of a recent sediment for organic geochemical analyses: *Geochimica et Cosmochimica Acta*, v. 42, p. 199-207.
- Tucker, M. E., and Wright, V. P., 1990 *Carbonate sedimentology*, Blackwell Science, 482 p.:
- Turner, E. C., and Jones, B., 2005, Microscopic calcite dendrites in cold-water tufa: implications for nucleation of micrite and cement: *Sedimentology*, v. 52, no. 5, p. 1043-1066.
- Van Wagoner, J. C., Mitchum, R. M., Campion, K. M., and Rahmanian, V. D., 1990, Siliciclastic sequence stratigraphy in well logs, cores, and outcrops: concepts for high resolution correlation of time and facies, American Association of Petroleum Geologists, *Methods in Exploration Series 7*, 55 p.:
- Vázquez-Urbez M., Pardo T. G., Arenas A. C., and Sancho, C., 2010, Fluvial diffluence episodes reflected in the Pleistocene tufa deposits of the River Piedra (Iberian Range, NE Spain): *Geomorphology*, v. 125, no. 1, p. 1-10.

- Viles, H. A., and Goudie, A. S., 1990, Tufas, travertines and allied carbonate deposits: *Progress in Physical Geography*, v. 14, p. 19-41.
- Walker, J., Cliff, R. A., and Latham, A. G., 2006, U–Pb isotopic age of the StW 573 hominid from Sterkfontein, South Africa: *Science*, v. 314, p. 1592–1594.
- Warren, J. K., 2006, *Evaporites: Sediment, Resources and Hydrocarbons*, Springer, 1035 p.:
- , 2010, Evaporites through time: Tectonic, climatic and eustatic controls in marine and nonmarine deposits: *Earth-Science Reviews* v. 98, p. 217–268.
- Weidie, A. E., and Murray, G. E., 1967, Geology of Parras Basin and adjacent areas of Northeastern Mexico: *American Association of Petroleum Geologist Bulletin*, v. 51, no. 5, p. 678-695.
- Winsborough, B. M., Seeler, J. S., Golubic, S., Folk, R. L., and Maguire, B., 1994, Recent fresh-water lacustrine stromatolites, stromatolitic mats, and oncoids from Northeastern Mexico, *in* Bertrand-Sarfati, J., and Monty, C., eds., *Phanerozoic Stromatolites, Volume II: The Netherlands*, Kluwer Academic Publishers, p. 71-100.
- Woodhead, J., Hellstrom, J., Maas, R., Drysdale, R., Zanchetta, G., Devine, P., and Taylor, E., 2006, U-Pb geochronology of speleothems by MC-ICPMS: *Quaternary geochronology* v. 1, p. 208-221.
- Woodhead, J., and Hergt, J. M., 2001, Strontium, neodymium, and lead isotope analyses of NIST glass certified reference materials: SRM 610, 612, 614: *Geostandards Newsletter* v. 25, p. 261-266.
- Woodhead, J. D., Hellstrom, J., Paton, C., Hergt, J. M., Greig, A., and Maas, R., 2008, A guide to depth profiling and imaging applications of LA-ICP-MS, *in* Sylvester, P., ed., *Laser Ablation ICP–MS in the Earth Sciences: Current Practices and Outstanding Issues* Mineralogical Association of Canada p. 135-145.
- Wright, V. P., and Platt, N. H., 1995, Seasonal wetland carbonate sequences and dynamic catenas: a re-appraisal of palustrine limestones: *Sedimentary Geology*, v. 99, no. 2, p. 65-71.
- Wright, V. P., and Tucker, M. E., 1991, Calcretes: an introduction, *in* Wright, V. P., and Tucker, M. E., eds., *Calcretes, Volume 2, IAS Reprint Series 2*, Blackwell Scientific Publication, p. 1-22.

## **APPENDICES**

**Plus-Carlo Erba: Carbon Isotope Analysis**

martes, 16 de noviembre de 2010  
 J. Macquaker  
 A. Pye  
 $\delta^{13}C$

**Memorial University  
 CREAT Network - TERRA Facility  
 Stable Isotope Lab**

Please quote OurLabID when making enquiries about your samples.

Sample ID	Date Time	Analysis	Comment	Amount (mg)	Peak Amplitude (mV)	Delta of Peak	Mean Delta of All Analyses	StdDev of Deltas of All Analyse s	%C for applicable media	Mean %C of All Analyses	StdDev of %C of All Analyses	Last Name	Submit Date	Medium	Project Purpose
N12-3	16/11/2010	D-24362		1.212	17758	-6.28	-6.28		13.01	13.01		Macquaker	09/06/2010	25 -> G, Org C, organic C	Mayran Fm TOC
N12-4	16/11/2010	D-24363		1.241	17981	-6.61	-6.61		12.97	12.97		Macquaker	09/06/2010	25 -> G, Org C, organic C	Mayran Fm TOC
N12-5	16/11/2010	D-24364		1.479	20281	-6.15	-6.15		12.40	12.40		Macquaker	09/06/2010	25 -> G, Org C, organic C	Mayran Fm TOC
N12-6	16/11/2010	D-24367		1.449	20695	-6.38	-6.38		12.88	12.88		Macquaker	09/06/2010	25 -> G, Org C, organic C	Mayran Fm TOC
N12-7	16/11/2010	D-24368		1.582	21964	-6.69	-6.69		12.40	12.40		Macquaker	09/06/2010	25 -> G, Org C, organic C	Mayran Fm TOC
N12-9	24/11/2010	D-24750	re-runs	7.098	2298	-15.77	-15.77		0.27			Macquaker	09/06/2010	25 -> G, Org C, organic C	Mayran Fm TOC
N12-10	24/11/2010	D-24751	re-runs	1.101	15721	-7.10	-7.10		12.70			Macquaker	09/06/2010	25 -> G, Org C, organic C	Mayran Fm TOC
N12-11	16/11/2010	D-24371		1.240	18109	-6.44	-6.44		13.14	13.14		Macquaker	09/06/2010	25 -> G, Org C, organic C	Mayran Fm TOC
N12-12	16/11/2010	D-24373		1.410	20819	-6.34	-6.34		13.20	13.20		Macquaker	09/06/2010	25 -> G, Org C, organic C	Mayran Fm TOC
N12-14	16/11/2010	D-24374		1.250	16735	-5.49	-5.49		12.08	12.08		Macquaker	09/06/2010	25 -> G, Org C, organic C	Mayran Fm TOC
N12-15	16/11/2010	D-24375		1.196	17016	-5.94	-5.94		12.72	12.72		Macquaker	09/06/2010	25 -> G, Org C, organic C	Mayran Fm TOC
N21B-1	16/11/2010	D-24376		1.213	17349	-6.00	-6.00		12.81	12.81		Macquaker	09/06/2010	25 -> G, Org C, organic C	Mayran Fm TOC
N21B-2	16/11/2010	D-24377		1.491	20985	-5.39	-5.39		12.64	12.64		Macquaker	09/06/2010	25 -> G, Org C, organic C	Mayran Fm TOC
N21B-4	16/11/2010	D-24380		1.302	18877	-6.82	-6.82		13.15	13.15		Macquaker	09/06/2010	25 -> G, Org C, organic C	Mayran Fm TOC
N21B-5	16/11/2010	D-24381		1.041	13836	-5.54	-5.54		11.95	11.95		Macquaker	09/06/2010	25 -> G, Org C, organic C	Mayran Fm TOC
N21B-6	16/11/2010	D-24382		1.016	14720	-5.84	-5.84		12.99	12.99		Macquaker	09/06/2010	25 -> G, Org C, organic C	Mayran Fm TOC
N21B-7	16/11/2010	D-24383		1.153	16251	-5.66	-5.66		12.68	12.68		Macquaker	09/06/2010	25 -> G, Org C, organic C	Mayran Fm TOC
N21B-9	16/11/2010	D-24384		1.096	13984	-5.68	-5.68		11.39	11.39		Macquaker	09/06/2010	25 -> G, Org C, organic C	Mayran Fm TOC
N21B-12	16/11/2010	D-24386		1.162	16890	-5.83	-5.83		12.97	12.97		Macquaker	09/06/2010	25 -> G, Org C, organic C	Mayran Fm TOC
N21B-13	16/11/2010	D-24387		1.223	13967	-5.50	-5.50		10.19	10.19		Macquaker	09/06/2010	25 -> G, Org C, organic C	Mayran Fm TOC
N21B-15	16/11/2010	D-24388		1.011	14690	-5.78	-5.78		13.07	13.07		Macquaker	09/06/2010	25 -> G, Org C, organic C	Mayran Fm TOC
N21B-17	16/11/2010	D-24389		1.585	23090	-6.42	-6.42		13.08	13.08		Macquaker	09/06/2010	25 -> G, Org C, organic C	Mayran Fm TOC
N7C-4	16/11/2010	D-24390		1.648	22814	-6.94	-6.94		12.33	12.33		Macquaker	09/06/2010	25 -> G, Org C, organic C	Mayran Fm TOC
N7C-6	16/11/2010	D-24393		1.080	16552	-6.40	-6.40		13.77	13.77		Macquaker	09/06/2010	25 -> G, Org C, organic C	Mayran Fm TOC
N7C-7	16/11/2010	D-24394		1.534	21883	-6.06	-6.06		12.78	12.78		Macquaker	09/06/2010	25 -> G, Org C, organic C	Mayran Fm TOC
N7C-9	16/11/2010	D-24395		1.386	20476	-5.77	-5.77		13.16	13.16		Macquaker	09/06/2010	25 -> G, Org C, organic C	Mayran Fm TOC
N7C-12	16/11/2010	D-24396		1.093	12866	-6.29	-6.29		10.55	10.55		Macquaker	09/06/2010	25 -> G, Org C, organic C	Mayran Fm TOC
N7C-14	16/11/2010	D-24397		1.062	15343	-6.73	-6.73		12.89	12.89		Macquaker	09/06/2010	25 -> G, Org C, organic C	Mayran Fm TOC
N7C-15	16/11/2010	D-24399		1.252	17337	-6.36	-6.36		12.45	12.45		Macquaker	09/06/2010	25 -> G, Org C, organic C	Mayran Fm TOC
N7C-16	16/11/2010	D-24400		1.517	22154	-6.56	-6.56		13.13	13.13		Macquaker	09/06/2010	25 -> G, Org C, organic C	Mayran Fm TOC
N7C-7	24/11/2010	D-24752	re-runs	1.034	14502	-6.24	-6.24		12.49			Macquaker	09/06/2010	25 -> G, Org C, organic C	Mayran Fm TOC

**Appendix 1**

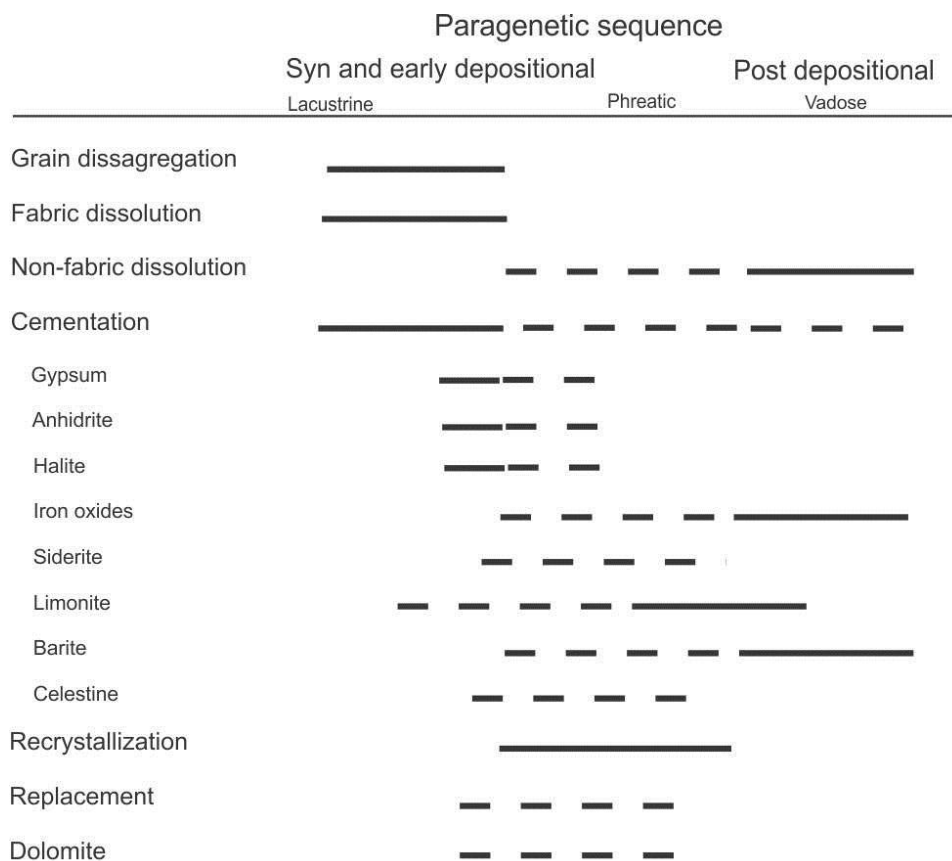
**Additional information for carbon analysis by EA-CF-IRMS**

Column heading	Explanation
OurLabID	This is the sample identification assigned by our lab for your sample. This number is used for tracing all analyses applied to the sample. If you have any questions about a particular analysis, please refer to the OurLabID number.
Analysis	This is the analysis number assigned by the data acquisition software.
Delta of Peak	This number is the isotope ratio ( $\delta^{13}\text{C}$ VPDB) determined from the valid peak for the individual sample.
Mean Delta of All Analyses	If a sample has been analysed more than once during a run, this number will be the mean of all of the valid analyses.
StdDev of Deltas of All Analyses	If a sample has been analysed more than once during a run, this number will be the standard deviation of all of the valid analyses.
%C for applicable media	This number is the elemental percentage determined from the valid peak for the individual sample, based on mass.
Mean %C of All Analyses	If a sample has been analysed more than once during a run, this number will be the mean of all of the valid analyses.
StdDev of %C of All Analyses	If a sample has been analysed more than once during a run, this number will be the standard deviation of all of the valid analyses.

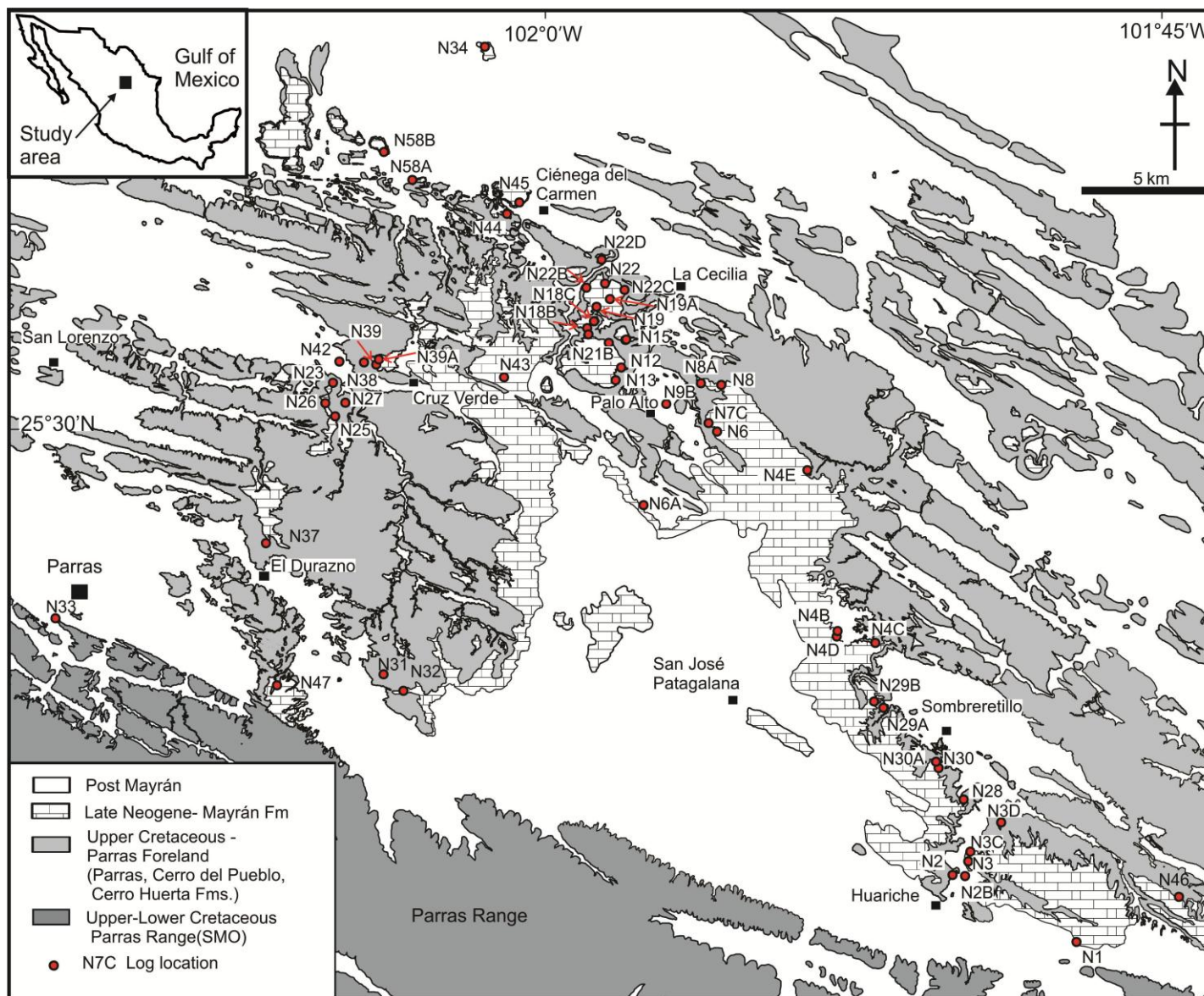
**Reference Material Known/Accepted Values**

OurLabID	Standard ID	Carbon wt. %	$\delta^{13}\text{C}$ VPDB	Comments
G-27	IAEA-CH-6	42.11	$-10.45 \pm 0.13$ <sup>1</sup>	<sup>1</sup> Coplen et.al. 2006: New guidelines for $\delta^{13}\text{C}$ measurements. Analytical Chemistry.
G-24	USGS-24	100	$-16.05 \pm 0.11$ <sup>1</sup>	<sup>1</sup> Coplen et.al. 2006: New guidelines for $\delta^{13}\text{C}$ measurements. Analytical Chemistry.
C-131	LSVEC	16.26	$-46.6 \pm 0.15$ <sup>1</sup>	<sup>1</sup> Coplen et.al. 2006: New guidelines for $\delta^{13}\text{C}$ measurements. Analytical Chemistry.
C-132	MUN-CO-1	12.00	$-21.02 \pm 0.10$	internal standard
C-133	MUN-CO-2	12.00	$-40.11 \pm 0.15$	internal standard
G-32/G-42	Sulphanilamide	41.85		
G-33/G-43	MUN Sulfanilamide	41.85		priming sample
G-34/G-44	BBOT	72.53		
G-35/G-45	B2153	$1.65 \pm 0.02$	$-27.46 \pm 0.11$	Elemental Microanalysis Certificate of Analysis, Batch 2822; <sup>2</sup> Revised for VCDT scale defined in Coplen et.al. 2002: USGS WRIR 01-4222
C-132 and C-133 are used for carbon isotope calibration.				
G-35/G-45 is used for elemental calibration of carbon.				
G-35/G-45 is a check standard for carbon isotope analysis.				
Note: Due to balance precision, smaller masses will have an increased error in elemental determinations. Samples smaller than ~800 mg are more affected, with error increasing with decrease in sample size.				

Appendix 1 Continue



















**Appendix 2.** Paragenetic sequence inferred for the Mayrán carbonates. Fabric dissolution includes burrowing and fenestral porosity, non-fabric dissolution includes vug pores. Solid line-main diagenetic pathway, dashed line-subordinated diagenetic pathway.




Appendix 3. Basin scale log location map

**FIGURE KEY AND ABBREVIATIONS**






















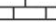
**BIOGENIC**

-  Charophyte
-  Ostracode
-  Gastropod
-  Bivalves
-  Bioclast undetermined
-  Oncolid
-  Stromatolite Type 1
-  Stromatolite Type 2
-  Calcified microbial filament
-  Macrophyte mold/cast
-  Bryophyte mold/cast
-  Phytocast
-  Pelloid / Clott
-  Fish
-  Bone fragment undetermined
-  Root cast









**Bioturbation**

-  Low
-  Moderately
-  Highly




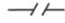




**DEPOSITIONAL & POST-DEPOSITIONAL**

-  Lamination
-  Cross stratification
-  Wavy stratification
-  Structureless
-  Normal grading
-  Reverse grading
-  Mudcrack
-  Fenestral pores
-  Tepee
-  *Microcodium*
-  Mottling
-  Extraclasts
-  Calcareous nodules
-  Intraclasts
-  Gypsum Interval
-  Gypsum crystals
-  Gypsum nodules
-  Selenite
-  Anhydrite crystals
-  Halite crystals
-  Dolomite crystal
-  Calcrete crust
-  Calcareous interval

**LITHOLOGY**

-  Horizontally bedded limestone / Tufa
-  Marlstone
-  Calcareous sandy mudstone
-  Siliciclastic mudstone
-  Non-channelized conglomerate
-  Channelized conglomerate & Pebbly sandstone
-  Gypsum
-  Halite

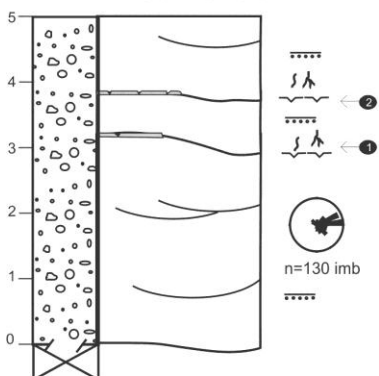
**OTHERS**

-  K/N Unconformity
-  Truncation
-  52°  
Bedrock dip
- KCP Cretaceous Cerro del Pueblo Formation
- KCP Cretaceous Cerro Huerta Formation
-  Basal contact not observed/covered
-  Paleocurrent data (azimut of clast imbrication)  
n=13 imb
-  Depositional cycle
-  Mined interval
-  Sample site

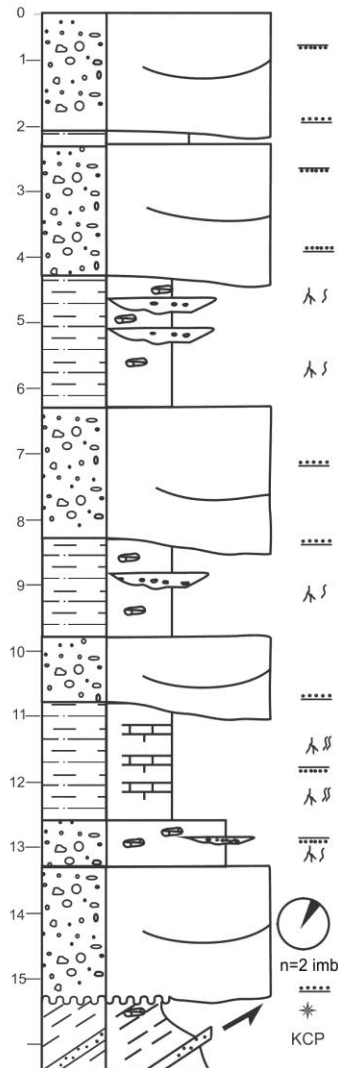
**Appendix 4**



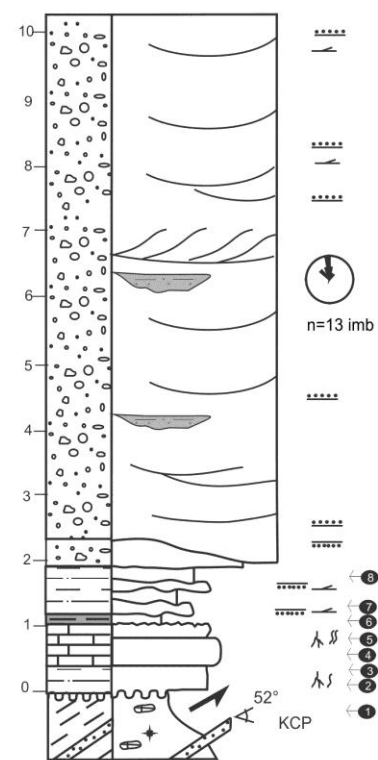
(m) N1  
CLASTIC GRAIN SIZE  
Mud Sand Gavel  
C S L F M C G C  
I I I I I I I I I I I I I I I I I I



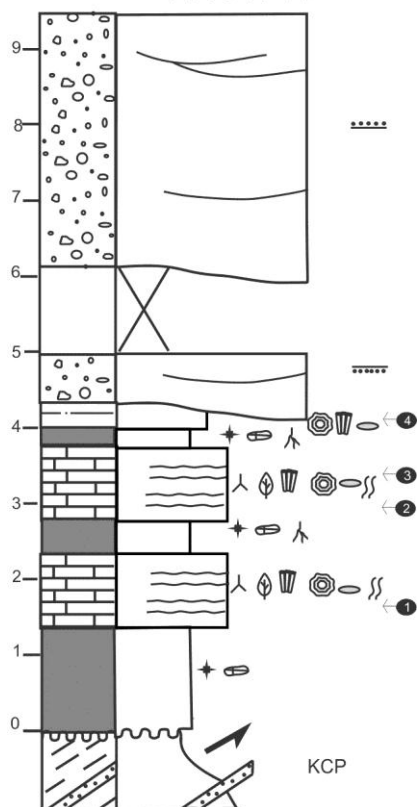
(m) N2  
CLASTIC GRAIN SIZE  
Mud Sand Gavel  
C S L F M C G C  
I I I I I I I I I I I I I I I I I I



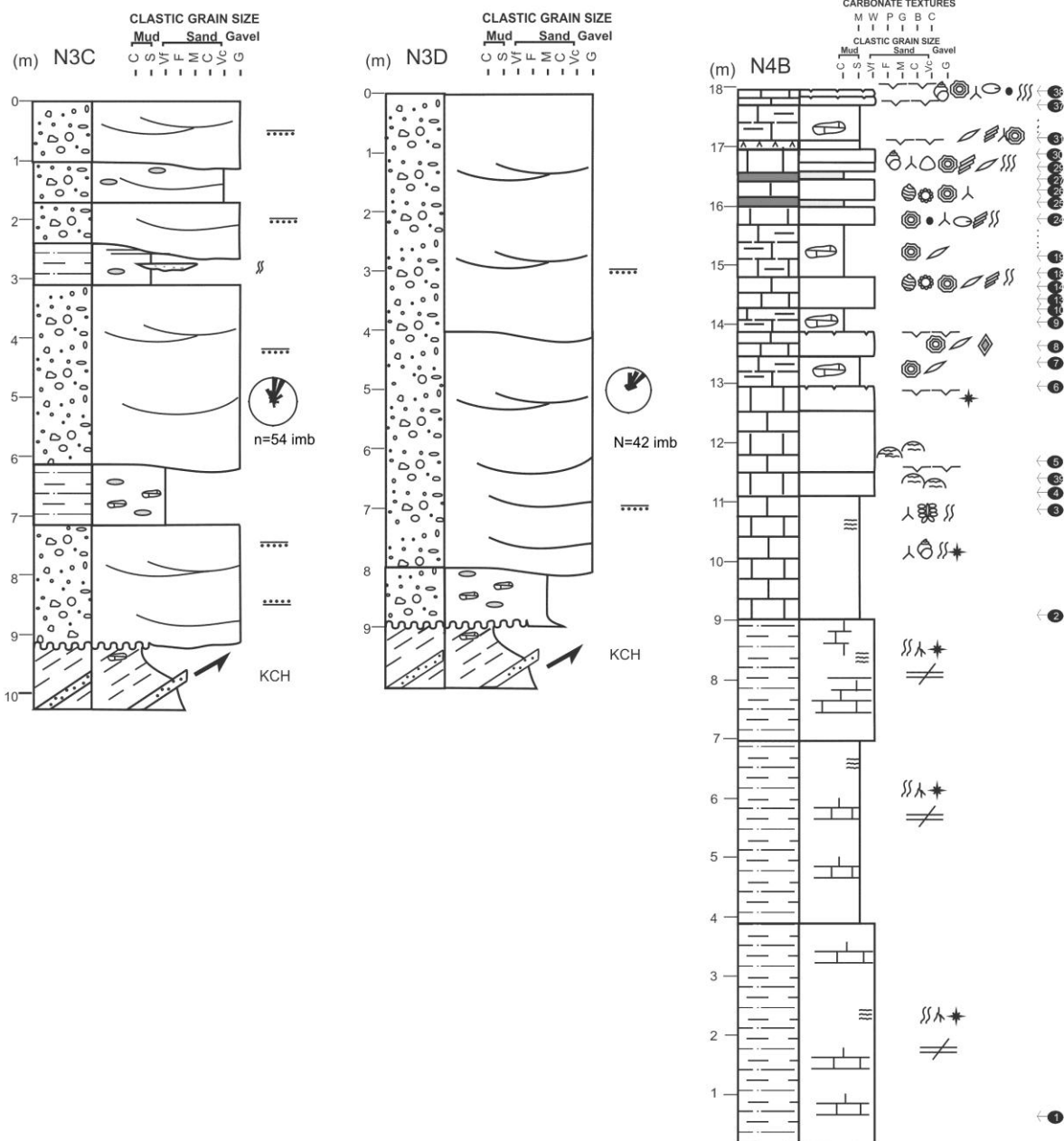
(m) N3  
CARBONATE TEXTURES  
M W P G B C  
I I I I I  
CLASTIC GRAIN SIZE  
Mud Sand Gavel  
C S L F M C G C  
I I I I I I I I I I I I I I I I I I



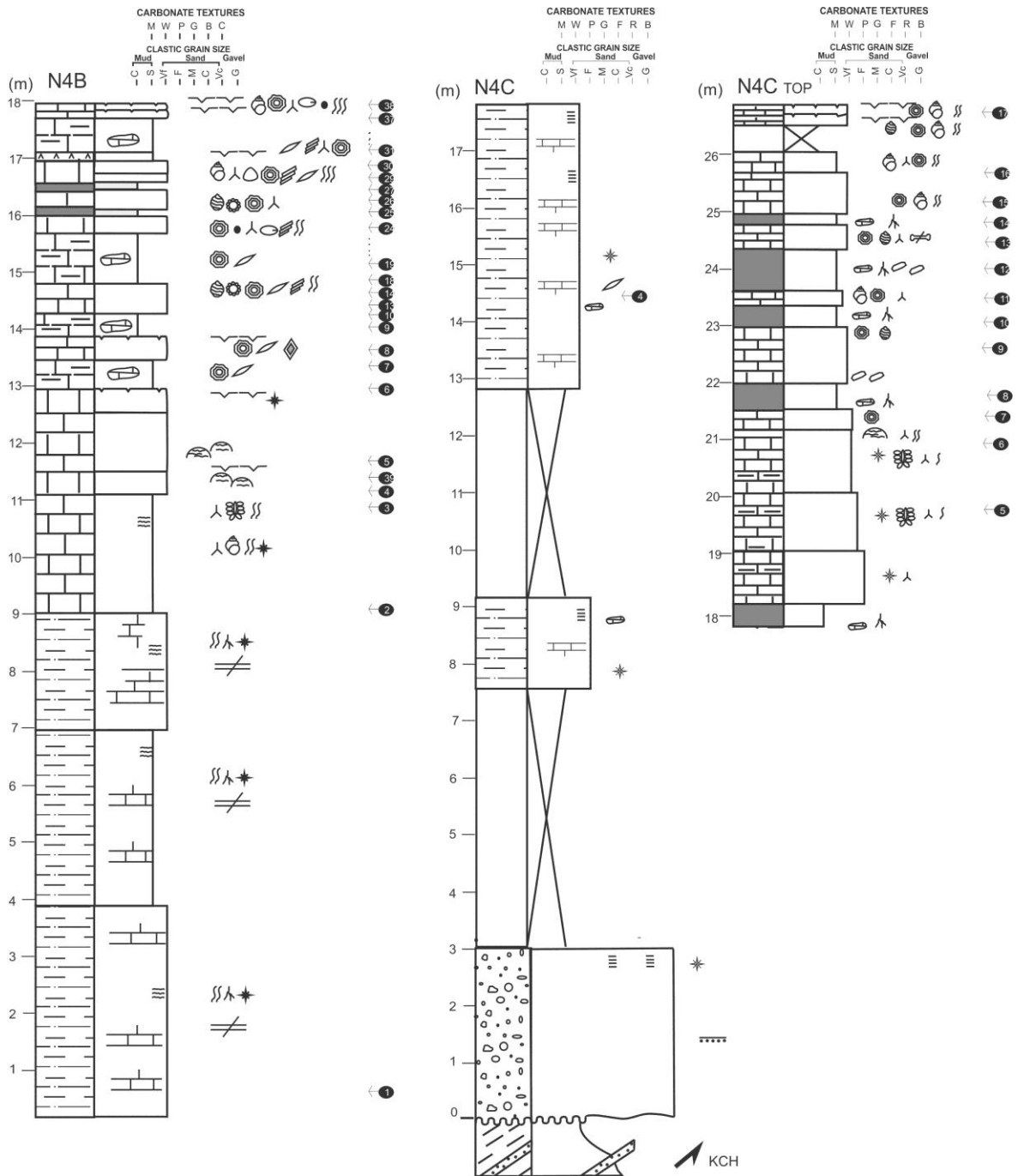
(m) N2B  
CARBONATE TEXTURES  
M W P G B C  
I I I I I  
CLASTIC GRAIN SIZE  
Mud Sand Gavel  
C S L F M C G C  
I I I I I I I I I I I I I I I I I I



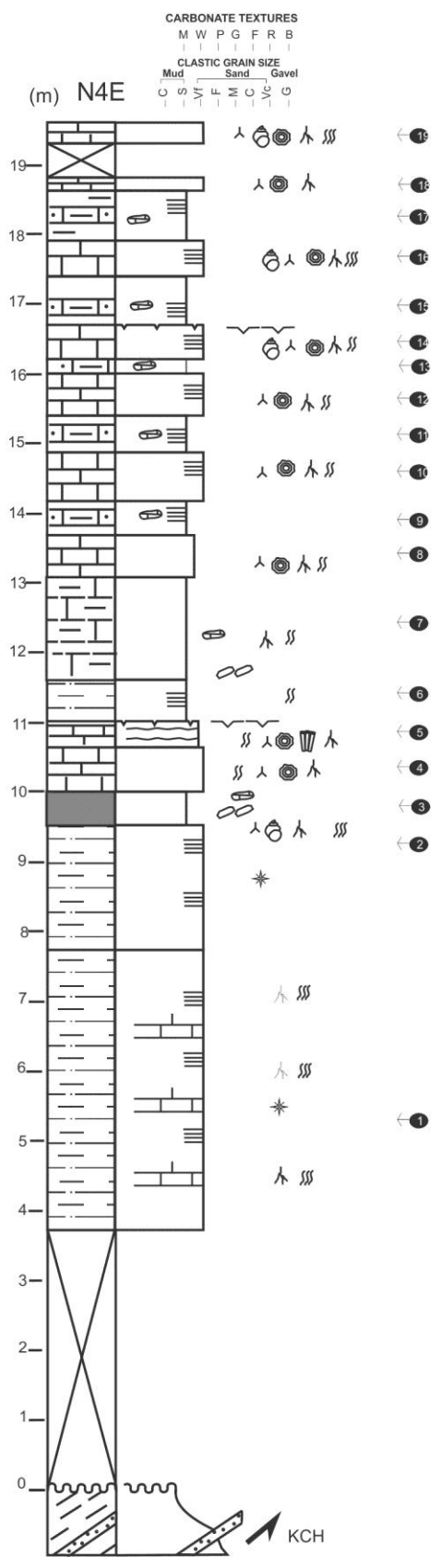
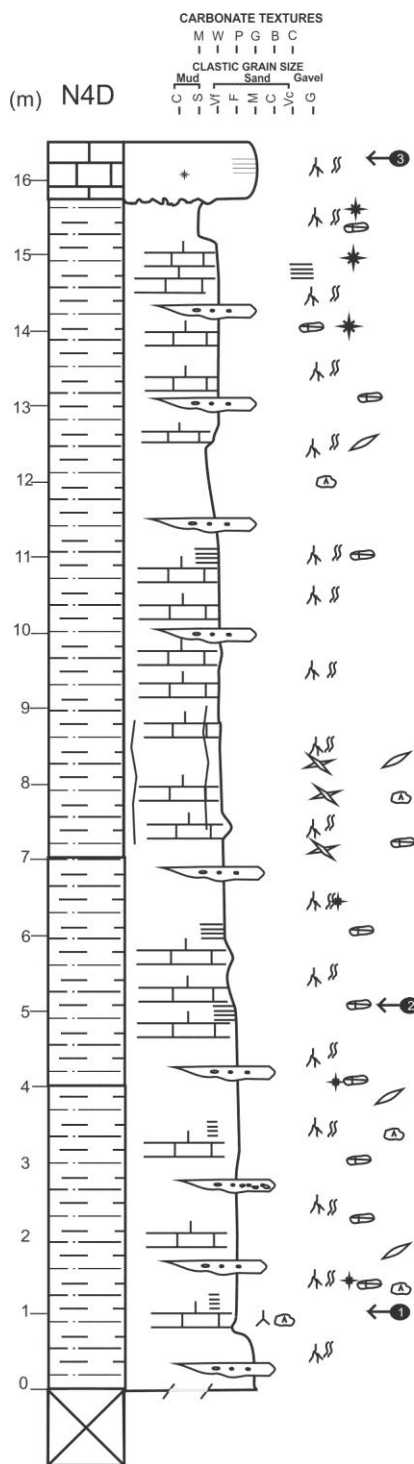
Appendix 5



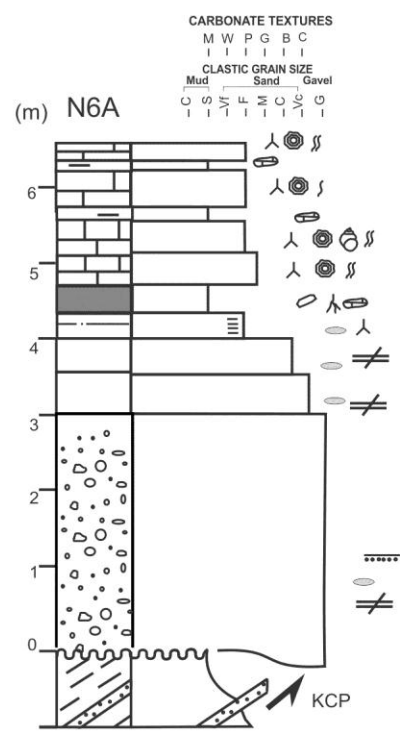
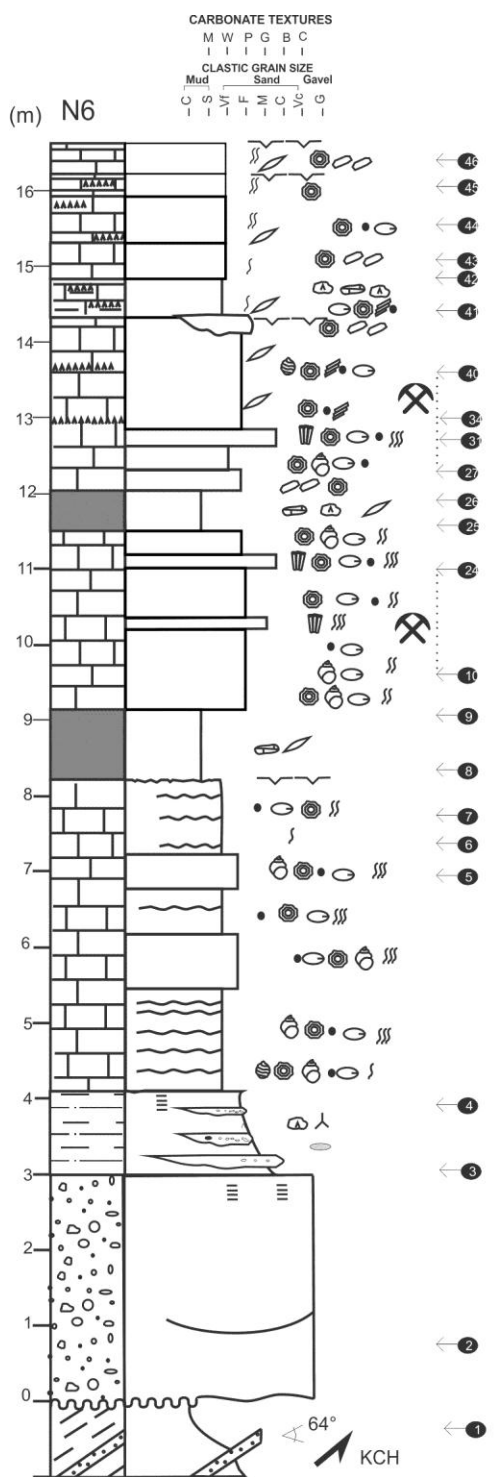
Appendix 6



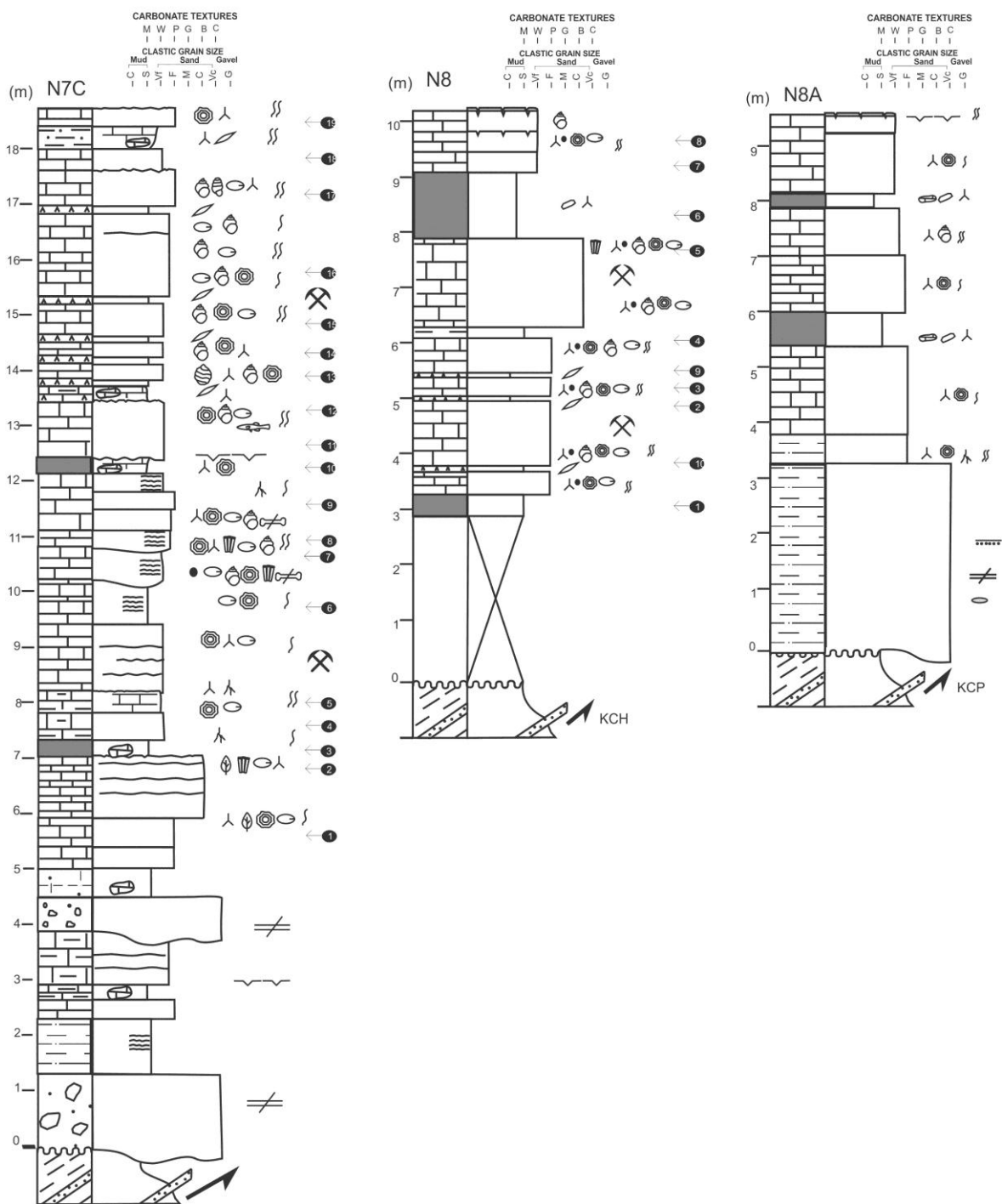
Appendix 7



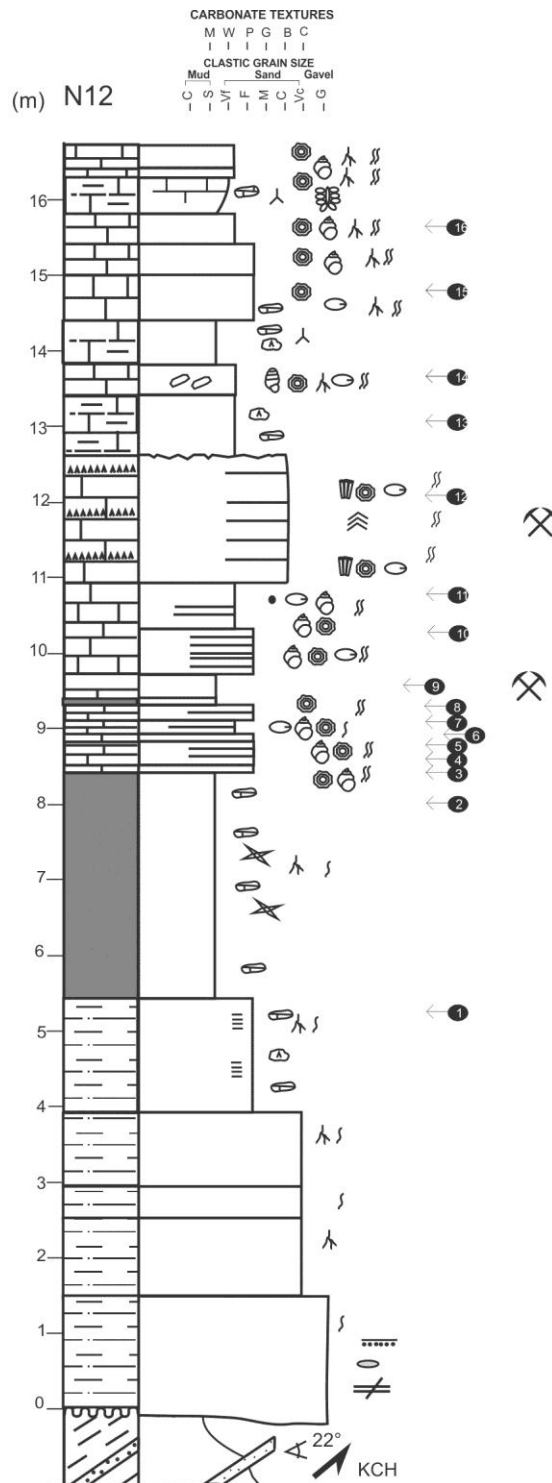
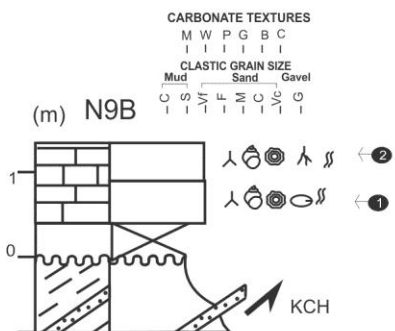
Appendix 8



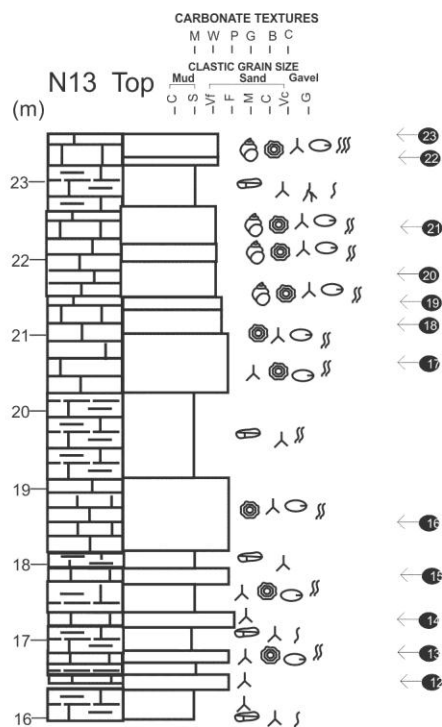
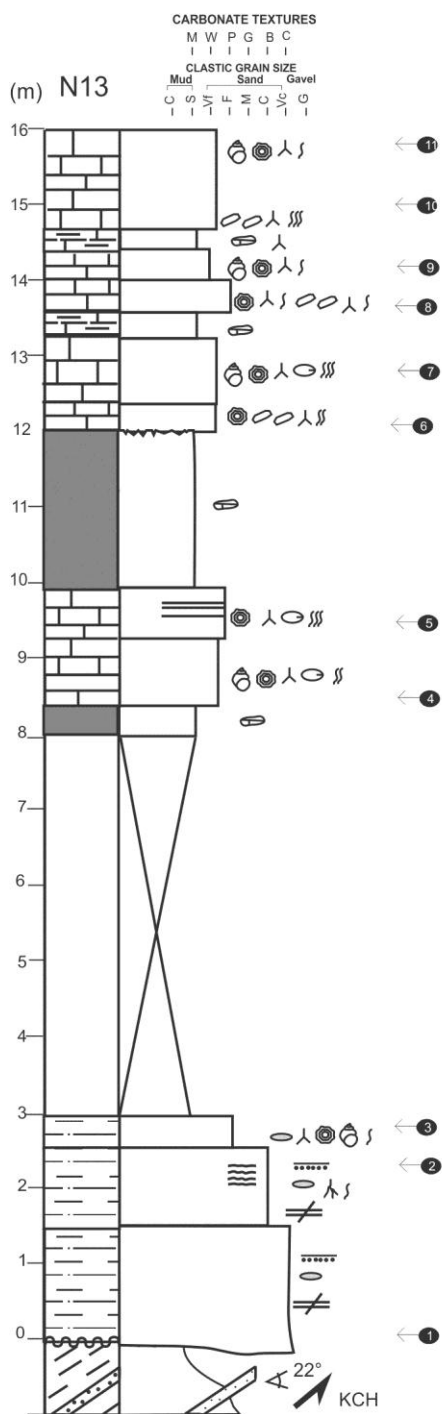
Appendix 9



Appendix 10

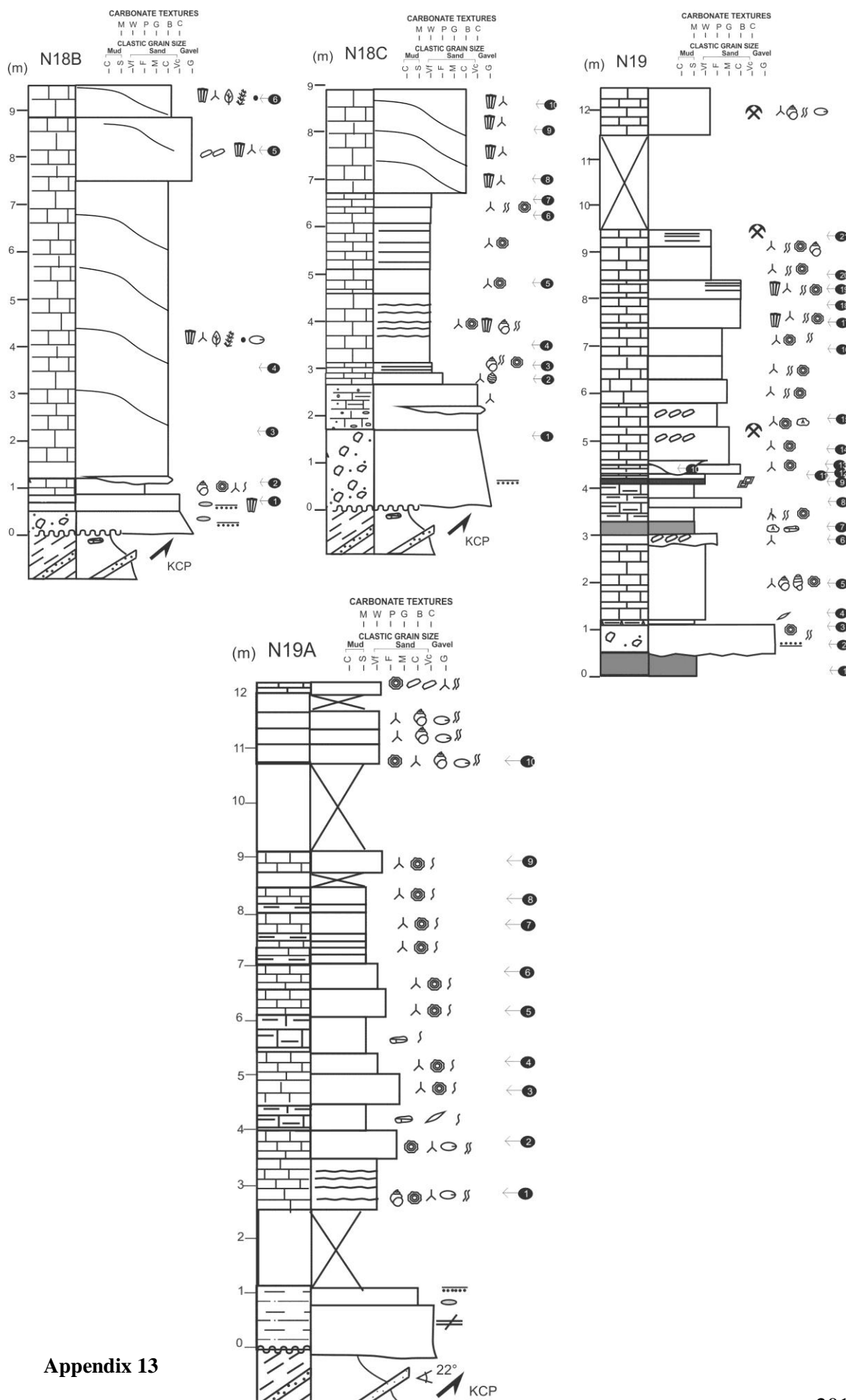


Appendix 11

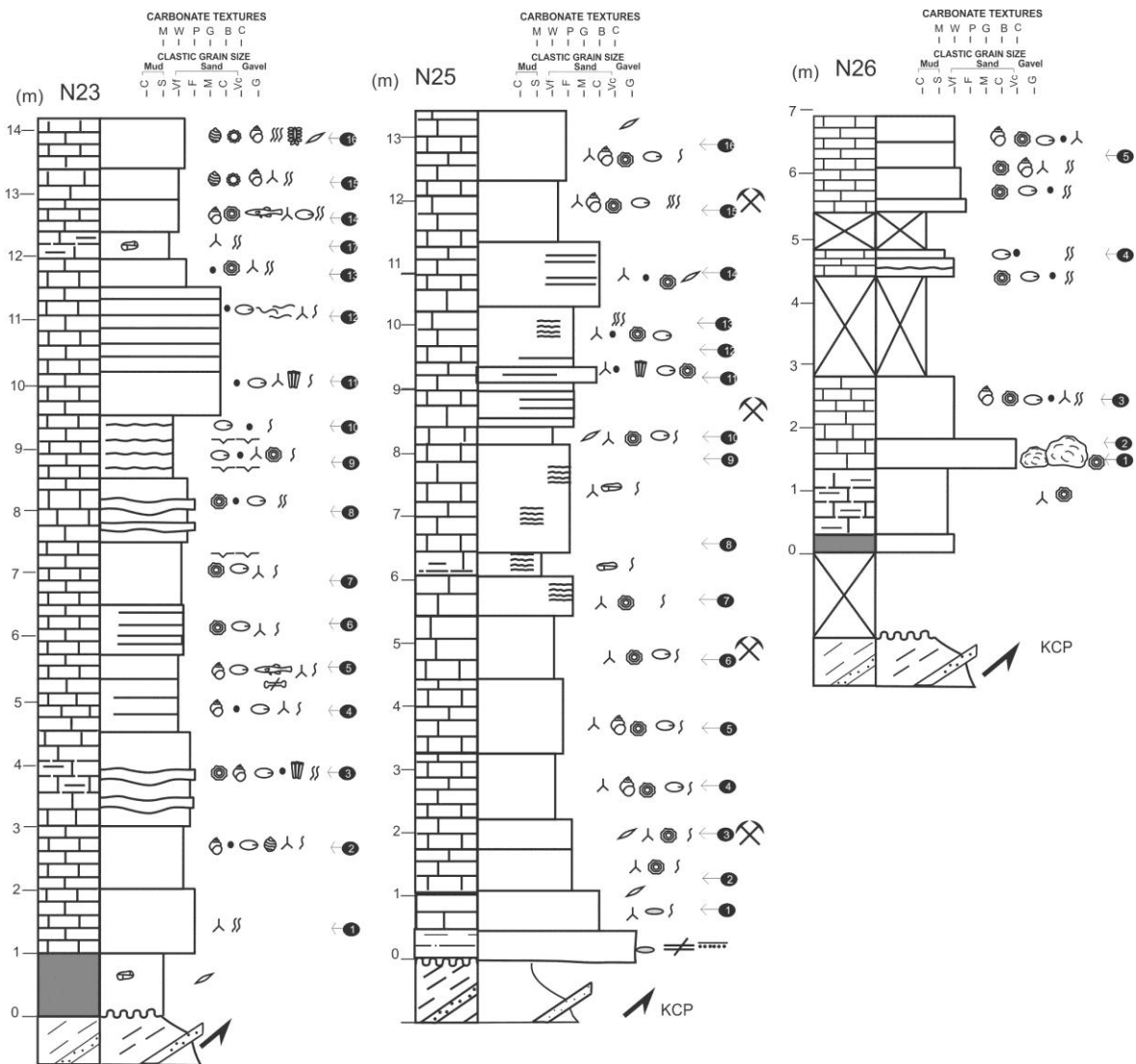


Appendix 12

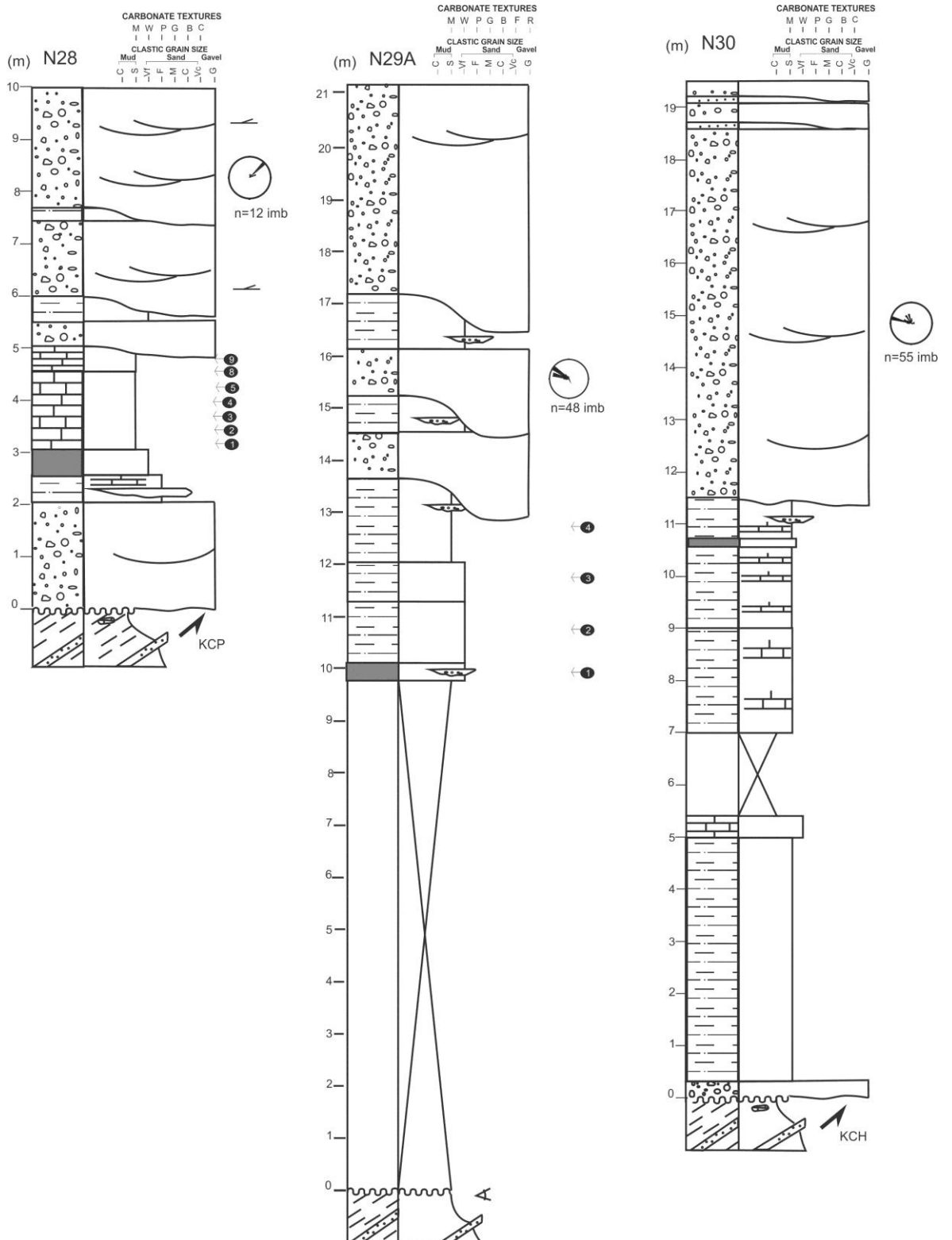




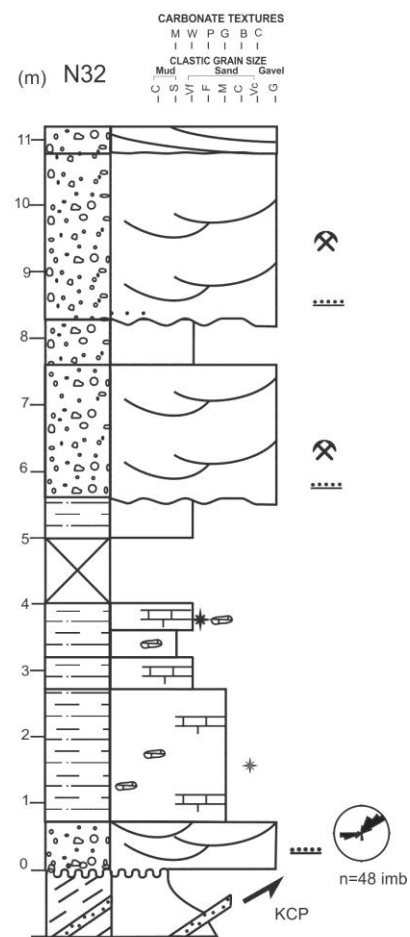
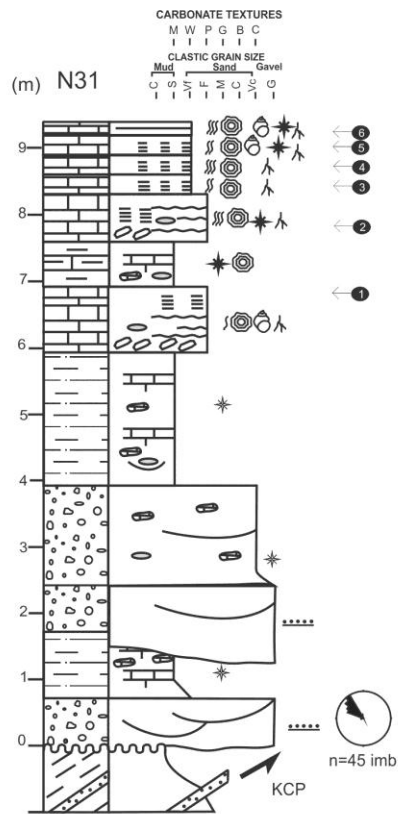
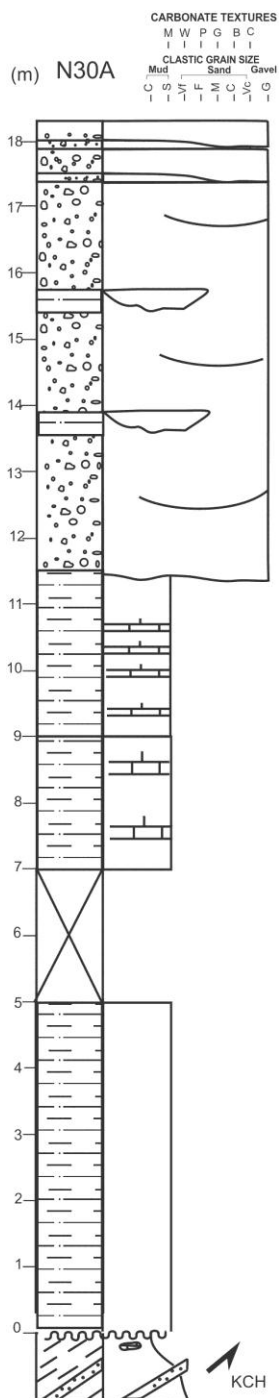
Appendix 13



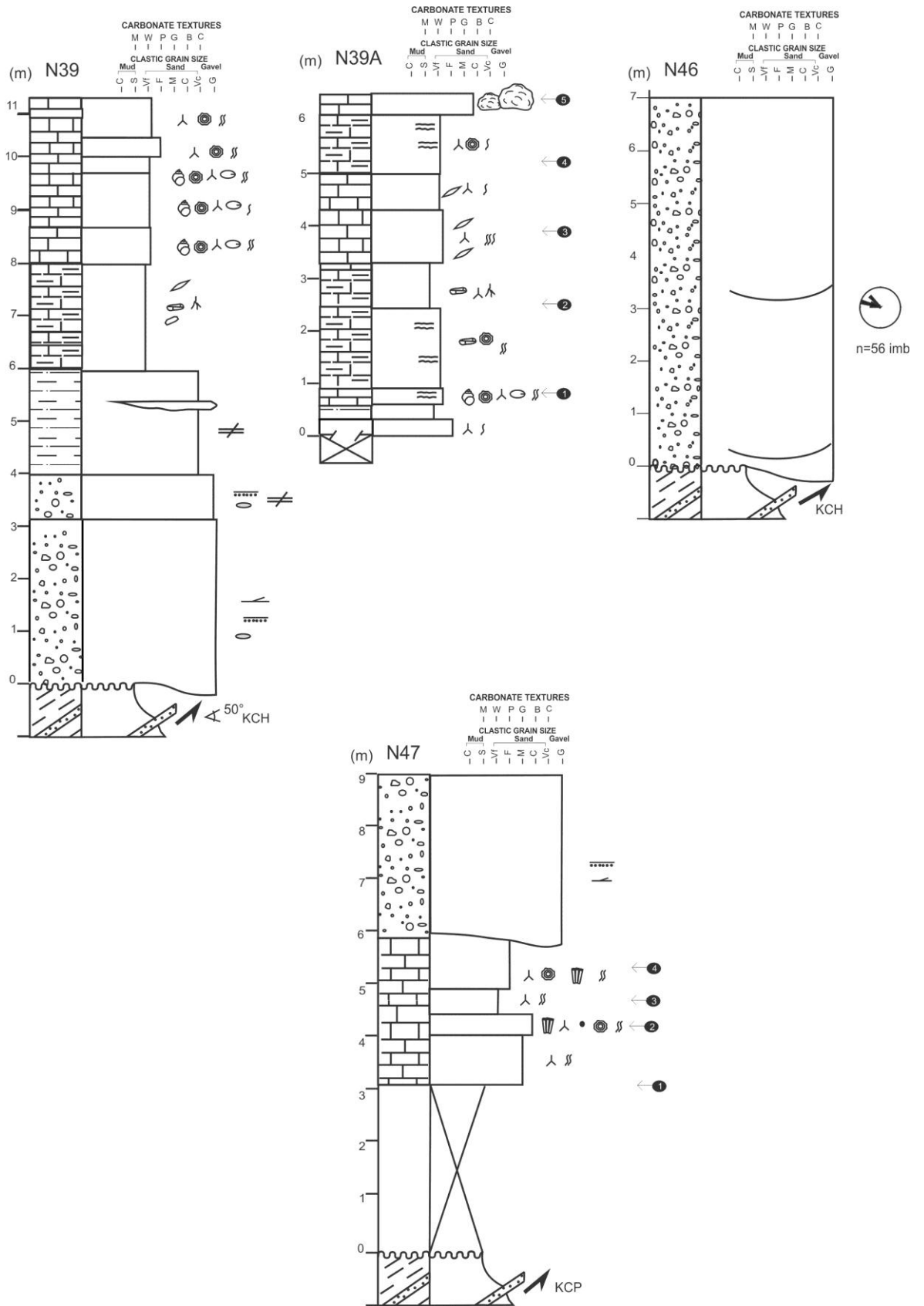
Appendix 14



Appendix 15



Appendix 16



Appendix 17